Low Oxidation State Main-Group Diamides

Liu, Han-Ying Dennis

Award date:
2023

Awarding institution:
University of Bath

Low Oxidation State Main-Group Diamides

Han-Ying Liu

A thesis submitted for the degree of Doctor of Philosophy

University of Bath

Department of Chemistry

June 2023

"...I am just passionately curious." –Albert Einstein.

Contents

I. Acknowledgements

First and foremost, I would like to thank my supervisor, Prof. Mike Hill, for offering me the opportunity to do a PhD and all his support during this journey. Perhaps it is a bit of a cliché saying that he is not an ordinary supervisor, the daily coffee session in the morning (of course it is following the COVID guidelines) and all the google maps searches reflect that it is more pure good vibes. Also, I am grateful for the abundance of freedom and suggestions provided in my project, it has been an enjoyable process with a lot of satisfying observations. It really has been a privilege to work with Mike.

The Hill group members are also essential for the completion of this thesis. Kieran, Bibian, Andy, and Louis have provided help about the chemistry and living in Bath. Special thanks go to Anne-Fred for helping me in the setting up stage; Ryan for all the help in the alumanyl and the first step in the sodium-magnesium chemistry; and Kyle for the insights into the chemistry and help during my writing. Henry, Dom, and Ollie also deserve special mention for the lengthy office chats, especially Henry with all his memes and Ollie with random quotes. I also appreciate the help and chats from Dave, Carla, Tom, Laura, and the Liptrot group members in the same part of building.

This thesis would not have been possible without computational support from Dr Claire M^{c}Mullin and Dr Sam Neale, they have provided great insights and perspectives into the chemistry and put a lot more depth into some random observations I have made. I am grateful for Dr Emma Richards for her help in all the EPR experiments, although we would often observe a signal where we did not expect one and got really confused. I would also like to thank Dr John Lowe and Dr Catherine Lyall for the help with NMR experiments. A special thank you goes to Dr Mary Mahon for all her help with crystallography, especially her patience and hard work in rectifying data from some of my questionable choice of X-ray diffraction samples.

This body of work also marked the tenth year of my adventure in chemistry. It would not have been the case if Prof. Ching-Wen Chiu had not offered me the chance to conduct undergraduate and masters research in her group. I am, therefore, eternally grateful for her supervision and help during those projects and her support in my application for PhD positions. It is also a good time to say thank you to Dr Chao-Tang Shen for equipping me with Schlenk techniques, one of the most useful and transferable skills (in organometallic chemistry).

Thank you to all my friends for all their support. Yi-Hsien for all her time and effort to host podcast length chats with me regardless of the time difference, and Bo-Jiun for his patience in understanding my academic challenges. Appreciation also goes to Jess for our (way too long)

coffee breaks, alongside Philip and Becca in our occasional Bath explorations. James, Matt, Laura, and Niamh also made my cohort a better group of people. It is also a good opportunity to express how fortunate I've felt to be able to work in Bath with all the great people in the same section of 1 South. Special thank you goes to Ross Stanley for everything, and my family for all the supports and attempts to understand what I am doing, albeit most of time they thought I am working with alloys.

Finally, I would like to thank my parents. My father for his unconditional support despite that that it might have gone beyond his understanding of career pathways. And my mother for inspiring me to do great things, and even foretold Bath to be an important city for me, hopefully she also foresaw the completion.

II. Publications as a Result of this Thesis

a. Publications as a Result of Work Contained Herein

1. *Reductive Dimerization of CO by a Na/Mg(I) diamide*. (Chapter 2)

H.-Y. Liu, R. J. Schwamm, S. E. Neale, M. S. Hill, C. L. M^{c}Mullin, and M. F. Mahon, *J. Am. Chem. Soc.,* **2021**, *143*, 17851–17856.

2. *Reduction of Na^{+} within a $\{Mg_2Na_2\}$ Assembly.* (Chapter 2)

H.-Y. Liu, S. E. Neale, M. S. Hill, C. L. M^{c}Mullin, M. F. Mahon, and E. Richards, *Angew. Chem. Int. Ed.* **2022**, *62*, e202213670.

3. *Cooperative Dihydrogen Activation at a $Na(I)_2/Mg(I)_2$ Ensemble*. (Chapter 2)

H.-Y. Liu, S. E. Neale, M. S. Hill, C. L. M^{c}Mullin, M. F. Mahon, and B. Morrison, *Chem. Commun.,* **2023**, *59*, 3846-3849.

4. *Seven-Membered Cyclic Potassium Diamidoalumanyls.* (Chapter 3)

R. J. Schwamm, M. S. Hill, H.-Y. Liu, M. F. Mahon, C. L. M^{c}Mullin, and N. A. Rajabi, *Chem. Eur. J.* **2021**, *27*, 14971-14980.

5. *Seven-membered Cyclic Diamidoalumanyls of the Heavier Alkali Metals: Structures and C–H activation of Arenes* (Chapter 3)

H.-Y. Liu, M. S. Hill, C. L. M^{c}Mullin, and M. F. Mahon, *manuscript submitted.*

6. *Diverse reactivity of an Al(I)-centred anion towards ketones.* (Chapter 3)

H.-Y. Liu, M. S. Hill, and M. F. Mahon, *Chem. Commun*., **2022**, *58*, 6938–6941.

7. *Ambiphilic Al−Cu Bonding.* (Chapter 4)

H.-Y. Liu, R. J. Schwamm, M. S. Hill, M. F. Mahon, C. L. M^{c}Mullin, and N. A. Rajabi, *Angew. Chem. Int. Ed.* **2021**, *60*, 14390– 14393

8. *On the reactivity of Al-group 11 (Cu, Ag, Au) bonds.* (Chapter 4)

H.-Y. Liu, S. E. Neale, M. S. Hill, M. F. Mahon, and C. L. M^{c}Mullin, *Dalton Trans*., **2022**, *51*, 3913-3924.

b. Publications as a Result of Other Work During this Thesis

I. *Structural Snapshots of an Al–Cu Bond-Mediated Transformation of Terminal Acetylenes.* (Related work to Chapter 4)

H.-Y. Liu, S. E. Neale, M. S. Hill, C. L. M^{c}Mullin, and M. F. Mahon, *Chem. Sci.,* **2023**, *14*, 2866-2876.

III. Abstract

Although small molecule activation was conventionally considered to be exclusive for transition-metal complexes, there have been significant developments in H_2 activation and other molecular transformations mediated by low oxidation state *p*-block species in the past two decades. There have, however, been limited reports concerning the *s*-block counterparts in H_2 activation and chemistry about low oxidation state aluminium anions.

Chapter 2 describes the synthesis of a low oxidation state magnesium diamide, which features sodium cations in its dimeric structure. Initial reactivity studies of the sodium magnesium complex demonstrate that the molecule exhibits a cooperative reactivity arising from the tetrameric unit. Addition of non-reducible Lewis bases to the molecule initiate an intramolecular reduction of Na^+, while activation of H_2, CO and various substrates has also been observed with this low oxidation state magnesium molecule.

Chapter 3 describes reactivity studies of a seven-membered cyclic diamidoalumanyl (anionic aluminium(I)) system, where the initial investigation disclosed that the potassium alumanyl exhibits Al(I)-centred characters. Heavier group 1 analogues of the potassium alumanyl have also been prepared, while an evaluation of their ability to conduct the C-H activation of benzene demonstrated that the identity of the counter cation influences the reactivity of this alumanyl system. An extensive studies of the potassium alumanyl in activation of organic substrates have also been performed, where particularly diverse reactivity was observed with a variety of ketone molecules. The potassium alumanyl also demonstrates a potent reducing ability towards *p*-block halides, indicating its potential utilisation as a homogeneous reductant.

Chapter 4 describes a series of group11-alumanyl species prepared by the salt metathesis process of a potassium alumanyl with ligand-supported coinage metal chlorides, demonstrating the application of the alumanyl in providing new aluminium−element bonds. The group 11-alumanyl complexes are evaluated with their reactivity towards heteroallenes, where copper, silver, and/or gold centred nucleophilicity was observed in some of the complexes, reflecting the influence of the co-ligand in this class of molecules.

Chapter 5 constitutes general synthetic notes and crystallographic data, while Chapter 6 describes some structures that demonstrate further applications and reactivity of some molecules contained within the thesis.

IV. Abbreviations

δ	Chemical shift
$\delta^{+/-}$	Partial positive/negative charge
ΔG	Change in Gibbs free energy
μL	Microlitre
χ	Pauling scale of electronegativity
{^{1}H}	Proton decoupled
°	Degrees
°C	Degrees Celsius
12-*c*-4	1,4,7,10-tetraoxacyclododecane
18-*c*-6	1,4,7,10,13,16-Hexaoxacyclooctadecane
2,2,2-crypt	(4,7,13,16,21,24-Hexaoxa-1,10-diazabicyclo[8.8.8]hexacosane)
Å	Angstrom
BCP	Bond critical point
Bn	Benzyl
br.	Broad NMR resonance
B_2pin_2	Bis(pinacolato)diboron
C_6D_6	d_6-Benzene
C_6F_6	Hexafluorobenzene
CAAC	Cyclic(alkyl)(amino)carbene
COD	1,5-Cyclooctadiene
COT	1,2,5,7-Cyclooctatetraene
Cp*	Pentamethylcyclopentadienyl
Cy	Cyclohexyl
d	Doublet
d	Deuterated
DAB	Diazabutadiene
DFT	Density Functional Theory
Dipp	2,6-Di-*iso*propylaniline
DOSY	Diffusion Ordered Spectroscopy
eV	Electronvolt

hept	Heptet
HMDS	Hexamethyldisilazane
HOMO	Highest occupied molecular orbital
Hz	Hertz
I	Nuclear spin
***i*-**	Ipso
ICP-OES	Inductively Coupled Plasma Optical Emission spectroscopy
***i*-Pr**	*Iso*-propyl
IMe	1,3-Dimethylimidazole-2-ylidene
IPr	1,3-Bis(2,6-di-*iso*propylphenyl)imidazol-2-ylidene
$^{x}J_{YY}$	Scalar coupling (J); Coupling constant over x Y-Y bonds ($^{X}J_{YY}$)
K	Kelvin
kcal	Kilocalorie
KC_8	Potassium graphite
kJ	Kilojoule
LUMO	Lowest unoccupied molecular orbital
m	Multiplet
***m*-**	Meta
mbar	Millibar
mg	Milligram
mL	Millilitre
mmol	Millimole
Me	Methyl
Mes	2,4,6-Trimethylbenzene
MHz	Megahertz
***n*-Bu**	*n*-Butyl
NaK	Sodium-potassium alloy
NBO	Natural bonding orbital
NHC	*N*-heterocyclic carbene
***n*-Hex**	*n*-Hexyl
nm	nanometre
NMR	Nuclear magnetic resonance

NON^{Dipp}	4,5-Bis(2,6-di-*iso*propylanilido)-2,7-di-*t*-Bu-9,9-dimethylxanthene
OSiN^{Dipp}	$[O(SiMe_2NDipp)_2]^{2-}$
***o*-**	Ortho
OTf	Trifluoromethanesulfonate
***p*-**	Para
Ph	Phenyl
ppm	Parts per million
q	Quartet
QTAIM	Quantum theory of atoms in molecules
^{R}BDI	$[HC\{(Me)CNR\}_2]^-$
^{R1R2}BDI	$[HC\{(R_1)CNR_2\}_2]^-$
R	Substituent
RT	Room temperature
s	Singlet
sept	Septet
SiN^{Dipp}	**[(**$CH_2SiMe_2NDipp)_2]^{2-}$
SiN^{Mes}	**[(**$CH_2SiMe_2NMes)_2]^{2-}$
t	Triplet
***t*-Bu**	Tertiary butyl
TD-DFT	Time-dependent density-functional theory
THF	Tetrahydrofuran
TMEDA	Tetramethylethylenediamine
Tol	Tolyl
UV-Vis	Ultraviolet–visible

1. Prologue

Referring to the formal charge borne by the constituents of a molecule, an atom's oxidation state is dictated by the number of electrons it loses or gains through the formation of its chemical bonds. An atom's oxidation state can, thus, be positive or negative, dependent on the number of electrons lost or gained, respectively. When forming a bond to any more electronegative atom, for example, an element formally increases its oxidation state by one positive charge. This concept can be sometimes confused with the valence state (or valency) of an element, which is dictated by the number of valence electrons it utilises in bond formation, irrespective of the polarisation of the interaction. As a result, the valence state of an element is always expressed as a number ≥0. Although the two descriptions are commonly interchangeable for more electropositive elements in their highest group oxidation states, the attribution of an atom's oxidation state can generally convey more information about of its electronic environment, particularly when covalently bonded to an identical atom.[1]

An element is in its highest oxidation state when it has formally lost all its valence electrons, resulting in a noble gas-like closed shell electronic configuration. Derivatives of main-group elements, particularly those of groups 1 and 2 and the lighter elements of groups 13-15, in their highest oxidation state tend to be most stable due to their ability to form strong chemical bonds. Whilst such species constitute the vast majority of main group systems, a variety of *s*- and *p*-block species in lower oxidation states have provided an intense area of study during recent decades. With suitable kinetic protection and/or electronic stabilisation, the reduction of precursors in higher oxidation states has resulted in the isolation of a plethora of main-group molecules with formally lower oxidation states. This latter class of low oxidation state main-group species has been observed to be capable of activating chemical bonds of small molecules.[2]

As the initial step of any chemical transformation, element-element bond activations have long attracted broad interest in synthetic chemistry. Although the activation of the simplest, yet relatively robust (432 kJ/mol), hydrogen-hydrogen bond of H_2 was conventionally considered to be exclusive for *d*-block molecules, recent studies have shown that various main-group molecules are also capable of mediating its conversion.[2-7] This reactivity is engendered by the energetically and spatially appropriate frontier orbital alignments, where the preparation of main-group species in low oxidation states has been demonstrated to provide a feasible approach. In this vein, this chapter will focus on the general strategies to achieve small molecule activation by *s*- or *p*-block centred molecules and will attempt to identify further

research opportunities in the low oxidation state main-group chemistry. The chemistry research described in thesis will, therefore, attempt to address these gaps through the preparation of novel species in which an *s*- or *p*-block element is in a formal low oxidation state, particularly those stabilised by sterically demanding diamide ligands, along with their corresponding reactivity.

"So it begins." –Theoden, *Lord of the Rings: The Two Towers*, 2002.

1.1 Main Group Centres as Transition Metals: Early Examples of H_2 Activation by Main Group Molecules

An inherent contrast in properties between transition metal complexes and main-group species arises from their respective valence electronic structures. The valence orbitals of *d*-block molecules are close in energy (<3 eV) and usually partially populated, giving rise to the characteristics of being coloured and reactive towards small molecules, with hydrogen providing the simplest archetype (**Figure 1. 1**). On the other hand, *s*- and *p*-block compounds are mostly colourless with fully occupied or empty frontier orbitals which are well separated energetically (>4 eV), such that covalent bond activation (e.g. H-H bond) is conventionally not kinetically feasible for these molecules.[2]

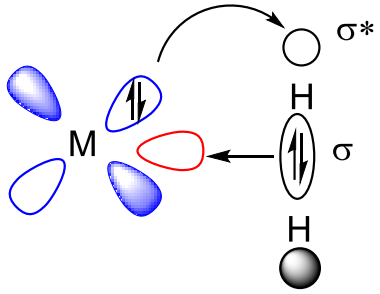

Figure 1. 1 : Visualisation of frontier orbital interactions during H_2 activation by a transition metal centre.

In the last two decades, however, numerous cases of reactivity that contradict this viewpoint of *p*-block chemistry have been reported.[2,3] In 2005, for example, Power and co-workers reported that the germanium analogue (**1.1**) (and later the tin analogue, **1.2**) of acetylene readily activates H_2 under mild conditions,[4,5] where compounds **1.1** and **1.2** exhibit frontier orbitals with appropriate energetic and spatial disposition for synergic engagement with the H–H bond (**Scheme 1.1**). Later, the development of Frustrated Lewis Pairs (FLPs), which possess 'unquenched' lone pairs and low energy vacant orbitals on spatially separated atoms, were demonstrated to be capable of splitting hydrogen reversibly in 2006 (**Scheme 1.2a**).[6] This reactivity can also be rationalised by the transition metal-like orbital interactions facilitated by this class of molecules, albeit the frontier orbitals in FLPs are introduced as spatially separated basic (HOMO) and acidic (LUMO) components (**Scheme 1.2b**).

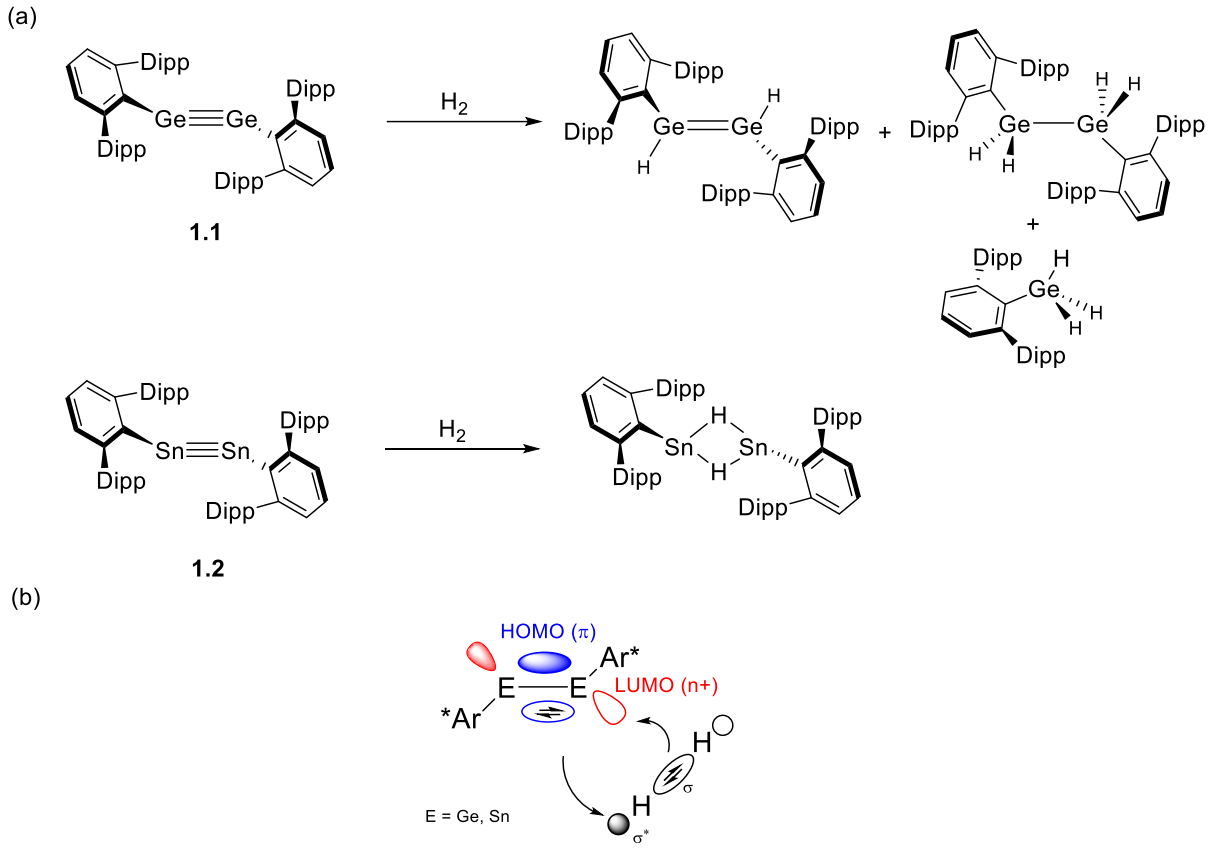

Scheme 1. 1 : (a) H_2 activation by 2,6-bis(2,6-di-isopropylphenyl)phenyldigermyne (**1.1**) and 2,6-bis(2,6-di-idopropylphenyl)phenyldistannyne (**1.2**) (b) Frontier orbital interactions during synergic H_2 activation by compounds **1.1** and **1.2** (where Dipp = 2.6-di-isopropylphenyl).[4,5]

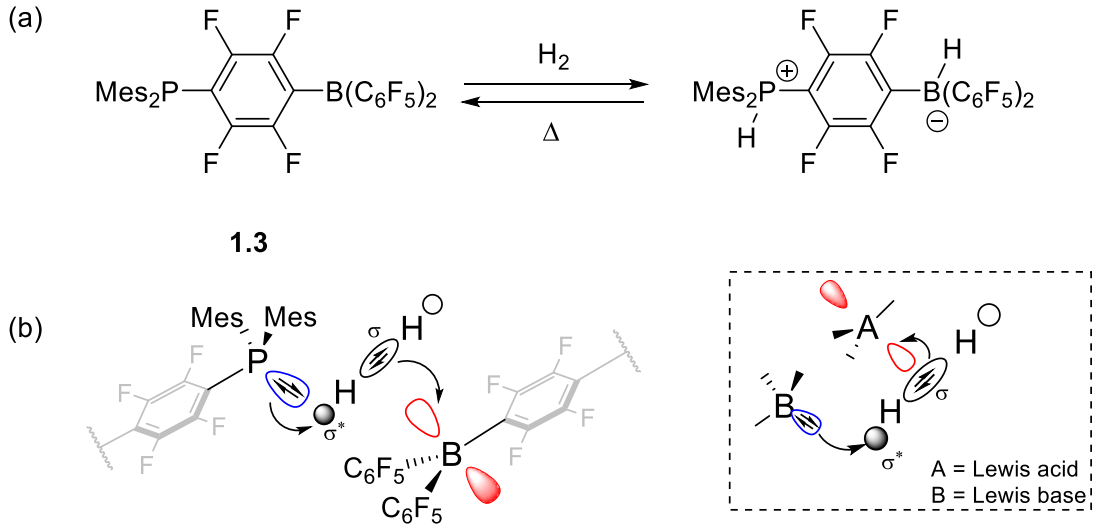

Scheme 1. 2 : (a) Metal-Free, reversible H_2 activation by compound **1.3** (b) Frontier orbital interactions during synergic H_2 activation by **1.3** and generalised illustration for Frustrated Lewis Pairs.[6]

Of most relevance to the research described in this thesis, transition metal-like behaviour may be achieved by the tailoring of accessible electron donor and acceptor orbital energy levels at individual low oxidation state *p*-block element centres to enable facile small molecule activation at a single atom centre. Furthermore, singlet carbenes comprising a low oxidation state carbon centre, have been identified as *p*-block centred derivatives capable of displaying such reactivity due to their possession of valence electronic structures reminiscent of those of typical transition metal complexes (**Figure 1.2**). In 2007, this deduction was verified by Bertrand and co-worker's report in which they described the facile splitting of hydrogen at a single carbon centre of a cyclic(alkyl)(amino)carbene (**1.4**) and an acyclic(alkyl)(amino)carbene (**1.5**) under mild conditions (**Scheme 1. 3**).[7,8]

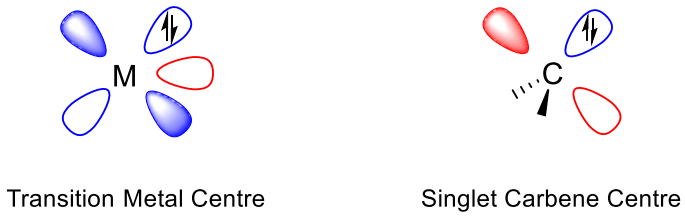

Figure 1. 2 : Depiction of frontier molecular orbitals of a transition metal centre and a singlet carbene centre.

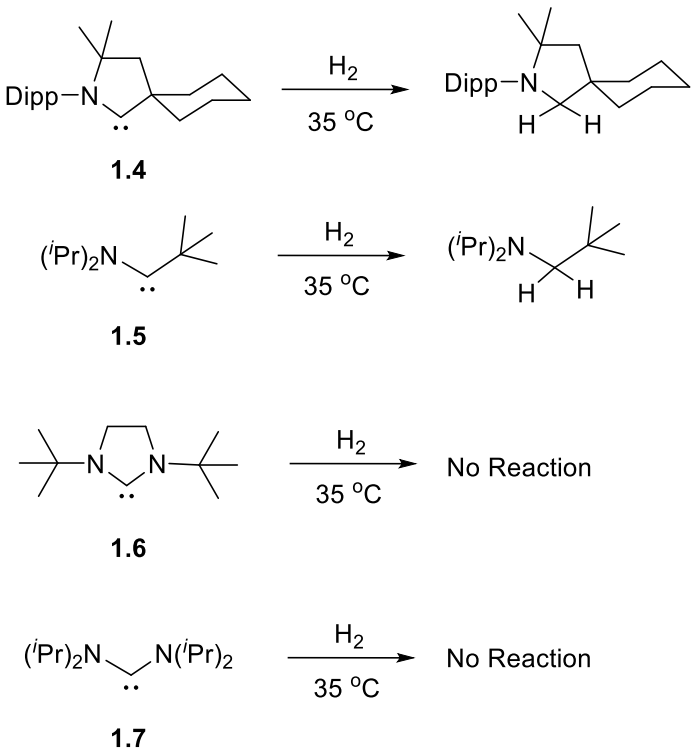

Scheme 1. 3: Reactions of various carbenes (**1.4 - 1.7**) with H_2.[7]

As shown in **Scheme 1.3**, whilst both the cyclic and acyclic (alkyl)(amino)carbene (**1.4** and **1.5**, respectively) were observed to react with H_2, their diamino-substituted counterparts (**1.6** and **1.7**) remained unreacted under the same reaction conditions despite their similar frontier orbital structures. This contrasting reactivity can be rationalised by the narrower HOMO-LUMO gap in (alkyl)(amino)carbenes (**Figure 1.3**),[7, 9] such that the smaller energy difference at the carbon-centred frontier orbitals more closely resembles that of a *d*-block complex.[8, 9]

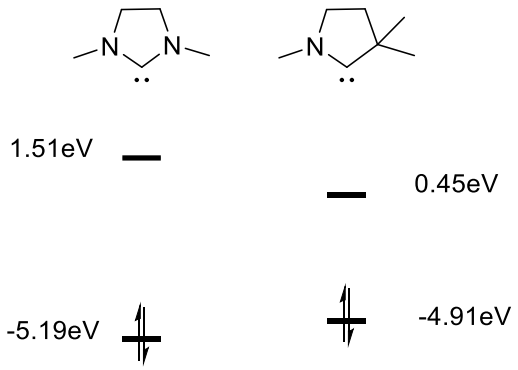

Figure 1. 3 : Energy (eV) of frontier orbitals of cyclic di(amino)carbenes and cyclic (alkyl)(amnio)carbenes calculated at the B3LYP/6-31G* level.[9]

Thermodynamic stabilisation of the carbenoid carbon centre is typically provided by adjacent σ-withdrawing and π-donating atoms to the low oxidation state carbene centre (**Figure 1.4**). Consequently, the low valent carbon centres in diamino-substituted carbenes (**1.6** and **1.7**) feature a larger energy HOMO-LUMO separation and exhibit relative stability toward formal oxidative addition, whilst the relatively destabilising orbital interactions in (alkyl)(amino)carbenes (**1.4** and **1.5**) facilitate their reactivity towards H_2 arising from the narrowed frontier orbital gap.

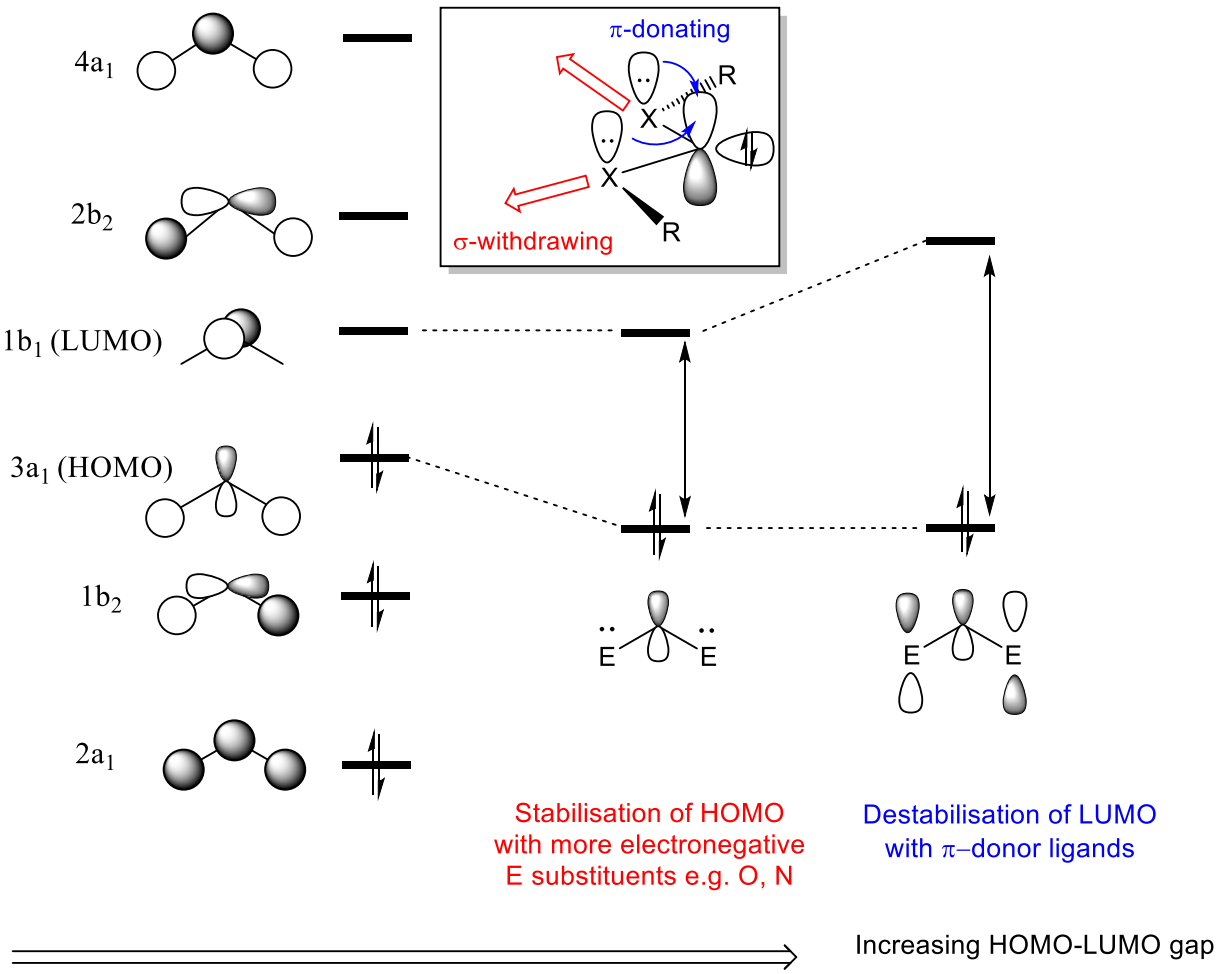

Figure 1. 4 : General approach to achieve the electronic stabilisation of singlet carbenes.

1.2 Main Group Centres as Transition Metals: Small Molecule Activation by Main Group Singlet Carbene Analogues

As showcased by compounds **1.4** and **1.5**, singlet carbenes with valence orbitals close in energy (<3 eV) can indeed display reactivities comparable to that of transition metal complexes, and fine-tuning of the electronic structure in such molecules can be readily manifested through appropriate molecular design (**Figure 1.4**). Inspired by this observation, a phenomenal amount of research in main group chemistry has since been conducted in the synthesis of singlet carbene analogues. Many of these compounds display suitably narrow frontier orbital energy gaps that mimic *d*-block species in their ability to initiate small molecule activation.

1.2.1 Singlet Carbene Analogues in Group 14

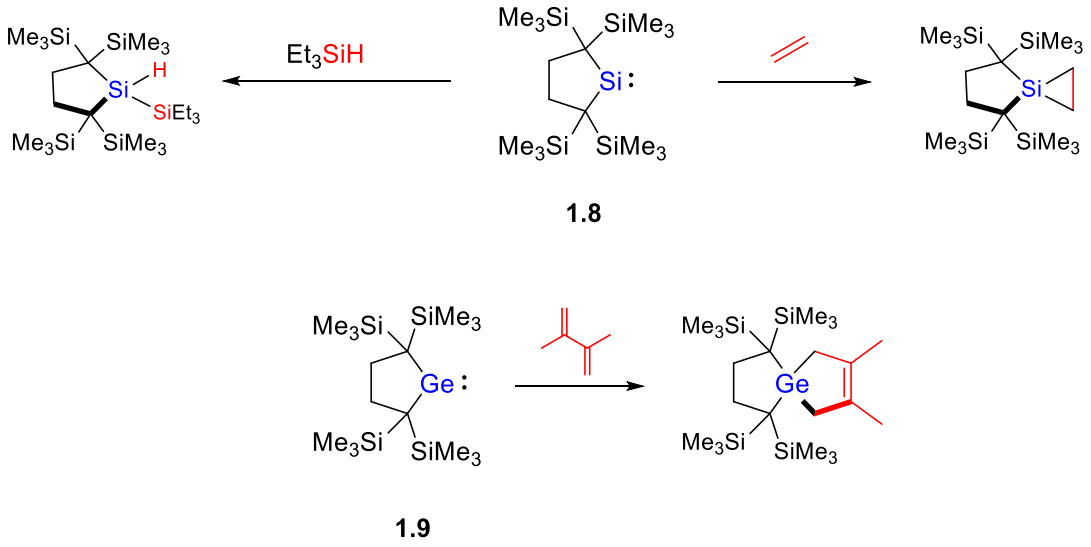

Scheme 1. 4 : Selected Examples of oxidative addition at singlet carbene analogues **1.8** and **1.9**.[10,11]

Although thermodynamic stabilisation of heavier congeners of singlet carbenes in group 14 (i.e. E = Si, Ge, Sn, Pb), is again often provided by adjacent σ-withdrawing and π-donating atoms to the low oxidation state metallylene centre (**Figure 1.4**), and these molecules typically feature at least one such stabilising interaction with nitrogen, wholly carbon-substituted species can be isolated when the ligand structure provides sufficient kinetic protection.[10,11] As depicted in **Scheme 1.4**, these latter heavier carbene analogues (**1.8**, E = Si; **1.9**, E= Ge) are purely stabilised by bulky substituents and undergo relatively facile oxidative addition with various reagents that is facilitated by the higher energy ($3a_1$ HOMO, **Figure 1.4**) electron pair and the

more energetically accessible vacant *p* orbital ($1b_1$ LUMO, **Figure 1.4**). In this manner, a wide variety of metallomimetic examples with varied frontier orbital energies have now been reported for the heavier group 14 elements.[12] For example, a narrower HOMO - LUMO energy gap can be realised in a tin(II) species by deploying either one or two more σ-donating and non-π donor boryl groups (**1.10** and **1.11**, respectively) to the formally low oxidation state element centre. Resultant reactivity studies with H_2 evidence an increasing ability to undergo H-H oxidative addition, and further support the general design principle in enabling main-group molecules with transition metal properties (**Scheme 1.5**).[13]

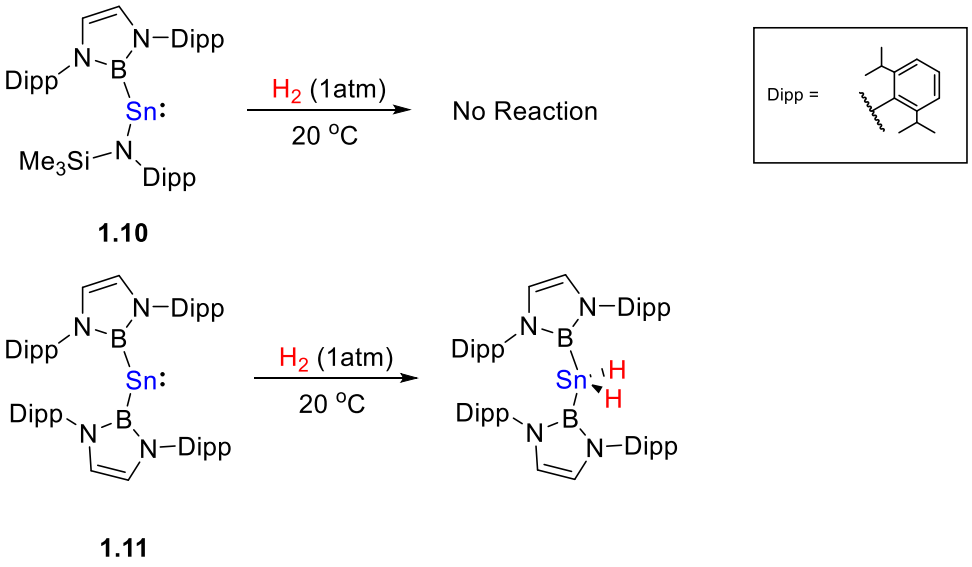

Scheme 1. 5 : Contrasting reactivity towards H_2 of mono-boryl and bis-boryl substituted stannylenes (**1.10** and **1.11**).[13]

1.2.2 Singlet Carbene Analogues in Group 15

Featuring a relatively stable non-bonding electron lone pair, the development of phosphenium cations even predated the isolation of isoelectronic singlet carbenes. Again, as depicted in **Figure 1.4**, the di-substituted cationic phosphorus molecules were realised due to the stabilisation of the empty phosphorus p-orbital by adjacent π-donor heteroatoms as well as their inductive stabilisation of the lone pair.[14] This class of molecule has also been observed to perform small molecule activation, even mediating catalytic transformations.[14,15] Neutral group 15 molecules have also been identified as potential main group species for transition metal-like small molecule activation, and have been applied to catalysis due to their two readily accessible oxidation states (+III and +V) and a lone pair of electrons. The geometrically constrained phosphorus compound **1.12**, which enables the catalytic hydrogenation of organic molecules

authenticated this viewpoint (**Scheme 1.6a**), where the origin of such chemical behaviour can be rationalised from the backbone-enforced modulation of frontier orbital alignment (**Scheme 1.6b**).[16] As depicted in **Scheme 1.6b**, compound **1.12** indeed exhibits an electronic configuration broadly comparable to that of singlet carbenes, an observation which has since motivated a significant volume of group 15 metallomimetic chemistry.[17-20] A further consideration arising in this system involves the necessary manipulation of its steric environment at the central atom to constrain its geometry. This type of chemistry, therefore, will not be further investigated in this thesis.

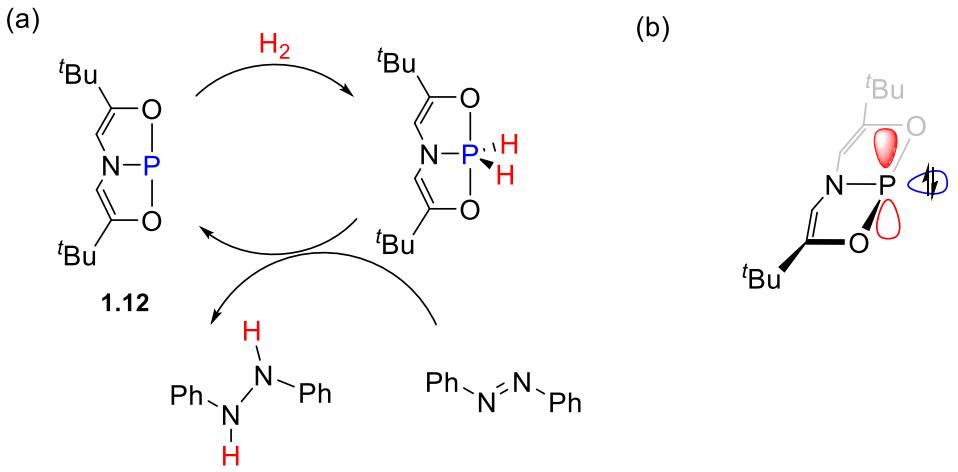

Scheme 1. 6 : (a) Catalytic H_2 transformation mediated by the geometrically constrained compound **1.12**. (b) Illustration of the P- centred frontier orbital configurations in compound **1.12**.[16]

1.2.3 Singlet Carbene Analogues in Group 13

1.2.3.1 Boron

Although the neutral boron counterpart of a singlet carbene, a mono-substituted borylene [:BR] (where R = mono-anionic substituent), has yet to be isolated due to the difficulty of supplying sufficient protection with only one substituent, its properties have been examined by trapping experiments and theoretical calculations.[21-24] Ground state borylenes were found to possess a singlet electronic configuration, where the HOMO of the molecule approximates to the lone pair of electrons of boron whilst two empty *p*-orbitals provide the LUMO and LUMO+1.[23,24]

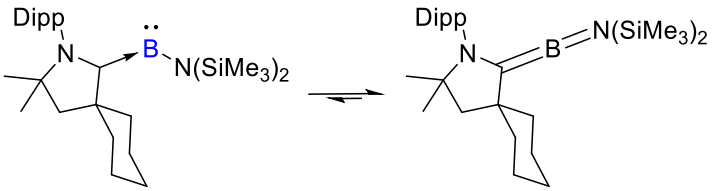

1.13

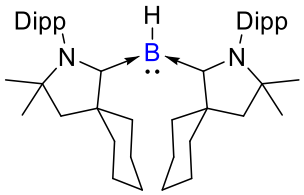

1.14

Figure 1. 5 : Selected examples of isolated borylenes.[23,25,26]

On the other hand, borylenes with differing numbers of coordinated Lewis bases have been extensively prepared and studied thanks to the increased electronic and kinetic stabilisation supplied by the donor ligand (**1.13**, **1.14**; **Figure 1.5**).[23,25,26] With inherently narrow energetic gaps in their frontier orbitals, small molecule activation has also been reported to be facilitated by borylenes (**1.15**, *in-situ* generated by photolysis; **1.16**, *in-situ* generated by reduction) regardless of the presence of coordinating ligands, including H_2 activation and even N_2 fixation, which had previously been confined to *d*- and *f*-block complexes (**Scheme 1.7**).[23,24,26,27]

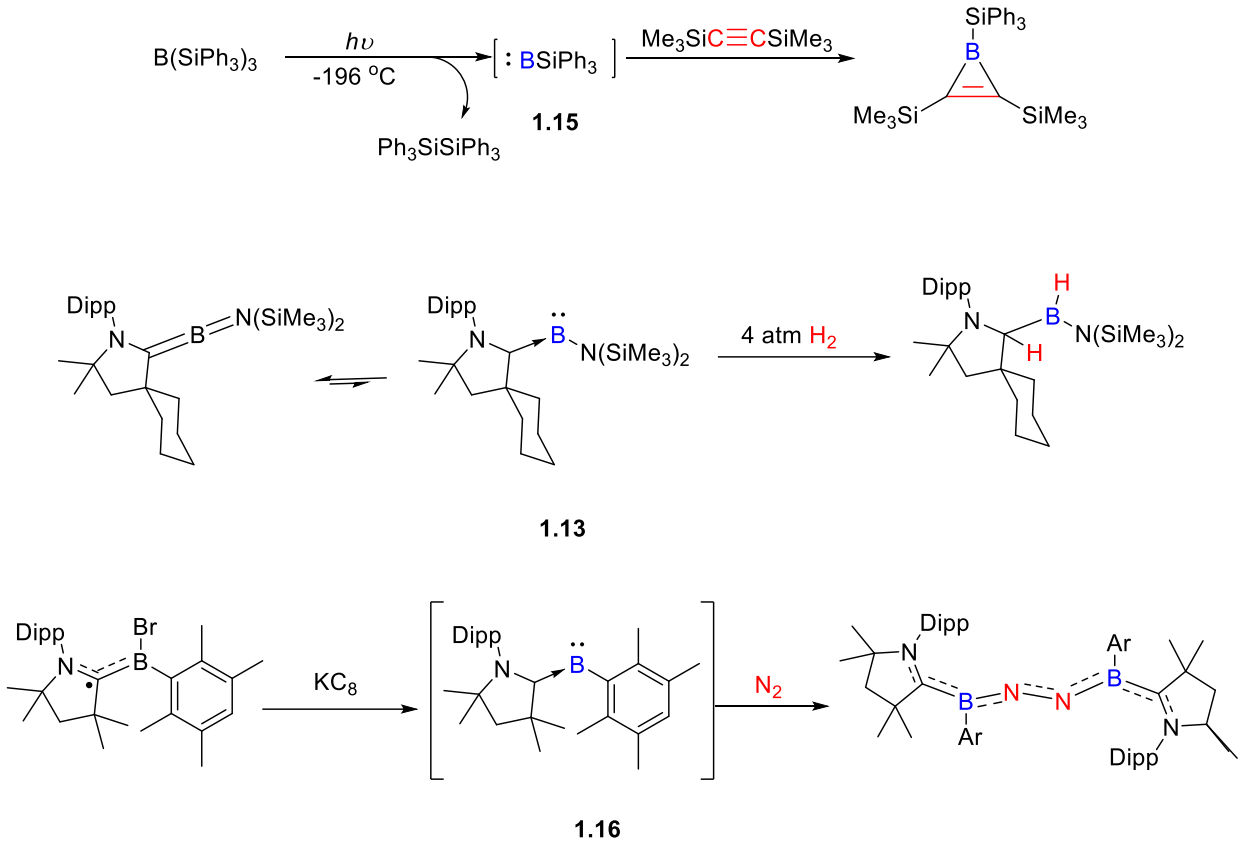

Scheme 1. 7 : Selected examples of the reactivity of borylenes **1.13**, **1.15**, and **1.16**.[23,24,26,27]

Featuring an electropositive boron and violating the octet rule, the isoelectronic boron analogues of a *N*-heterocyclic singlet carbene, the boryl anion, was prepared long after its theoretical prediction.[28,29] Such a molecule was realised by Yamashita and co-workers with the synthesis of the *N*-heterocyclic boryllithium (**1.17**), in which the stability of the singlet boron centre is attained by its interaction with an even more electropositive Li atom alongside the stabilisation provided by the diamido groups.[28] This first isolated *N*-heterocyclic boryllithium (**1.17**), featuring a lone pair of electrons and a relatively low-lying p_π-orbital of boron, again induces small molecule activation (such as H_2) under mild conditions alongside exhibiting reactivity characteristic of a boron-centred nucleophile (**Scheme 1.8**).[28,30,31] Since the initial preparation of **1.17**, various *s*-block metal-boryl derivatives (**1.18** – **1.21**) have also been reported, featuring various ligand environments and synthetic routes (**Figure 1.6**).[31-34]

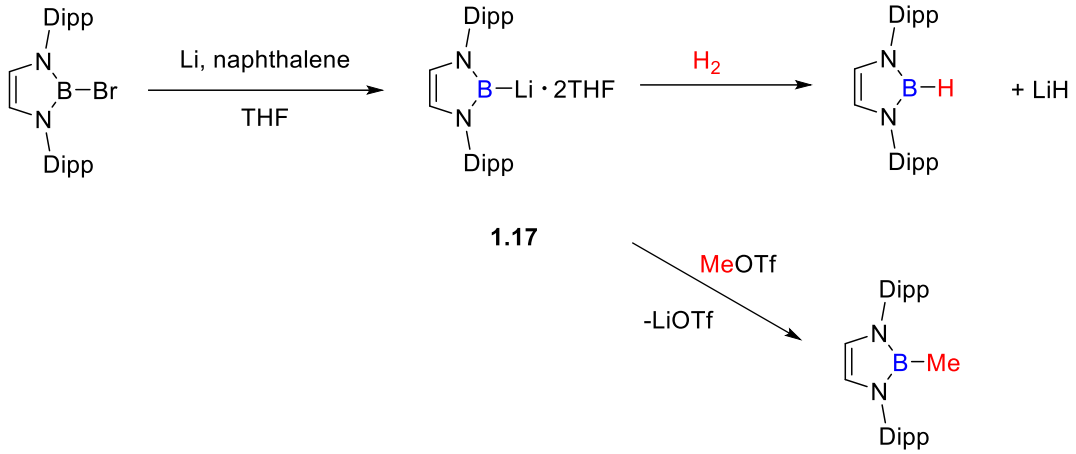

Scheme 1. 8: Synthesis and selected reactions of the first isolated boryllithium (**1.17**) [28,30,31]

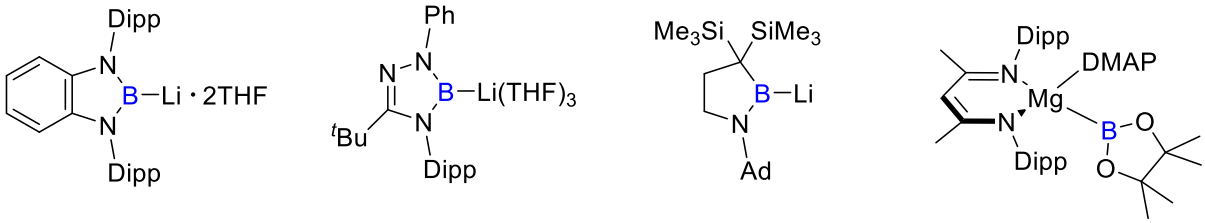

1.18 **1.19** **1.20** **1.21**

Figure 1. 6 : Selected examples of *s*-block metal-boryl derivatives (**1.18** – **1.21**).[31-34]

1.2.3.2 Aluminium

Although the spectroscopic observation of the meta-stable AlCl and later the structural characterisation of the tetrameric [Al{η^5-(C_5Me_5)}]$_4$ ([AlCp*]$_4$; **1.22**) provided initial examples in the field,[35,36] the first well-defined monomeric Al(I) singlet carbene analogue, [{^{Dipp}BDI}Al] (**1.23**) (where ^{Dipp}BDI = CH(CMeNDipp)$_2$, Dipp = 2,6-diisopropylphenyl), was only reported in 2000.[37] As previously illustrated in **Figure 1.4**, the β-diketiminate backbone thermodynamically stabilises the Al(I) oxidation state through its adjacent π-donating and σ-withdrawing nitrogen atoms, in conjunction with the provision of a significant level of steric protection to the aluminium centre. More recently, it has been demonstrated that enhancement of the steric bulk of the cyclopentadienyl group prohibits the oligomerisation previously observed in **1.22**, allowing the isolation of the monomeric cyclopentadienyl-Al(I) derivative (**1.24**).[38] Furthermore, the mono-substituted aluminylene (**1.25**) has been realised with an extremely bulky terphenyl group, further highlighting the importance of kinetic stabilisation in the synthesis of low oxidation state main group molecules (**Figure 1.7**).[39]

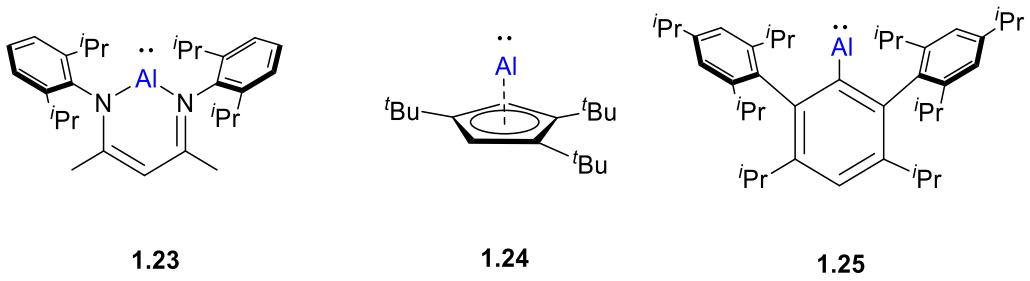

Figure 1. 7 : Selected examples of neutral Al(I) complexes.[37-39]

Similar to the reactivity that has been observed with main group singlet carbene analogues with small HOMO-LUMO gaps, compounds **1.23** and **1.24** readily undergo oxidative addition with small molecules. High nucleophilicity and a potent reducing ability have also been observed as the primary characteristics of such neutral Al(I) carbenoids, behaviour which can be attributed to the high in energy Al(I)-based lone pair of electrons and the inherently low electronegativity of aluminium, respectively (**Scheme 1.10**).[38,40,41]

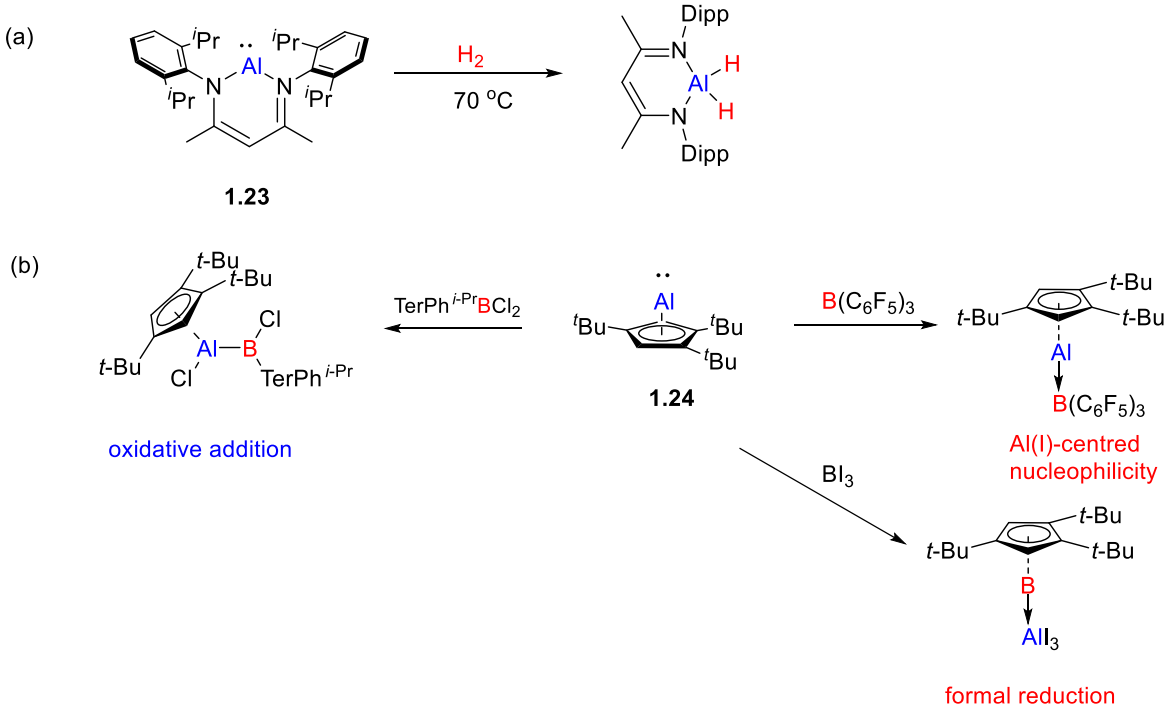

Scheme 1. 9 : (a) H_2 activation by **1.23**; (b) diverse reactivity of **1.24**.[38,40]

Bearing one of the most electropositive *p*-block elements, an isoelectronic anionic aluminium counterpart of a singlet carbene remained elusive until the recent realisation of **1.25** by Aldridge, Goicoechea and co-workers (**Scheme 1.11**).[42] The stability of the anionic Al(I) carbenoid centre in the potassium alumanyl, [{NON^{Dipp}}AlK]$_2$ (**1.25**), was provided by steric protection from the bulky substituents and thermodynamic stabilisation by the neighbouring

nitrogen atoms (as previously illustrated in **Figure 1.4**). In comparison to the neutral Al(I) species (**1.23**), compound **1.25** exhibits enhanced reactivity and readily undergo H_2 oxidative addition at room temperature. This may be rationalised by the HOMO of **1.25**, which approximates to the non-bonding orbital of the Al-based lone pair, and which is further destabilised by the negative charge at the aluminium centre. This observation is again in line with the general design principle for enabling main-group molecules with transition metal properties, where a narrower HOMO-LUMO energetic separation results in enhanced transition metal-like reactivity.

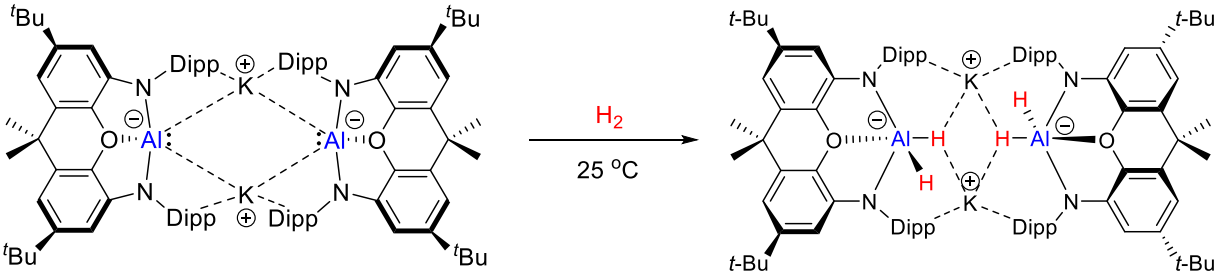

1.25

Scheme 1. 10 : [{NON^{Dipp}}AlK]$_2$ (**1.25**) and its H_2 activation.[42]

Shortly after the report of compound **1.25**, various broadly analogous *N*-heterocyclic aluminium(I) anions were synthesised in the forms of the *N,N'*-heterocycles (**1.26**, **1.27**), a cyclic(alkyl)(amino) carbene analogue (**1.28**), and a dialkyl-substituted aluminium(I) species (**1.29**) (**Figure 1.8**).[43-48] Although a variety of formally anionic aluminium(I)-centred molecules have, thus, been reported, correlated reactivity studies were underreported at the start of this project. This chemistry will be described in further detail in **Chapter 3**.

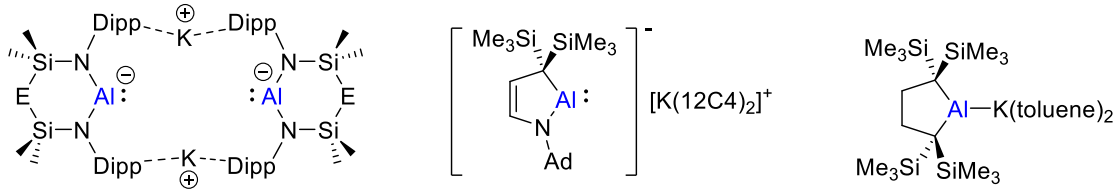

1.26, E = O
1.27, E= $(CH_2)_2$

1.28

Ad = 1-adamantyl
12C4 = 12-crown-4 ether

1.29

Figure 1. 8 : Selected examples of anionic aluminium(I) singlet carbene analogues **1.26**-**1.29.**[43-48]

1.2.3.3 Gallium

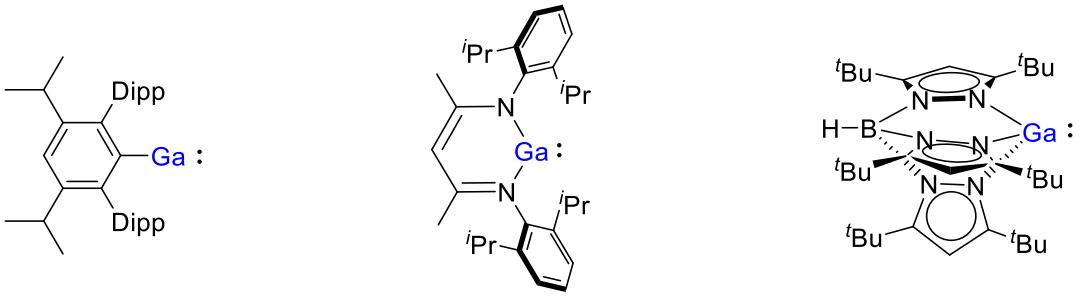

1.30 **1.31** **1.32**

Figure 1. 9 : Selected examples of reported neutral Ga(I) molecules.[49-51]

Persistent neutral gallium(I) molecules that are broadly analogous to singlet carbenes have been prepared with various coordination environments of the metal centre. Whilst mono-substituted carbene analogues have only been identified spectroscopically and dimerise in the solid state (with the exception of compound **1.30** which was reported later),[49,52] the tri-coordinated species (**1.32**) was structurally characterised over a quarter of century ago, albeit with the shortcoming of exclusively displaying Lewis basicity for the lack of an empty valence orbital (**Figure 1.9**).[50] Enhanced reactivity was again achieved by the use of a β-diketiminate backbone to afford the gallium(I) species, [{^{Dipp}BDI}Ga] (**1.31**).[51] In this case, the backbone provides a mono-anionic and bi-dentate support, granting protection for the gallium centre possessing an electron pair but a still energetically accessible empty *p*-orbital. The molecule (**1.31**) is, thus, capable of inducing E-H σ–bond oxidative addition *via* its transition metal-like frontier orbital configurations (**Scheme 1.12**).[53]

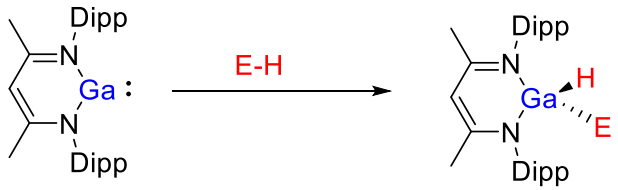

1.31 E = $SnPh_3$, OEt, NEt_2, PPh_2

Scheme 1. 11 : E-H bond activation by [{^{Dipp}BDI}Ga] (**1.31**). [53]

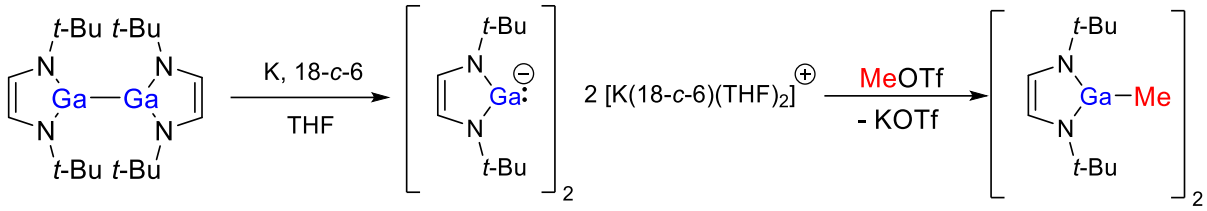

1.33

Scheme 1. 12 : Synthetic route of the first gallyl anion (**1.33**) and its reaction towards MeOTf.[54,55]

As a result of its marginally smaller atomic size and higher electronegativity, examples of molecules containing formally negatively charged gallium(I) were prepared and predated their lighter analogues. The first anionic group 13 element in +I oxidation state to be synthesised was the gallyl anion, $[(^{t}BuNCH)_2Ga]^-$ (**1.33**), in 1999 as part of an alkali metal salt,[54] where the counter potassium cation was sequestered by a crown ether (**Scheme 1.13**). The reactivity of compound **1.33** was later elaborated by Schmidbaur and co-workers, where the anionic gallium(I) centre was reacted with methyl triflate to yield the corresponding dimeric $[(t\text{-}BuNCH)_2GaMe]_2$ and potassium triflate (**Scheme 1.13**).[55] Although compound **1.33** did not exhibit reactivity reminiscent of *d*-block complexes, its nucleophilic substitution towards MeOTf unambiguously evidenced its Ga(I)-centred reactivity, indicating the low oxidation state nature of the gallium centre in compound **1.33**. The successful isolation of **1.33** encouraged further investigations into gallium(I) compounds. Although various anionic gallium(I) species have since been prepared and extensively utilised as coordinating ligands, few examples of gallium-centred small molecule activation have been described, which may be attributed to the inherently larger singlet-triplet gap present in gallium.[56-59]

1.2.3.4 Indium and Thallium

Like its lighter counterparts, the neutral monomeric indium(I) singlet carbene analogue, [{^{Dipp}BDI}In] (**1.34**), was synthesised with a β-diketiminate backbone, and compound **1.34** did indeed undergo oxidative addition, albeit only towards more readily reducible organic substrates (**Scheme 1.14a**).[60,61] On the other hand, the first example of the heaviest congeners in group 13 was realised as [{CH(CPhNSiMe$_3$)$_2$}Tl] (**1.35**, **Scheme 1.14b**).[62] This is plausibly due to the increased atom size of thallium and the requirement for a larger β-diketiminate ligand to provide sufficient protection to prevent the self-aggregation observed in the attempted synthesis of less sterically encumbered thallium β-diketiminate derivatives.[63]

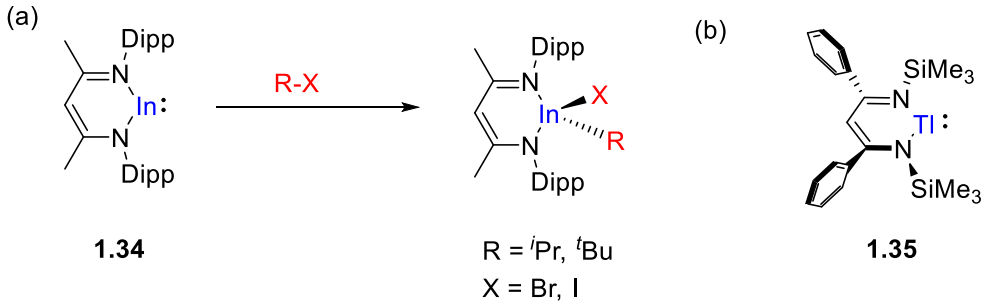

Scheme 1. 13 : [{^{Dipp}BDI}In] (**1.34**) and its reaction with alkyl halides (b) [{CH(CPhNSiMe$_3$)$_2$}Tl] (**1.35**). [60-62]

The sole example of an anionic analogue of a singlet carbene featuring an indium or a thallium as the central atom was reported by Coles and co-workers in 2018. With the implementation of the sterically encumbered bis(amidodimethyl)disiloxane ligand {OSiN^{Dipp}} (where the {OSiN^{Dipp}} = [O(SiMe$_2$NDipp)$_2$]$^{2-}$, Dipp = 2,6-diiospropylphenyl), the group have successfully isolated indyl derivatives, [{OSiN^{Dipp}}In]$^{-}$, as an indyl-lithium complex (**1.36**), an ion-separated pair (**1.37**), and a contact ionic dimeric indyl-potassium complex (**1.38**) (**Scheme 1.15**).[64,65] Both compounds **1.36** and **1.37** have been observed to exhibit nucleophilic behaviour, whilst indyl-imide formation was observed when **1.38** was reacted with an organic azide.

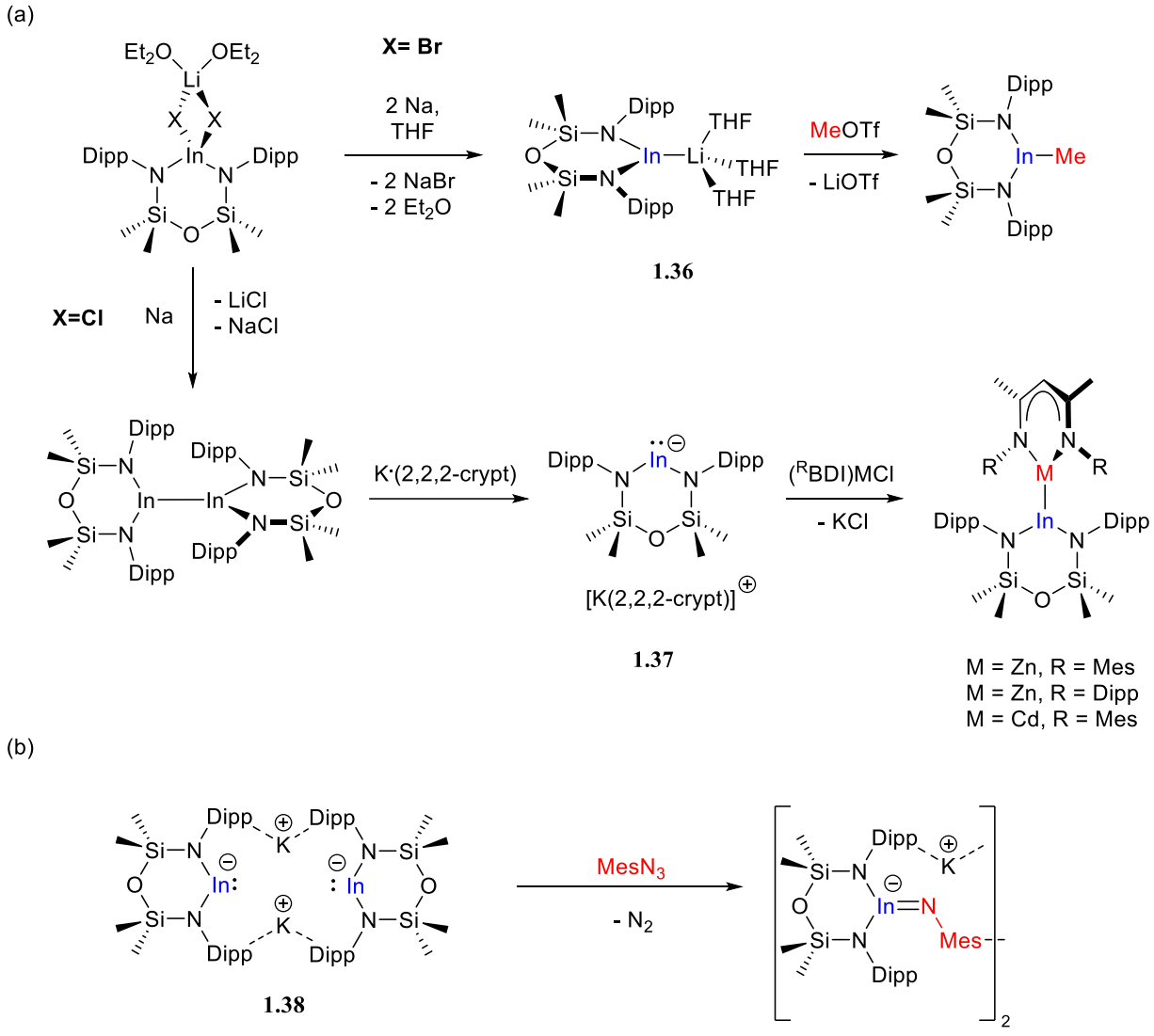

Scheme 1. 14 : Synthesis and reactivity of indyl derivatives [{OSiN^{Dipp}}In]$^{-}$ **1.36** – **1.38**.[64,65]

1.2.4 Singlet Carbene Analogues in the *s*-block

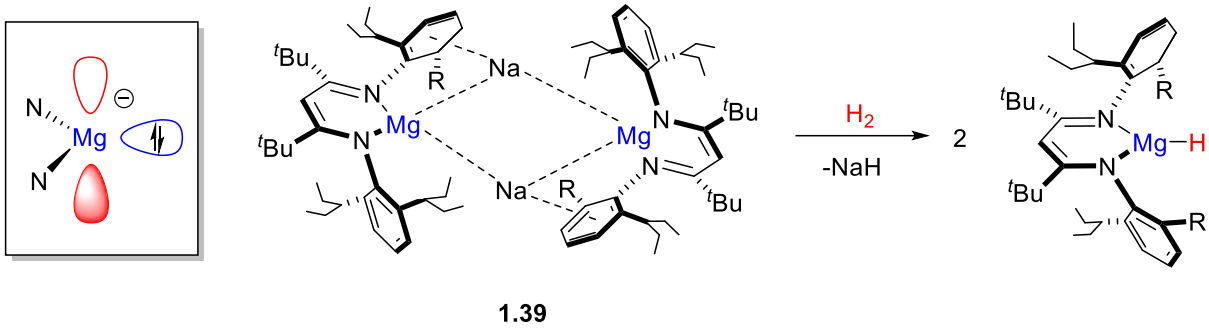

1.39

Scheme 1. 15 : Reaction of [{^{tBuDipep}BDI}MgNa]$_2$ (**1.39**) with H_2 and visualisation of the magnesium-based frontier orbitals of compound **1.39**.[66]

Harder and co-workers' recent report of the extremely sterically encumbered β-diketiminato Mg(0) species, [{^{tBuDipep}BDI}MgNa]$_2$ (**1.39**), represented the first singlet carbene analogue in the *s*-block. Its capability of activating H_2 under mild conditions has further authenticated the general design principle in enabling main-group molecules with transition metal-like reactivity (**Scheme 1.16**),[66] Jones and co-workers' β-diketiminate stabilised Mg(I) dimer derivatives also exhibit frontier orbital alignment suitable for transition metal-like reactivity,[67-69] where the [Mg-Mg] unit features the two-electron occupied orbital and a low-lying empty orbital (**Figure 1.10**). This class of magnesium(I) dimers have indeed demonstrated reactivity in a broad array of small molecule activation processes, such as the Lewis base coordinated derivatives of [{^{Dipp}BDI}Mg]$_2$ (**1.40**) mediated CO trimerisation,[70] and/or the C–C σ bond activation of cyclopropanes by **1.40** (**Scheme 1.17**).[71] The direct reaction of H_2 by **1.40** or related derivatives, however, is yet to be reported despite its thermodynamic viability,[72] indicating further research may be required in the field of Mg(I) chemistry. This class of chemistry will be described in more detail in **Chapter 2**.

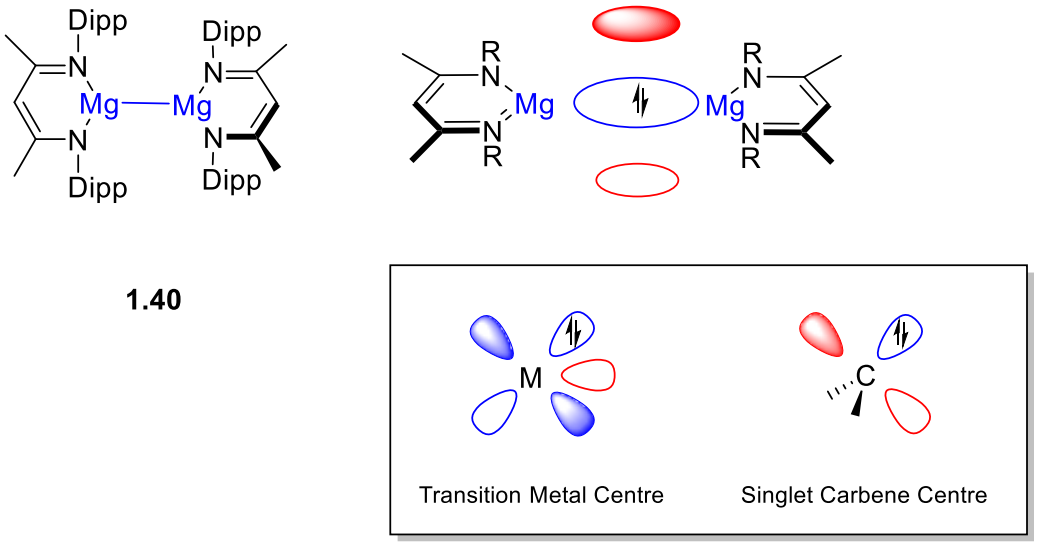

Figure 1. 10 : The frontier orbitals of the Mg-Mg bond in β-diketiminate stabilised Mg(I) dimer derivatives (and the example [{^{Dipp}BDI}Mg]$_2$ (**1.40**)).

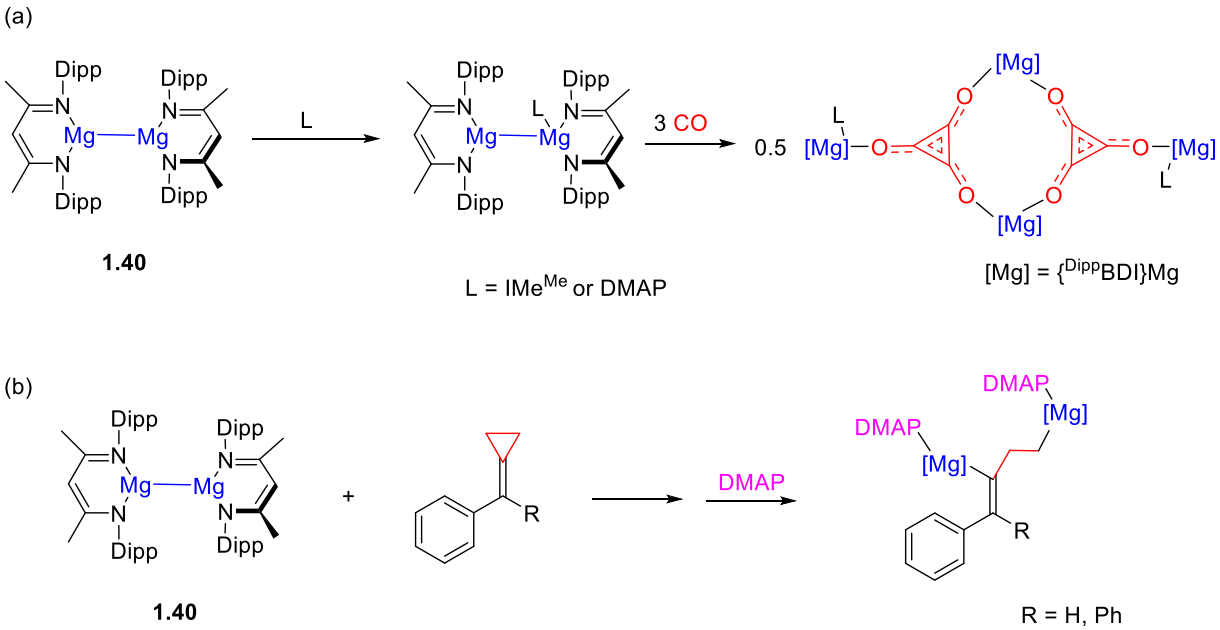

Scheme 1. 16 : (a) Base-coordinated [{^{Dipp}BDI}Mg]$_2$ derivatives mediated CO trimerisation (b) C–C σ bond activation by [{^{Dipp}BDI}Mg]$_2$ (**1.40**).[70, 71]

1.3 Research Objective

As highlighted by this brief literature review, the general principle of facilitating *d*-block element-like chemical behaviour is now extensively studied and well established in *p*-block chemistry. Analogous research in *s*-block-derived reactivity, however, remains relatively limited. Arising from the comprehensive studies of dimeric Mg(I) derivatives, it may be inferred that this class of molecule indeed exhibits a frontier orbital alignment suitable for transition metal-like reactivity. While examples of the low oxidation state $[\{^{Dipp}BDI\}Mg]_2$ (**1.40**) mediated small molecule activation have been reported, H_2 activation by magnesium(I) species remained unreported at the start of this project. A detailed literature review and further investigation in the field will, therefore, be conducted as part of this thesis.

Featuring one of the most electropositive elements in the *p*-block, chemistry arising from the isoelectronic aluminium analogue of a singlet carbene of aluminium, namely the alumanyl anion, was still in its preliminary stages at the start of this project. Although $[\{SiN^{Dipp}\}AlK]_2$ (**1.27**) had already reported in the Hill group, its reactivity remained relatively unexplored. This project will, thus, also conduct a more detailed review of alumanyl chemistry, and an exploration of the chemical behaviour and application of the potassium alumanyl (**1.27**) and its derivatives.

1.4 References

1. G. Parkin, *J Chem Educ*, 2006, **83**, 791.
2. P. P. Power, *Nature*, 2010, **463**, 171-177.
3. R. L. Melen, *Science*, 2019, **363**, 479-484.
4. G. H. Spikes, J. C. Fettinger and P. P. Power, *J Am Chem Soc*, 2005, **127**, 12232-12233.
5. Y. Peng, M. Brynda, B. D. Ellis, J. C. Fettinger, E. Rivard and P. P. Power, *Chem Commun*, 2008, 6042-6044
6. G. C. Welch, R. R. San Juan, J. D. Masuda and D. W. Stephan, *Science*, 2006, **314**, 1124-1126.
7. G. D. Frey, V. Lavallo, B. Donnadieu, W. W. Schoeller and G. Bertrand, *Science*, 2007, **316**, 439-441.
8. M. Melaimi, R. Jazzar, M. Soleilhavoup and G. Bertrand, *Angew Chem Int Ed Engl*, 2017, **56**, 10046-10068.
9. D. Martin, N. Lassauque, B. Donnadieu and G. Bertrand, *Angew Chem Int Ed Engl*, 2012, **51**, 6172-6175.
10. M. Kira, S. Ishida, T. Iwamoto, M. Ichinohe, C. Kabuto, L. Ignatovich and H. Sakurai, *Chem Lett*, 1999, 263-264.
11. Y. Mizuhata, T. Sasamori and N. Tokitoh, *Chem Rev*, 2009, **109**, 3479-3511.
12. Y. Mizuhata, T. Sasamori and N. Tokitoh, *Chem Rev*, 2009, **109**, 3479-3511.
13. A. V. Protchenko, J. I. Bates, L. M. Saleh, M. P. Blake, A. D. Schwarz, E. L. Kolychev, A. L. Thompson, C. Jones, P. Mountford and S. Aldridge, *J Am Chem Soc*, 2016, **138**, 4555-4564.
14. A. H. Cowley and R. A. Kemp, *Chem Rev*, 1985, **85**, 367-382.
15. B. Rao, C. C. Chong and R. Kinjo, *J Am Chem Soc*, 2018, **140**, 652-656.
16. N. L. Dunn, M. Ha and A. T. Radosevich, *J Am Chem Soc*, 2012, **134**, 11330-11333.
17. H. W. Moon and J. Cornella, *ACS Catalysis*, 2022, **12**, 1382-1393.
18. J. M. Lipshultz, G. Li and A. T. Radosevich, *J Am Chem Soc*, 2021, **143**, 1699-1721.
19. K. Chulsky, I. Malahov, D. Bawari and R. Dobrovetsky, *J Am Chem Soc*, 2023, **145**, 3786-3794.
20. T. Chu and G. I. Nikonov, *Chem Rev*, 2018, **118**, 3608-3680.
21. H. Braunschweig, T. Herbst, D. Rais, S. Ghosh, T. Kupfer, K. Radacki, A. G. Crawford, R. M. Ward, T. B. Marder, I. Fernandez and G. Frenking, *J Am Chem Soc*, 2009, **131**, 8989-8999.
22. M. Krasowska, M. Edelmann and H. F. Bettinger, *J Phys Chem A*, 2016, **120**, 6332-6341.
23. M. A. Legare, C. Pranckevicius and H. Braunschweig, *Chem Rev*, 2019, **119**, 8231-8261.
24. B. Pachaly and R. West, *Angew Chem Int Ed Engl*, 1984, **23**, 454-455.
25. R. Kinjo, B. Donnadieu, M. A. Celik, G. Frenking and G. Bertrand, *Science*, 2011, **333**, 610-613.
26. F. Dahcheh, D. Martin, D. W. Stephan and G. Bertrand, *Angew Chem Int Ed Engl*, 2014, **53**, 13159-13163.

27. M.-A. Légaré, G. Bélanger-Chabot, R. D. Dewhurst, E. Welz, I. Krummenacher, B. Engels and H. Braunschweig, *Science*, 2018, **359**, 896.
28. Y. Segawa, M. Yamashita and K. Nozaki, *Science*, 2006, **314**, 113.
29. M. Wagner, N. J. R. van Eikema Hommes, H. Noeth and P. v. R. Schleyer, *Inorg Chem*, 1995, **34**, 607-614.
30. M. Yamashita, Y. Suzuki, Y. Segawa and K. Nozaki, *J Am Chem Soc*, 2007, **129**, 9570-9571.
31. A.-F. Pécharman, A. L. Colebatch, M. S. Hill, C. L. McMullin, M. F. Mahon and C. Weetman, *Nat Commun*, 2017, **8**, 15022.
32. Y. Segawa, Y. Suzuki, M. Yamashita and K. Nozaki, *J Am Chem Soc*, 2008, **130**, 16069-16079.
33. W. Lu, H. Hu, Y. Li, R. Ganguly and R. Kinjo, *J Am Chem Soc*, 2016, **138**, 6650-6661.
34. H. Kisu, T. Kosai, T. Iwamoto and M. Yamashita, *Chem Lett*, 2021, **50**, 293-296.
35. W. Klemm, E. Voss and K. Geiersberger, *Zeitschrift für anorganische Chemie*, 1948, **256**, 15-24.
36. C. Dohmeier, C. Robl, M. Tacke and H. Schnöckel, *Angew Chem Int Ed Engl*, 1991, **30**, 564-565.
37. C. Cui, H. W. Roesky, H.-G. Schmidt, M. Noltemeyer, H. Hao and F. Cimpoesu, *Angew Chem Int Ed*, 2000, **39**, 4274-4276.
38. A. Hofmann, C. Pranckevicius, T. Tröster and H. Braunschweig, *Angew Chem Int Ed*, 2019, **58**, 3625-3629.
39. J. D. Queen, A. Lehmann, J. C. Fettinger, H. M. Tuononen and P. P. Power, *J Am Chem Soc*, 2020, **142**, 20554-20559.
40. T. Chu, I. Korobkov and G. I. Nikonov, *J Am Chem Soc*, 2014, **136**, 9195-9202.
41. M. Zhong, S. Sinhababu and H. W. Roesky, *Dalton Trans*, 2020, **49**, 1351-1364.
42. J. Hicks, P. Vasko, J. M. Goicoechea and S. Aldridge, *Nature*, 2018, **557**, 92-95.
43. K. Koshino and R. Kinjo, *J Am Chem Soc*, 2020, **142**, 9057-9062.
44. S. Kurumada, S. Takamori and M. Yamashita, *Nat Chem*, 2020, **12**, 36-39.
45. R. J. Schwamm, M. D. Anker, M. Lein and M. P. Coles, *Angew Chem Int Ed Engl*, 2019, **58**, 1489-1493.
46. R. J. Schwamm, M. P. Coles, M. S. Hill, M. F. Mahon, C. L. McMullin, N. A. Rajabi and A. S. S. Wilson, *Angew Chem Int Ed Engl*, 2020, **59**, 3928-3932.
47. G. Feng, K. L. Chan, Z. Lin and M. Yamashita, *J Am Chem Soc*, 2022, **144**, 22662-22668.
48. S. Grams, J. Eyselein, J. Langer, C. Färber and S. Harder, *Angew Chem Int Ed*, 2020, **59**, 15982-15986.
49. Z. Zhu, R. C. Fischer, B. D. Ellis, E. Rivard, W. A. Merrill, M. M. Olmstead, P. P. Power, J. D. Guo, S. Nagase and L. Pu, *Chem Eur J*, 2009, **15**, 5263-5272.
50. M. C. Kuchta, J. B. Bonanno and G. Parkin, *J Am Chem Soc*, 1996, **118**, 10914-10915.
51. N. J. Hardman, B. E. Eichler and P. P. Power, *Chem Commun*, 2000, 1991-1992.
52. N. J. Hardman, R. J. Wright, A. D. Phillips and P. P. Power, *Angew Chem Int Ed*, 2002, **41**, 2842-2844.
53. A. Seifert, D. Scheid, G. Linti and T. Zessin, *Chem Eur J*, 2009, **15**, 12114-12120.
54. E. S. Schmidt, A. Jockisch and H. Schmidbaur, *J Am Chem Soc*, 1999, **121**, 9758-9759.

55. E. S. Schmidt, A. Schier and H. Schmidbaur, *J Chem Soc, Dalton Trans*, 2001, 505-507.
56. R. J. Baker, R. D. Farley, C. Jones, M. Kloth and D. M. Murphy, *J Chem Soc, Dalton Trans*, 2002, 3844-3850.
57. R. J. Baker and C. Jones, *Coord Chem Rev*, 2005, **249**, 1857-1869.
58. M. Asay, C. Jones and M. Driess, *Chem Rev*, 2011, **111**, 354-396.
59. I. L. Fedushkin, A. N. Lukoyanov, G. K. Fukin, S. Y. Ketkov, M. Hummert and H. Schumann, *Chem Eur J*, 2008, **14**, 8465-8468.
60. M. S. Hill and P. B. Hitchcock, *Chem Commun*, 2004, 1818-1819.
61. M. S. Hill, P. B. Hitchcock and R. Pongtavornpinyo, *Inorg Chem*, 2007, **46**, 3783-3788.
62. Y. Cheng, P. B. Hitchcock, M. F. Lappert and M. Zhou, *Chem Commun*, 2005, 752-754.
63. M. S. Hill, R. Pongtavornpinyo and P. B. Hitchcock, *Chem Commun*, 2006, 3720-3722.
64. R. J. Schwamm, M. D. Anker, M. Lein, M. P. Coles and C. M. Fitchett, *Angew Chem Int Ed*, 2018, **57**, 5885-5887.
65. M. D. Anker, M. Lein and M. P. Coles, *Chem Sci*, 2019, **10**, 1212-1218.
66. B. Rösch, T. X. Gentner, J. Eyselein, J. Langer, H. Elsen and S. Harder, *Nature*, 2021, **592**, 717-721.
67. S. P. Green, C. Jones and A. Stasch, *Science*, 2007, **318**, 1754-1757.
68. S. P. Green, C. Jones and A. Stasch, *Angew Chem Int Ed*, 2008, **47**, 9079-9083.
69. S. J. Bonyhady, C. Jones, S. Nembenna, A. Stasch, A. J. Edwards and G. J. McIntyre, *Chem Eur Jl*, 2010, **16**, 938-955.
70. K. Yuvaraj, I. Douair, A. Paparo, L. Maron and C. Jones, *J Am Chem Soc*, 2019, **141**, 8764-8768.
71. R. Y. Kong and M. R. Crimmin, *J Am Chem Soc*, 2020, **142**, 11967-11971.
72. A. Datta, *J Phy Chem C*, 2008, **112**, 18727-18729.

2. Synthesis and Reactivity Studies of a Mg(I) Diamide

Amongst the most abundant elements in the Earth's crust, the alkaline earth metals have been widely studied and are commonly used in a variety of industries.[1] Their intrinsic low electron affinities have hampered studies concerning reduced species in oxidation states <+2 and related potential applications. Recent years have, however, seen a number of reports of low oxidation state group 2 chemistry, with especially significant advances in the isolation of reduced magnesium complexes.[2-4] This can be attributed to the properties of group 2 elements; beryllium(2+) being the most difficult element to be reduced, where the strength of Be–element bonds ensure that any reduced Be molecule readily reacts with other substrates. In contrast, it is an increasing challenge to attain sufficient kinetic protection for low oxidation state calcium species and those of larger elements (**Figure 2.1**).[3-5] This chapter will, therefore, focus on the reduction of a magnesium(II) diamide, as an initial investigation of molecules in which the group 2 atom displays a formal low oxidation state.

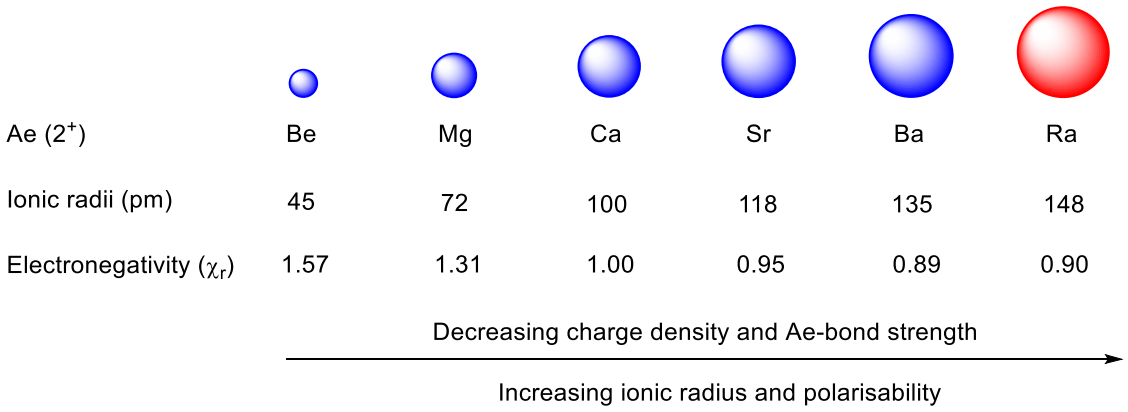

Figure 2. 1 : Overview of properties of group 2 ions.[3,5]

"I prefer bonding with myself." –Olenna Tyrell, *Game of Thrones*, 2011.

2.1 Developments in the Chemistry of Isolable Reduced Magnesium Species

Although the feasibility of low oxidation state magnesium species has been predicted by theoretical calculation since the 1980s,[6-8] initial reports of this class of metastable magnesium complexes were limited to spectroscopic observations under low temperature matrix conditions.[9,10]

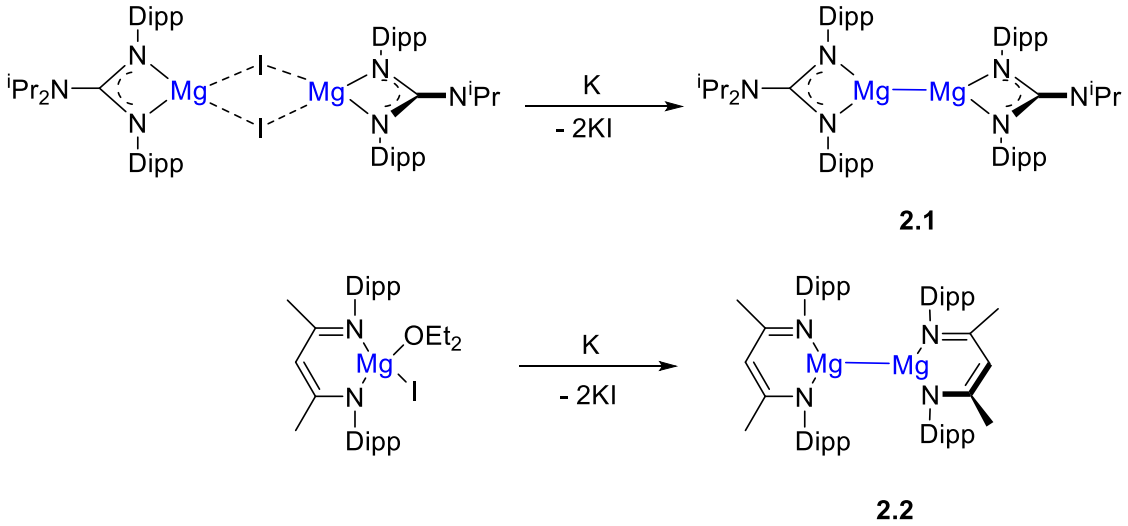

Scheme 2. 1 : First reported isolable dimeric Mg(I) molecules.[11]

As is the case for many low oxidation state main group derivatives, the isolation of reduced Mg compounds required appropriate ligand environment to provide sufficient kinetic stabilisation.[7,8] In 2007, the first isolation of well-defined Mg(I) molecules were reported by Jones and co-workers. Their initial publication described the potassium reduction of guanidinate- and β-diketiminate-supported magnesium(II) halide derivatives to provide the respective stable magnesium(I) dimers, **2.1** and **2.2** (**Scheme 2.1,** where **2.2** was previously described as **1.40** in **Section 1.2**).[11] It is considered that the stability of the low oxidation state magnesium complexes originates from the steric protection of the neighbouring bulky substituents, delocalisation of electron density within the six-membered backbone, as well as formation of the Mg-Mg bond (Mg-Mg distance = 2.8505(12) Å for **2.1** and 2.8457(8) Å for **2.2**) quenching the inherent open-shell electron configuration of the magnesium centre in +I oxidation state.[2,11]

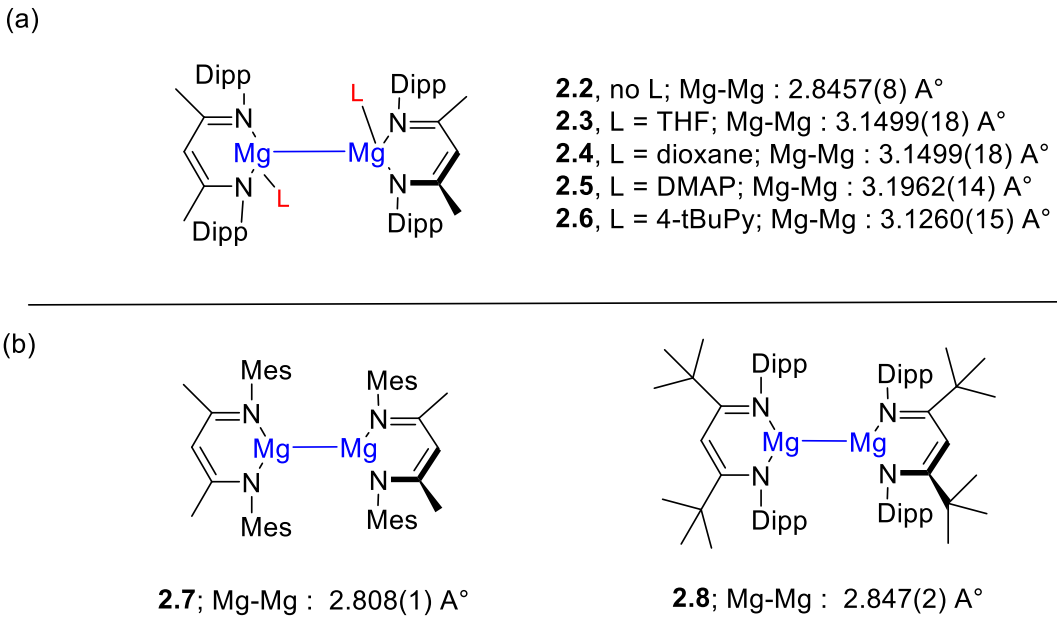

Figure 2. 2: Selected examples of structurally characterised magnesium(I) dimers and correlated Mg-Mg distances.[11-13]

A considerable number of variants of the dimeric β-diketiminato Mg(I) compound (**2.2**) have been prepared and studied since this original realisation. The introduction of a stoichiometric amount of a neutral Lewis base to the dimer provided a collection of stable adducts, all of which exhibit an elongated Mg-Mg distance (3.1260(15)Å －3.1962(14)Å) compared to the base-free molecule **2.2** with a positive correlation between the increase of the metal-metal bond length and the donating strength of the coordinated base (**Figure 2.2a**).[12] Further magnesium dimers have also been prepared through modification of the supporting ligand. A significantly shortened Mg-Mg bond (2.808(1) Å) is observed in the smaller mesityl-substituted β-diketiminate-supported magnesium(I) (**2.7**), whilst a marginally enhanced steric demand has been demonstrated to elongate the Mg-Mg separation (2.847(2) Å) in [{$^{t\text{BuDipp}}$BDI}Mg]$_2$ (**2.8**), highlighting the high malleability of the Mg-Mg bond towards its steric environment (**Figure 2.2b**).[13] Remarkably, the [{$^{\text{Mes}}$BDI}Mg]$_2$ derivative (**2.7**) was found to be capable of reducing diiminophosphinate Mg(II) halides and giving the corresponding reduced heterocyclic magnesium(I) dimer **2.9**, further indicating the significant impact of the supporting ligand and the nature of each molecule in this class of complexes (**Scheme 2.2**).[14]

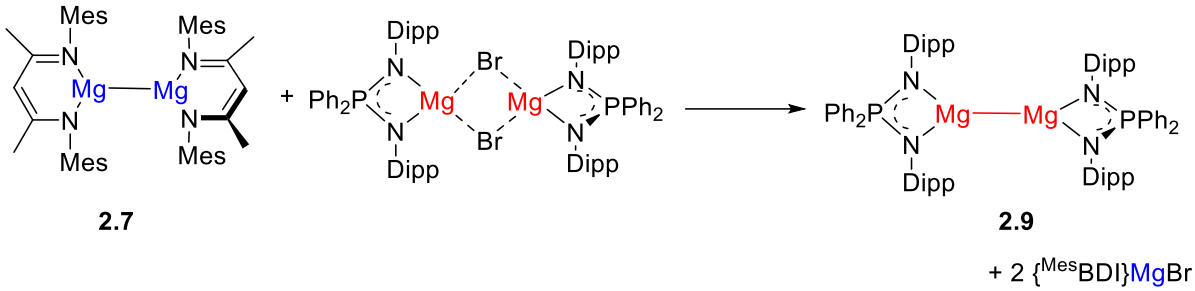

Scheme 2. 2 : Synthesis of **2.9** via a Mg(I)/Mg(II) redox reaction.[14]

Although a notable amount of unprecedented reactivity has been observed with such magnesium(I) dimers, the general class of compound has been found to be relatively inert towards substrates with stronger chemical bonds such as CO or H_2. Moreover, in an unexpected reflection of longer Mg-Mg interactions in compounds **2.3** — **2.6**, no evidence of escalated reactivity was found in these molecules. This can be explained by the more sterically encumbered environment around the reduced element centre, hampering any potential interaction between the reactive sites of the dimer and the introduced substrates.

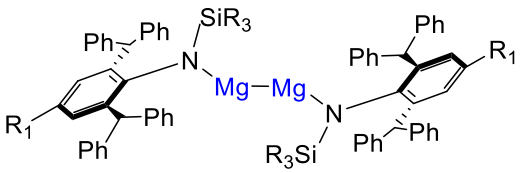

2.10, R_1 = ^{i}Pr, R_2 = Me; Mg-Mg = 2.8223(11)A°
2.11, R_1 = Me, R_2 = ^{i}Pr; Mg-Mg = 2.8501(13)A°

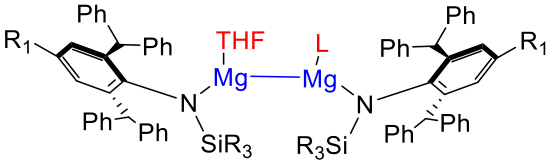

2.12, R_1 = ^{i}Pr, R_2 = Me, L = THF; Mg-Mg = 2.930(2)A°
2.13, R_1 = Me, R_2 = ^{i}Pr, no L; Mg-Mg = 2.9049(17)A°

Figure 2. 3 : Di-substituted Mg(I) dimers and their THF adducts.[15]

Manipulation of the coordination environment was, therefore, conducted in order to further expose the bimetallic centre of the complexes. Implementation of a super bulky amido ligand facilitated the synthesis and structural characterisation of Mg(I) molecules comprising two-coordinated metal centres as well as the related adducts with one or two coordinated molecules of THF (**2.10**—**2.13**, **Figure 2.3**). In these cases, Mg-Mg separations (2.8223(11) Å —2.930(2)Å) fall within the range of previously reported compounds.[2,15] Tripodal diimine-enolate ligands have also been utilised in synthesis of the magnesium(I) dimer **2.14**, which possesses a very constrained environment from the backbone. As illustrated in **Figure 2.4**, the symmetry enforced by the tripodal backbone hampers the mesomeric effect by disrupting the

orbital interaction, plausibly one of the reasons why compound **2.14** readily activates CO_2 and SO_2 despite bearing very sterically hindered magnesium centres.[16]

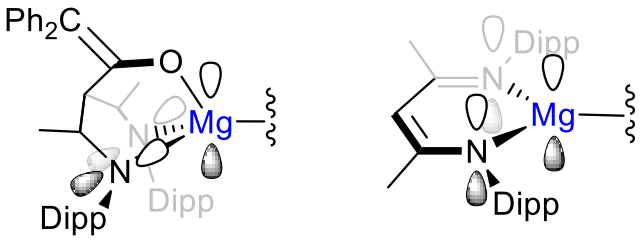

2.14 **2.2**

Figure 2. 4 : Illustration of frontier orbital interaction in compound **2.2** and **2.14**. Multiple bonds in the tripodal backbone of **2.14** are omitted for clarity.

Particularly comprehensive research has also been conducted with regards to the reactivity and application of [{^{Dipp}BDI}Mg]$_2$ (**2.2**) and its derivatives. These molecules are notable for their potent reducing ability, and compound **2.2** has in particular enabled the preparation of numerous reduced species and provided access to a wide variety of low oxidation state *p*-block molecules.[17] Dimeric magnesium(I) β-diketiminates have also been found to be capable of reductively activating CO_2, giving CO as a by-product, reactivity which had previously been exclusively demonstrated with low oxidation state *f*-block complexes (**Scheme 2.3a**).[18] Moreover, activation of CO has been shown to be viable with derivatives of compound **2.2**, either through the hydrogenative coupling of CO facilitated by a hydrogenated Mg(I) dimer (**2.15**), itself prepared by prior treatment of **2.2** with cyclohexa-1,3-diene (**Scheme 2.3b**);[19] or the reductive trimerisation of carbon-monoxide mediated by the "activated" magnesium(I) dimer **2.16** and **2.17** (**Scheme 2.3c**).[20] In the latter case, enhanced reactivity was attained by coordination of a neutral Lewis base to only one of the metal centres in the molecule, striking a balance between activation of the Mg-Mg interaction without introducing too much steric hindrance to the bimetallic moiety. Numerous further applications of the reduced magnesium(I) complexes have also been explored, including the homogeneous preparation of Grignard reagents, and catalysis resulting in the hydroboration of organic molecules.[21,22]

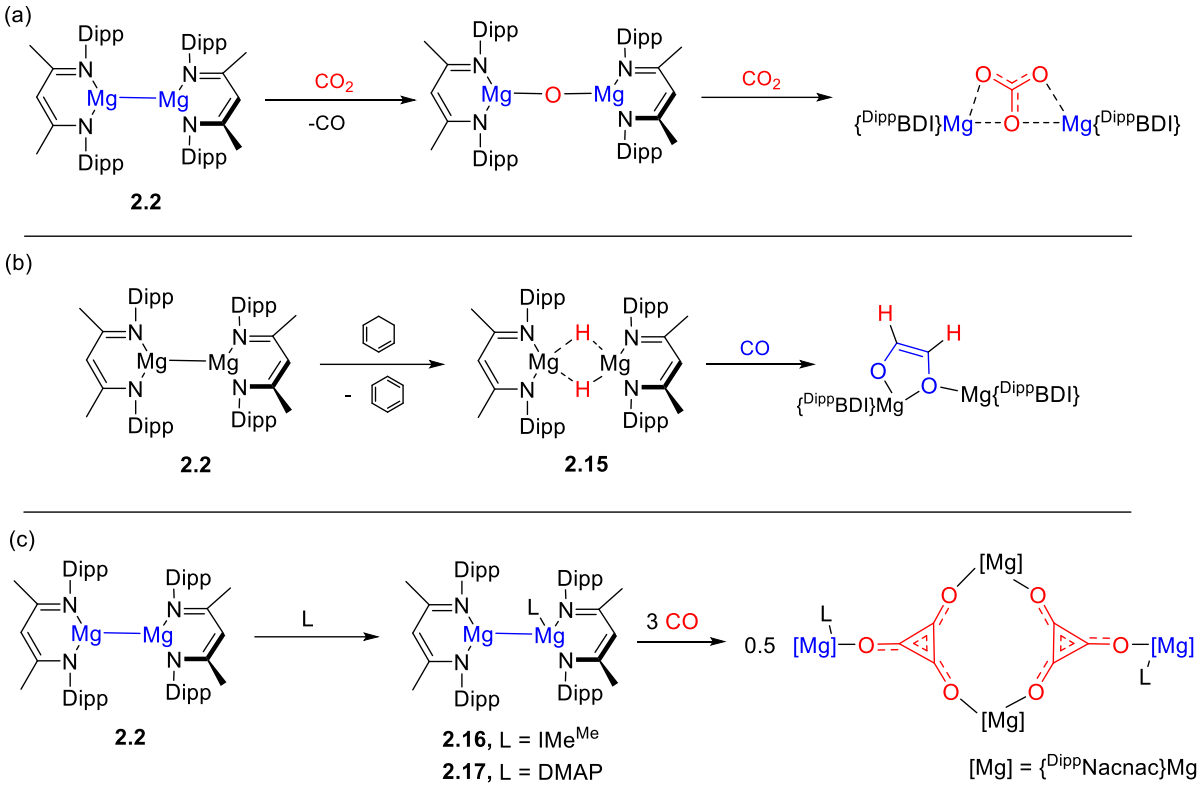

Scheme 2. 3 : Selected Examples of small molecule activation by [{^{Dipp}BDI}Mg]$_2$ (**2.2**) and its derivatives.[18-20]

A deduction arising from these reports regarding the chemistry of magnesium(I) β-diketiminate derivatives is that a weakening of the diatomic interaction between the two magnesium centres delivers higher reactivity. This observation can be rationalised from consideration of the electronic structure of atomic magnesium(I), namely an elongation of the Mg-Mg bond induces more Mg(I) radical type reactivity. This speculation is supported by several observations where the elongated Mg-Mg moiety exhibits increased lability in spite of only moderately increased steric hindrance,[2,20,22] and has inspired several of the latest studies in the field of low oxidation state magnesium chemistry. Harder and co-workers have recently described a series of even bulkier β-diketiminate-supported Mg(II) halides and their respective properties upon reduction. [{^{Dipep}BDI}Mg]$_2$ (**2.18**), which displays an exceptionally elongated Mg-Mg distance (3.051(1) Å) for a base-free dimeric magnesium(I) derivative, which was viewed as the reactive species and shown to readily reduce benzene when its preparation was conducted in the presence of sodium metal and TMEDA (Scheme **2.4**a).[23] In addition, an unusual Mg-Mg compound (**2.19**) was identified when the even more crowded ^{tBuDipep}BDI ligand was used. With the same ligand, a unique magnesium(0) complex (**2.20,** previously described as **1.39** in **Section 1.2**) has also been synthesised when sodium was applied as the reductant (**Scheme 2.4b**).[24,25] The further reduced Mg(0) species **2.20** exhibits significantly

enhanced reactivity in comparison to its Mg(I) counterparts. Of particular note, dihydrogen activation was achieved by the magnesium(0) dimer **2.20** under mild conditions, and the remarkable trinuclear [{^{tBuDipep}BDI}Mg-Mg-Mg{^{tBuDipep}BDI}] was isolated after heating **2.20** at moderately elevated temperature (56 ˚C), highlighting the contrasting thermal stability of **2.20** in comparison to that of reported Mg(I) species (**Scheme 2.5**).[24,25]

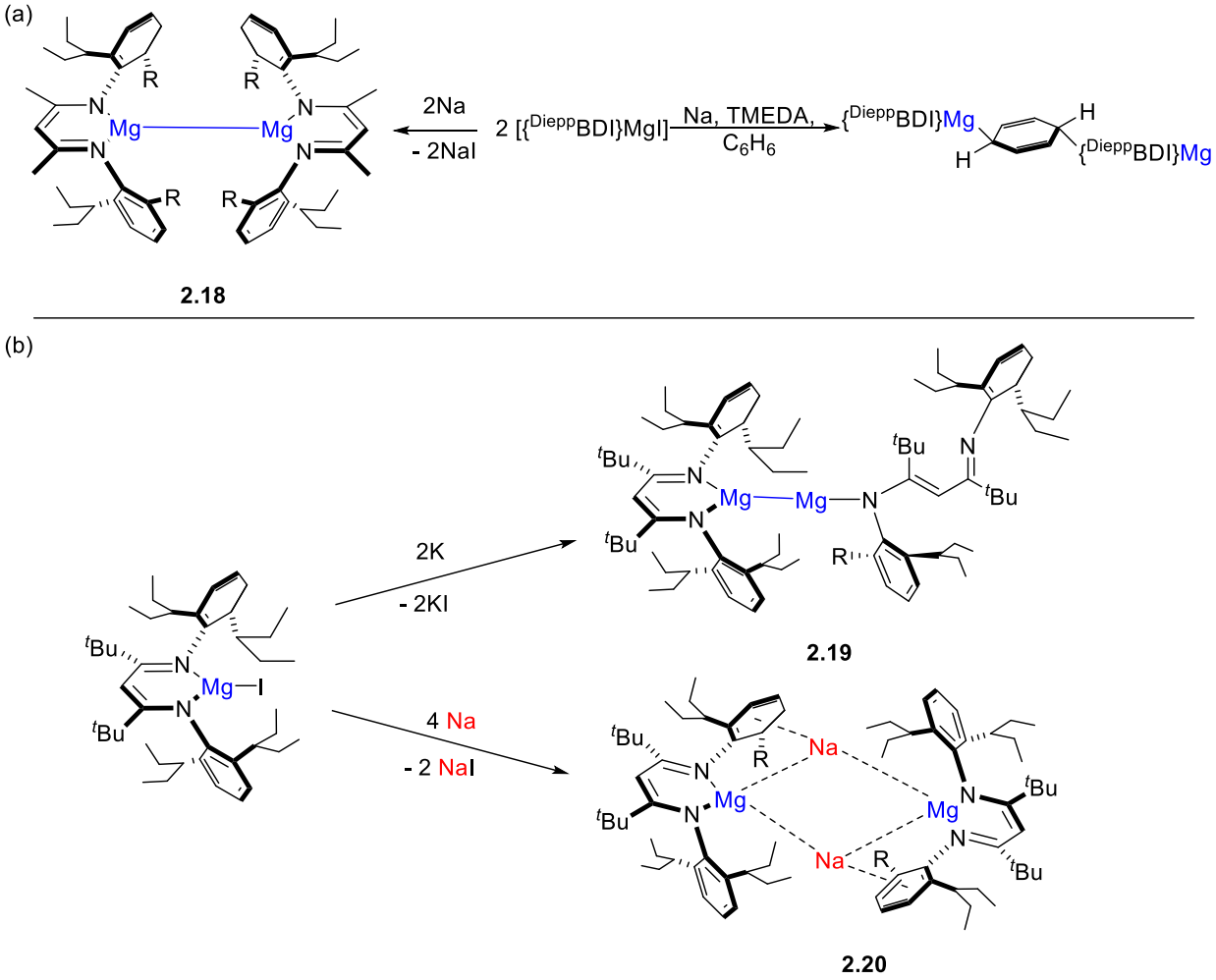

Scheme 2. 4 : Selected examples of low oxidation magnesium complexes with a super bulky ligand backbone.[23-25]

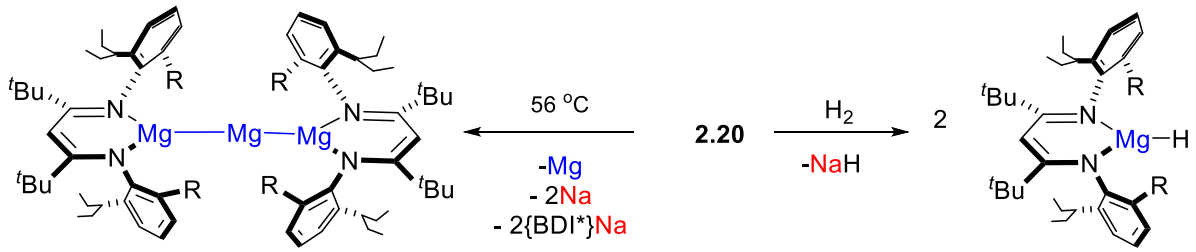

Scheme 2. 5 : Selected examples of reported reactivity of compound **2.20**. [24,25]

In a sharp contrast to the mono-anionic backbones exemplified by the β-diketiminate ligand, there have been very limited reports of low oxidation state magnesium chemistry employing di-anionic backbones. Prior to this project, the field has only seen Yang and co-workers' reports of dimeric diamine- supported Mg(I) derivatives, **2.21 – 2.23** (**Figure 2.5**).[26,27] In all these cases, a substantial association between the potassium cation and the planar delocalised ligand backbone was observed in all the formally negatively charged magnesium(I) dimers, suggestive of a ligand-based reduction. The distances between the magnesium atoms (2.8261(16)—2.957(1) Å) found in these formally anionic Mg(I) dimers are comparable to those of their neutral counterparts. Only limited reactivity towards reducible substrates has been reported for these compounds, suggesting that further scrutiny of these charged magnesium dimers might be justified. In addition, preparation of a low oxidation state magnesium species with a non-reducible di-anionic backbone appears not to have been further investigated.

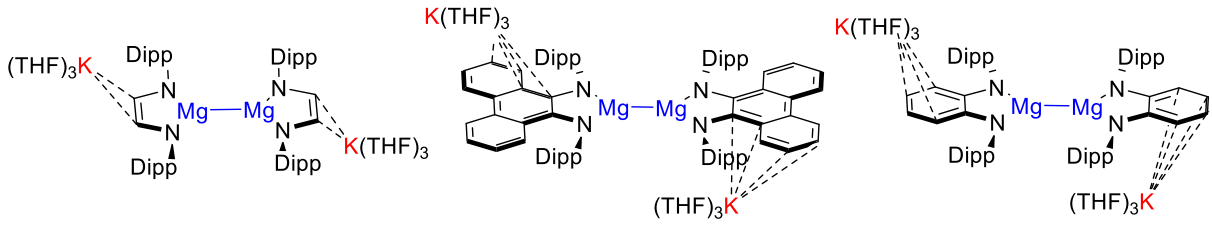

2.21 **2.22** **2.23**

Figure 2. 5 : Reported examples of ion paired magnesium(I) dimers. [26,27]

2.2 Preparation and Characterisation of a Sodium-Magnesium Diamide

In light of the above detailed description of the advances in low oxidation state magnesium chemistry, the utilisation of a redox non-active di-anionic ligand to support a Mg(II) molecule and its related reduced species was identified as a viable entry point for the project. With a previously reported six-membered chelating diamido ligand $\{SiN^{Dipp}\}^{2-}$ (where $\{SiN^{Dipp}\} = \{CH_2SiMe_2N(Dipp)\}_2$) by the Hill group,[28] a preliminary examination of the reduction of the magnesium diamide [$\{SiN^{Dipp}\}$Mg] (**2.24**) was performed *in silico* by Dr Claire M^{c}Mullin. These computed results implied that either sodium or potassium reduction of **2.24** is a significantly exergonic process (**Scheme 2.6**). Compound **2.24** was, thus, prepared for the experimental investigation.

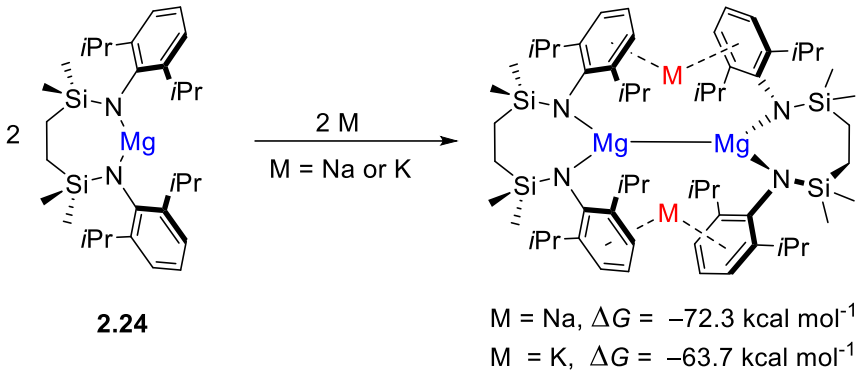

2.24

Scheme 2. 6 : DFT-computed (BP86-D3BJ/BS2(benzene)//BP86/BS1) free energy changes for the sodium and potassium reduction of compound **2.24**.

Synthesis of **2.24** was performed by the reaction of the diamine pro-ligand, $\{SiN^{Dipp}\}H_2$, and di-*n*-butyl magnesium in hexane at room temperature. Overnight stirring of the reaction mixture under a weak flow of argon provided a colourless solution, which, upon removal of all volatiles, afforded the targeted magnesium diamide [$\{SiN^{Dipp}\}$Mg] (**2.24**) in a multi-gram scale. Whilst the analytically pure [$\{SiN^{Dipp}\}$Mg] can be isolated from the described process, it rapidly forms the corresponding adducts upon introduction of aromatic solvents (within 1 hour). The full characterisation of the magnesium diamide was, therefore, conducted on colourless crystals obtained from respective arene solutions as its Mg-η^1-benzene (**2.24**·benzene) and Mg- η^1-toluene (**2.24**·toluene) adducts by X-ray diffraction analysis (**Figure 2.6**). Although the molecules displayed no features of particular note, the seven-membered cyclic configuration and the Mg-η^1-arene interaction of **2.24** were validated by their structural characterisation (**Figure 2.6**).

" It's turning yellow!" – R. J. Schwamm, June 2021.

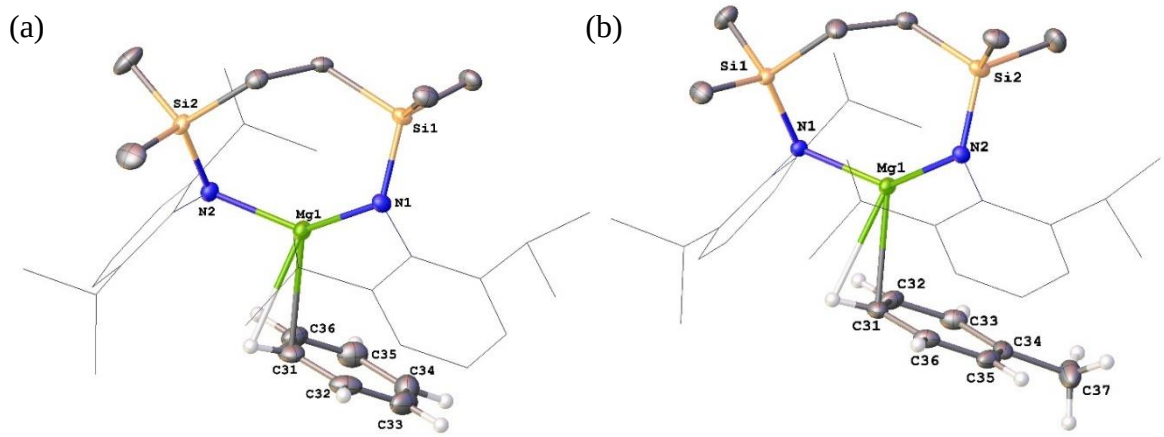

Figure 2. 6 : Displacement ellipsoid plots of (a) compound **2.24**·benzene and (b) compound **2.24**·toluene (30% probability ellipsoids). Dipp substituents are shown as wireframe and hydrogen atoms, except those of the coordinated arenes, are omitted for clarity. Selected bond lengths (Å) and angles (°); **2.24**·benzene: Mg1-N1 1.947(2), Mg1-N2 1.948(2), Mg1-C31 2.501(3), N1-Mg1-N2 132.52(10), N1-Mg1-C31 120.17(11), N2-Mg1-C31 104.32(11); **2.24**·toluene: Mg1-N1 1.962(2), Mg1-N2 1.960(3), Mg1-C312.469(3), N2-Mg1-N1 133.92(11), N1-Mg1-C31 104.49(12), N2-Mg1-C31 118.82(12).

Prompted by the higher thermodynamic viability indicated by theoretical calculations, sodium reduction was then conducted on **2.24**. Overnight stirring of excess 5 wt% Na/NaCl in a solution of **2.24** in benzene yielded a bright yellow solution with a grey suspension. Removal of precipitates and all volatiles provided a yellow waxy solid, which could then be crystallised by keeping a concentrated solution of the product in toluene at −30 ˚C. ^{1}H NMR spectroscopic characterisation of the purified product, **2.25**, demonstrated a noticeable asymmetry across the {SiN^{Dipp}} backbone. This was particularly apparent for the $SiMe_2$ signals, where two singlets (each integrating to 6H) appeared at δ 0.52 and −0.21 ppm (**Figure 2.6**), and which may be attributed to the loss of the mirror plane through the seven-membered magnesocycle, [{SiN^{Dipp}}Mg]. In addition, an EXSY NMR experiment conducted on **2.25** did not display any level of coherence transfer between the silyl-methyl resonances, indicating no conformational exchange of these resonances arising from the ligand environment. Subsequent single crystal X-tray diffraction analysis confirmed the inference made from the ^{1}H NMR spectrum, and verified **2.25** as a tetranuclear hetrobimetallic complex, [{SiN^{Dipp}}MgNa]$_2$, where two {SiN^{Dipp}}Mg units are bridged by twofold Na-η^6-Dipp interactions (**Figure 2.8**) .

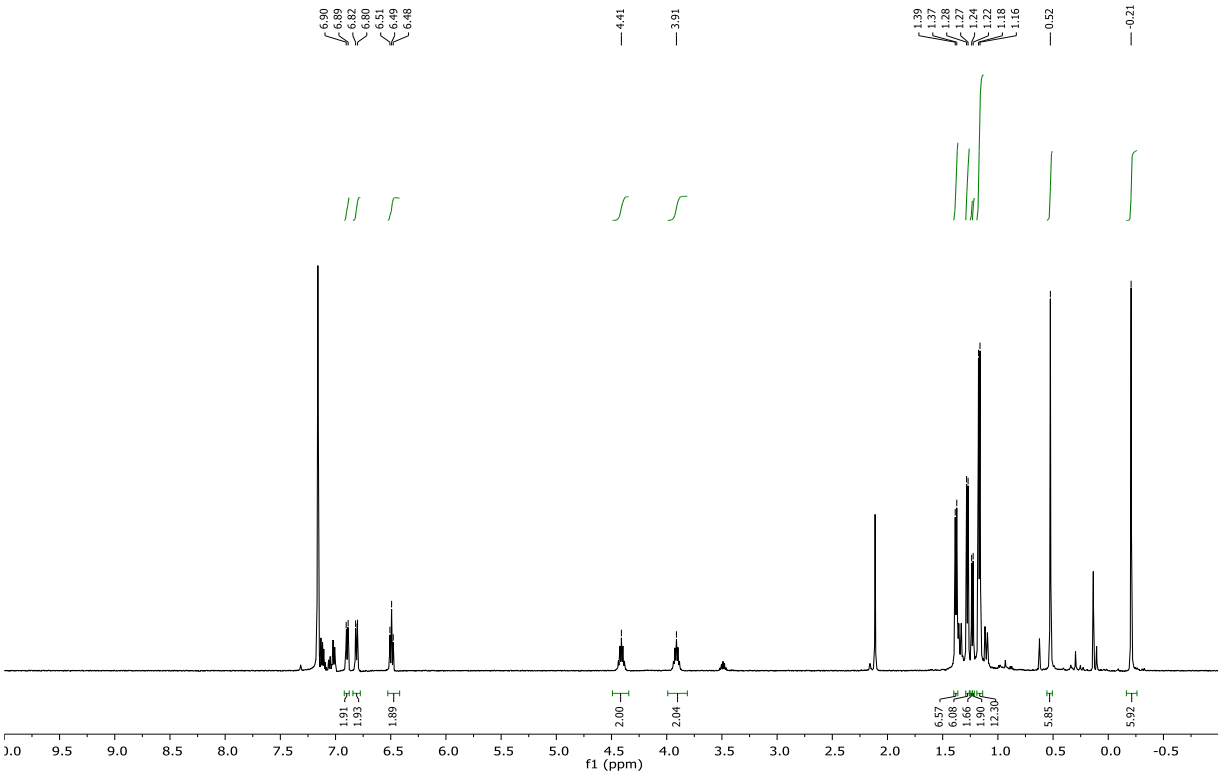

Figure 2. 7 : ^{1}H NMR Spectrum (500 MHz, 298 K, C_6D_6) of compound **2.25**.

The triclinic unit cell of **2.25** is composed of a racemate, that is, the Mg1/Mg2- and Mg3/Mg4-containing molecules describe right- and left-handed helices, respectively. While there are variations across the metric data of both molecules, the gross constitutions are effectively identical. The observed Mg-Mg separations in the molecules (Mg1-Mg2 = 3.2077(10) Å, Mg3-Mg4 3.2124(11) Å) are longer than any previously reported Mg-Mg distance (3.1962(14) Å).[12] On the other hand, the N-Mg bonds found in **2.25** (avg. 2.0831 Å), while significantly elongated from those of its precursor **2.24** (avg. 1.9454 Å), are more comparable with the reported N-Mg distances in [{^{Dipp}BDI}Mg]$_2$ **2.2** (avg. 2.0604 Å),[11] rather than the formal nitrogen-Mg(0) interactions (avg. 2.117 Å) displayed in compound **2.20**.[25] The structural data are, therefore, in good agreement with the attribution of a +I oxidation level to magnesium.

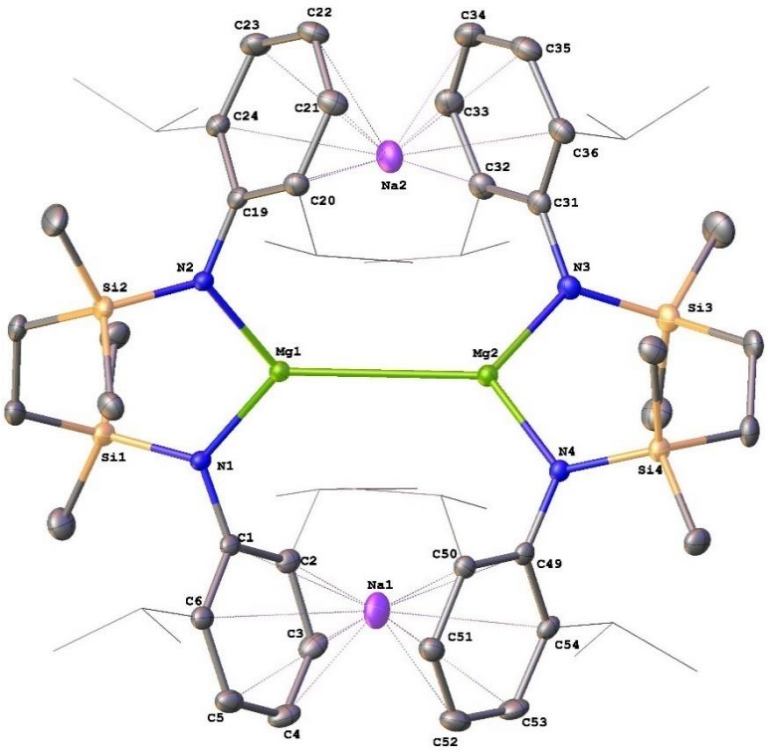

Figure 2. 8 : Displacement ellipsoid plot (30% probability) of the Mg1/Mg2-containing molecule of compound **2.25**. Hydrogen atoms and disordered molecules of solvent are omitted, and *iso*-propyl groups are shown as wireframe for clarity. Selected bond lengths (Å) and angles (°): Mg1-Mg2 3.2077(10), Mg3-Mg4 3.2124(11), Mg1-Na2 3.7229(13), Mg1-N1 2.0843(18), Mg1-N2 2.0786(19), Mg2-Na2 3.7014(13), Mg2-N3 2.090(2), Mg2-N4 2.0794(19), Mg3-Na3 3.6290(12), Mg4-Na3 3.6691(12), N2-Mg1-N1 109.76(7), N3-Mg2-N4 110.77(8), N5-Mg3-N6 110.03(8), N8-Mg4-N7 110.41(8).

In a similar fashion to compound **2.20**, notable levels of both Na-Mg and Na-aryl interactions are evident from the solid-state data of **2.25**. The closest Na-Mg distance in **2.25** (Mg3-Na3 3.6290(12) Å) is elongated in comparison to the Na-Mg contacts reported for compound **2.20** (3.4529(7) Å), in which a weak Mg–Na bonding was supported by the QTAIM analysis. In contrast, the Na-$C_{centroid}$ distances to the Dipp substituents (avg. 2.414 Å) of **2.25** are significantly shorter in comparison to the Na-$C_{centroid}$ separations observed in compound **2.20** (2.604 Å).[25] In the latter case, rapid solution exchange of both sites of *N*-Aryl substituents was inferred as no difference between Na-coordinated and non-coordinated aryl substituents could be discriminated by NMR spectroscopy. This observation is in sharp contrast to the solution properties of compound **2.25**, where the geometry of each [{SiN^{Dipp}}Mg] unit in the dimer is evidently 'locked' into its solid-state conformation by a combination of persistent Mg-Mg and Na-Dipp interactions. As a result, the enantiomers observed in the solid-state structures cannot interconvert, imposing the loss of symmetry in {SiN^{Dipp}} ligand environments indicated by NMR spectroscopy.

(a)

(b)

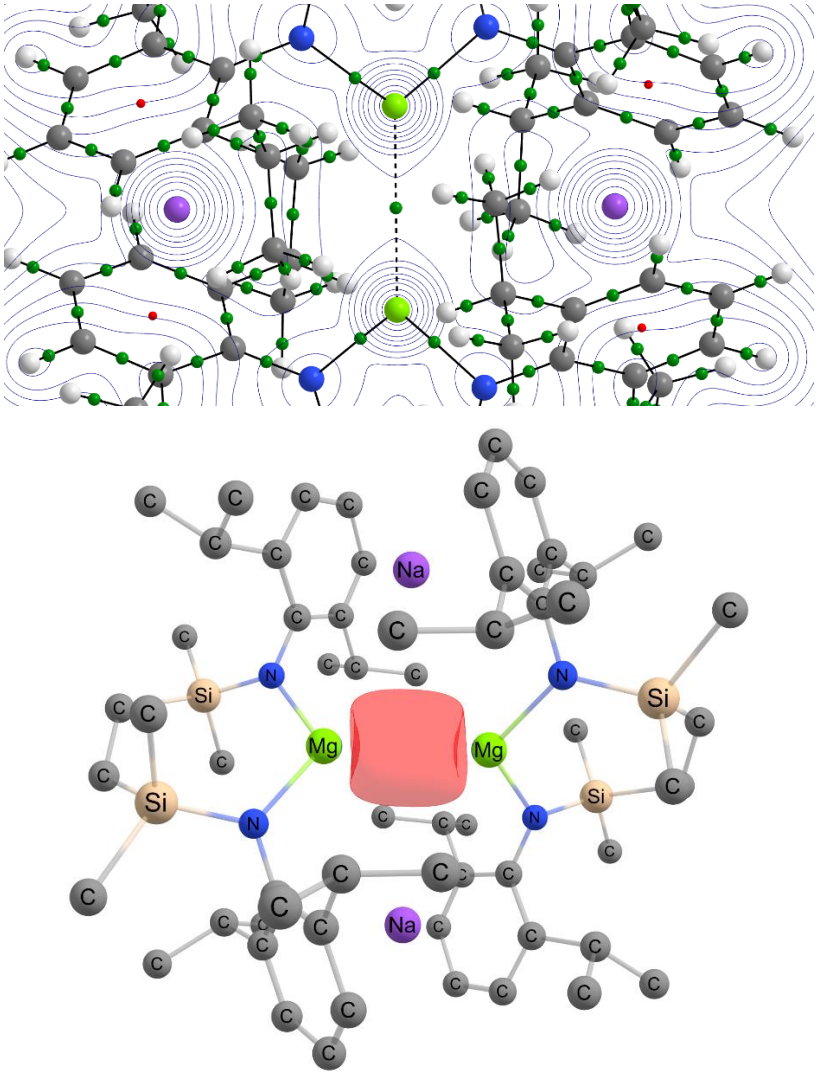

Figure 2. 9 : (a) QTAIM molecular graph of the BP86-optimised geometry of **2.25**. The electron density contours are computed in the {Mg-N} planes with bond critical points (BCPs) shown as small green spheres. (b) Natural Localized Molecular Orbital of the Mg-Mg bond in **2.25**.

Insight into the interatomic interactions in compound **2.25** was also acquired by a computational investigation performed by Dr Sam Neale and Dr M^{c}Mullin. Quantum theory of atoms in molecules (QTAIM) topological analysis conducted for [{SiN^{Dipp}}MgNa]$_2$ (**2.25**) found that the Mg-Mg bond critical point (ρ = 0.0194) has a negative energy density (H(r) = –0.00362) and Laplacian ($\nabla^2\rho(r)$ = –0.0136) indicative of a stabilising covalent bond (**Figure 2.9a**). This is further supported by NBO analysis through the identification of a natural localised molecular orbital of a Mg-Mg σ-bond with a roughly equal contribution from the 3s orbitals of each Mg centre (**Figure 2.9b**). Furthermore, QTAIM analysis revealed two weak bond critical points (where ρ = 0.0034) between the Na cations and the Mg-Mg bond critical point itself. Perturbation energy analysis of this unusual interaction with both Na^+ cations estimated an overall σ-donation strength between the Mg-Mg bond and each Na^+ cation of

$\Delta E^{(2)} \approx 25$ kcal mol^{-1}, suggesting the nature of **2.25** may be better considered as a supported $[Na_2Mg_2]^{4+}$ core rather than an isolated $[Mg\text{-}Mg]^{2+}$ unit, highlighting a notable contrast to the previously reported di-anionic ligand-supported low oxidation state magnesium species (**2.21-2.23**).[26,27]

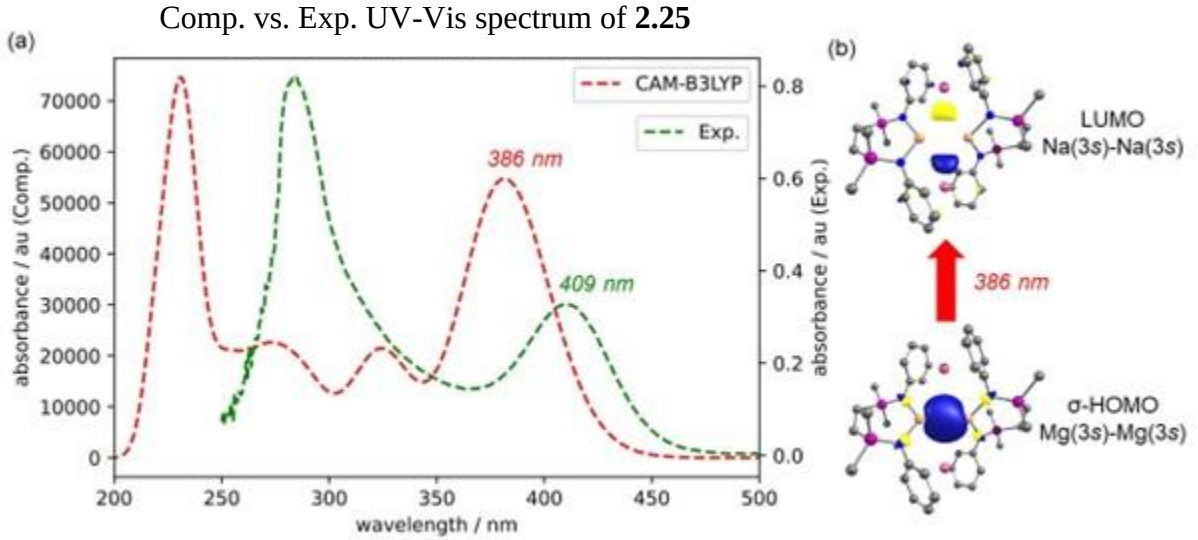

Figure 2. 10 : (a) Experimental (benzene, 8.5×18^{-8} M, green) and TD-DFT simulated (CAMB-3LYP/def2-TZVPP//BP86/def2-SVP - ORCA 5, red) UV-Vis absorbance spectra of compound **2.25**; (b) the HOMO → LUMO transition attributed to the experimental absorption centred at 409 nm.

To shed light further onto the electronic structure of compound **2.25**, its UV-Vis absorption was scrutinised both experimentally and computationally. The UV-Vis spectrum (250 – 500 nm) of an 8.5×10^{-8} M solution of **2.25** in benzene was recorded (**Figure 2.10a**). Consistent with its bright yellow appearance, the lowest energy electronic transition at 409 nm appears as a moderately intense absorption, whilst a more intense band exhibits at 285 nm with a shoulder. TD-DFT calculations were performed using the CAM-B3LYP functional in order to simulate the spectrum and provide an indication of the nature of the observed transitions. Although appreciable blue shifts of *ca.* 20 - 40 nm can be observed in the individual transitions, these methods provided a reasonable qualitative correspondence with the experimental data (**Figure 2.10a**). On this basis, the lowest energy excitation is attributed to a HOMO→LUMO transition between the Mg-Mg σ-bond arising from overlapping of the magnesium 3s wavefunctions, and an MO represented by an out-of-phase combination of the sodium 3s atomic orbitals (**Figure 2.10b**). This observation is reminiscent of the aforementioned examination of the $\{Mg_2Na_2\}$ core using QTAIM and NBO methods and is, again, consistent with a significant degree of cooperativity between the alkali and alkaline earth element components.

2.3 Cooperative Reactivity of the {Mg_2Na_2} Unit

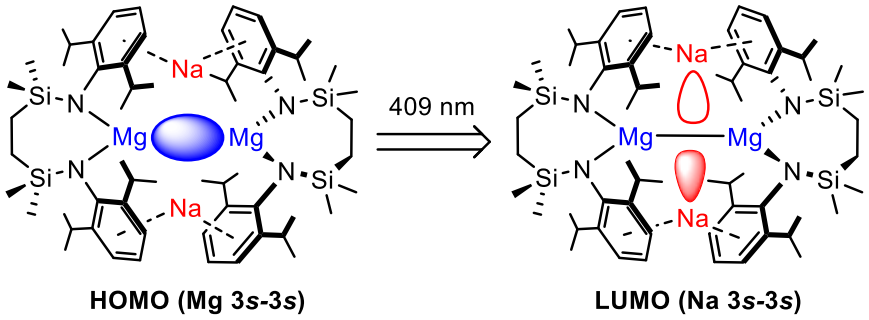

Figure 2. 11 : Visualisation of the HOMO-LUMO transition in compound **2.25**.

As discussed in the previous section, both experimental and computational investigations of the electronic structure of compound **2.25** have indicated that the magnesium-sodium complex is best considered as a ligand supported {Mg_2Na_2} unit, where the intense UV-Vis absorption can be attributed to the electron transition of σ(Mg-Mg) to 3s(Na) orbitals (**Figure 2.11**). This cooperative interaction across the bimetallic {Mg_2Na_2} unit was further verified by an examination of the solubility of [{SiN^{Dipp}}MgNa]$_2$ (**2.25**) in THF, whereupon a grey precipitate and colourless solution were rapidly obtained upon addition of the solvent. In light of this observation, the reaction was then meticulously repeated in a stoichiometric fashion, namely by addition of two molar equivalents of tetrahydrofuran *via* a micropipette to a solution of **2.25** in C_6D_6. A decolourisation of the bright yellow solution and deposition of a metallic mirror on the surface of reaction vessel appeared as the ethereal solvent diffused through the hydrocarbon solution, indicating the reaction between **2.25** and THF is a rapid and, most likely, stoichiometric reaction. The reaction product was then identified to be compound **2.26** by X-ray diffraction analysis performed on the colourless crystals obtained from the solution (in 83% yield), while the metallic mirror was confirmed to be exclusively (and of the entirety from **2.25** in the reaction) elemental sodium by ICP-OES (**Scheme 2.7**).

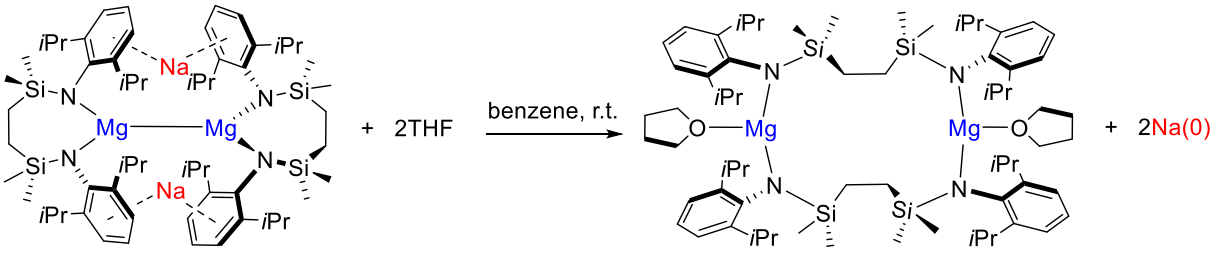

Scheme 2. 7 : Reaction of **2.25** with THF.

" Each ICP-OES test costs about 280 pilsners in Prague!" – ICOMC, 2022.

The resultant analysis conducted on the reaction of **2.25** with THF revealed that the extrusion of elemental sodium from **2.25** occurs through the oxidation of its {Mg(I)-Mg(I)} unit and ring opening of the 7-membered disilazide chelate structures, providing the deposition of a sodium mirror and the 14-atom macrocycle, in which the {SiN^{Dipp}}ligand adopts alternative {Mg-μ-κ1-N,κ1-N'-Mg'} bridging modes between the magnesium centres (**Figure 2.12**). The 3-coordinate Mg1 and Mg2 are each further ligated by a single molecule of THF, and the relevant Mg-N [Mg1-N1 1.9780(11), Mg1-N4 1.9795(11), Mg2-N2 1.9651(11), Mg2-N3 1.9671(11) Å] and Mg-O [Mg1-O1 2.0200(9), Mg2-O2 2.0311(10) Å] separations are consistent with a Mg(II) oxidation state assignment to both atoms. Although it cannot be verified whether **2.26** originates from a single parent molecule of **2.25**, the atomic specificity of this process advocates the reaction stoichiometry shown in **Scheme 2.7**.

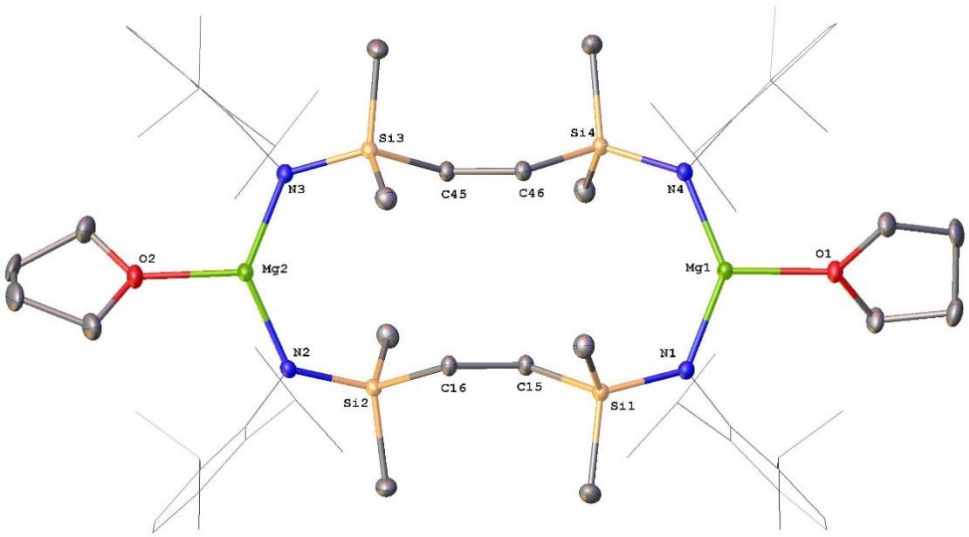

Figure 2. 12: Displacement ellipsoid (30% probability) plot of **2.26**. Hydrogen and disordered atoms and occluded benzene solvent have been omitted for clarity. Dipp substituents are shown as wireframe. Selected bond lengths (Å) and angles (°): Mg1-O1 2.0200(9), Mg1-N1 1.9780(11), Mg1-N4 1.9795(11), Mg2-O2 2.0311(10), Mg2-N2 1.9651(11), Mg2-N3 1.9671(11), N1-Mg1-O1 111.16(4), N1-Mg1-N4 136.66(4), N4-Mg1-O1 112.10(4), N2-Mg2-O2 111.89(4), N2-Mg2-N3 134.52(4), N3-Mg2-O2 113.59(4).

Intrigued by this behaviour, compound [{SiN^{Dipp}}MgNa]$_2$ (**2.25**) was then treated with two molar equivalents of the charge neutral, but more sterically encumbered, *N*- and *C*-donor bases, namely quinuclidine, 1,3-di-*iso*propyl-4,5-dimethyl-2-ylidene (*i*-Pr$_2$NHC(Me)$_2$) and 1,3-bis(2,6-di-*iso*propylphenyl)-2-ylidene (IPr). Although no discernible changes were observed by ^{1}H NMR spectroscopy, keeping these reaction mixtures at 40 °C for four weeks resulted in the deposition of a grey powder alongside the formation of subsequently insoluble colourless single crystals of compound **2.27** (**Figure 2.13a**). Although solution-state

characterisation of this species was limited by its low solubility, mechanical separation and X-ray diffraction analysis disclosed that **2.27** is a THF-free variant of compound **2.26** containing two 2-coordinate magnesium centres in all three cases (**Figure 2.13b**). These observations indicate a generic trend of sodium metal extrusion induced by introducing **2.25** to various bases, even if the coordination of the basic molecule to magnesium is hampered by the steric demands of the organic amine and/or Lewis donors.

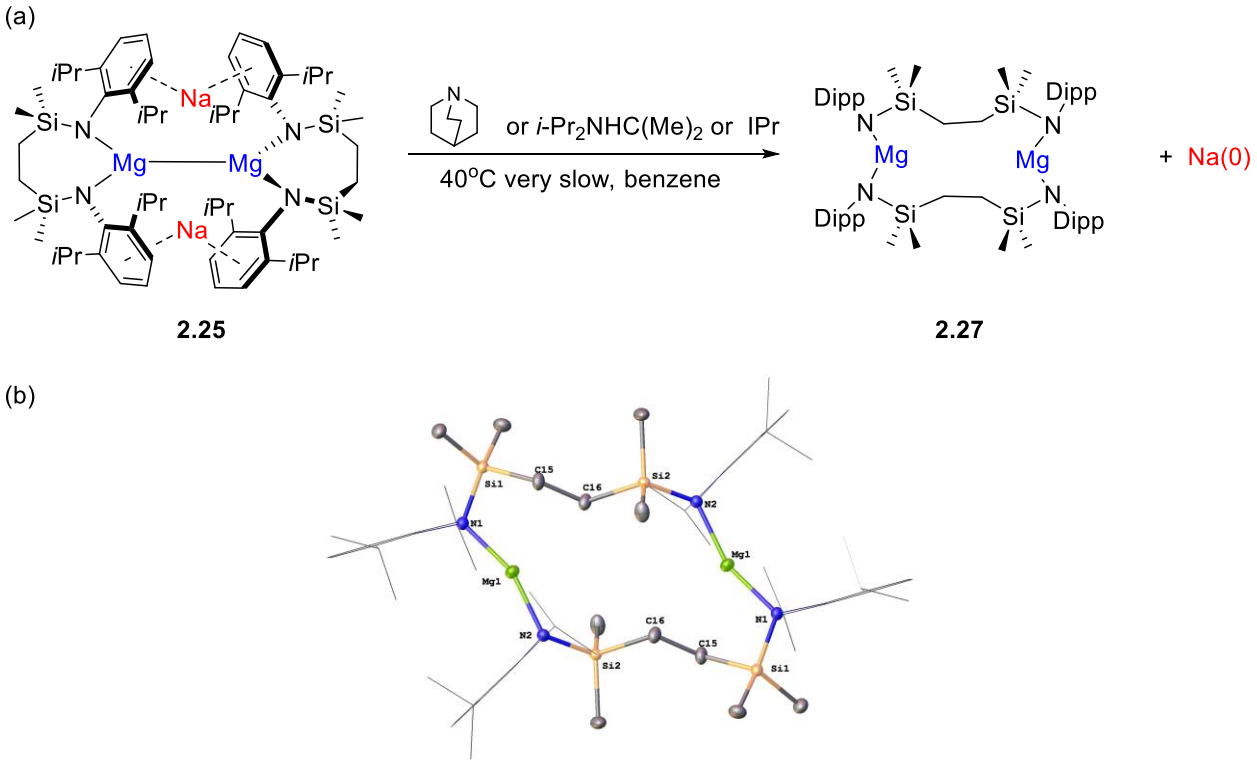

Figure 2. 13: (a) Synthetic routes to compound **2.27** and (b) displacement ellipsoid (30% probability) plot of **2.27**. For clarity, hydrogen and disordered atoms and occluded benzene solvent have been omitted. Dipp substituents are shown as wireframe. Selected bond lengths (Å) and angles (°): Mg1-N1 1.9207(12), Mg1-N2[1] 1.9360(11), N1-Mg1-N2[1] 160.17(5). Symmetry elements to generate equivalent atoms, [1] 1-x, 1-y, 1-z.

In a similar vein, compound **2.25** was also reacted with two molar equivalents of $NaNPh_2$, in which the *N*-donor nucleophile is negatively charged and less sterically demanding. Although the reaction rate was limited by the low solubility of the amide in benzene solvents, keeping the reaction mixture at 40 °C over 3 days was sufficient to consume all the magnesium-sodium complex (**2.25**), forming sodium metal as a grey powder along with a colourless solution. ^{1}H and ^{13}C NMR spectra of the colourless solution indicated that a single species (**2.28**) was the predominant product of the reaction between **2.25** and the sodium amide reagent. Compound **2.28** was subsequently isolated by removal of all volatiles, washing with hexane,

and crystallisation from hot benzene as colourless single crystals suitable for X-ray diffraction analysis (**Figure 2.14**).

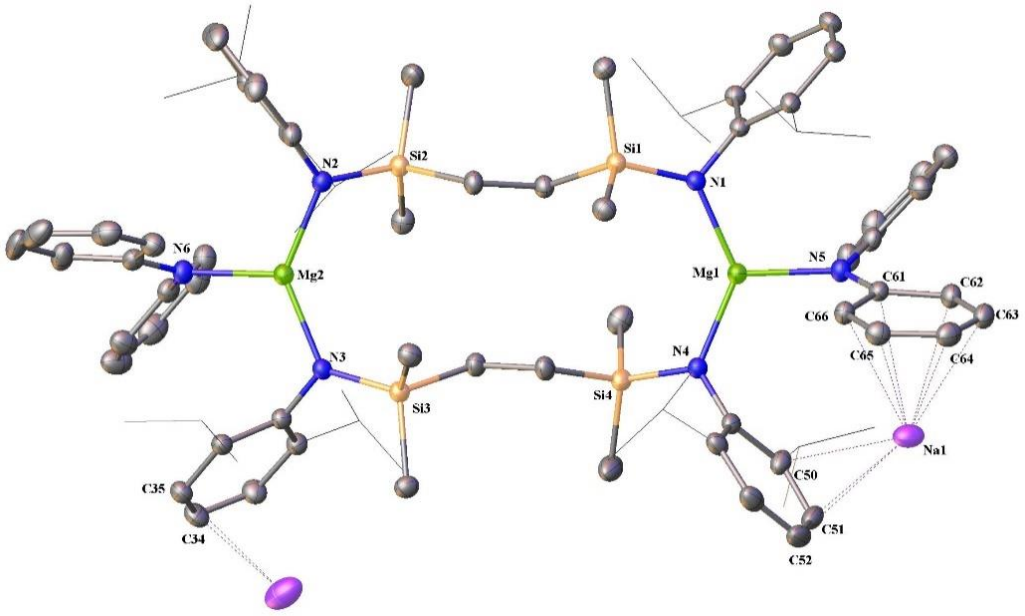

Figure 2. 14: Displacement ellipsoid (30% probability) plot of the asymmetric unit of compound **2.28**. Hydrogen and disordered atoms and occluded molecules of benzene solvent have been omitted for clarity. Dipp isopropyl substituents are shown as wireframe. Selected bond lengths (Å) and angles (°): Mg1-N1 2.0142(18), Mg1-N4 2.0130(19), Mg1-N5 2.0379(19), Mg2-N2 2.0057(19), Mg2-N3 2.0194(19), Mg2-N6 2.0341(19), N1-Mg1-N5 112.31(8), N4-Mg1-N1 133.02(8), N4-Mg1-N5 114.40(8), N2-Mg2-N3 133.16(8), N2-Mg2-N6 112.57(8), N3-Mg2-N6 114.05(8).

The asymmetric unit of **2.28** is based around a 14-atom macrocycle with Mg1 and Mg2 atoms being 3-coordinate, where both magnesium centres comprise magnesiate units resulting from *N*-coordination of a formally anionic diphenylamide moiety. Charge balance of **2.28** is attained by incorporation of Na1 and Na2 cations, located within coordination environments defined by the aromatic substituents of the diphenylamide and the SiN^{Dipp} ligand backbone. Whilst it is not possible to ascertain the origin of the sodium cations in **2.28**, the specificity of the sodium metal extrusion observed during the formation of compound **2.26**, supports the plausibility of an analogous process involving the reductive elimination of the sodium cations arising from the heterobimetallic starting material **2.25**.

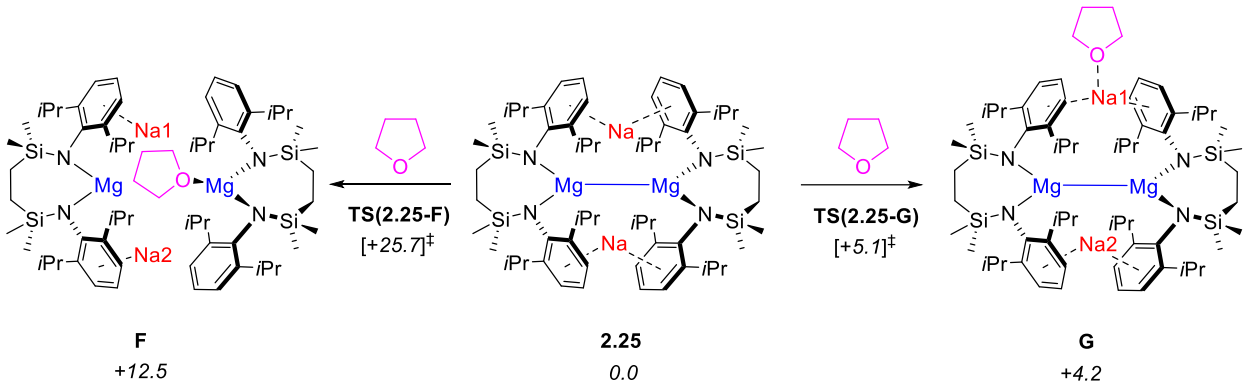

Figure 2. 15: DFT-computed (BP86-D3BJ/BS2(benzene)//BP86/BS1) free energies in kcal mol^{-1} for THF coordination to **2.25** at either the Mg (left) or Na centres (right).

Prompted by the transformation of **2.25** into compounds **2.26**, **2.27**, and **2.28**, computational mechanistic studies were performed by Dr Sam Neale with DFT calculations at the BP86-D3BJ(C_6H_6)/BS2//BP86/BS1 level of theory concerning the formation of **2.26**. Several scenarios were computed to identify the initial stage of the reaction, where a significant kinetic and thermodynamic preference was noted towards THF coordination at the Na1 centre, *via* **TS(2.25-G)** (+5.1 kcal mol^{-1}) to form **G** (+4.2 kcal mol^{-1}), rather than coordination at Mg *via* **TS(2.25-F)** (+25.7 kcal mol^{-1}) (**Figure 2. 15**). Moreover, the small barrier to formation of **G** at +5.1 kcal mol^{-1} is qualitatively consistent with the observation of an immediate colour change upon addition of THF to the benzene solution of **2.25** at room temperature. QTAIM analysis was then conducted on compound **G**, in which the coordination of THF to Na^+ induces a disengagement of the sodium cation from the *N*-Dipp substituent and perturbs the structure of the {Mg_2Na_2} core by an elongation of the Mg···Na_{THF} interatomic distances in **G** compared to those of **2.25**.

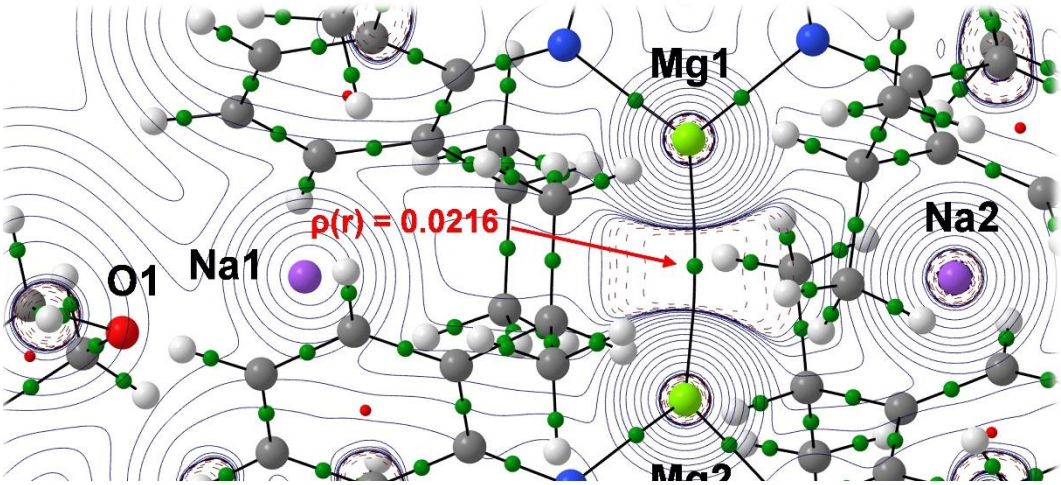

Figure 2. 16: QTAIM Laplacian plot of **G**, the initial THF adduct with **2.25**.

As shown in **Figure 2.16**, QTAIM analysis reveals that in comparison to **2.25**, the Mg1–Mg2 bond in **G** has a larger density at the bond critical point (BCP), where ρ(r) = 0.0216 (versus 0.0194 in **2.25**), and more negative Laplacian ($\nabla^2\rho(r) = -0.0155$ for **G**, versus −0.0136 in **2.25**) and energy density values (where H(r) = −0.0411 in **G** vs. −0.0362 in **2.25**). In addition, the Mg1–Mg2 bond path now exhibits a slight curvature towards the Na2 atom, further supporting the inference that formation of the Na_{THF} unit has disrupted the previously characterised interactions between the Mg-Mg bond and Na cations in **2.25**. Analysis of BCPs of low density in **G** revealed a small, yet appreciable Na2 – Mg1 BCP, where ρ(r)= 0.005 and $\nabla^2\rho(r)$ = +0.0074. While the density at this BCP has, thus, increased from that characterised in **2.25** (ρ(r)= 0.0034), no appreciable BCP between the $Na1_{THF}$ unit and the Mg–Mg bond could now be found. Any further theoretical analysis of the formation of **2.26** would be speculative and complicated by the observed macrocyclisation of the [{SiN^{Dipp}}Mg] units of **2.25**. The computational mechanistic studies on the formation of **2.26** have, however, further validated the proposed frontier orbital configuration as illustrated in Figure **2.11**.

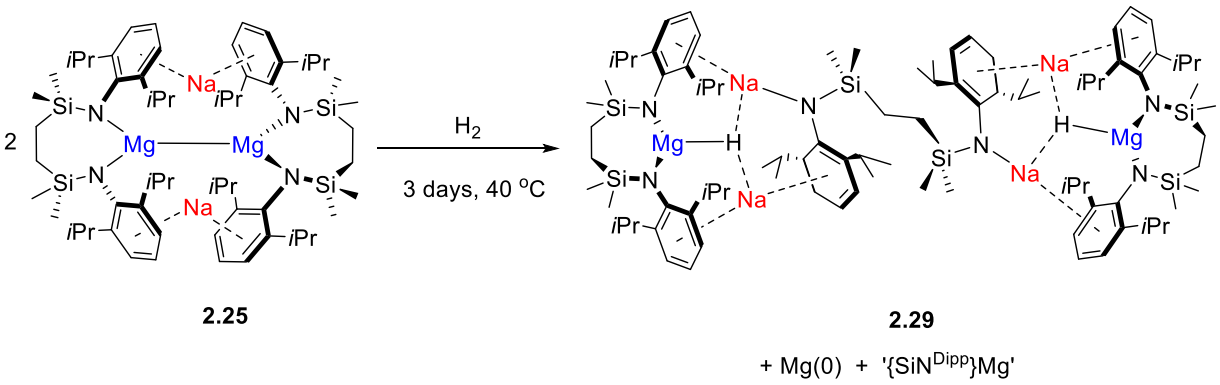

Scheme 2. 8 : Reaction of **2.25** with H_2.

Encouraged by the observation that the $\{Mg_2Na_2\}$ tetrametallic unit displays reactivity as a contiguous assembly with primarily *s*-block derived frontier orbitals, compound **2.25** was assessed in its capability to activate hydrogen. A reaction mixture was prepared by charging a degassed benzene solution of **2.25** with 2 atm. of hydrogen gas. Whilst no evidence of any transformation of **2.25** was observed over the course of 12 hours at room temperature, ^{1}H NMR spectroscopic monitoring indicated the formation of a predominant new compound under gentle heating and prolonged reaction time (40 °C, 3 days). The conversion of **2.25** took place with the simultaneous formation of a grey precipitate, from which, upon removal of all volatiles, compound **2.29** was isolated as colourless crystals *via* recrystallisation from a solution in hexane (**Scheme 2.8**). As shown in **Figure 2.17**, the resultant X-ray diffraction

analysis disclosed compound **2.29** to be a heterobimetallic hydride, while a quantitative ICP-OES analysis conducted on an acid digested solution of the metallic precipitate confirmed its identity as magnesium and the stoichiometry illustrated in **Scheme 2.8**.

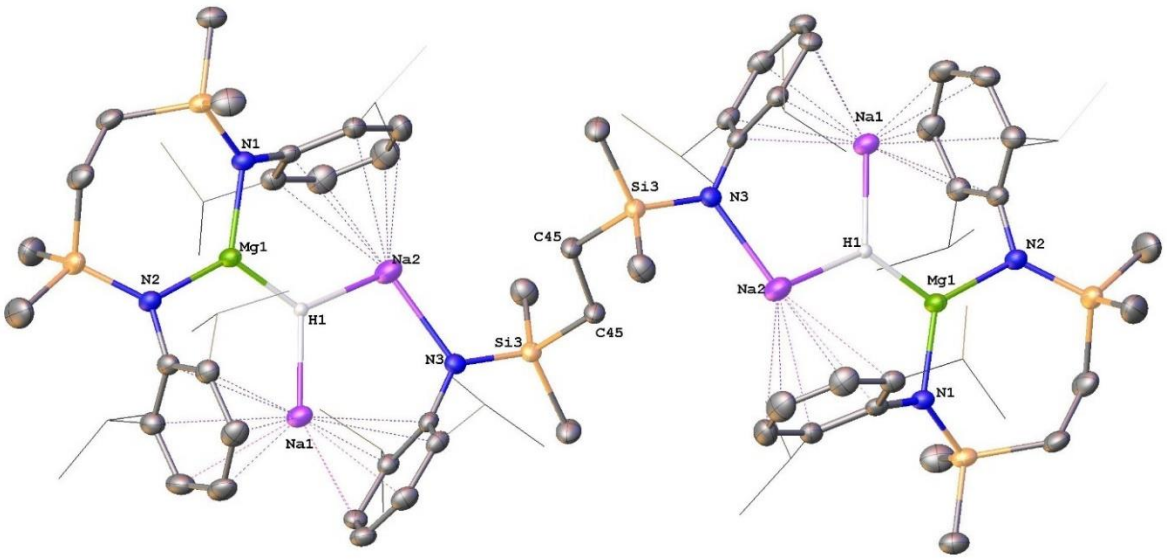

Figure 2. 17 : Displacement ellipsoid (30% probability) plot of compound **2.29**. H atoms, apart from H1 and H1[1], and occluded hexane solvent have been removed and iso-propyl groups are shown as wireframe for clarity. Selected bond lengths (Å) and angles (°): Mg1-N1 1.9795(13), Mg1-N2 1.9711(14), Na1-C22 2.7776(18), Na1-C33 2.7840(16), Na1-C34 2.7344(16), Na2-N3 2.2895(14), Na2-C1 3.1096(16), Na2-C2 3.0148(17), Na2-C3 2.9391(19), Na2-C4 2.948(2), Na2-C5 3.023(2), Na2-C6 3.1209(18), N1-Mg1-N2 126.44(6), N1-Mg1-N2 126.44(6). Symmetry operations to generate equivalent atoms: [1] −x, 2−y, 1−z.

The asymmetric unit of **2.29** is composed of half the molecule with the remainder generated *via* a crystallographic inversion centre (**Figure 2.17**), where both hydrides are trigonally encapsulated by a seven membered chelate [{SiN^{Dipp}}Mg] unit and two sodium cations. While Na1/Na1[1] is bound in a η^6-fashion by the aromatic substituents of the [{SiN^{Dipp}}Mg] and further polyhapto- interactions with C31-C36 (and C31[1]-C36[1]) comprising the Dipp substituents of the additional {SiN^{Dipp}} unit, the coordination spheres of Na2/Na2[1] are completed by the η^6-interactions with the *N*-Dipp on the [{SiN^{Dipp}}Mg] and N3/N3[1]. The observed Mg-N lengths in compound **2.29** are consistent with the oxidation of Mg(I), in that the Mg1-N1 [1.9795(13) Å] and Mg1-N2 [1.9711(14) Å] bonds of **2.29** are significantly shorter than the Mg–N distances observed in **2.25** (avg. 2.08 Å). Furthermore, whilst the presence of the halides in **2.29** could not be identified by ^{1}H NMR spectroscopy in d_6-benzene solution, dihydrogen was confirmed as the source of the hydride ligands of **2.29** by performance of a further reaction of **2.25** with D_2. This process provided similar results and the isolation of **2.29**-

d_2, giving a singlet signal at δ 4.16 ppm as the sole observable resonance in its ^{2}H NMR spectrum in benzene.

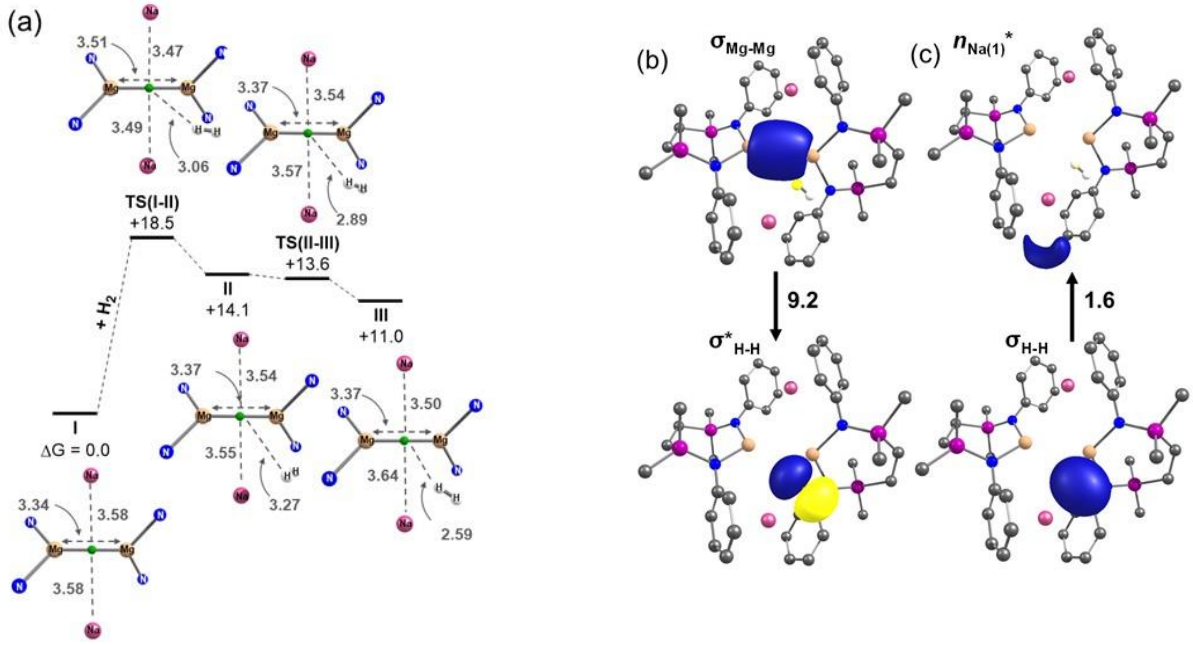

Figure 2. 18 : (a) Computed free energy profile (BP86-D3BJ/BS2-(benzene)//BP86/BS1), in kcal mol^{-1} for initial addition of H_2 to **2.25/I**. (SiN^{Dipp} ligand backbone and aromatic rings removed for clarity, and interatomic distances, and distances between each Na and the Mg–Mg midpoint (green) quoted in Å). (b) $\sigma_{Mg–Mg} \rightarrow \sigma^*_{H–H}$ interaction of **III**, identified by second-order perturbation energy analysis of the Fock matrix in NBO basis; (c) the corresponding $\sigma_{H–H} \rightarrow n^*_{Na(3s)}$ interaction of **III**. The donor-acceptor interaction energies, $\Delta E^{(2)}$, are quoted in kcal mol^{-1}.

Although several amido-derived Na/Mg hydrides have been reported as resulting from either β-C–H elimination or metal amide/Si–H metathesis,[29,30] compound **2.29** provides the first example where the hydrides arise from direct activation of dihydrogen by a Mg/Na complex. To further shed light on this unique reactivity, DFT calculations (BP86-D3BJ/BS2-(benzene)//BP86/BS1 level of theory) were performed by Dr Neale and Dr M^{c}Mullin to assess the kinetics of H_2 addition to **2.25** (denoted as **I** in the computational study) and the structure of the resulting H_2 adduct. Initial H_2 addition was identified to take place via **TS(I-II)** and a barrier of +18.5 kcal mol^{-1} to form **II** (+14.1 kcal mol^{-1}). Subsequent H_2 reorientation *via* a low-lying saddle point **TS(II-III)** (+13.6 kcal mol^{-1}) affords a more stable adduct, **III** (+11.0 kcal mol^{-1}), in which the H–H bond is directed towards the Mg–Mg σ bond (**Figure 2.18a**). NBO-based donor-acceptor interaction analysis of **III** revealed two appreciable interactions between the H_2 unit and the tetrametallic Mg_2Na_2 centre; a $\sigma_{Mg–Mg} \rightarrow \sigma^*_{H–H}$ interaction ($\Delta E^{(2)}$ = 9.2 kcal mol^{-1}; **Figure 2.18b**) supplemented by a smaller but still significant engagement *via* $\sigma_{H–H} \rightarrow n^*_{Na(3s)}$ ($\Delta E^{(2)}$ = 1.6 kcal mol^{-1}; **Figure 2.18c**).

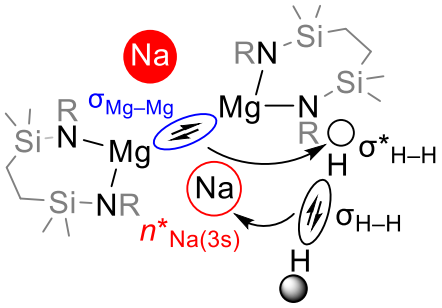

Figure 2. 19 : Illustration of the computationally inferred frontier orbital interactions between compound **2.25** and dihydrogen.

Although the semi-heterogeneous nature of the Mg(0) extrusion process and the structural complexity of **2.29** prevents any further meaningful mechanistic analysis, the nature of the H_2 activation process may be rationalised as a direct consequence of the cooperative behaviour arising from low oxidation state assembly of the magnesium and sodium centres (**Figure 2.19**). The computed frontier orbital interactions invoked in the initial coordination of H_2 to **2.25** bear some analogy to those of the generalised *d*- and *p*-block-derived systems depicted in **section 1.1**.

2.4 Reductive Reactivity of [{SiN^{Dipp}}MgNa]$_2$

As previously discussed in **section 2.1**, a strong reducing ability has been the characteristic feature shared by the various reported low oxidation state magnesium(I) dimers. The intrinsic reductive reactivity of the low oxidation state magnesium complex **2.25** was, thus, also investigated.

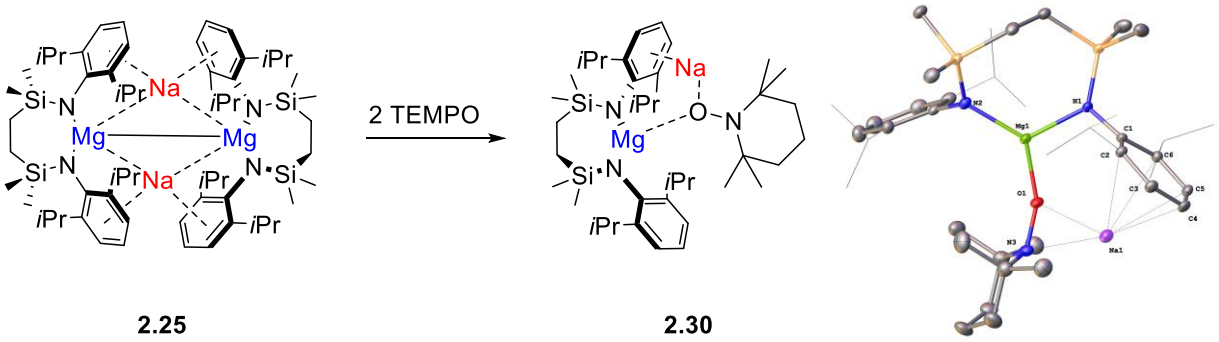

2.25 **2.30**

Scheme 2. 9 : Reaction of [{SiN^{Dipp}}MgNa]$_2$ with TEMPO and displacement ellipsoid plot (30% probability) of compound **2.30**. Hydrogen atoms are omitted, and iso-propyl substituents are displayed in wireframes for clarity.

To assess the reducing nature of the magnesium centres, the magnesium sodium dimer **2.25** was firstly reacted with two molar equivalents of the free radical, 2,2,6,6-tetramethylpiperidin-1-yl-1-oxyl free radical (TEMPO). A gradual decolourisation was observed after the addition of the TEMPO radical to the bright yellow d_6-benzene solution of **2.25**, and, on standing at slightly elevated temperature (40 ^{o}C) overnight, the reaction mixture deposited colourless single crystals. X-ray diffraction analysis revealed the outcome of the reaction to be [({SiN^{Dipp}}Mg)(TEMPO)Na] (**2.30**), the one-to-one complex of the TEMPO single electron oxidant to each dimer half of the [{SiN^{Dipp}}MgNa]$_2$ molecule (**Scheme 2.9**). Although the solid-state data for compound **2.30** were of insufficient quality (R_1 = 0.0792, wR_2 = 0.2153) to justify detailed discussion, they unambiguously verified the inherent one-electron reducing property of each individual [{SiN^{Dipp}}MgNa] unit. The solubility of **2.30** in a more polar solvent ($CDCl_3$), however, allowed its NMR spectroscopic characterisation. A symmetrical disposition across the {SiN^{Dipp}}-backbone in the molecule could be inferred from its ^{1}H NMR spectrum, in which the diagnostic iso-propyl methine and $SiMe_2$ peaks were each observed to resonate as single environments (**Figure 2.20**). This observation is consistent with a more labile monomeric constitution and the loss the of the more rigid structure imposed by the Mg-Mg interactions between the [{SiN^{Dipp}}Mg] moieties in compound **2.25**.

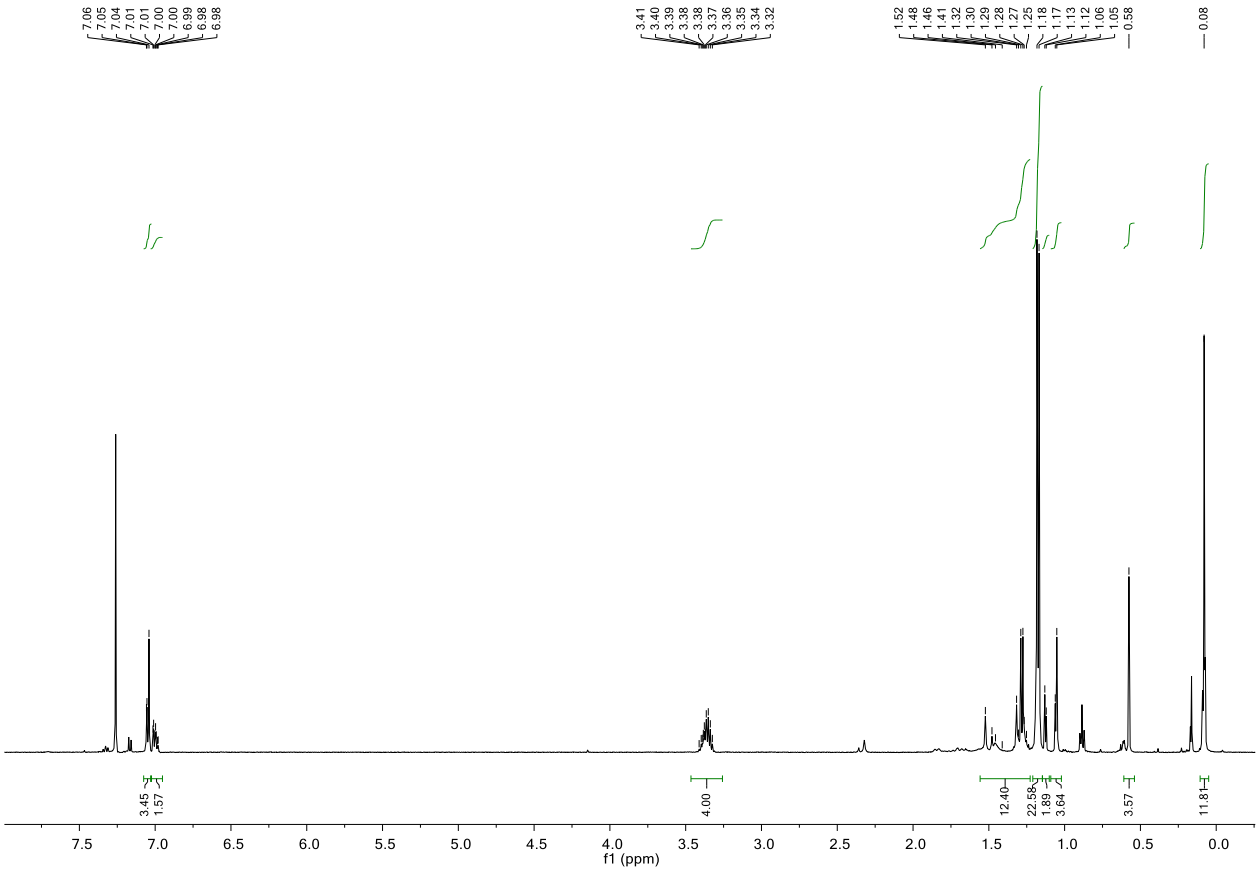

Figure 2. 20 : ^{1}H NMR spectrum of **2.30** (500 MHz, 298 K, $CDCl_3$).

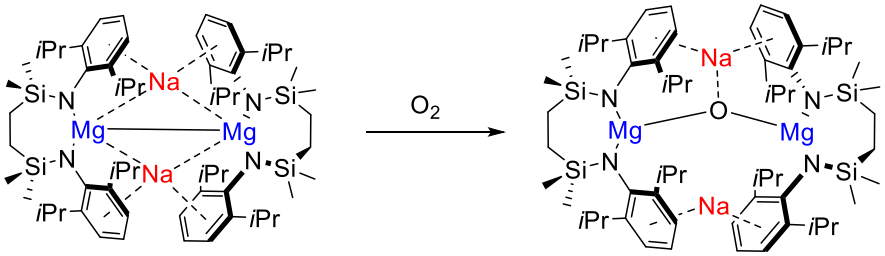

2.25 **2.31**

Scheme 2. 10 : Synthesis of **2.31**.

Quantitative solid-state characterisation of the outcome of a reaction between $[\{SiN^{Dipp}\}MgNa]_2$ and molecular oxygen was provided by the serendipitous isolation of an oxidised product of the magnesium(I) sodium complex (**2.25**). Colourless crystals, presumably obtained during storage of a benzene solution of **2.25** in a leaky Young's tube, were shown by X-ray diffraction analysis to be $[Na_2(\{SiN^{Dipp}\}MgOMg\{SiN^{Dipp}\})]$ (**2.31**, **Scheme 2.10**), where an oxygen atom has been doubly reduced and now bridges between two magnesium centres (**Figure 2.21**). As shown in **Table 2.1**, the N-Mg distances exhibited in **2.31** (avg. 2.027 Å) are significantly shorter than those in **2.25** (avg. 2.0831 Å), supporting the higher oxidation state assigned to the magnesium centres in **2.31**; the N-Mg bond length is, however, elongated in

comparison to the length found in [{SiN^{Dipp}}Mg] (**2.24**) (avg. 1.9454 Å), which can plausibly be attributed to the higher coordination number of the magnesium centre. The Mg-O (1.8610(4) Å) and Mg-N (avg. 2.027 Å) separations in compound **2.31** are analogous to those in the dimagnesium-oxo-complex obtained from formal oxidation of [{^{Dipp}BDI}Mg]$_2$ (**2.2**) (Mg-O, 1.8080(5) Mg-N, avg. 2.104 Å**),**[18] despite some structural variations arising from the latter case being isolated as a THF adduct.

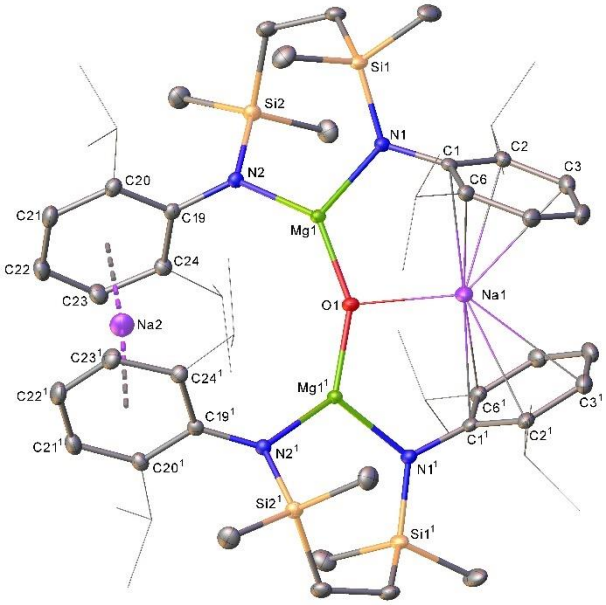

Figure 2. 21 : Displacement ellipsoid plot (30% probability) of compound **2.31**. The asymmetric unit comprises half of a dimer, and the remainder of the bimetallic complex is generated by a crystallographic 2-fold rotation axis. Hydrogen atoms and solvent molecules are omitted, and iso-propyl groups are shown as wireframe for clarity.

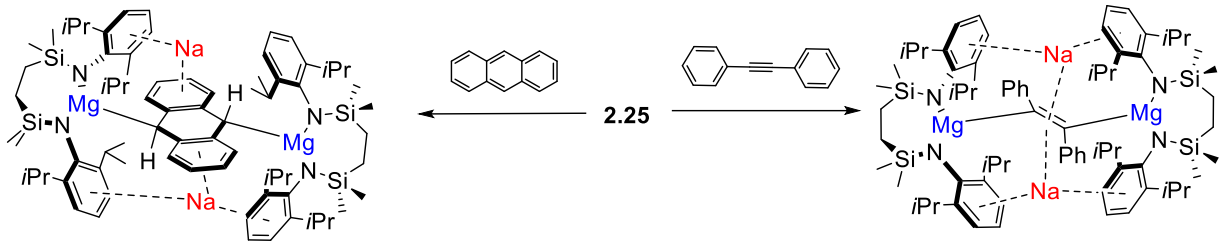

2.32 **2.33**

Scheme 2. 11 : Reaction of [{SiN^{Dipp}}MgNa]$_2$ (**2.25**) towards diphenylacetylene and anthracene.

Prompted by the observation that compound **2.25** indeed demonstrates magnesium centred reducing ability, [{SiN^{Dipp}}MgNa]$_2$ was then reacted with electron rich, yet reducible, organic substrates (**Scheme 2.11**; anthracene, $E_{1/2}$ = –1.98 V vs SCE; diphenylacetylene, E^o = –2.11 V vs SCE).[31] Whilst compound **2.32** crystallised directly from the reaction mixture of **2.25** and anthracene, the ^{1}H NMR spectrum recorded in d_8-toluene indicated that the reaction

of compound **2.25** towards diphenylacetylene provides a single predominant product (**2.33**). Slow evaporation of the latter reaction at low temperature provided crystals of **2.33**. The resultant X-ray diffraction analyses revealed that both compounds **2.32** and **2.33** comprise the relevant reduced carbon-based dianions, which bridge two [{SiN^{Dipp}}Mg] moieties with two arene-encapsulated sodium cations balancing the overall charge of the molecule (**Figure 2.22**).

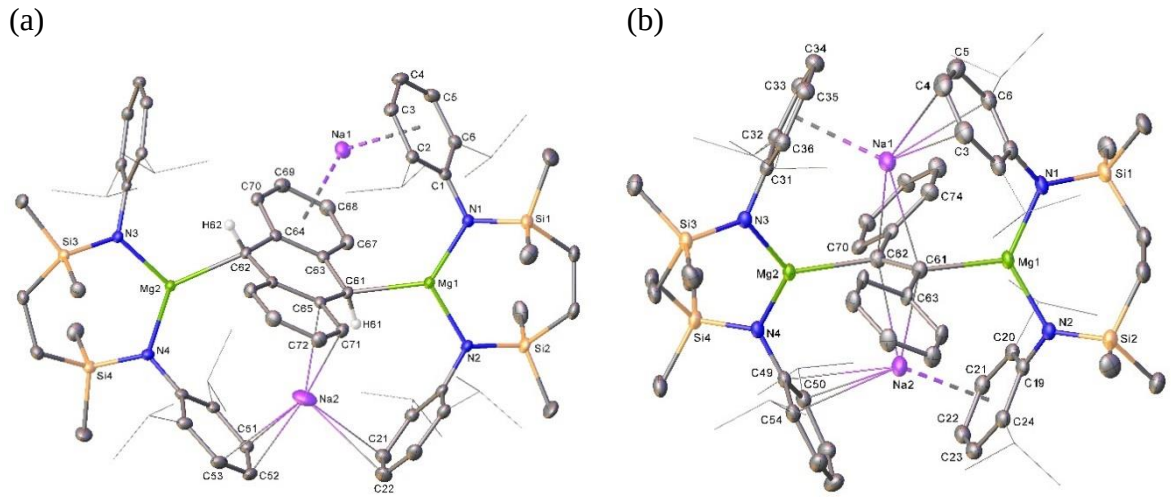

Figure 2. 22 : Displacement ellipsoid plots (30% probability) of (a) compound **2.32** and (b) compound **2.33**. Hydrogen atoms (except H61 and H62 in **2.32**) and solvent molecules are omitted, and iso-propyl groups are shown as wireframe for clarity.

Although all attempts to redissolve **2.32** in any common solvents induced degradation of the compound and regeneration of free anthracene in solution, the reaction of **2.25** with anthracene reproducibly provided colourless crystals of **2.32** in moderate yields (50%−60%). On the other hand, the ^{1}H NMR spectrum of compound **2.33** in d_8-toluene exhibited broad resonances, and all attempts to change the solvent resulted in decomposition of the molecule with the protonated [{SiN^{Dipp}}H$_2$] as the main identifiable product. Although the nature of the compounds precludes more detailed spectroscopic analysis of these compounds, it can be inferred from these observations that both **2.32** and **2.33** exhibit rapid conformational change in solution, giving rise to the high lability of both species and the apparent fluxional behaviour of **2.33**.

	2.31	2.32	2.33
Mg1-N1	2.0366(9)	1.9990(12)	2.049(3)
Mg1-N2	2.0537(9)	2.0098(12)	2.057(3)
Mg2-N3	-	2.0043(11)	2.043(3)
Mg2-N4	-	2.0099(12)	2.038(3)
Mg1-C61	1.8610(4) †	2.2342(13)	2.221(4)
Mg2-C62	-	2.2408(13)	2.228(4)

Table 2. 1: Selected bond distances (Å) for compounds **2.31** – **2.33**. † Mg1-O1.

In contrast to the issues encountered with their solution state characterisation, solid state analysis of **2.32** and **2.33** was readily achieved by X-ray diffraction (**Figure 2. 22, Table 2. 1**). In compound **2.32**, the sodium cations are found to be polyhapto- encapsulated by the aromatic moieties of both of the [{SiN^{Dipp}}Mg] and anthracene units. Furthermore, the Mg-N separations (avg. 2.0057 Å) are observed to be notably shorter in compound **2.32** in comparison to those in compound **2.25** (avg. 2.0831 Å). Both this value and the alternating C-C bond distances (C61-C63 1.4895(19) Å, C63- C64 1.4277(18) Å, C64-C62 1.4751(18) Å, C62-C66 1.4795(18) Å, C66-C65 1.4259(18) Å, C65-C61 1.4958(18) Å) observed in the C61-C63-C64-C62-C66-C65 cycles are, thus, consistent with a Mg(II) assignment and the formal reduction of anthracene moiety. Polyhapto- cation-arene interactions are also found between the sodium cations and Dipp substituents of the [{SiN^{Dipp}}Mg] unit in compound **2.33**, in this case with their coordination sphere was completed by a Na-η^2-C=C interaction with the dianionic acetylide moiety. The solid-state data of **2.33** are again consistent with the formal reduction of diphenylacetylene and the oxidation of the magnesium centre, with a now elongated C61-C62 distance (1.370(7) Å) and contracted Mg-N bonds (avg. 2.047 Å).

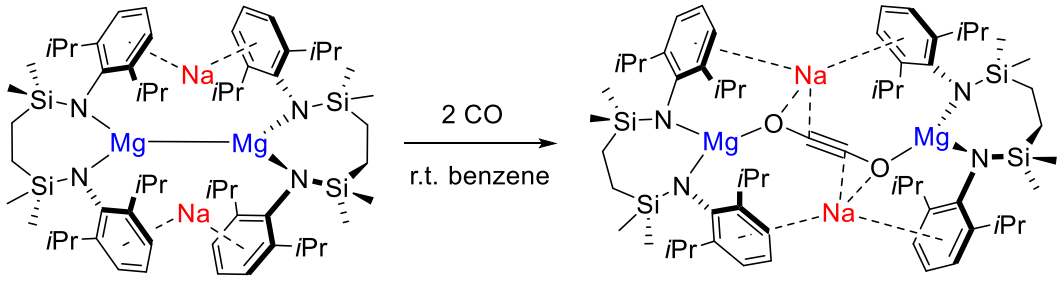

2.25 **2.34**

Scheme 2. 12: Synthesis of **2.34**.

Encouraged by the potent reducing nature displayed by compound **2.25**, a solution of compound **2.25** in benzene was treated with 2 atm. of ^{13}CO at room temperature. The conversion of **2.25** was complete after 3 days to provide the quantitative generation of a single new species (**2.34**, **Scheme 2.12**). The formation of the new species **2.34** was characterised in solution by the loss of asymmetry apparent in the {SiN^{Dipp}} backbone environments of **2.25** in the resultant ^{1}H NMR spectrum and, more characteristically, the emergence of a single new ^{13}C-enriched peak at δ 50.2 ppm in the corresponding $^{13}C\{^{1}H\}$ NMR spectrum. While the carbon centres of Jones' deltate $[C_3O_3]^{2-}$ originating from magnesium(I) dimers (**2.16**, **2.17**) could not be observed by $^{13}C\{^{1}H\}$ NMR spectroscopy for comparison,[20] a strongly reminiscent ^{13}C environment has previously been identified in Evans and co-workers' observation of the ethynediolate ^{13}C nuclei in the charge separated complex $[\{(Me_3Si)_2N\}_3Y(\mu\text{-}OC{\equiv}CO)Y\{N(SiMe_3)_2\}_3][K(18\text{-cr-}6)(THF)_2]_2$ (δ_C = 55.5 ppm). In this latter species, reductive dimerisation of two molecules of CO was mediated by the Y^{2+} centres generated *in-situ* by addition of excess potassium to $[Y\{N(SiMe_3)_2\}_3]$.[32] The inference of compound **2.34** being an analogous [{SiN^{Dipp}}Mg((μ-OC≡CO)Mg{SiN^{Dipp}}Na$_2$] was confirmed by X-ray diffraction analysis of a single crystal obtained by slow evaporation of a hexane solution at room temperature (**Figure 2. 23**).

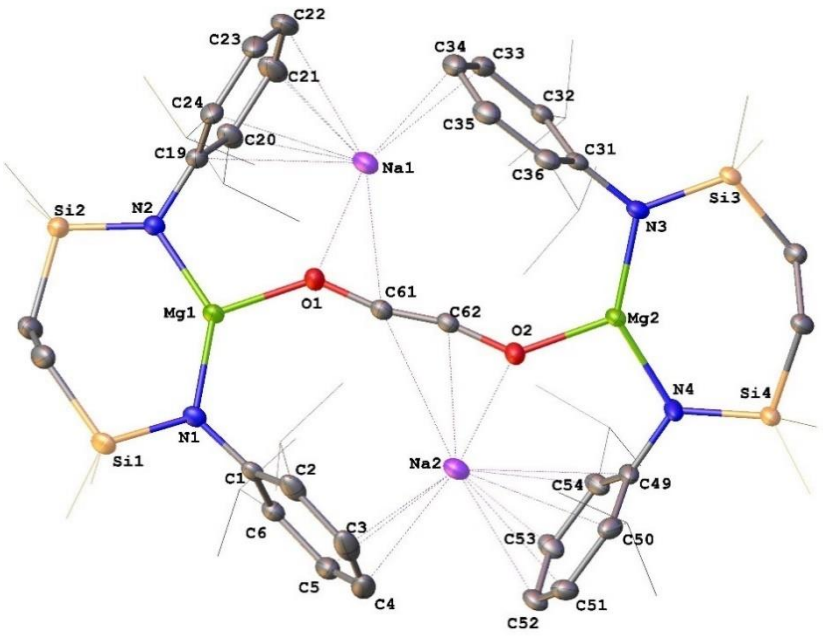

Figure 2. 23: Displacement ellipsoid (30% probability) of compound **2.34**. Hydrogen atoms, disordered atoms and disordered molecules of solvent are omitted for clarity. Dipp isopropyl and $SiMe_2$ methyl substituents are shown as wireframe. Selected bond lengths (Å) and angles (°): Mg1-N1 1.9684(11), Mg1-N2 1.9739(12), Mg2-N3 1.9694(12), Mg2-N4 1.9739(13), Mg1-O1 1.8904(11), Mg2-O2 1.8959(10), Na1-O1 2.2477(12), Na1-C61 2.6156(15), Na2-O2 2.3019(11), Na2-C61 3.1107(15), Na2-C62 2.5930(14), C61-C62 1.196(2), N1-Mg1-N2 138.34(5), N3-Mg2-N4 137.29(5), C62-C61-O1 166.82(14), C61-C62-O2 166.62(14).

The structure of **2.34** exhibits a (μ-OC≡CO) dianion bridging two [{SiN^{Dipp}}MgNa] units in which the magnesium and sodium centres are coordinated by the {SiN^{Dipp}} diamide chelate and a series of polyhapto- interactions with the *N*-Dipp substituents, respectively. The dianionic ethynediolate moiety is bound *via* terminal Mg-O [Mg1-O1 1.8904(11); Mg2-O2 1.8959(10) Å] and η^2-C-O contacts with the Na1 (Na1-O1 2.2477(12); Na1-C61 2.156(15) Å) and Na2 (Na2-O2 2.3019(11), Na2-C62 2.5930(14) Å) atoms. In the {O-C≡C-O} unit, the extremely short C61-C62 bond (1.196(2) Å) is comparable to that determined by powder X-ray diffraction in [NaOC≡CONa] (1.19(0.3)Å),[33]suggesting the C-C triple bond is unaffected by the proximity of the sodium cations, albeit the O1-C61-C62 (166.82(14)°) and O2-C62-C61 (166.62(14)°) angles highlight a significant deviation of the ethynediolate moiety from linearity.

"This molecule really just does whatever it wants." – K. G. Pearce, 2022.

2.5 Conclusion and Future Work

Sodium reduction of the {SiN^{Dipp}} backbone-supported magnesium(II) starting material (**2.24**) gives the bright yellow heterotetrametallic complex [{SiN^{Dipp}}MgNa]$_2$ (**2.25**). Compound **2.25** exhibits a considerable absorption at 409 nm, which can be qualitatively attributed to a σ(Mg-Mg) → 3s*(Na,Na) transition by theoretical calculations. This implied interconnected property between the metal centres was further validated by the cooperative behaviour of the {Mg_2Na_2} unit when reacted with non-reducible bases, inducing the formation of a variety of 14-atom magnesium containing macrocycles (**2.26** – **2.28**) and the deposition of metallic sodium. Compound **2.29** also provides the first example of a Na/Mg hydride complex prepared by the direct activation of dihydrogen with a low oxidation state sodium magnesium complex. The H_2 activation is suggested to be facilitated by the frontier orbitals derived from the magnesium and sodium atoms, further advocating the cooperative behaviour of the tetrametallic core of the molecule. The intrinsic reducing reactivity of **2.25** was also investigated by treating it with more readily reducible substrates, yielding a collection of novel species featuring formally oxidised magnesium centres and new magnesium-element bonds (**2.30** – **2.34**).

A primary conclusion arising from these observations, especially of the cooperative behaviour of the {Mg_2Na_2} unit, is that compound **2.25** is best considered as a supported $[Na_2Mg_2]^{4+}$ core rather than an isolated $[Mg\text{-}Mg]^{2+}$ unit. This highlights the contrast between the newly prepared low oxidation state magnesium complex (**2.25**) and previously reported mono- or bimetallic examples. In addition, the conceptual framework provided by the computed orbital interactions between H_2 and **2.25** (as illustrated in Figure **2.19**) implies a general applicability to manipulate the frontier orbitals of related systems, where the design and preparation of an assembly of further low oxidation state arrays of dissimilar *s*-block element centres may facilitate the activation of even more challenging small molecule substrates.

"DFT said you can do it with potassium as well." – C. L. M^{c}mullin, 2021.

2.6 Experimental data

[{SiN^{Dipp}}Mg] (2.24)

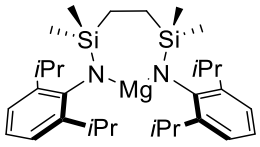

A heptane solution of $MgBu_2$ (1.0M, 16mL, 16mmol) was added dropwise to a solution of [{SiN^{Dipp}}H_2] (8.0g, 16mmol) in hexane (50mL) at room temperature. The reaction mixture was then left stirring at room temperature for 18 hours under a weak flow of argon, yielding a clear solution. The removal of all volatiles under vacuum gives a white waxy powder of the title compound. Yield 7.8 g, 94%. Anal Calc'd for $C_{30}H_{50}MgN_2Si_2$ (**2.24**, 519.22): C, 69.40; H, 9.71; N, 5.40 %. Found: C, 69.24; H, 9.69; N, 5.25 %. Compound **2.24** rapidly forms corresponding adducts upon introduction of aromatic solvents, forming the **2.24**-benzene or **2.24**-toluene molecules. Single crystals suitable for X-ray crystallography were obtained as colourless blocks from slow evaporation of the respective arene solutions. ^{1}H NMR (500 MHz, 298 K, Benzene-d_6) δ 7.12 – 7.03 (m, 4H, *m*-C$_6$*H*$_3$), 7.05 – 6.97 (m, 2H, *p*-C$_6$*H*$_3$), 3.87 (sept, *J* = 6.9 Hz, 4H, C*H*Me$_2$), 1.20 (d, *J* = 6.9 Hz, 24H, CH*Me*$_2$), 1.13 (s, 4H, SiC*H*$_2$), 0.26 (s, 12H, Si*Me*$_2$). ^{13}C{^{1}H} NMR (126 MHz, 298 K, Benzene-d_6) δ 144.2 (*i*-*C*$_6$H$_3$), 130.6 (*o*-*C*$_6$H$_3$), 123.8 (*m*-*C*$_6$H$_3$), 120.9 (*p*-*C*$_6$H$_3$), 27.7 (*C*HMe$_2$), 25.0 (CH*Me*$_2$), 12.7 (Si*C*H$_2$), 1.1 (Si*Me*$_2$).

[{SiN^{Dipp}}MgNa]$_2$ (2.25)

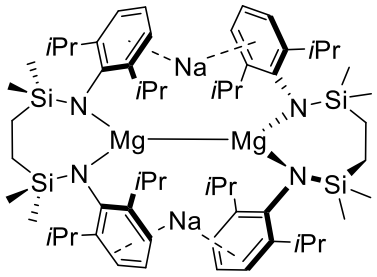

[{SiN^{Dipp}}$_2$Mg] (**2.24**,0.5g, 0.987mmol) and 5 wt.% Na/NaCl (1.4g, 3.04mmol) were charged into a Schlenk flask, followed by addition of benzene (40 mL) *via* cannula at room temperature. The reaction mixture was then stirred for 12 hours, yielding a yellow solution with a grey suspension. All the solid was then filtered, and all volatiles were removed under vacuum. Toluene (5 mL) was then added to give a yellow solution which was kept at –30 ˚C, yielding bright yellow crystals of **2.25**. Yield 0.384 g, 72%. Anal Calc'd for $C_{67}H_{108}Mg_2Na_2N_4Si_4$ (**2.25**.C_7H_8, 1176.56): C, 68.40; H, 9.25; N, 4.76 %. Found: C, 68.20; H, 9.03; N, 4.71 %. ^{1}H NMR (500 MHz, 298 K, Benzene-d_6) δ 6.89 (d, *J* = 8.8 Hz, 2H, *m*-C$_6$*H*$_3$), 6.81 (d, *J* = 8.8 Hz, 2H, *m*-C$_6$*H*$_3$), 6.53-6.45 (m, 2H, *p*-C$_6$*H*$_3$), 4.41 (sept, *J* = 6.9 Hz, 2H, C*H*Me$_2$), 3.91 (sept, *J* = 6.9 Hz, 2H, C*H*Me$_2$), 1.38 (d, *J* = 6.9 Hz, 6H, CH*Me*$_2$), 1.28 (d, *J* = 6.9 Hz, 4H, CH*Me*$_2$), 1.24 (s, 2H, SiC*H*$_2$), 1.22 (s, 2H, SiC*H*$_2$), 1.17 (d, *J* = 6.9 Hz, 12H, CH*Me*$_2$, overlapping), 0.52 (s, 6H, Si*Me*$_2$), -0.21 (s, 6H, Si*Me*$_2$). ^{13}C{^{1}H} NMR (126 MHz, 298K, Benzene-d_6) δ 156.6 (*i*-*C*$_6$H$_3$), 148.3 (*o*-*C*$_6$H$_3$), 147.06 (*o*-*C*$_6$H$_3$), 125.0 (*m*-*C*$_6$H$_3$), 123.5 (*m*-*C*$_6$H$_3$), 118.2 (*p*-*C*$_6$H$_3$), 28.4 (CH*Me*$_2$), 27.4 (*C*HMe$_2$), 27.04 (CH*Me*$_2$), 26.48 (*C*HMe$_2$), 25.1 (CH*Me*$_2$), 25.1 (CH*Me*$_2$), 23.9 (Si*C*H$_2$), 4.0 (Si*Me*$_2$), 1.9 (Si*Me*$_2$). *toluene impurity from recrystallisation observed.

[{SiN^{Dipp}}$_2$Mg$_2$·THF$_2$] (2.26)

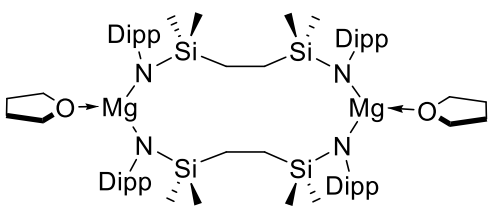

In a J Young's tube, [{SiN^{Dipp}}MgNa]$_2$ (**2.25**, 21.6 mg, 0.02 mmol) was dissolved in 0.4 mL of d_6-benzene before the addition of tetrahydrofuran (3.2 μL, 2.8 mg, 0.04 mmol) *via* a micropipette to the bright yellow solution. Upon addition, the reaction mixture turned reddish purple during the diffusion of tetrahydrofuran, and a metallic mirror was observed to be formed within a few seconds. The

reaction mixture was observed to become colourless within a few minutes after the formation of the metallic mirror. The reaction mixture was then filtered, and the filtrate was kept at room temperature to afford **2.26** as colourless crystals, from which a single crystal suitable for X-ray diffraction was obtained. Yield 19.6 mg, 83 %. Anal Calc'd for $C_{68}H_{116}Mg2N_4O_2Si_4$ (**2.26**, 1182.65): C, 69.06; H, 9.89; N, 4.74 %. Found: C, 68.69; H, 10.19; N, 4.30 %. ^{1}H NMR (500 MHz, 298 K, Benzene-d_6) δ 7.05 (d, J = 7.6 Hz, 8H, m-C_6H_3), 6.89 (t, J = 7.6 Hz, 4H, p-C_6H_3), 4.14 (sept, J = 6.9 Hz, 8H, CHMe$_2$), 2.33 (s br, 8H, OCH_2CH$_2$), 1.37 (d, J = 6.9 Hz, 24H, CHMe_2), 1.26 (s, 8H, SiCH_2), 1.09 (d, J = 6.9 Hz, 24H, CHMe_2), 0.69 (s br, 8H, OCH$_2$CH_2), 0.34 (s, 24H, SiMe_2). ^{13}C{^{1}H} NMR (126 MHz, 298 K, Benzene-d_6) δ 152.7 (i-C_6H_3), 144.8 (o-C_6H_3), 123.5 (m-C_6H_3), 120.0 (p-C_6H_3), 69.4 (OCH$_2$CH$_2$) 27.4 (CHMe$_2$), 25.4 (CHMe_2), 25.2 (OCH$_2$$CH_2$), 25.0 (CH$Me_2$), 14.7 (SiCH$_2$), 1.9 (Si$Me_2$). Identification of the metallic mirror was conducted by ICP-OES analysis in Butterworth Lab, and it was confirmed to be Na metal; Anal Calc'd: Na, 1001; Mg 0 mg/L; Found: Na, 975; Mg, <1 mg/L.

[{SiN^{Dipp}}$_2$Mg$_2$] (2.27)

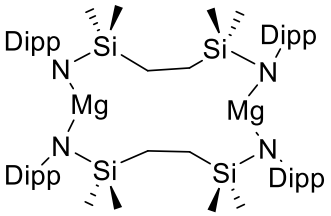

In J Young's tubes, [{SiN^{Dipp}}MgNa]$_2$ (**2.25**, 21.6 mg, 0.02 mmol) was dissolved in 0.4 mL of d_6-benzene. Various bulky bases were then added to each tube of the bright yellow solution. Entry a, Quinuclidine (4.4 mg, 0.04 mmol); entry b, 1,3-diisopropyl-4,5-dimethyl-2-ylidene (7.2 mg, 0.04 mmol); entry c. 1,3-bis(2,6-diisopropylphenyl)-2-ylidene (15.5 mg, 0.04 mmol). All reaction mixtures were kept at 40 °C and monitored by ^{1}H NMR spectroscopy over a long reaction period (*ca.* 1 month). Whilst no significant changes were observed in the ^{1}H NMR spectra of the reaction mixtures, a grey powder and colourless crystals appeared from each reaction mixture. The identity of the colourless crystal was then confirmed by X-ray crystallography to be **2.27**.

[({SiN^{Dipp}}$_2$Mg$_2$-(NPh$_2$)$_2$)Na$_2$] (2.28)

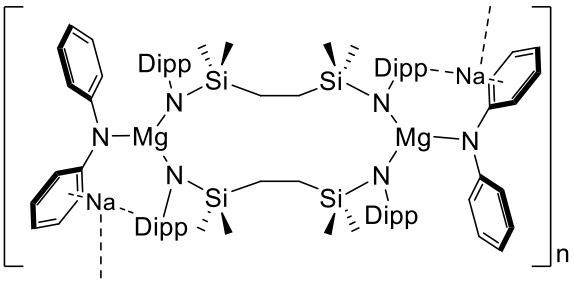

In a J Young's tube, [{SiN^{Dipp}}MgNa]$_2$ (**2.25**, 21.6 mg, 0.02 mmol) was dissolved in 0.4 mL of d_6-benzene before the addition of NaNPh$_2$ (7.6 mg, 0.04 mmol) to the bright yellow solution. No significant change was observed by ^{1}H NMR spectroscopy after the reaction mixture was kept at room temperature for 12 hours. The reaction mixture was then kept at 40 °C for 3 days before the complete conversion of the starting material was observed. The reaction mixture exhibited as a colourless solution with a grey powder after being kept at elevated temperature for 3 days. The reaction mixture was then filtered, and kept under vacuum to remove all volatiles, washed with hexane (0.5ml x2) affording **2.28** as pale-yellow powder. Yield 24.3 mg, 64%, Anal Calc'd for $C_{120}H_{156}Mg_2N_6Na_2Si_4$ (**2.28**, 1889.46): C, 71.01; H, 9.89. Found: C, 71.78; H, 7.91 %. A colourless single crystal suitable for X-ray crystallography was obtained by gradually cooling down a saturated solution of **2.28** in benzene from 60 °C. ^{1}H NMR (500 MHz, 298 K, Benzene-d_6) δ 7.12 – 6.93 (m, 4H, m-C_6H_3), 6.86 – 6.76 (m, 6H, ArH on NPh$_2$), 6.54 – 6.50 (m, 2H, p-C_6H_3), 6.44 – 6.33 (m, 4H, ArH on NPh$_2$), 4.17 (sept, J = 6.8 Hz, 4H, CHMe$_2$), 1.38 (s, 4H, SiCH_2), 1.35 (d, J = 6.8 Hz, 12H, CHMe_2), 1.03 (d, J = 6.8 Hz, 12H, CHMe_2), 0.41 (s, 12H, SiMe_2). ^{13}C{^{1}H} NMR (126 MHz, 298 K, Benzene-d_6) δ 153.7 (i-ArC on NPh$_2$), 146.2 (i-C_6H_3), 144.4 (o-C_6H_3), 130.4 (ArC on NPh$_2$), 123.4 (m-C_6H_3), 122.7 (ArC on NPh$_2$), 118.7

(Ar*C* on NPh_2), 117.5 (*p*-C_6H_3), 27.9 (*C*HMe_2), 25.9 (CH*Me*$_2$), 24.8 (CH*Me*$_2$), 15.9 (Si*C*H_2), 2.1 (Si*Me*$_2$).

[{SiN^{Dipp}}Mg(H)Na$_2${SiN^{Dipp}}Na$_2$(H)Mg{SiN^{Dipp}}](2.29)

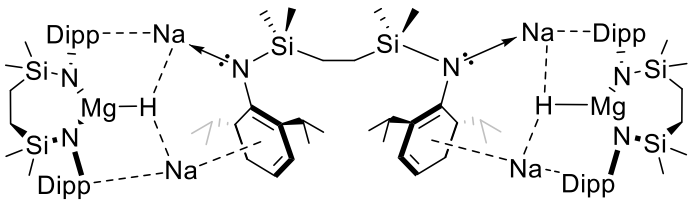

In a J Young's tube, [{SiN^{Dipp}}MgNa]$_2$ (**2.25**, 21.6 mg, 0.02 mmol) was dissolved in 0.4 mL of d_6-benzene. The bright yellow solution was degassed by three freeze-pump-thaw cycles, before being charged with 2 atm. of hydrogen gas. The reaction mixture was observed to transform into a colourless solution with black precipitates after being kept at 40 ˚C for 3 days. The powder was then removed by filtration, and removal of all volatiles of the filtrate *under vacuo* afforded **2.29** as a white powder. Yield 17.9 mg, 78%. The reaction was also carried out in the same procedure with $^2H_2$, and the resulting powder was dissolved in C_6H_6 to record a ^{2}H NMR spectrum. Anal Calc'd for $C_{96}H_{166}Mg_2N_6Na_4Si_6$ (**2.29**, 1713. 51): C, 67.29; H, 9.77; N, 4.90 %. Found: C, 66.82; H, 9.42; N, 4.82 %. Single crystals suitable for X-ray crystallography was obtained by slow evaporation of a hexane solution of X at room temperature. ^{1}H NMR (500 MHz, 298 K, Benzene-d_6) δ 7.03 – 6.93 (m, 4H, *m*-C$_6H_3$), 6.90 (d, *J* = 7.5 Hz, 8H, *m*-C6*H*3 on {SiN^{Dipp}}Mg), 6.82 – 6.78 (m, 2H, *p*-C$_6H_3$), 6.74 (t, *J* = 7.5Hz, 4H, *p*-C$_6H_3$ on {SiN^{Dipp}}Mg), 3.96 (sept, *J* = 7.0 Hz, 8H, C*H*Me$_2$ on {SiN^{Dipp}}Mg), 3.90 (sept, *J* = 6.9 Hz, 4H, C*H*Me$_2$), 1.28 (d, *J* = 7.0 Hz, 24H, CH*Me*$_2$ on {SiN^{Dipp}}Mg), 1.23 (d, *J* = 6.9 Hz, 12H, CH*Me*$_2$), 1.19 (d, *J* = 6.9 Hz, 12H, CH*Me*$_2$), 1.17 (s, 8H, SiCH_2 on {SiN^{Dipp}}Mg), 1.13 (s, 4H, SiCH_2), 0.87 (d, *J* = 7.0 Hz, 24H, CH*Me*$_2$ on {SiN^{Dipp}}Mg), 0.25 (s, 36H, SiMe$_2$)*overlapping peaks. ^{2}H NMR (77 MHz, 298 K, C_6H_6) δ 4.16. ^{13}C{^{1}H} NMR (126 MHz, 298 K, Benzene-d_6) δ 156.6 (*i*-C_6H_3), 152.1 (*i*-C_6H_3 on {SiN^{Dipp}}Mg), 147.1 (*o*-C_6H_3), 146.0 (*o*-C_6H_3 on {SiN^{Dipp}}Mg), 129.3 (m-C_6H_3), 123.1 (*p*-C_6H_3), 122.7 (*m*-C_6H_3 on {SiN^{Dipp}}Mg), 119.9 (*p*-C_6H_3 on {SiN^{Dipp}}Mg), 27.4 (*C*HMe$_2$), 27.1 (*C*HMe$_2$ on {SiN^{Dipp}}Mg), 25.6 (CH*Me*$_2$ on {SiN^{Dipp}}Mg), 25.2 (CH*Me*$_2$), 24.0 (CH*Me*$_2$), 23.8 (CH*Me*$_2$ on {SiN^{Dipp}}Mg), 13.2 (Si*C*H_2 on {SiN^{Dipp}}Mg), 13.0 (Si*C*H_2), 1.2 (Si*Me*$_2$)*overlapping peaks.

[{SiN^{Dipp}}Mg(TEMPO)Na](2.30)

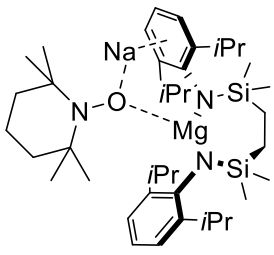

In a J Young's tube, [{SiN^{Dipp}}MgNa]$_2$ (**2.25**, 21.6 mg, 0.02 mmol) was dissolved in 0.4 mL of d_6-benzene before the addition of TEMPO (3.1 mg, 0.02 mmol) to the bright yellow solution. The reaction mixture was then kept at room temperature for a period of 3 days, during which time a gradual decolourisation and formation of colourless crystals was observed. The colourless crystals were found suitable for X-ray diffraction analysis of the connectivity of **2.30**. The colourless crystalline solids were then collected and washed with hexane (0.2mL x 2) before removal of all volatiles *in vacuo*, providing **2.30** as a colourless powder. Yield 16 mg, 65%. No meaningful result was obtained for elemental analysis after multiple attempts. ^{1}H NMR (500 MHz, Chloroform-*d*) δ 7.06 – 7.03 (m, 4H, *m*-C$_6H_3$), 7.02-6.97 (m, 2H, *p*-C$_6H_3$), 3.43-3.30 (m, 4H, C*H*Me$_2$), 1.55 – 1.23 (m, 12H, NC*Me*$_2$ of TEMPO), 1.18 (d, *J* = 6.9 Hz, 12H, CH*Me*$_2$), 1.15-1.11 (m, 2H, NCMe$_2$CH$_2$CH_2 of TEMPO), 1.09-1.02 (m, 4H, NCMe$_2$CH_2CH$_2$ of TEMPO), 0.58 (s, 4H, SiCH_2), 0.08 (s, 12H, SiMe$_2$). ^{13}C{^{1}H} NMR (126 MHz, Chloroform-*d*) δ 143.9 (*i*-C_6H_3), 143.7 (*o*-C_6H_3), 123.1, 123.0 (*m*-C_6H_3 and *p*-C_6H_3), 70.4 (N*C*Me$_2$ of TEMPO), 40.0 (NCMe$_2$*C*H$_2$*C*H$_2$ of TEMPO), 31.7 (NCMe$_2$CH$_2$*C*H$_2$ of

TEMPO), 28.3 (*C*HMe$_2$), 23.7 (CH*Me*$_2$), 22.8 (NC*Me*$_2$ of TEMPO) 17.4 (NC*Me*$_2$ of TEMPO), 9.6 (Si*C*H$_2$), -1.6 (Si*Me*$_2$).

[Na$_2$({SiN^{Dipp}}MgOMg{SiN^{Dipp}})] (2.31)

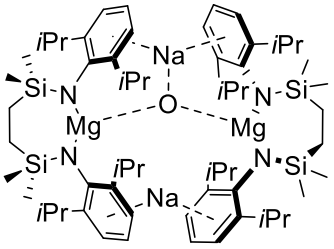

In a J Young's tube, [{SiN^{Dipp}}MgNa]$_2$ (**2.25**) was dissolved in 0.4 mL of d_6-benzene to make a bright yellow solution. The Young's tube was kept at ambient temperature over the period of a month, during which time the solution was observed to become pale yellow with the formation of colourless crystals suitable for single crystal X-ray diffraction analysis at the edge of the solution. X-ray crystallography revealed the identity of the colourless crystals to be **2.31**.

[Na$_2$({SiN^{Dipp}}Mg(C$_{14}$H$_{10}$)Mg{SiN^{Dipp}})](2.32)

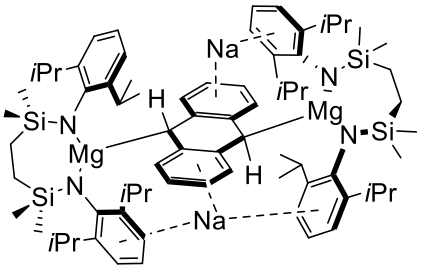

In a J Young's tube, [{SiN^{Dipp}}MgNa]$_2$ (**2.25**, 21.6 mg, 0.02 mmol) was dissolved in 0.2 mL of d_6-benzene before the addition of anthracene (3.6 mg, 0.02 mmol) to the bright yellow solution. The reaction mixture was then kept at 40 °C for a period of 3 days, exhibiting a gradual decolourisation and formation of colourless crystals suitable for X-ray diffraction analysis as **2.32**. The supernatant was then carefully decanted, and the crystalline solids were collected and washed with hexane (0.1mL x 2) before removal of all volatiles *in vacuo*, giving **2.32** as a colourless powder. Yield 14.5 mg, 57.5%. All attempts to redissolve **2.32** in any common solvents (C_6D_6, d_8-toluene, d_8-THF, $CDCl_3$) induced degradation of **2.32** and regeneration of free anthracene in the solution. The described process is, however, reproducible with moderate yields of **2.32** (14.5 mg, 57.5%; 12.5 mg, 49.6%; 14 mg, 55.5%; 15.2mg, 60.3%; 14 mg, 55.5%).

[Na$_2$({SiN^{Dipp}}Mg(PhCCPh)Mg{SiN^{Dipp}})](2.33)

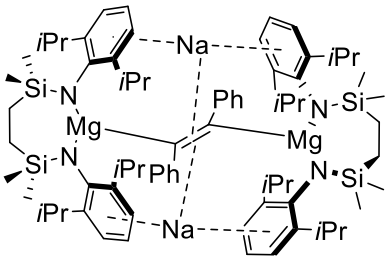

In a J Young's tube, [{SiN^{Dipp}}MgNa]$_2$ (**2.25**, 21.6 mg, 0.02 mmol) was dissolved in 0.4 mL of d_8-toluene before the addition of diphenylacetylene (3.6 mg, 0.02 mmol) to the bright yellow solution. The reaction mixture was then kept at 40 °C for a period of 3 days, whereupon the ^{1}H NMR spectrum indicated the formation of a new predominant species and consumption of all starting materials. The tube was then taken into glovebox and the now yellowish orange solution was decanted into a vial. Slow evaporation of the solution provided **2.33** as pale orange crystals suitable for X-ray diffraction analysis. Yield 17 mg, 67%. No meaningful result was obtained for elemental analysis after multiple attempts. ^{1}H NMR (500 MHz, 298 K, Toluene-d_8) δ 7.36 – 7.26 (m, 2H, C$_6$*H*$_3$ on SiN^{Dipp}), 7.26– 7.18 (m, 5H, C$_6$*H*$_5$ on PhCCPh), 6.87 – 6.49 (m, 10H, C$_6$*H*$_3$ on SiN^{Dipp}), 6.60 – 6.50 (m, 5H, C$_6$*H*$_5$ on PhCCPh), 4.15 – 3.65 (m, 4H, C*H*Me$_2$) 3.65 – 3.02 (m, 4H, C*H*Me$_2$), 1.38 – 1.05 (m, 30H, CH*Me*$_2$), 1.05 – 0.65 (m, 18H, CH*Me*$_2$), 0.65 – 0.44 (m, 8H, Si*C*H$_2$), 0.35 – -0.05 (m, 24H, Si*Me*$_2$). ^{13}C{^{1}H} NMR (101 MHz, 298 K, Toluene-d_8) δ 156.9 (4°*C* of C$_6$H$_3$ on SiN^{Dipp}), 153.6 (4°*C* of of C$_6$H$_3$ on SiN^{Dipp}), 144.3 (Ar*C* of PhCCPh), 139.8 (Ar*C* of PhCCPh), 132.1 (4°*C* of PhCCPh), 131.9 (Ar*C* of C$_6$H$_3$ on SiN^{Dipp}), 126.9 (4°*C* of PhCCPh), 123.3 (Ar*C* of C$_6$H$_3$ on SiN^{Dipp}), 119.4 (Ar*C* of PhCCPh), 28.5 (CH*Me*$_2$), 27.3 (*C*HMe$_2$), 23.6 (CH*Me*$_2$), 9.8 (Si*C*H$_2$), -1.6 (Si*Me*$_2$).

[Na_2({SiN^{Dipp}}Mg(OCCO)Mg{SiN^{Dipp}})](2.34)

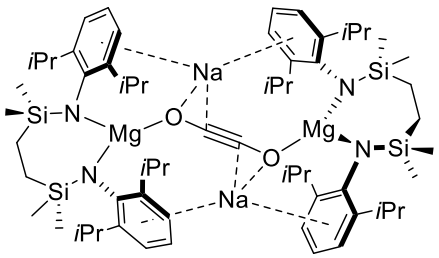

[{SiN^{Dipp}}MgNa]$_2$ (**2.25**,10.8mg, 0.01mmol) was dissolved in 0.4 mL of C_6D_6 inside a J Young's NMR tube. The solution was then degassed by three cycles of freeze-pump-thaw before the tube was charged with 2 atm of ^{13}CO. A diagnostic peak at 50 ppm in the ^{13}C NMR spectrum was observed to form within an hour after the gas was added to the reaction mixture. Quantitative conversion into compound **2.34** (determined by ^1H NMR) was observed after the reaction mixture was left at room temperature for 3 days. All volatiles were then removed under vacuum, giving **2.34** as a colourless solid. Crystals suitable for X-ray diffraction analysis were obtained by slow evaporation of a hexane solution at room temperature. Yield 9.0 mg, 79%. No meaningful result was obtained for elemental analysis after several attempts. ^1H NMR (500 MHz, 298 K, Benzene-d_6) δ 6.88 (d, *J* = 7.4 Hz, 4H, *m*-C_6H_3), 6.65 (t, *J* = 7.4 Hz, 2H, *p*-C_6H_3), 4.02 (sept, *J* = 6.8 Hz, 4H, C*H*Me_2), 1.31 (d, *J* = 6.8 Hz, 12H, CH*Me*$_2$), 1.11 (s, 4H, SiCH_2), 0.97 (d, *J* = 6.8 Hz, 12H, CH*Me*$_2$), 0.19 (s, 12H, Si*Me*$_2$). $^{13}C\{^1H\}$ NMR (126 MHz, 298 K, Benzene-d_6) δ 153.8 (*i*-C_6H_3), 147.5 (*p*-C_6H_3), 121.6 (*m*-C_6H3), 118.3 (*p*-C_6H_3), 50.2 (C_2O_2), 27.3 (*C*HMe_2), 25.1 (CH*Me*$_2$), 23.7 (CH*Me*$_2$), 11.9 (Si*C*H_2), 1.1 (Si*Me*$_2$). Peaks observed at 160-180 ppm, no correlation with proton observed in ^1H-^{13}C HSQC, HMBC, plausibly ^{13}C labelled impurities.

2.7 References

1. D. A. Young, in *Phase Diagrams of the Elements*, University of California Press, Berkeley, 1991, pp. 78-87.
2. A. Stasch and C. Jones, *Dalton Trans*, 2011, **40**, 5659-5672.
3. B. Rösch and S. Harder, *Chem Commun*, 2021, **57**, 9354-9365.
4. L. A. Freeman, J. E. Walley and R. J. Gilliard, *Nat Synth*, 2022, **1**, 439-448.
5. R. M. Pashley and J. N. Israelachvili, *J Colloid Interface Sci*, 1984, **97**, 446-455.
6. P. G. Jasien and C. E. Dykstra, *J Am Chem Soc*, 1983, **105**, 2089-2090.
7. Y. Xie, H. F. Schaefer and E. D. Jemmis, *Chem Phys Lett*, 2005, **402**, 414-421.
8. A. Velazquez, I. Fernández, G. Frenking and G. Merino, *Organometallics*, 2007, **26**, 4731-4736.
9. L. A. Tjurina, V. V. Smirnov, D. A. Potapov, S. A. Nikolaev, S. E. Esipov and I. P. Beletskaya, *Organometallics*, 2004, **23**, 1349-1351.
10. X. Wang and L. Andrews, *J Phys Chem A*, 2004, **108**, 11511-11520.
11. S. P. Green, C. Jones and A. Stasch, *Science*, 2007, **318**, 1754-1757.
12. S. P. Green, C. Jones and A. Stasch, *Angew Chem Int Ed*, 2008, **47**, 9079-9083.
13. S. J. Bonyhady, C. Jones, S. Nembenna, A. Stasch, A. J. Edwards and G. J. McIntyre, *Chem Eur Jl*, 2010, **16**, 938-955.
14. A. Stasch, *Angew Chem Int Ed*, 2014, **53**, 10200-10203.
15. A. J. Boutland, D. Dange, A. Stasch, L. Maron and C. Jones, *Angew Chem Int Ed*, 2016, **55**, 9239-9243.
16. A. J. Boutland, I. Pernik, A. Stasch and C. Jones, *Chem Eur J*, 2015, **21**, 15749-15758.
17. C. Jones, *Nat Rev Chem*, 2017, **1**, 0059.
18. R. Lalrempuia, A. Stasch and C. Jones, *Chem Sci*, 2013, **4**, 4383-4388.
19. R. Lalrempuia, C. E. Kefalidis, S. J. Bonyhady, B. Schwarze, L. Maron, A. Stasch and C. Jones, *J Am Chem Soc*, 2015, **137**, 8944-8947.
20. K. Yuvaraj, I. Douair, A. Paparo, L. Maron and C. Jones, *J Am Chem Soc*, 2019, **141**, 8764-8768.
21. C. Bakewell, A. J. P. White and M. R. Crimmin, *J Am Chem Soc*, 2016, **138**, 12763-12766.
22. J. Li, M. Luo, X. Sheng, H. Hua, W. Yao, S. A. Pullarkat, L. Xu and M. Ma, *Org Chem Front*, 2018, **5**, 3538-3547.
23. T. X. Gentner, B. Rösch, G. Ballmann, J. Langer, H. Elsen and S. Harder, *Angew Chem Int Ed*, 2019, **58**, 607-611.
24. B. Rösch, T. X. Gentner, J. Eyselein, A. Friedrich, J. Langer and S. Harder, *Chem Commun*, 2020, **56**, 11402-11405.
25. B. Rösch, T. X. Gentner, J. Eyselein, J. Langer, H. Elsen and S. Harder, *Nature*, 2021, **592**, 717-721.
26. Y. Liu, S. Li, X.-J. Yang, P. Yang and B. Wu, *J Am Chem Soc*, 2009, **131**, 4210-4211.
27. M. Ma, H. Wang, J. Wang, L. Shen, Y. Zhao, W.-H. Xu, B. Wu and X.-J. Yang, *Dalton Trans*, 2019, **48**, 2295-2299.

28. R. J. Schwamm, M. P. Coles, M. S. Hill, M. F. Mahon, C. L. McMullin, N. A. Rajabi and A. S. S. Wilson, *Angew Chem In Ed*, 2020, **59**, 3928-3932.
29. D. J. Gallagher, K. W. Henderson, A. R. Kennedy, C. T. O'Hara, R. E. Mulvey and R. B. Rowlings, *Chem Commun*, 2002, 376-377.
30. D. J. Liptrot, M. S. Hill and M. F. Mahon, *Chem Eur Jl*, 2014, **20**, 9871-9874.
31. M. Szostak, M. Spain and D. J. Procter, *J Org Chem*, 2014, **79**, 2522-2537.
32. M. Fang, J. H. Farnaby, J. W. Ziller, J. E. Bates, F. Furche and W. J. Evans, *J Am Chem Soc*, 2012, **134**, 6064-6067.
33. E. Weiss and W. Büchner, *Chemische Berichte*, 1965, **98**, 126-130.

3. Synthesis and Reactivity Studies of Al(I) Diamides

In contrast to the relatively limited reports of isolable examples in the low oxidation state chemistry of the group 2 elements,[1,2] the past few decades have seen significant developments in low oxidation state group 13 chemistry, especially with regards to singlet carbene analogues in their +I oxidation state. The closed-shell electronic configuration and higher electron affinity of the group 13 centre in this class of molecules renders higher stability in comparison to the reduced group 2 species in oxidation state <+II, facilitating more wide ranging studies.[3,4]

Although a considerable number of low oxidation state group 13 carbene analogues have now been described, until recently only a limited number featured a low oxidation state aluminium centre. This lacuna can be attributed to the element's larger size and lower electron affinity compared to that of boron, whilst in the heavier elements of group 13 the +I oxidation state is increasingly favoured due to the inert pair effect. While the initial preparation and isolation of neutral Al(I) dates from the early 1990s,[5-7] their negatively charged counterparts have only been realised in more recent years.[4,8] Reactivity arising from the enhanced electron density imparted to the electropositive aluminium in these latter species, particularly novel aluminium(I) diamido anions, will be the focus of this chapter.

"I gotta get one of those." – Mandalorian, *The Mandalorian*, 2020.

3.1 Development of Aluminium(I) Analogues of Singlet Carbenes

3.1.1 Formally neutral aluminium centres

The report of gaseous AlCl at 1000 °C in 1948 initiated studies of the chemistry of molecular aluminium(I).[5] It was not until 1989, however, that the Schnöckel group reported a toluene/diethyl ether solution of AlCl which is metastable at −78 °C.[9] The availability of this reagent enabled the preparation of the first room-temperature stable aluminium(I) molecule, namely the tetrameric $[AlCp^*]_4$ ($Cp^* = \{\eta^5\text{-}(C_5Me_5)\}$).[6] The tetrameric structure observed in the solid state can be attributed to the interactions of the lone pair of each AlCp* moiety with the low-lying σ*(Al-C) orbital of the other units, stabilising the compound both thermodynamically and kinetically. Reactivity studies of $[AlCp^*]_4$, however, revealed that the molecule behaves as four individual units of pentamethylcyclopentadienyl-aluminium(I), either reacting as a Lewis base donor or as a two electron reductant *via* oxidative addition at the metal centre (**Scheme 3.1**).[10-12]

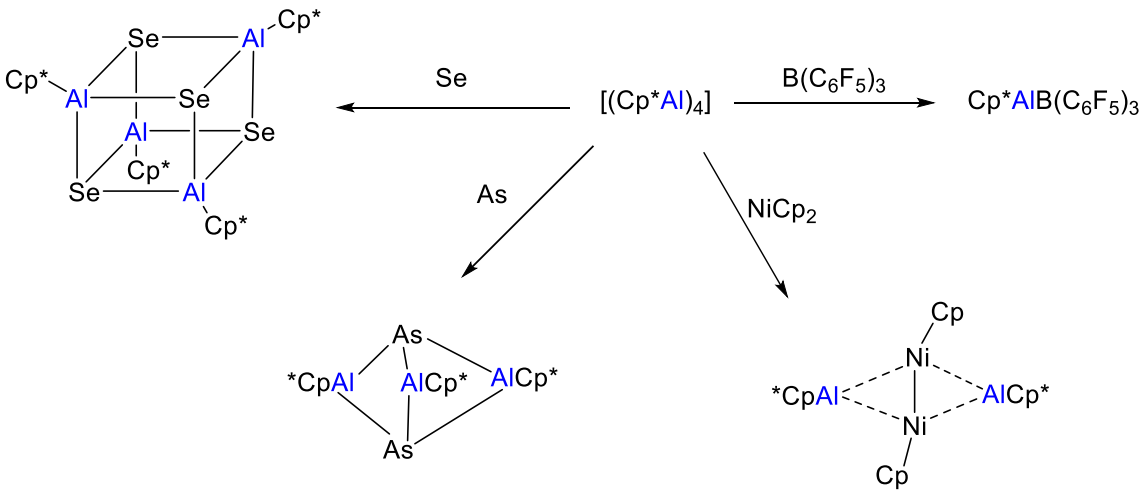

Scheme 3. 1 : Selected examples of reactions of $[Al\{\eta^5\text{-}(C_5Me_5)\}]_4$.[10-12]

The first structurally characterised monomeric neutral aluminium(I) singlet carbene analogue was made possible with the β-diketiminate backbone, $\{^{Dipp}BDI\}$ (where ^{Dipp}BDI = $CH(CMeNDipp)_2$, Dipp = 2,6-diisopropylphenyl). In this case, the adjacent nitrogen atoms stabilise the metal centre thermodynamically whilst providing considerable steric hindrance with its substituents, rendering kinetic stability as a monomer in solid state.[7] The chemistry of $[\{^{Dipp}BDI\}Al]$ (**3.1**, previously described as **1.23** in **Section 1.2**) has been comprehensively documented since its initial report, with the vast majority of its reactivity predicated on oxidative addition across the Al(I) centre. **3.1** displays small molecule activation chemistry

reminiscent of that of a *d*-block organometallic complex, such as various oxidative addition reactions of E-X bonds (**Scheme 3.2a**).[13] [1+2] cycloadditions of **3.1** with ethyne have also been reported, where a three-membered aluminacyclopropene (**3.2**) can be obtained when the temperature is kept under −50 ˚C. In contrast, compound **3.3** was isolated when the reaction was warmed back to room temperature in the presence of an excess amount of acetylene (**Scheme 3.2b**).[14] The latter molecule (**3.3**) can be considered as the result of further reaction from **3.2**, exhibiting an enhanced reactivity originating from the highly strained three-membered cyclic structure. This behaviour was subsequently elaborated through a thermally more stable aluminacyclopropene derivative **3.4** (**Scheme 3.2c**).[15]

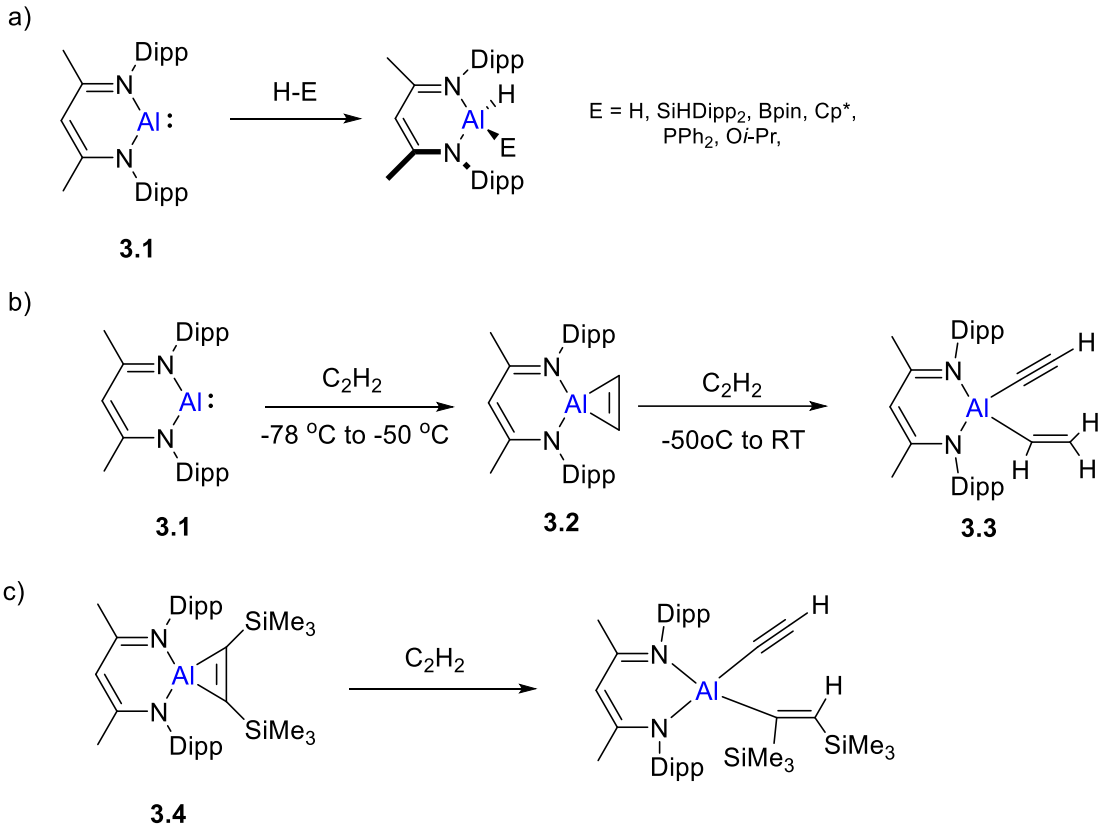

Scheme 3. 2 : Selected reactions of [{^{Dipp}BDI}Al(I)] (**3.1)** and its derivatives.[13-15]

The *d*-block like behaviour and oxidative addition at the Al(I) centre arising from compound **3.1** can be rationalised by its non-bonding electron pair and a low-lying empty p_π orbital at the Al centre, providing a valence electronic structure reminiscent of that of a transition metal (As previously discussed in **Section 1.1**). Subsequently, other monomeric neutral aluminium(I) carbenoids have also been realised with various supporting groups. Advancing from the previously reported tetramer $[AlCp^*]_4$, the recent implementation of a bulkier cyclopentadienyl group hampers the interaction between individual aluminium centres

and subsequently facilitates the isolation of monomeric derivatives.[16,17] Even more recently, 1-coordinate aluminium(I) has also been realised through the use of various super bulky C- and N-donor ligands (**Figure 3.1**).[18,19]

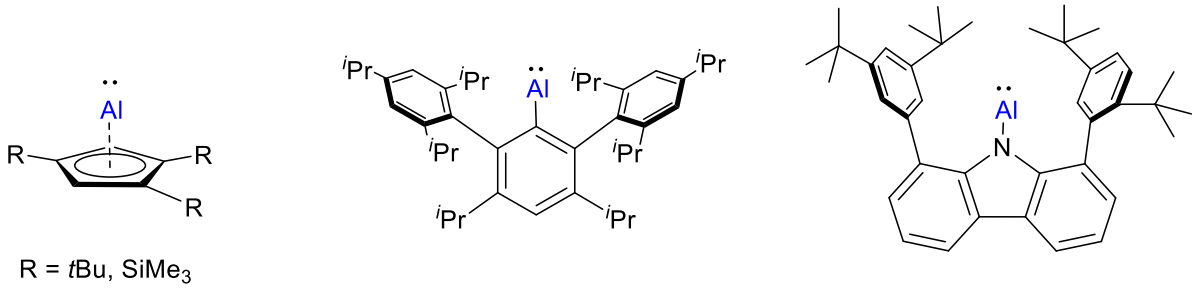

Figure 3. 1 : Selected examples of monomeric Al(I) carbenoids.[16-19]

3.1.2 Formally mono-anionic aluminium centres

3.1.2.1 Diamido ligand backbones

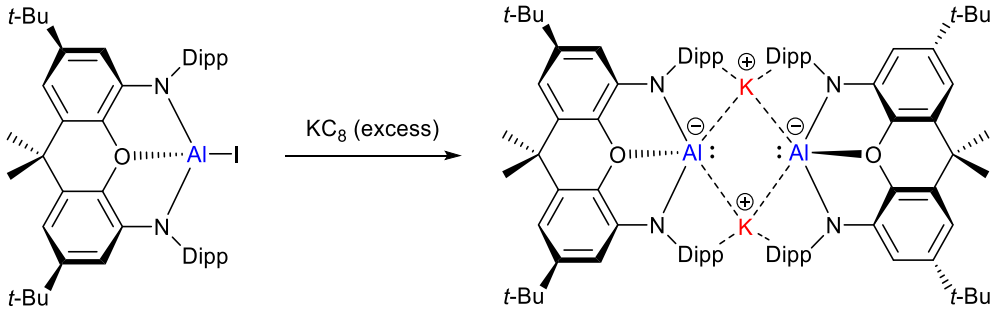

3.5

Scheme 3. 3 : Preparation of [{NON^{Dipp}}AlK]$_2$ (**3.5**).[8]

Although it is now 20 years since the first report of compound **3.1**, and various monomeric neutral aluminium(I) species have now been prepared, the realisation of the first anionic aluminium(I) carbene analogue was only achieved by Aldridge, Goicoechea and co-workers in 2018. The co-ligand [NON^{Dipp}]$^{2-}$ (NON^{Dipp} = 4,5-bis(2,6-di-isopropylanilido)-2,7-di-tert-butyl-9,9-dimethylxanthene) withdraws excess electron density from the reduced aluminium centre, coordinates the low-lying 3p-orbital with an oxygen atom, and provides significant steric protection. These features stabilise the anionic aluminium(I) complex [{NON^{Dipp}}AlK]$_2$ (**3.5,** previously described as **1.25** in **Section 1.2**), which was synthesised by potassium reduction of its corresponding Al(III) iodide, [{NON^{Dipp}}AlI] (**Scheme 3.3**).[8] X-ray crystallography revealed that **3.5** exists as a dimeric structure in the solid state, in which potassium-arene contacts propagate each dimer unit and plausibly further stabilise the highly reactive aluminium(I) centres. In addition, the solid-state data suggest the absence of any significant

interaction between the aluminium centres (Al-Al > 6.6 Å), while the elongated Al-N separations (1.956(2) and 1.963(2) Å, where Al-N = 1.846(2) Å in {NON^{Dipp}}AlI) further supported the attribution of a +I oxidation state to the aluminium centres.

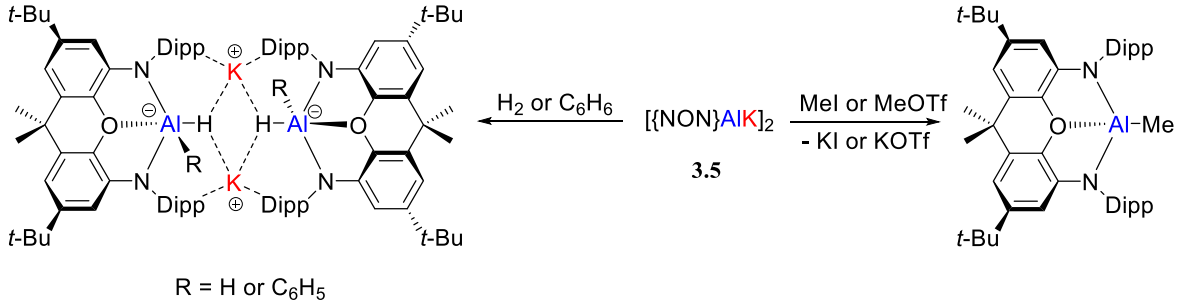

Scheme 3. 4 : Selected examples of reactions of [{NON^{Dipp}}AlK]$_2$ (**3.5**).[8]

Compound **3.5** exhibits enhanced, and unprecedented reactivity compared to its neutral counterparts, plausibly due to the higher nucleophilicity of the aluminium-centred lone pair resulting from the formal negative charge. [{NON^{Dipp}}AlK]$_2$ (**3.5**) readily activates small molecules such as H_2 and benzene, cleaving the respective H-H and C-H bonds to yield the formal oxidative addition products and generate new aluminium-element bonds (**Scheme 3.4**). In addition, compound **3.5** has been demonstrated to behave as a potent aluminium centred nucleophile. For instance, Al-C bonded complexes were obtained through the reaction of [{NON^{Dipp}}AlK]$_2$ (**3.5**) with carbon-centred electrophiles (e.g. MeI and MeOTf), indicating nucleophilic attack of the electrophilic carbon centres by the aluminium centre (**Scheme 3.4**).[8] This type of nucleophilic substitution has also subsequently been employed in the formation of a range of unsupported Al-element bonds (selected Al-E bonds: E = Li, Be, Mg, Al, Cu, Zn, Ag, Au), chemistry which will be described in detail in **Section 4.1**.[8,20-23]

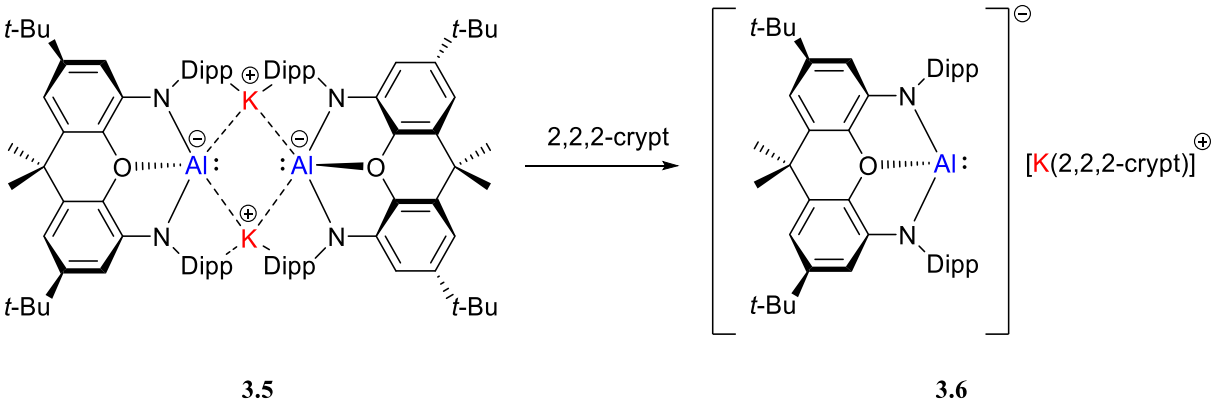

3.5 **3.6**

Scheme 3. 5 : Preparation of the monomeric aluminium(I) anion **3.6**.[24]

As discussed previously, the dimeric nature of **3.5** is considered as a stabilising factor in the isolation of the anionic aluminium(I) complex, and the removal of the cation-arene interaction can drastically alter its behaviour. In this vein, Aldridge, Goicoechea and co-workers prepared a monomeric aluminium anion by adding two molar equivalents of the group 1 metal abstractor, [2,2,2]-cryptand (4,7,13,16,21,24-hexaoxa-1,10-diazabicyclo[8.8.8]hexacosane), to compound **3.5**, obtaining the charge separated molecule [K(2,2,2-crypt)][Al{NON^{Dipp}}] (**3.6**) (**Scheme 3.5**).[24] The monomeric nature of **3.6** was confirmed by its solid state X-ray diffraction analysis (all K···Al interactions > 7 Å), and, more notably, its reaction with benzene provides reversible C=C bond activation of the arene *via* the formation of two new Al-C bonds (**Scheme 3.6**). This contrasts significantly with the C-H bond activation of benzene exhibited by the dimeric aluminium(I) species **3.5**, implying the K$^+$-Dipp interaction is indeed an influential feature in the reactivity of compound **3.5**.[24]

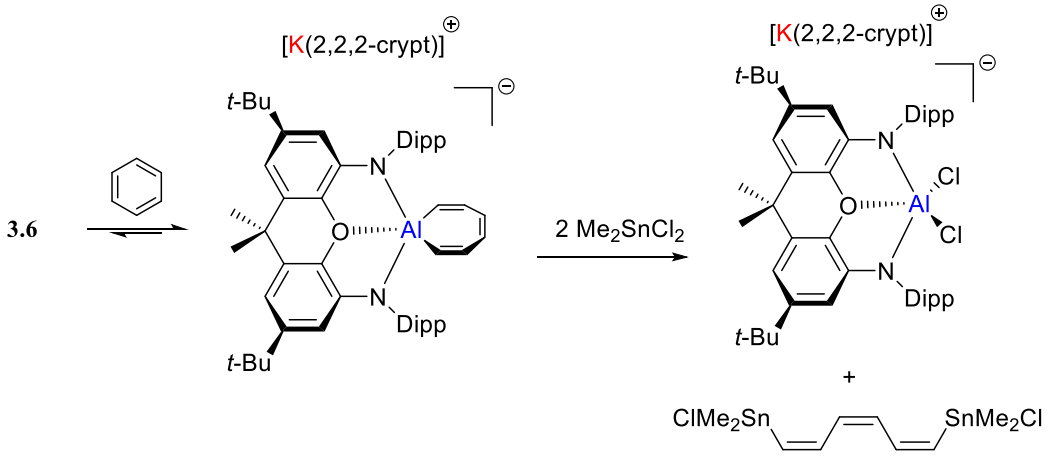

Scheme 3. 6 : The C-C activation and functionalisation of benzene using compound **3.6**.[24]

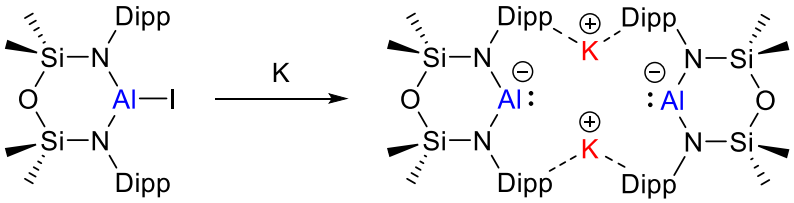

3.7

Scheme 3. 7 : Synthesis of [{OSiN^{Dipp}}AlK]$_2$ (**3.7**).[25]

Encouraged by the successful isolation of complex **3.5**, Coles and co-workers prepared a novel alumanyl anion (**3.7,** previously described as **1.26** in **Section 1.2**) with the dianionic bis(amidodimethyl)disiloxane ligand {OSiN^{Dipp}} ({OSiN^{Dipp}} = [O(SiMe$_2$NDipp)$_2$]$^{2-}$), which had previously been reported to facilitate the isolation of other low oxidation state *p*-block molecules.[26] Similar to [{NON^{Dipp}}AlK]$_2$ (**3.5**), [{OSiN^{Dipp}}AlK]$_2$ (**3.7**) was prepared by

potassium reduction of its aluminium(III) iodide precursor (**Scheme 3.7**).[25] Compound **3.7** again exhibited a dimeric structure originating from two-fold potassium-arene associations between each [{OSiN^{Dipp}}Al] moiety and the potassium cations in the solid state. Moreover, this structural characterisation found neither a chemical bond between the aluminium centres (Al-Al = 5.673(1) Å), nor an O-to-Al coordination (Al-O = 3.356(2) and 3.418(2) Å) which was a feature of compound **3.5**. The reactivity of **3.7** has been scrutinised towards various substrates since its initial report. An aromatic $[COT]^{2-}$ dianion was obtained by the two-electron reduction conducted by $[\{OSiN^{Dipp}\}AlK]_2$ (**3.7**), in which the planar aromatic moiety exhibits μ_2-η^2:η^8-interactions with the aluminium centre and the potassium cations. Disruption of the polymeric structure arising from this interaction was achieved with 18-crown-6, resulting in a further transformation into [K(18-*c*-6)][({OSiN^{Dipp}}Al)(COT)], which is essentially the (1+4) cycloaddition product of COT to the aluminium centre (**Scheme 3.8a**);[25] a reactivity redolent of that of the neutral [{^{Dipp}BDI}Al] (**3.1**).[27] A selection of hetero element-aluminium bonds have also been realised through the formal oxidation of compound **3.7**, including the synthesis of Al-selenium multiple bonded species (**Scheme 3.8b**).[28] Both described low oxidation state aluminium species (**3.5** and **3.7**) were also recently reported to facilitate reductive couplings of CO molecules. In these cases, the C–C bond formation products varied according to the applied reaction conditions, highlighting the enhanced reactivity of the anionic aluminium(I) centre.[29,30]

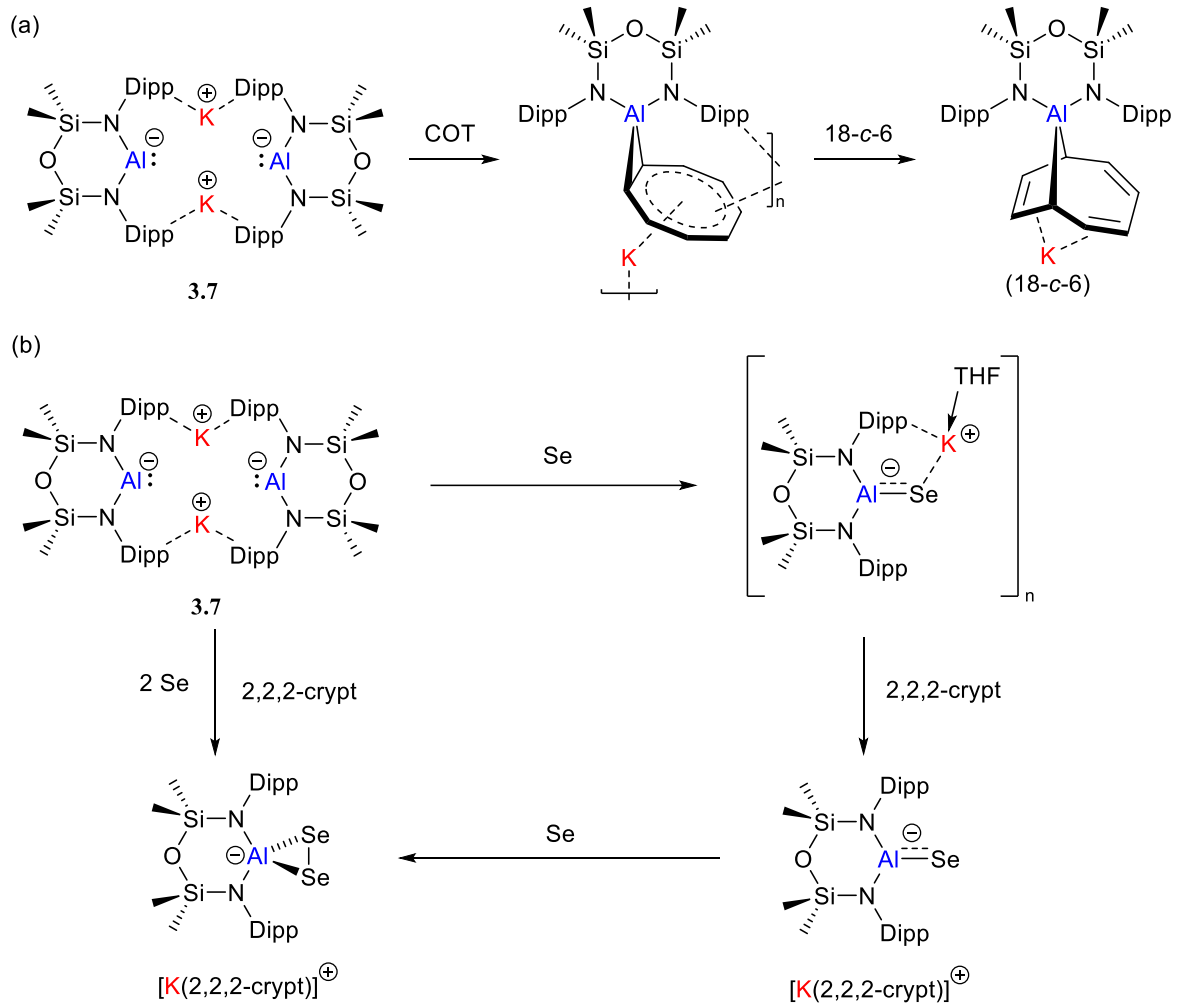

Scheme 3. 8 : Selected examples of reactions of [{OSiN^{Dipp}}AlK]$_2$ (**3.7**).[25,28]

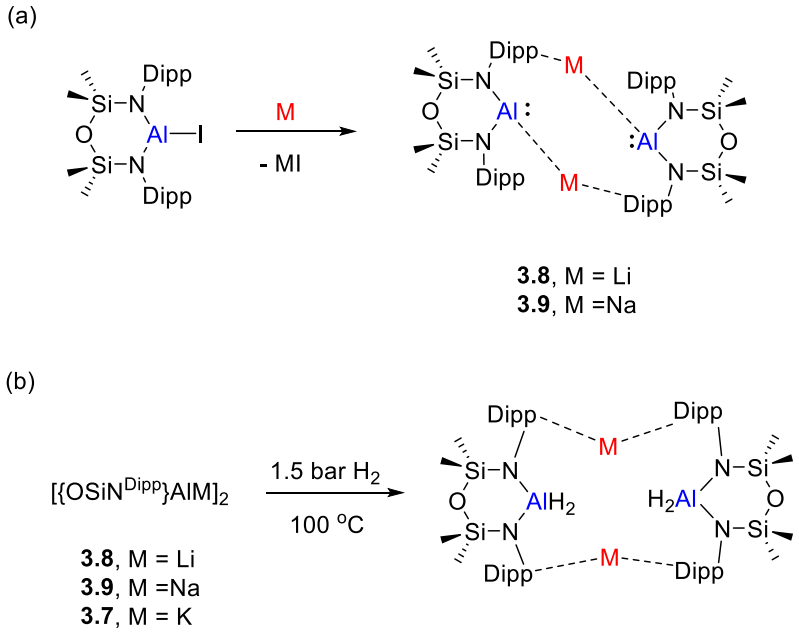

Scheme 3. 9 : (a) Lithium and sodium reduction of [{OSiN^{Dipp}}AlI] (b) H_2 activation mediated by compounds **3.8**, **3.9**, and **3.7**.[31]

The consequences of changing the identity of the group 1 metal in the Al(I) species have also been investigated. Lithium and sodium analogues of [{OSiN^{Dipp}}AlK]$_2$ (**3.7**) can be prepared by direct reduction of the aluminium(III) iodide with the respective metal ([{OSiN^{Dipp}}AlLi]$_2$ (**3.8**), [{OSiN^{Dipp}}AlNa]$_2$ (**3.9**), **Scheme 3.9a**), or by treatment of **3.7** with lithium iodide in diethyl ether giving the lithium congener **3.8**.[31] In a sharp contrast, the lithium reduction of [{NON^{Dipp}}AlI] only gives the Al-N bond cleavage product, while the related sodium reduction exclusively gives the dialumane,[{NON^{Dipp}}Al-Al{NON^{Dipp}}]. Isolation of [{OSiN^{Dipp}}AlK]$_2$ (**3.7**) and its lighter analogues (**3.8** and **3.9**) has enabled the preparation of a series of novel aluminium hydrides (**Scheme 3.9b**).[31] The formal oxidative addition of H_2 to the aluminium centres was found to require harsher conditions (100 ^oC, 1.5 bar of H_2) in the {OSiN^{Dipp}} systems compared to that in **3.5**. A difference in the H_2 activation rate was observed across the dissimilar group 1-[{OSiN^{Dipp}}Al] species, where the time required for 50% conversion of the starting materials is in a relative order of Li (1.5 days), Na (6 days), and K (12 days). On the other hand, the heavier alkali metal counterparts (**3.10** and **3.11**) of **3.7** have also been prepared by the respective rubidium and caesium reduction of [{OSiN^{Dipp}}AlI] (**Scheme 3.10**).[32] Like compound **3.7**, [{OSiN^{Dipp}}AlRb] (**3.10**) and [{OSiN^{Dipp}}AlCs] (**3.11**) were found to exhibit dimeric structures *via* persistent cation-arene interactions in the solid state. The geometry of each [{OSiN^{Dipp}}Al] unit in the dimer was found to be dependent on the identity of the group 1 metal, in that considerable angles were observed between the two Al-N-Si-O-Si-N heterocyclic planes (66.55(4)° in **3.10** and 66.31(5)° in **3.11**). Furthermore, C-H activation of C_6H_6 was found to be exclusively mediated by [{OSiN^{Dipp}}AlCs] (**3.11**) across all the group 1 analogues of **3.7**, indicating the significant influence of the identity of group 1 metal in this class of molecule.[31,32]

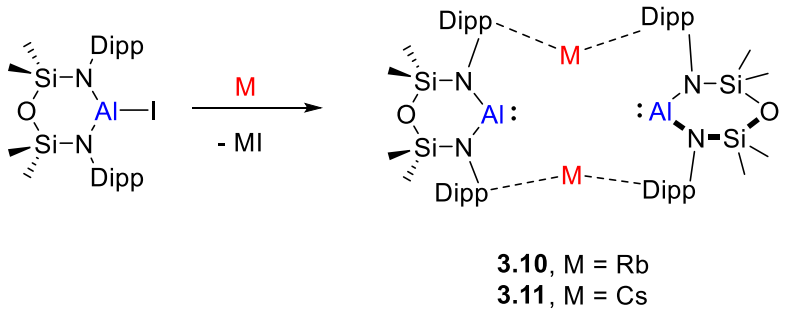

Scheme 3. 10 : Rubidium and caesium reduction of [{OSiN^{Dipp}}AlI].[32]

Several similar species bearing formally negatively charged aluminium(I) centres supported by a diamido-ligand backbone have been reported since the initial reports of

compounds **3.5** and **3.7**. Shortly after the report of **3.7**, Hill and co-workers demonstrated that closely related seven-membered potassium alumanyls can be prepared following an analogous reaction protocol (**3.12**, **3.13**, **Figure 3.2,** where **3.12** was previously described as **1.27** in **Section 1.2**),[33,34] although the synthesis of less sterically encumbered [{SiN^{Mes}}AlK]$_2$ (**3.13**) always gives an inseparable mixture of the Al(I) and Al(II) species. Furthermore, Harder and co-workers have reported that the treatment of KHMDS with **3.1** provides the related potassium diamido-aluminium(I) complexes (**3.14**),[35] and the corresponding heavier and lighter group 1 congeners have also been isolated (**3.15 — 3.18**, **Figure 3.2**).[36] Very recently, the field has also delivered a novel six-membered [{C$_3$NDipp}AlK]$_2$ complex (**3.19**), which facilitated the synthesis of an unprecedented Al-Sc bonded species.[37] Moreover, an acyclic anionic diamido aluminium(I) complex (**3.20**) has also been realised by Liptrot, Hicks and co-workers (**Figure 3.2**).[38]

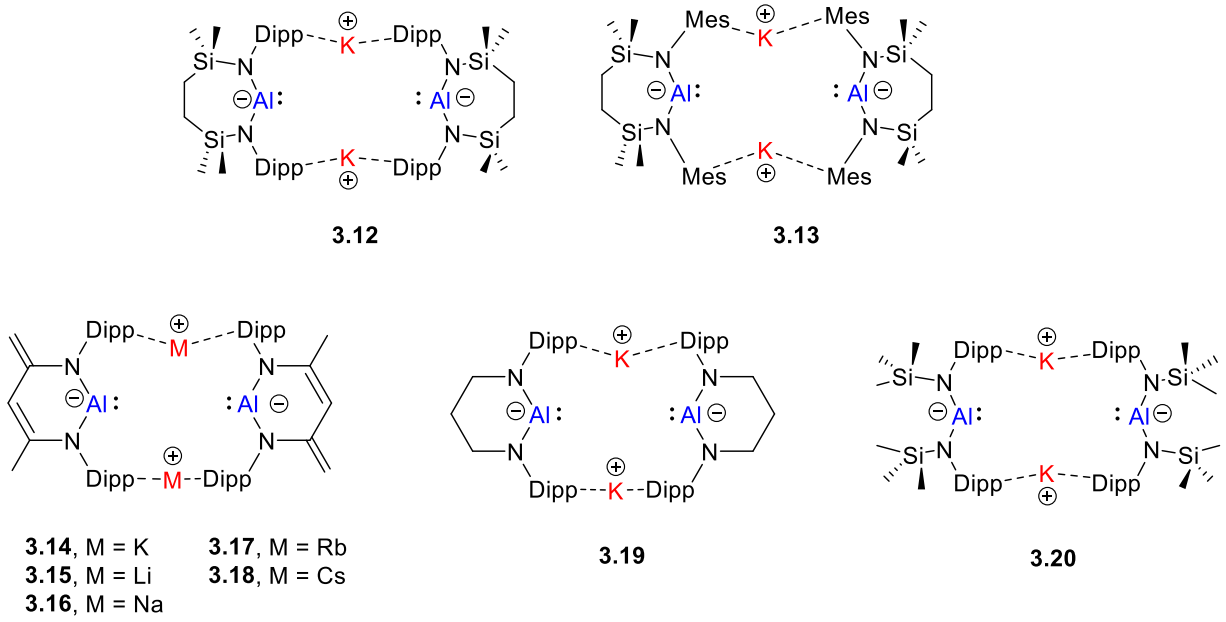

Figure 3. 2 : Examples of potassium diamido aluminium(I) complexes.[33-38]

3.1.2.2 Dialkyl and alkylamido ligand backbones

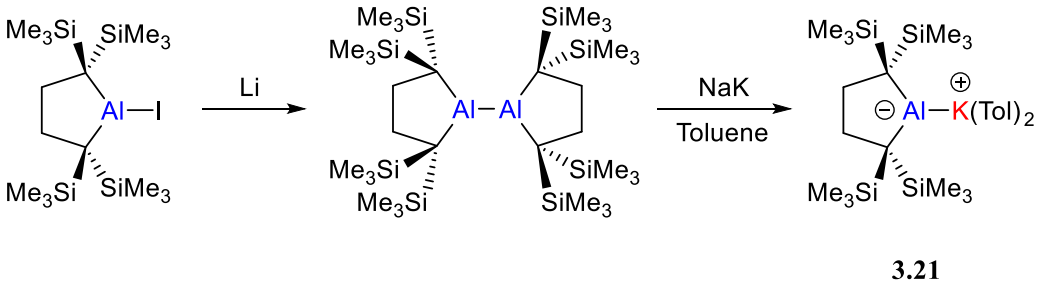

Scheme 3. 11: The synthesis of the dialkyl-substituted anionic alumanyl complex (**3.21**) (Tol = toluene).[39]

As previously described in **Section 1.1** and **1.2**, the adjacent substituents heavily influence the behaviour of the low-oxidation state carbon centre of singlet carbenes. In this vein, chelating C,C'-(dialkyl) and C,N-(alkyl)(amido) ligands have been utilised in the preparation of related anionic Al(I) species. Prompted by its previous successful implementation in silylene chemistry,[40] the tetrakis(trimethylsilyl)butylene ligand was selected by Yamashita and co-workers in the synthesis of an anionic aluminium(I) species supported by a wholly carbon-based donor system. Lithium reduction of the corresponding aluminium(III) iodide complex gives the dialumane, which was subsequently reduced by sodium-potassium alloy to afford the aluminum(I) species (**3.21**, **Scheme 3.11**).[39] In contrast to the potassium alumanyls (**3.5**, **3.7**, **3.12 – 3.14**, **3.19**, **3.20**) described previously, compound **3.21** was determined by X-ray diffraction studies to be a monomeric five-membered aluminium-containing heterocycle in the solid state. In addition, a significant interaction between the aluminium centre and the potassium cation can be inferred from its significantly shorter Al-K separation (3.4549(5) Å) compared to those in **3.5**, **3.7**, and **3.12** (5.673(1)-6.627(1) Å).

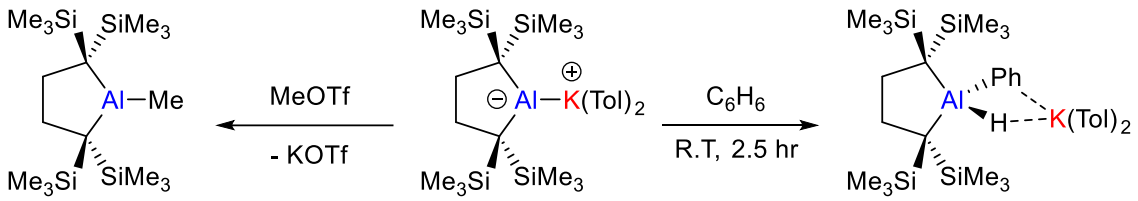

3.21

Scheme 3. 12 : Selected examples of the reactivity exhibited by compound **3.21**.[39]

In a similar manner to compound **3.5**, the aluminium centre in **3.21** exhibits nucleophilicity evident from its nucleophilic attack on the electrophilic carbon centre of MeOTf (**Scheme 3.12**).[39] On the other hand, C-H activation of benzene transpired within 2.5 hours after the introduction of **3.21** to the solution, yielding the formally C-H oxidative addition product (**Scheme 3.12**).[39] The remarkably milder conditions compared to that required for the related reaction between **3.5** and benzene (4 days at 60 °C) highlights the effect of the alkyl substituents next to the low oxidation state element centre (as previously described in **Figure 1.4**).

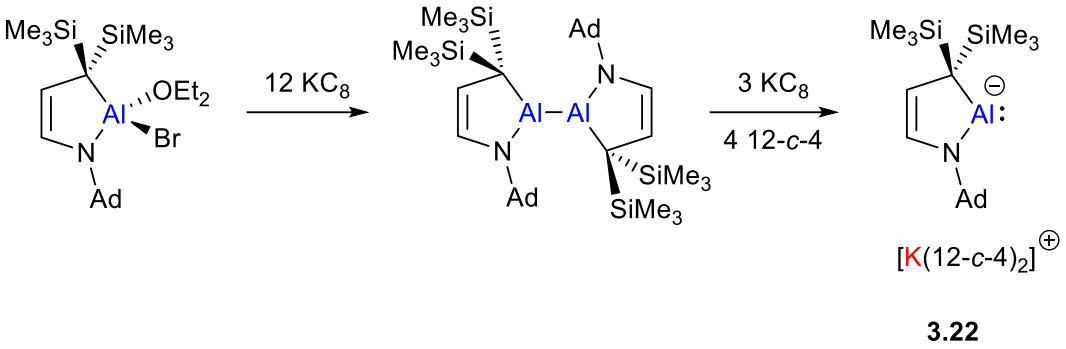

Scheme 3. 13 : Synthetic route to an alkylamido-substituted alumanyl **3.22**.[41]

Kinjo and co-workers expanded this class of alumanyl chemistry by pursuing an aluminium analogue of a CAAC. In a similar synthetic route to that employed in the synthesis of **3.21**, reduction of the corresponding dialumane achieves the preparation of an alkylamido-substituted alumanyl (**3.22**, **Scheme 3.13**).[41] Compound **3.22** provides an unprecedented trigonal *σ*-aromatic heteroatomic group 13 ring concomitant with a three-centre, two-electron AlB_2 bond when treated with Me_2S-BH_3. In contrast, oxidative addition of the E-H bond to the aluminium metal centre was observed when reacting **3.22** with phenylsilane and ammonia, illustrating the *d*-block-like nature of this alumanyl system (**Scheme 3.14**).[41]

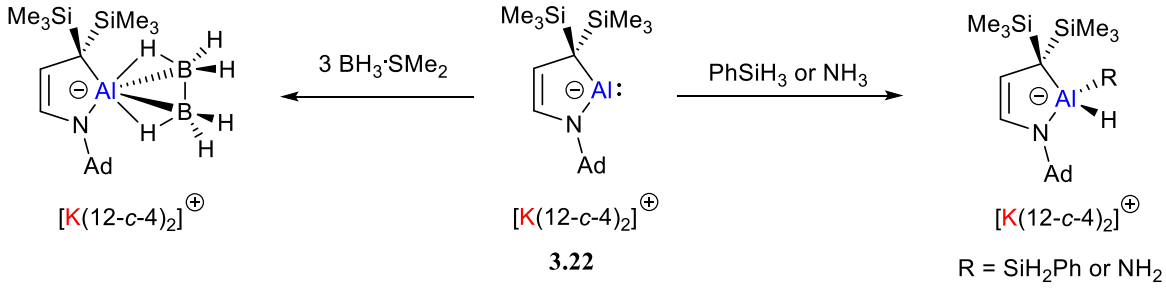

Scheme 3. 14 : Selected examples of the reactivity exhibited by compound **3.22**.[41]

3.1.2.3 Electronic structures of the anionic aluminium(I) centres

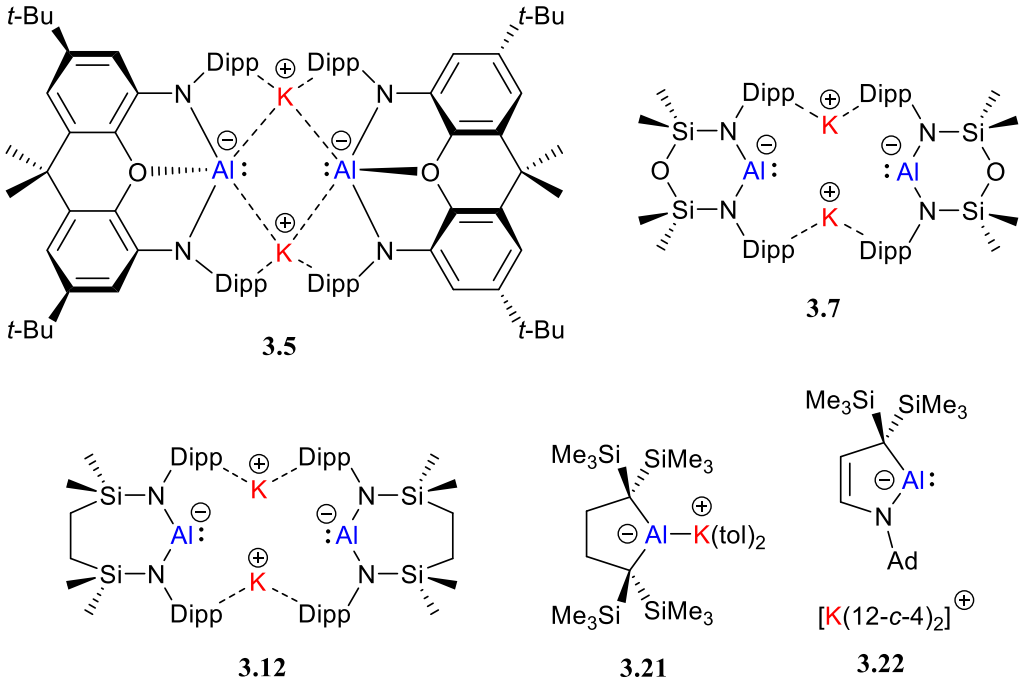

Figure 3. 3 : The five alumanyl systems discussed herein.[42]

To shed light on the reactivity of the negatively charged aluminium(I) centres, Aldridge, Goicoechea and co-workers performed DFT calculation on the electronic structures on five of the discussed alumanyl species (**3.5**, **3.7**, **3.12**, **3.21**, **3.22**, **Figure 3.3**). In a similar vein to the low oxidation state carbon centres in various *N*-heterocyclic carbenes described in **Section 1. 1**, these aluminium(I) species were analysed *in silico* by the energy separations between their occupied and vacant orbitals at the Al(I) centre (namely the lone pair of electrons and the empty p_{π}-orbital, respectively).[42] Although the computational study was conducted on the monomeric anions with any effects exercised by the interactions with the counter-cations disregarded, the analysis still provides qualitative insight into the influences of the amido and/or the alkyl substituents on the anionic alumnium(I) centred behaviour.

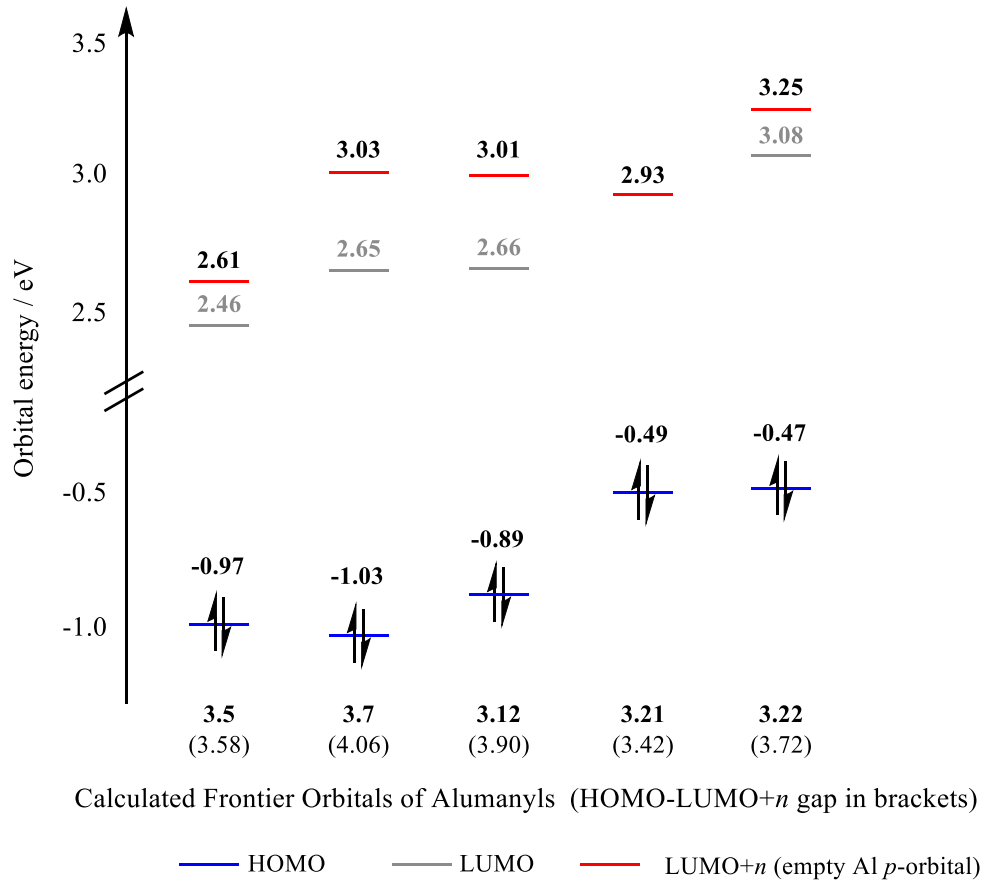

Figure 3. 4 : The computed frontier orbital energies (eV) of HOMO, LUMO and LUMO+n in five representative alumanyl species (**3.5**, **3.7**, **3.12**, **3.21**, **3.22**) at the DFT-D3, PBE0, Def-TZVP level of theory, where LUMO+n represents the orbital associated with the empty aluminium p_π-orbital.[42]

The HOMO approximates to a non-bonding orbital localised on the aluminium centre in each alumanyl, largely the Al(I) electron lone pair. As shown in **Figure 3.4**, the HOMOs in diamido alumanyls (**3.5**, **3.7**, **3.12**) exhibit comparable orbital energies, with the HOMOs in the alkyl-substituted systems (**3.21**, **3.22**) higher in energy. This divergence in orbital energies may be rationalised by the absence of one or two α-electron withdrawing groups for **3.22** and **3.21**, respectively.

On the other hand, the LUMOs were found to be ligand-based unoccupied orbitals in all the selected aluminium(I) species apart from compound **3.21**, in which the LUMO is attributed to the Al p_π-orbital. As a result, the dialkyl- substituted species (**3.21**) exhibits the smallest energy gap between the HOMO and the Al p_π-orbital (3.42 eV) across the assayed alumanyls. In the alkylamido-substituted alumanyl (**3.22**), the aluminium p_π-orbital is found to be the LUMO+1, notably higher in energy than that of **3.21** despite the similarity in energy of their HOMOs. This observation may be attributed to the π-donation from the single adjacent amido

substituent, which 'destabilises' the aluminium p_z-orbital and results in the larger energy separation (3.72 eV) observed by the DFT study.

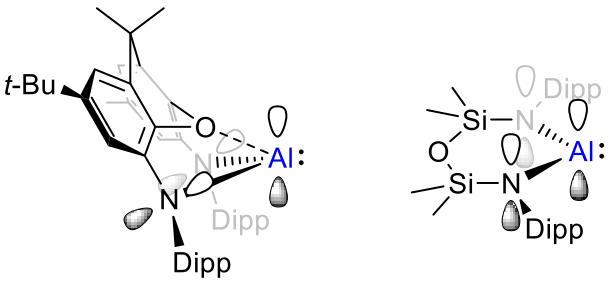

3.5 **3.7**

Figure 3. 5 : Visualisation of the orbitals involved in the N-Al π-interaction in compounds **3.5** and **3.7**.

As depicted in **Figure 3.5**, the planar geometry of the [{OSiN^{Dipp}}Al] moiety in compound **3.7** allows an enhanced Al-N π-interaction in comparison to that in compound **3.5**. The stronger mesomeric effect from the α-amido substituents, therefore, provides the higher energy Al p$_\pi$-orbitals in compound **3.7**. With its lower energy electron lone pair, compound **3.7** features the largest energy separation (4.02 eV) in the class of aluminum(I) species. Furthermore, the non-planar geometry of compound **3.5** enforced by the xanthene backbone provides a N-Al-N angle of 53.7° and considerably longer Al-N bonds (2.022(1)/2.049(1) Å) compared to those in **3.7** (1.879(2)-1.896(2) Å). The N→Al π-donation is thus severely perturbed, and the Al p$_\pi$-orbital in **3.5** is therefore more energetically accessible, as quantified by a separation in energy of 3.57 eV.

Whilst featuring a comparable planar diamido-backbone to that of compound **3.7**, compound **3.12** exhibits a slightly smaller energy separation (3.90 eV) between the HOMO and the aluminium p$_\pi$-orbital in comparison to that imposed by the siloxane-derived ligand {OSiN^{Dipp}}. This divergence may be rationalised by the larger chelate size of **3.12** enforcing a wider N-Al-N angle (**3.7**: 103.89(8)°; **3.12**: 108.84(9)°), increasing the s character in the Al-N bond and in turn destabilising the Al(I) centred lone-pair orbital.

3.1.3 Seven-membered cyclic potassium diamidoalumanyl (**3.12**)

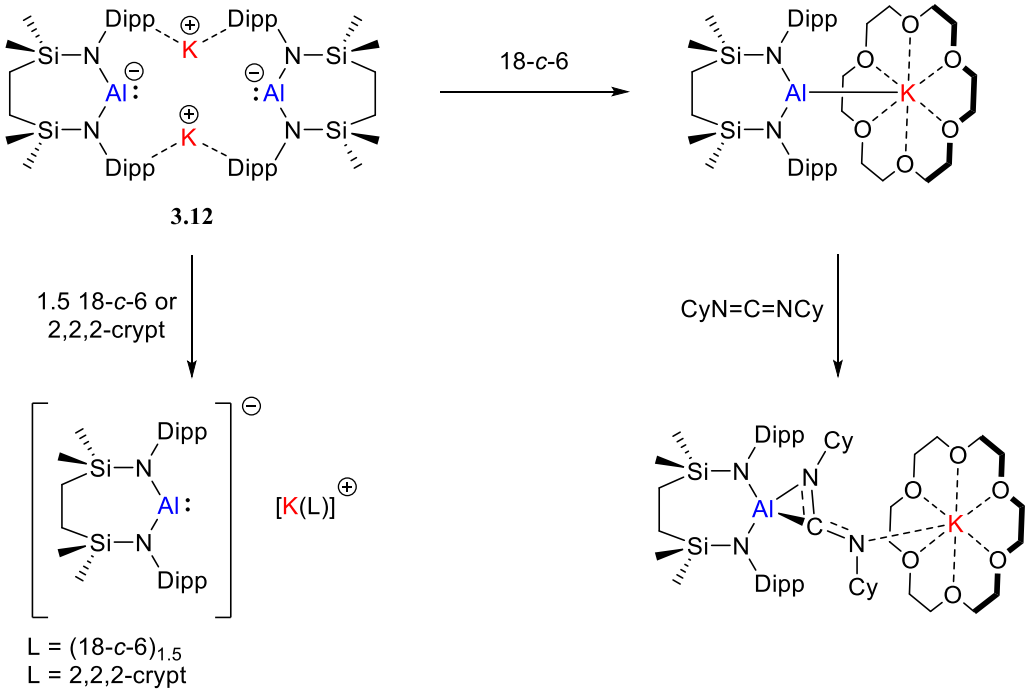

Scheme 3. 15 : Synthesis of monomeric derivatives of **3.12** and related reactivity studies.[33,34]

Although the comparable six-membered cyclic potassium diamidoalumanyl [{OSiN^{Dipp}}AlK]$_2$ (**3.7**) has been reported, and its reactivity was in the process being studied and described by Coles and coworkers at the start of this project, the difference in the aluminium(I) based frontier orbital between compound **3.7** and the seven membered [{SiN^{Dipp}}AlK]$_2$ (**3.12**) encourages further investigation of compound **3.12**.[33, 34] Furthermore, although the preparation of monomeric derivatives of **3.12** (**Scheme 3.15**) and related reactivity studies had been conducted in the Hill group, reactivity studies of **3.12** were still in their preliminary stages at the start of this project (**Scheme 3.15**). This chapter will, therefore, focus on a more wide-ranging scrutiny of the chemistry of seven-membered cyclic potassium diamidoalumanyls exemplified by [{SiN^{Dipp}}AlK]$_2$ (**3.12**).

3.2 Assessment of the Aluminium(I) Centred Behaviour in [{SiN^{Dipp}}AlK]$_2$

As discussed in the previous section, aluminium centred Lewis basicity and/or nucleophilicity is the diagnostic property of an aluminium(I) species. The reactivity of [{SiN^{Dipp}}AlK]$_2$ (**3.12**) was, therefore, firstly examined by treatment of a boron-centred Lewis acid and a carbon-based electrophile (**Scheme 3.16**).

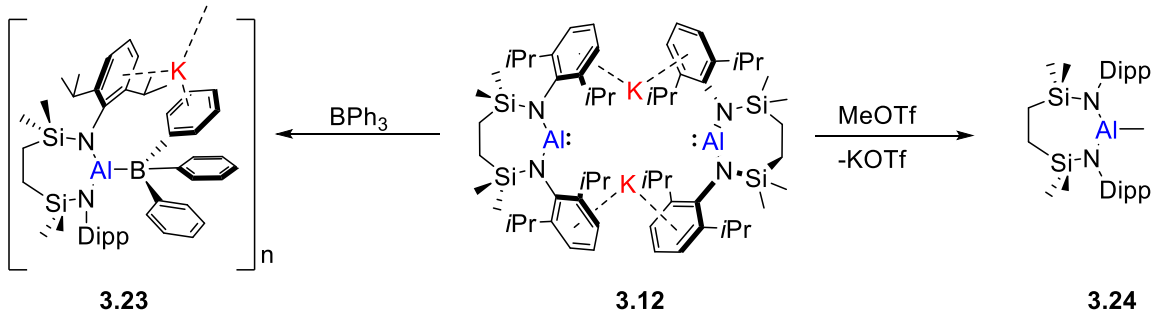

3.23 **3.12** **3.24**

Scheme 3. 16 : Reaction of [{SiN^{Dipp}}AlK]$_2$ (**3.12**) with BPh$_3$ and MeOTf.

Reaction of compound **3.12** with two molar equivalents of triphenylborane (a one-to-one stoichiometry of aluminium to boron) gives compound **3.23** as the single product in moderate yield (67%). Although *in-situ* monitoring of the formation of **3.23** was hampered by its low solubility in arene solutions, its NMR characterisation was enabled by the more polar solvent CDCl$_3$. ^{1}H and ^{13}C{^{1}H} NMR spectra of **3.23** comprise a single set of *i*-Pr signals, indicating a significant level of free rotation within the molecule. On the other hand, no resonance correlated to the formation of 4-coordinated boron environments could be found in the corresponding ^{11}B NMR spectrum, supporting the incorporation of boron into a non-spherically symmetric environment and its bonding to a similarly quadrupolar ^{27}Al atom (*I*=5/2; 100 %). This deduction was confirmed by X-ray diffraction analysis of a single crystal obtained from a saturated toluene solution of **3.23**, which was identified to be a potassium aluminaborate species (**Figure 3.6**, **Table 3.1**). Consistent with its low solubility in non-polar solvents, compound **3.23** features a polymeric structure, where a network of the aluminaborate anions are propagated by a combination of polyhapto K-B*Ph* and K-N*Dipp* interactions. The Al1−B1 separation (2.190(3) Å) in compound **3.23** lies marginally outside the range of Al−B bond lengths (2.1147(15)–2.183(3) Å) previously described in B(C$_6$F$_5$)$_3$ and 9-borafluorene adducts with the charge neutral cyclopentadienyl substituted Al(I) species and [{BDI^{Dipp}}Al].[12,43-45]

"Is that like the Gomberg dimer?" – A. -F. Pécharman, 2019.

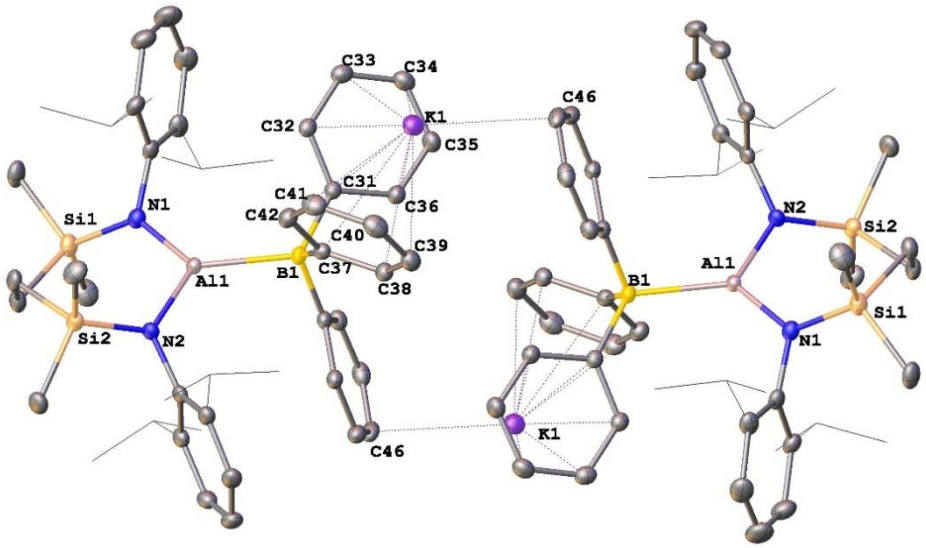

Figure 3. 6 : Displacement ellipsoid plots (30% probability) of parts of the polymeric structures of compound **3.23**. (Symmetry operations to generate equivalent atoms, [i]−1/2+x, 3/2−y, −1/2+z; [ii] 1−x,1−y,1−z; [iii] 1/2+x, 3/2−y, 1/2+z). Minor components of disordered atoms and hydrogen atoms have been removed for clarity. Wireframe view has been employed for some groups, also for visual simplicity.

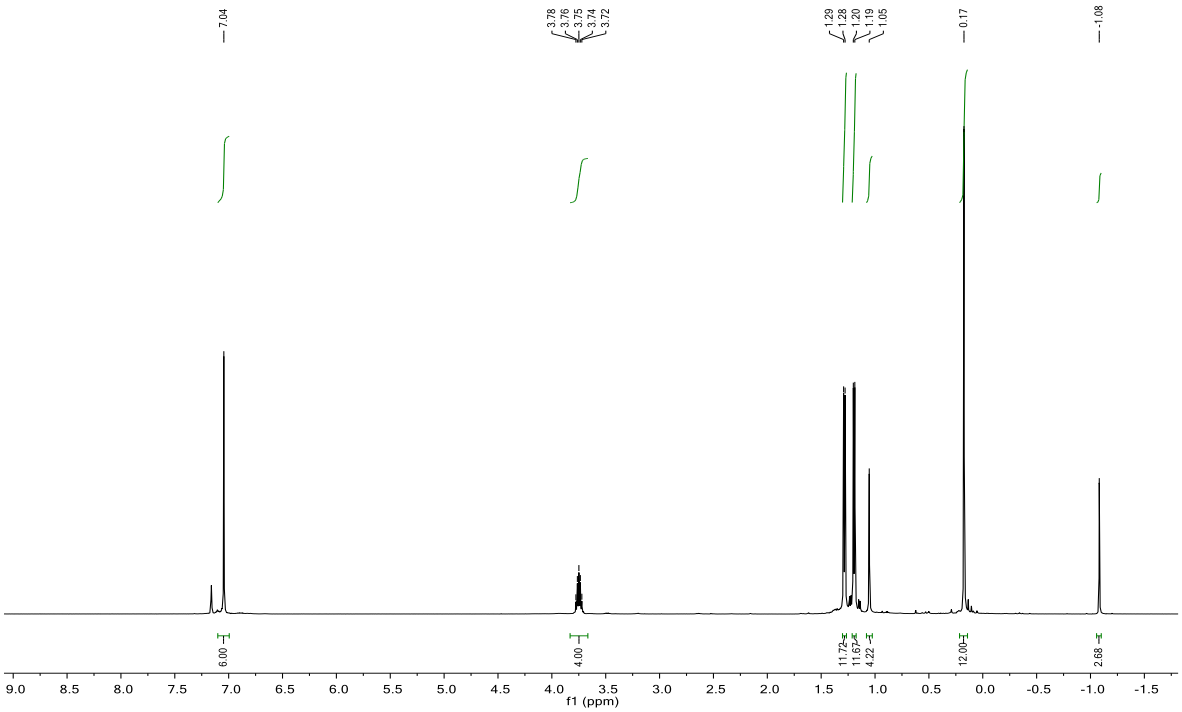

Figure 3. 7 : The *in-situ* generated ^{1}H NMR (500 MHz, 298 K, C_6D_6) spectrum of **3.24**.

Analogous to the described nucleophilic reactivity of **3.5** and **3.21**,[8,39] reaction of [{SiN^{Dipp}}AlK]$_2$ with MeOTf readily provided the related methyldiamidoalumane (**3.24**, **Figure 3.7**). Quantitative formation of [{SiN^{Dipp}}AlMe] (**3.24**) was confirmed by ^{1}H and ^{13}C NMR spectroscopy by comparison with the previously reported spectra of the methylalumane, **3.24**. The reaction of **3.12** with triphenylborane to provide the Lewis adduct (**3.23**) and the nucleophilic substitution product (**3.24**) yielded by MeOTf imply compound **3.12** indeed exhibits a Al(I)-centred nucleophilicity, characteristic of a low oxidation state aluminium species.

	3.23	**3.25**	**3.26**
Al1-N1	1.863(2)	1.7964(11)	1.8426(10)
Al1-N2	1.874(2)	1.7990(12)	1.8458(10)
Al1-X	2.190(3) [a]	2.0074(14) [b]	2.7330(6) [c]
N1−Al1−N2	111.34(10)	121.14(5)	114.28(5)
N1−Al1−X	127.75(11) [a]	124.67(6) [b]	124.21(3) [c]
N2−Al1−X	120.84(11) [a]	114.12(6) [b]	121.50(3) [c]

Table 3. 1: Selected bond lengths (Å) and angles (°) of compounds **3.23**, **3.25**, **3.26**. [a] X= B1; [b] X=C31; [c] X=Al1[1].

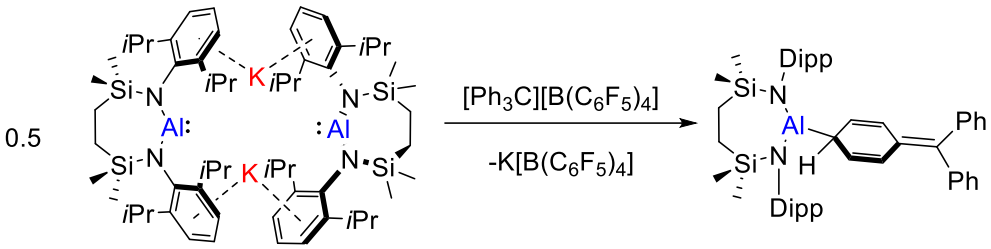

3.12 **3.25**

Scheme 3. 17 : Synthesis of **3.25**.

In contrast to its straightforward behaviour towards neutral electrophiles, the reaction of **3.12** with the BPh$_3$-isoelectronic trityl cation of [Ph$_3$C][B(C$_6$F$_5$)$_4$] demonstrated a series of rapid colour changes to green to bright red to light yellow within 10 minutes, alongside the

deposition of a crystalline material, which was identified as $K[B(C_6F_5)_4]$ by a unit cell check. Inspection of the remaining solution by ^1H NMR spectroscopy indicated the formation of one predominant new compound (**3.25**, **Scheme 3.17**), which was characterised by the appearance of two mutually coupled doublet of doublets resonances and a triplet signal at δ_H 5.99 (2H), 4.39 (2H) and 2.09 (1H) ppm, respectively (**Figure 3.8**). This observation was subsequently verified by X-ray diffraction analysis conducted on a colourless single crystal of **3.25**, revealing it to be a neutral diamidoalumane bearing a cyclohexadienyl substituent with an Al1−C31 bond length of 2.0074(14) Å (**Figure 3.9a**, **Table 3.1**). The cyclohexadienyl moiety inferred in the ^1H NMR spectrum of **3.25** is evident in its short C32−C33, C35−C36, and C34−C37 separations (1.340(2) Å, 1.340(2) Å, 1.369(2) Å), and the sum of angles at C37 of 359.6°. Whilst the formation of the cyclohexadienyl group is strongly reminiscent of the methylenecyclohexadiene resulting from the head-to-tail dimerisation of the trityl (Gomberg) radical,[46] the potassium borate by-product suggests that this reactivity is initiated by a metathesis process similar to that observed in the reaction of **3.12** with MeOTf.

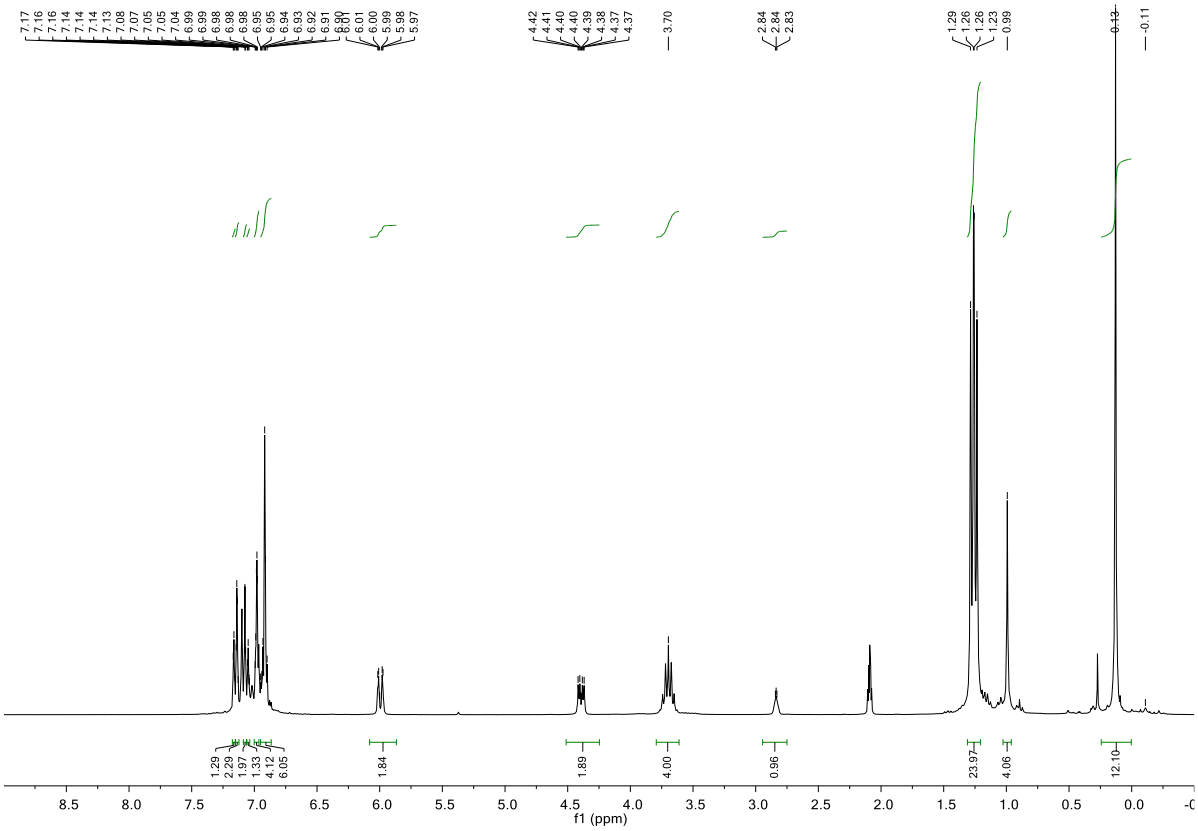

Figure 3. 8 : ^1H NMR (300 MHz, 298 K, d_8-Toluene) spectrum of **3.25**.

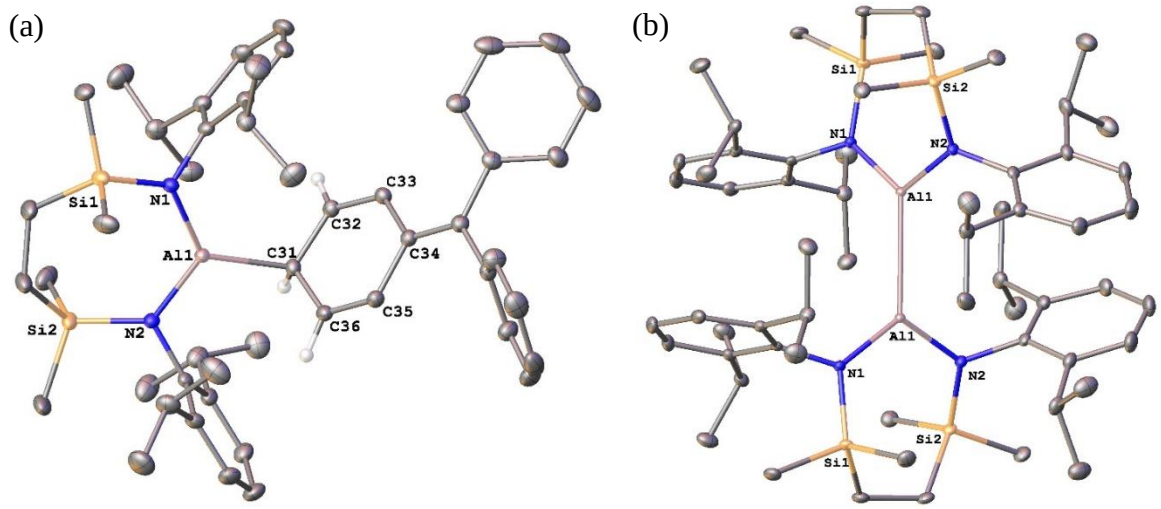

Figure 3. 9 : Displacement ellipsoid plots (30% probability) of (a) compound **3.25**. Hydrogen atoms (except those of C31, C32, C36) have been removed for clarity. (b) compound **3.26**. Hydrogen atoms have been removed for clarity, symmetry operations to generate equivalent atoms, 3/2−x, y, 1−z.

Intrigued by the potential redox reactivity of **3.12** implied by the formation of compound **3.25**, a variety of oxidising reagents were then utilised to examine the reducing nature of the compound **3.12**. Although most reactions between **3.12** and oxidants (TCNE, $[Cp_2Fe][BF_4]$, AgOTf) provided intractable mixtures, single crystals of the Al(II) compound **3.26** were found to be accessible by the treatment of compound **3.12** with the organic electron acceptor 7,7,8,8-tetracyanoquinodimethane (TCNQ, E^0=+0.2 V vs. SCE or Ag/AgCl)[47] and subsequent mechanical separation. The centrosymmetric structure of compound **3.26** (**Figure 3.9**, **Table 3.1**) displays a pronounced elongated Al-Al distance of 2.7330(6) Å in comparison to the dialane(II) derivatives related to other reported alumanyl species (related dialane of **3.5**, Al-Al 2.646(1) Å; related dialane of **3.13**, Al-Al 2.5850(5) Å; related dialane of **3.21**, Al-Al 2.6696(11) Å; related dialane of **3.22**, Al-Al 2.5926(12) Å.),[8,33,34,39,41] plausibly due to the more sterically crowded environment provided by the $\{SiN^{Dipp}\}$ ligand. Although pure bulk quantities of compound **3.26** could not be obtained, this observed redox behaviour in the formation of **3.26**, alongside other described reactivity in this section, is indicative of the aluminium(I) centred properties of compound **3.12**.

3.3 Aluminium(I) Centred C-H Activation of Benzene by the [{SiN^{Dipp}}Al] Moiety

Prompted by the observation of the aluminium(I) centred behaviour of compound **3.12**, as well as the narrower computed energy gap between its HOMO and empty aluminium p_z-orbital in comparison to that of compound **3.7**, a comparative study of the reactivity of [{OSiN^{Dipp}}AlK]$_2$ (**3.7**) and [{SiN^{Dipp}}AlK]$_2$ (**3.12**) was performed to further scrutinise the nature of compound **3.12**.

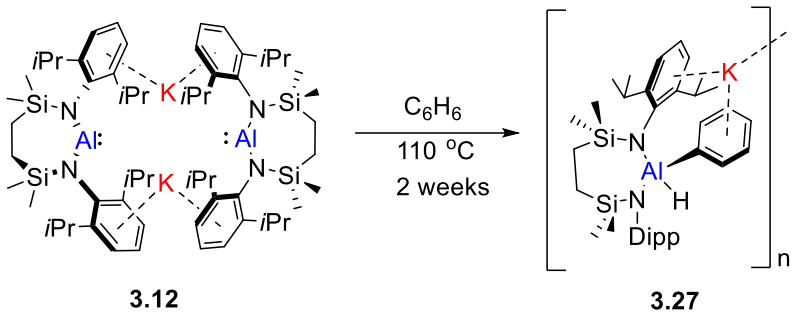

3.12 **3.27**

Scheme 3. 18 : Reaction of **3.12** with benzene.

Although no reactivity of compound **3.7** towards benzene has been described at the time of writing, its heaviest group 1 counterpart, [{OSiN^{Dipp}}AlCs]$_2$ (**3.11**), has been reported to mediate the C-H activation of benzene to give [{OSiN^{Dipp}}Al(H)(Ph)Cs] as the product.[32] In this vein, compound **3.12** was first assessed in its capability to activate a molecule of benzene. In a contrast to the inert behaviour of **3.7** in benzene, the solution of **3.12** in benzene was observed to undergo a gradual decolourisation at 110 ˚C over the course of two weeks. While the full conversion of **3.12** could be inferred from the resultant ^{1}H NMR spectrum, compound **3.27** was observed to simultaneously precipitate from the solution as colourless crystals (**Scheme 3.18**). X-ray diffraction analysis conducted on the obtained single crystal identified the product to be the potassium (phenyl)(hydrido)diamdioaluminate (**3.27**), highlighting the dissimilarity in the reactivity of **3.12** and that of **3.7**. Dissolving **3.27** in the more polar and coordinating d$_8$-THF enabled its NMR spectroscopic characterisation, which features 2 sets of methine resonances (each integrated to 6H) arising from the isopropyl groups in the ^{1}H NMR spectrum, implying the loss of a mirror plane across the {SiN^{Dipp}} backbone of **3.12**.

" I would ask about other group 1 metals if I was the examiner." – M. S. Hill, Nov. 2022.

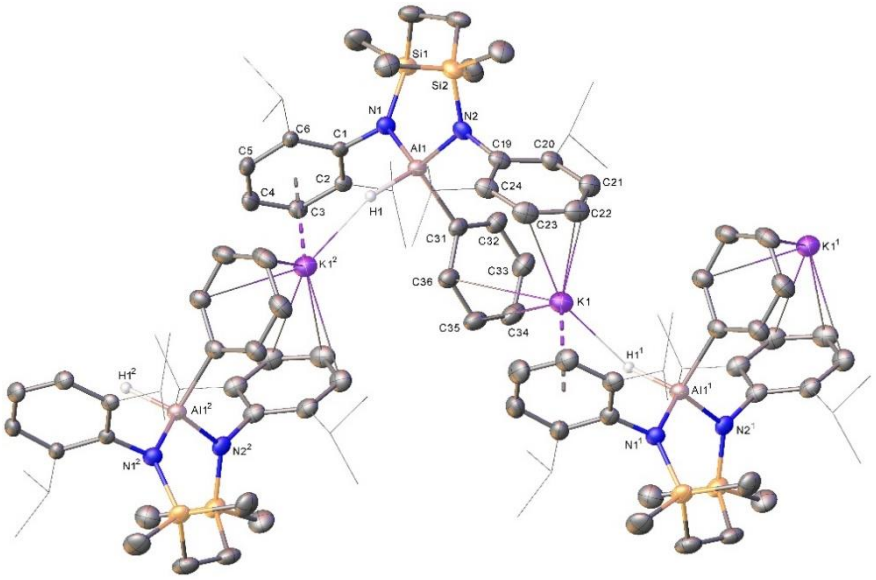

Figure 3. 10 : Displacement ellipsoid plot (30 % probability) of a section of the polymeric structure of compound **3.27**. Hydrogen atoms are omitted, and isopropyl groups are shown as wireframe for clarity. Symmetry operations to generate equivalent atoms [1]1-X,1/2+Y,1/2-Z; [2]1-X, -1/2+Y,1/2-Z.

The inference made from the spectra of compound **3.27** was confirmed by its solid-state data (**Figure 3.10**, **Table 3.2**). In concordance with its low solubility in non-coordinating solvents, the gross structure of **3.27** describes a 1-D polymer propagated by a combination of polyhapto-K-N*Dipp* interactions and cation- Al*Ph* associations. The {SiN^{Dipp}}-supported aluminium centre is now bonded to a hydride and a phenyl group, generating the asymmetrical environment throughout the [{SiN^{Dipp}}Al] moiety apparent in its ^{1}H and ^{13}C NMR spectra. The Al-N separations (avg. 1.872 Å) are now shorter than those measured in **3.12** (avg. 1.892 Å), which agrees with the higher oxidation state assigned to the aluminium centre in compound **3.27**. The structure of **3.27**, therefore, suggests that the reaction between **3.12** and benzene may be considered as an oxidative addition across the aluminium centre.

Encouraged by the enhanced reactivity observed with **3.12** in comparison to **3.7**, the synthesis of the full range of group 1 analogues of [{SiN^{Dipp}}AlK]$_2$ (**3.12**) was then attempted. Attempts to prepare the lithium counterpart of **3.12**, namely [{SiN^{Dipp}}AlLi], either *via* direct lithium reduction of the aluminium(III) iodide [{SiN^{Dipp}}AlI] or *via* salt metathesis with **3.12**, did not provide any tractable product. The sodium reduction (excess 5 wt% Na/NaCl) of [{SiN^{Dipp}}AlI] in hexane, however, reproducibly provided a pale-yellow solution with a grey suspension as the crude reaction product, which upon recrystallisation of the supernatant gave compound **3.28** as a colourless crystalline solid (**Scheme 3.19**). This reaction was then repeated in a smaller scale, where [{SiN^{Dipp}}AlI] was dissolved in C_6D_6 before addition of excess

Na/NaCl to the colourless solution in a J-Young's tube. The reaction mixture was then kept at 30 ˚C and continually shaken for 5 days. ^{1}H NMR spectroscopic inspection of this small-scale reaction provided data identical to that of the isolated product, indicating the exclusive formation of **3.28** under the applied reaction conditions.

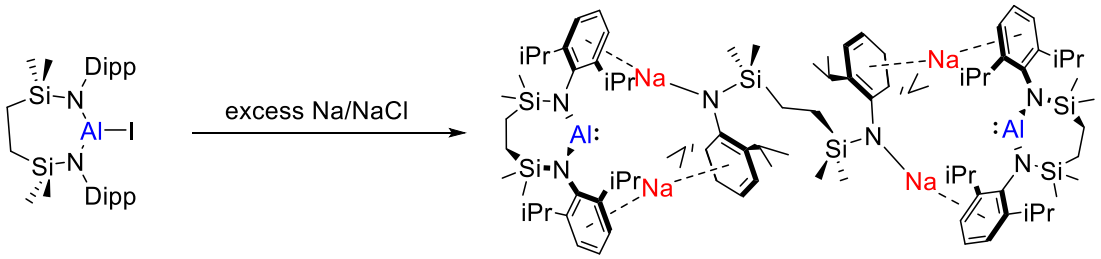

3.28

Scheme 3. 19 : Synthesis of **3.28** from the sodium reduction of [{SiN^{Dipp}}AlI].

The ^{1}H NMR spectrum of **3.28** displays two sets of {SiN^{Dipp}} backbone environments, which are characterised by the diagnostic *iPr*-methine resonances at δ_H = 3.77 and δ_H = 4.00 ppm to be in a two- to- one ratio (each integrated to 8H and 4H, respectively). This observation is redolent of the spectroscopic data provided by compound **2.29**, which comprises two [{SiN^{Dipp}}Mg] moieties bridged by four sodium cations, two hydrides, and a {SiN^{Dipp}} diamide ligand (**Section 2.3**). The resemblance was then verified by X-ray diffraction analysis performed on a colourless single crystal of **3.28**, revealing its structure comprises two [{SiN^{Dipp}}Al] anions and a {SiN^{Dipp}} diamide, with the charge balanced by four Na^{+} cations, which bridge between the units *via* a series of Na-N and Na-arene interactions (**Figure 3.11**, **Table 3.2**).

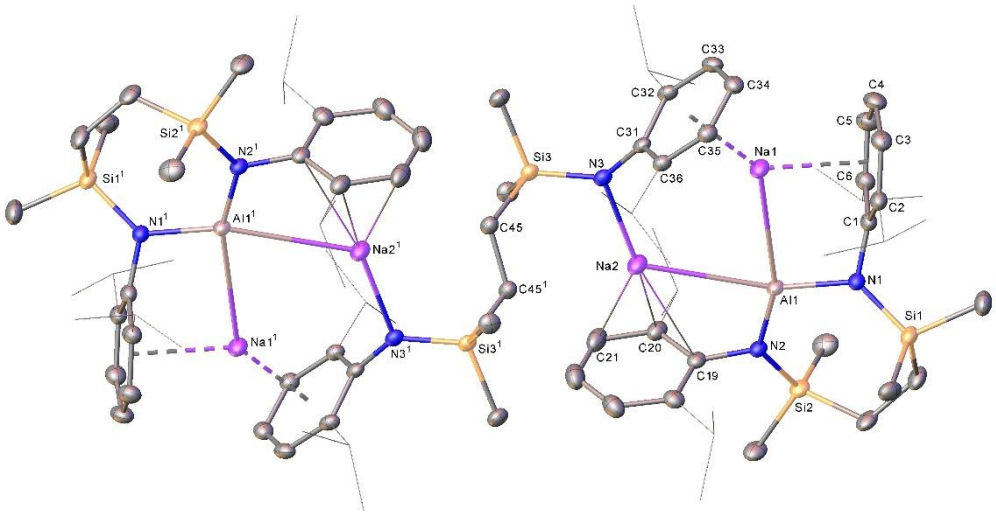

Figure 3. 11 : Displacement ellipsoid plot (30 % probability) of compound **3.27**. Hydrogen atoms are omitted, and isopropyl groups are shown as wireframe for clarity. Symmetry operations to generate equivalent atoms ^{1}-X,1-Y,1-Z.

As depicted in **Figure 3.11**, and like the structure of **2.29**, the asymmetric unit of **3.28** is composed of half the molecule with the remainder generated *via* a crystallographic inversion centre. Na1/Na1^{1} is bound in a η^6-fashion by the aromatic substituents of the [{SiN^{Dipp}}Al] and further polyhapto-interactions with C31-C36 (and C31^{1}-C36^{1}) of the Dipp substituents of the bridging diamide. The coordination spheres of Na2/Na2^{1} are composed of a η^6-interaction with an *N*-Dipp of the [{SiN^{Dipp}}Al] moiety and N3/N3^{1}. Unlike the similar constitutions of **3.9** to **3.7**, the sodium reduction product (**3.28**) of [{SiN^{Dipp}}AlI] is not the straightforward sodium analogue of **3.12**. Although the reactivity of compound **3.28** was still assessed in its facility to activate benzene molecule, no reaction was observed by ^{1}H NMR spectroscopy even when the reaction mixture was kept at 110 ˚C for over a month.

In contrast to the complexity observed in the sodium reduction of [{SiN^{Dipp}}AlI] and the subsequent isolation of **3.28**, rubidium and caesium reduction of the iododiamidoalumane provided straightforward access to the respective heavier analogues of **3.12**, namely [{SiN^{Dipp}}AlRb]$_2$ (**3.29**) and [{SiN^{Dipp}}AlCs]$_2$ (**3.30**) (**Scheme 3.20**). In both cases, a hexane solution of [{SiN^{Dipp}}AlI] was mixed with the respective alkali metal and stirred at room temperature for three days, affording bright yellow solutions with grey precipitates. Compounds **3.29** and **3.30** were then isolated as bright yellow crystalline powders by removal of all volatiles from each of the yellow filtrates. ^{1}H and ^{13}C NMR characterisation conducted on each compound provided clean and comparable spectra to those of **3.12**, suggesting **3.29** and **3.30** to be the rubidium and caesium congeners of **3.12**.

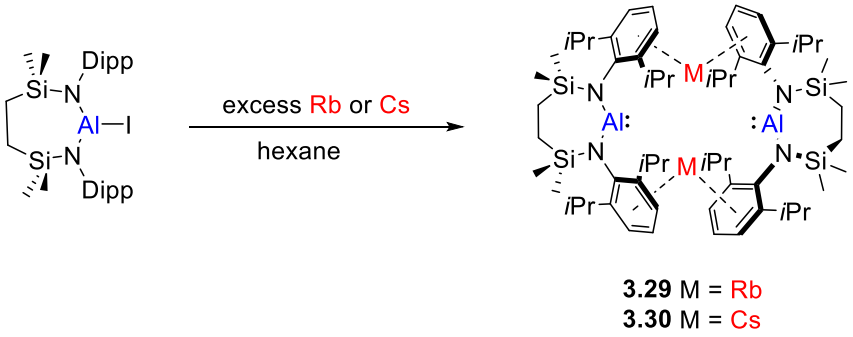

Scheme 3. 20 : Rubidium and caesium reduction of [{SiN^{Dipp}}AlI].

(a)

(b)

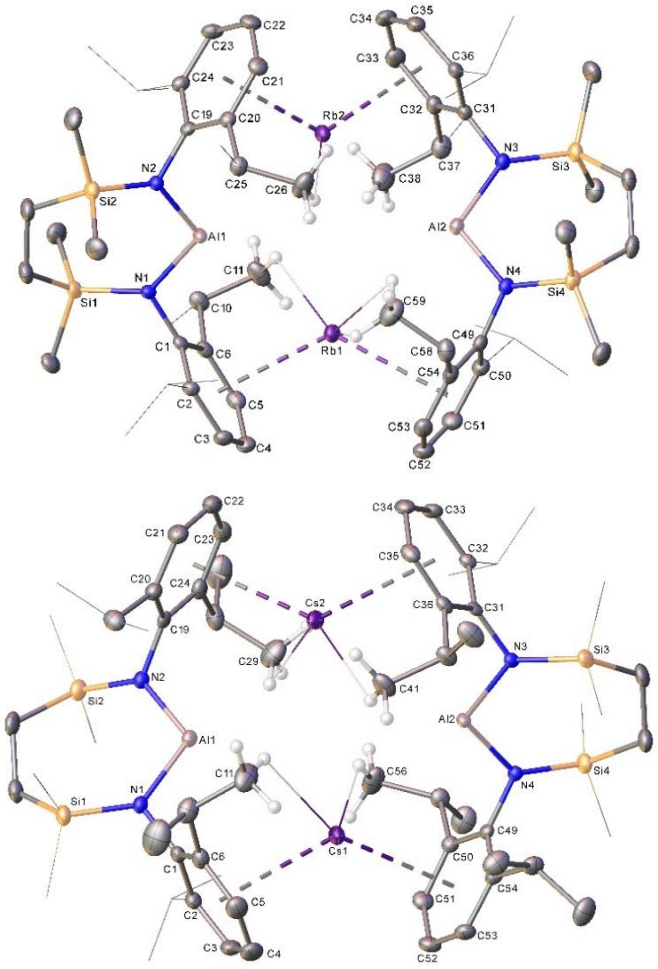

Figure 3. 12 : Displacement ellipsoid plots (30 % probability) of (a) compound **3.29**. Hydrogen atoms (except those of C11, C26, C38, C59) and solvent molecules have been removed, isopropyl groups (except those which have potential interactions with Rb) are shown as wireframe for clarity. (b) compound **3.30**. Hydrogen atoms (except those which have potential interactions with Cs) and solvent molecules have been removed for clarity, isopropyl and $SiMe_2$ group are shown as wireframe (except those which have potential interactions with Cs).

The deduced identities of **3.29** and **3.30** were confirmed by X-ray diffraction analysis performed on respective bright yellow single crystals (**Figure 3.12**, **Table 3.2**). Similar to that of compound **3.12**, compounds **3.29** and **3.30** were both observed to be dimeric structures

arising from the cation-arene interactions between individual alkali metals and *N*-Dipp substituents. In addition, the Al-N distances (avg. 1.892Å) in **3.29** and Al-N separations in **3.30** (avg. 1.892Å) are comparable to those observed (avg. 1.892Å) in compound **3.12**, in line with +I oxidation state assignments of the aluminium centres in all three molecules. On the other hand, the Al···Al separation (**3.12**, 5.7207(5) Å; **3.29**, 5.8547(10) Å; **3.30**, 6.0814(13) Å.) increases along with the size of the alkali metal cation, as has previously described by Coles and co-workers for their [{OSiN^{Dipp}}AlM]$_2$ systems.[32]

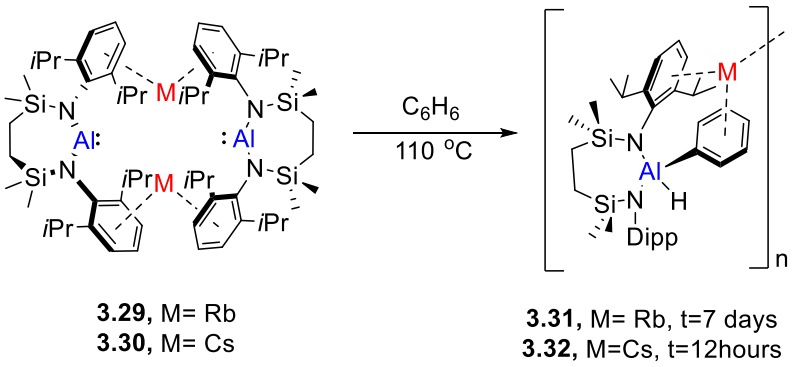

3.29, M= Rb
3.30, M= Cs

3.31, M= Rb, t=7 days
3.32, M=Cs, t=12hours

Scheme 3. 21 : C-H activation of benzene by [{SiN^{Dipp}}AlM]$_2$ molecules and related reaction time.

Intrigued by the observation of the divergence in the structural features between **3.12**, **3.29**, and **3.30**, their reactivity was then examined by comparing the reaction time required to achieve oxidative insertion towards the C-H bond of a benzene molecule (**Scheme 3.21**). Although the low solubility of the benzene activation products of **3.12**, **3.29**, and **3.30** (**3.27**, **3.31**, and **3.32**, respectively) prevented a quantitative kinetic study of these reactions, the depletion of the bright yellow colour and the corresponding ^{1}H NMR resonances of the starting material in each entry provided a qualitative indicator of conversion. As depicted in **Scheme 3.21**, the full consumption of **3.29** was observed within 7 days of heating the reaction mixture, while the full conversion of **3.30** required only 12 hours, indicating enhanced reactivity of [{SiN^{Dipp}}Al] anions with increasing size of their counter cation. NMR spectroscopic characterisation of **3.31** and **3.32** was, however, facilitated with the implementation of d_8-THF to provide the respective ^{1}H and ^{13}C NMR spectra which were comparable to those of **3.27**, indicating that the reactions of different [{SiN^{Dipp}}AlM]$_2$ towards benzene, whilst being different in the conversion rate, result in the analogous (phenyl)(hydrido)aluminate products.

	3.27	3.28	3.29	3.30	3.31	3.32
Al1-N1	1.877(2)	1.8886(18)	1.8866(15)	1.899(2)	1.878(2)	1.873(3)
Al1-N2	1.867(4)	1.8625(17)	1.8880(16)	1.903(2)	1.877(2)	1.889(3)
Al2-N3	-	2.3164(18)[a]	1.8960(16)	1.889(2)	-	1.873(3)
Al2-N4	-	3.1251(10)[b]	1.8989(16)	1.892(2)	-	1.881(3)
Al1-C31	2.000(3)	3.2368(11)[c]	-	-	2.010(3)	2.016(3)[e]
N1−Al1−N2	111.8(2)	111.73(8)	109.07(7)	109.64(9)	112.82(10)	112.99(12)[f]
N1−Al1−C31	114.02(11)	-	110.07(7)[d]	108.50(9)[d]	113.11(11)	108.56(13)[g]
N2−Al1−C31	106.7(2)	-	-	-	108.46(10)	113.27(13)[h]

Table 3. 2 : Selected bond lengths (Å) and angles (°) of compounds **3.27 ─ 3.32**.[a]Na2-N3; [b]Al1-Na1; [c]Al1-Na2; [d]N3-Al2-N4; [e]Al2-C67, 2.012(3) Å; [f]N3-Al2-N4, 112.92(12)°; [g]N3-Al2-C67, 109.58(12)°; [h]N4-Al2-C67, 112.35(13)°.

This inference was later verified by X-ray diffraction analysis conducted on the individual single crystals of **3.31** and **3.32** (**Figure 3.13**, **Table 3.2**), revealing their identity to be the Al(III) oxidative addition products [{SiN^{Dipp}}Al(H)(Ph)Rb] and [{SiN^{Dipp}}Al(H)(Ph)Cs], respectively. Comparable to that of **3.27**, the structures of **3.31** and **3.32** are polymers arising from the cation-arene interaction between the alkali metal and N-*Dipp* and Al-*Ph* groups. Furthermore, the Al-N bonds (**3.31**, avg. 1.878 Å; **3.32**, avg. 1.879 Å) in both molecules are found to be noticeably shorter than those measured in compound **3.12** (avg. 1.892 Å), again highlighting the oxidative nature of the Al(I) centred benzene activation.

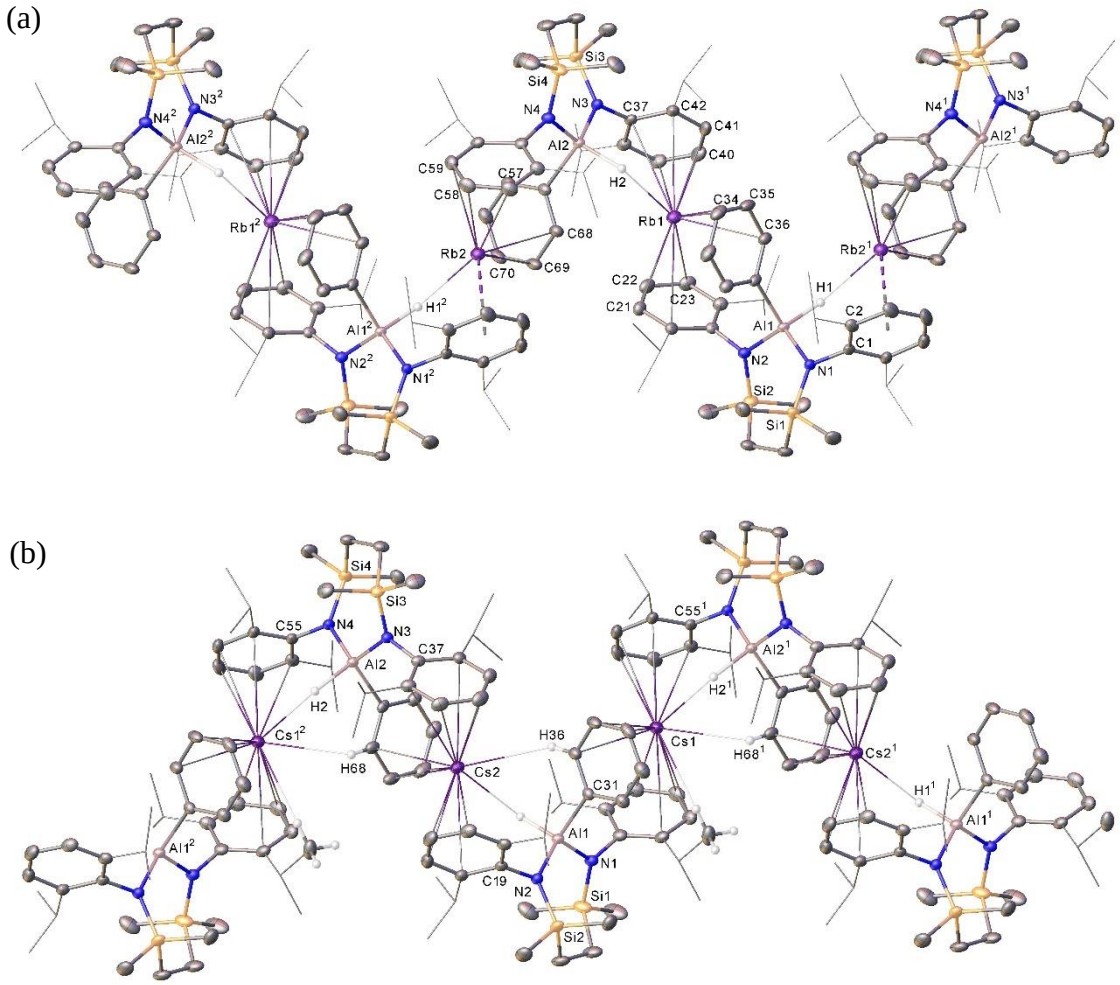

Figure 3. 13 : Displacement ellipsoid plots (30 % probability) of (a) a section of the polymeric structure of compound **3.31**. Hydrogen atoms (except those have potential interaction with Rb) and solvent molecules have been removed, isopropyl groups are shown as wireframe for clarity. Symmetry operations to generate equivalent atoms, ^{1}+X, -1+Y, +Z; ^{2}+X,1+Y, +Z. (b) a section of the polymeric structure of compound **3.32**. Hydrogen atoms (except those have potential interaction with Cs) and solvent molecules have been removed for clarity, isopropyl group are shown as wireframe (except those have potential interaction with Cs). Symmetry operations to generate equivalent atoms, ^{1}+X,1+Y, +Z; ^{2}+X, -1+Y, +Z.

3.4 Reactivity of [{SiN^{Dipp}}AlK]$_2$ Towards Organic Molecules

Prompted by the recent report of C-C bond activation facilitated by [{^{Dipp}BDI}Al] (**3.1**),[48,49] and the observations described in the previous section, the reactivity of [{SiN^{Dipp}}AlK]$_2$ (**3.12**) towards organic molecules was then investigated. Subsequent to the benzene activation by compound **3.12** portrayed in **Section 3.3**, its reactivity towards extended aromatic systems such as naphthalene, anthracene, and tetracene was explored.

Although anionic Al(I) centred activations of naphthalene have been described, where **3.5** and **3.21** were reported to undergo contrasting C-H activation and [1+4] cycloaddition, respectively.[24,50] A reaction of **3.12** with naphthalene was observed to exhibit a decolourisation in the hexane solution. The outcome of this transformation remained unclear at the time of writing due to the difficulty in obtaining a crystal suitable for X-ray diffraction analysis. The ^{1}H NMR spectrum of the reaction crude indicates the existence of multiple species, while attempts to repeat the reaction in d_6-benzene only provided **3.27** from the reaction of **3.12** with the solvent.

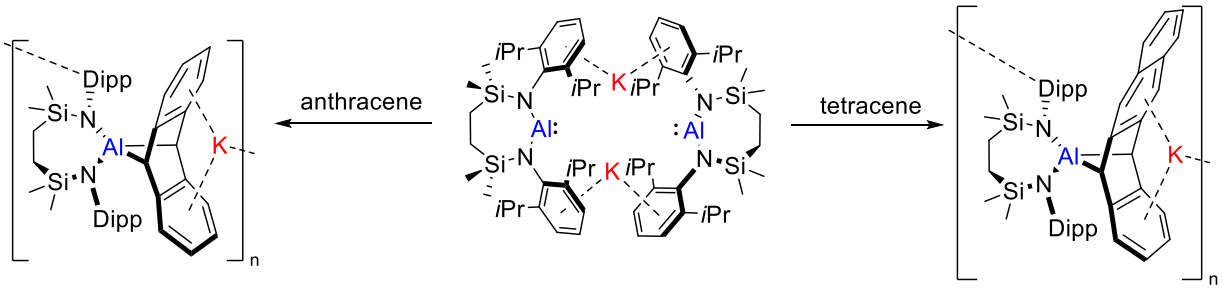

3.33 **3.12** **3.34**

Scheme 3. 22 : Reaction of **3.12** with anthracene and tetracene.

In a contrast to the issues encountered in monitoring the reaction of **3.12** and naphthalene, the reaction products of [{SiN^{Dipp}}AlK]$_2$ (**3.12**) with the more readily reducible anthracene and tetracene were fully characterised. In both reactions, a d_6-benzene solution of **3.12** was treated with the aromatic substrate and the reaction mixture was then kept at 60 ˚C for 16 hours. In both cases, a gradual decolourisation of the reaction mixture was observed along with the formation of colourless crystals of **3.33** and **3.34** as the products of the reactions with anthracene and tetracene, respectively (**Scheme 3.22**). The NMR spectroscopic characterisation of **3.33** and **3.34** was performed in d_8-THF solutions due to the inherent low solubility of both compounds in arene solvents. The resultant ^{1}H NMR spectra of **3.33** and **3.34** displayed broad peaks, most likely indicative of fluxional behaviour of these molecules in the solution state. Moreover, distinctive ^{1}H resonances (**3.33**, δ_H= 3.40ppm; **3.34** δ_H = 3.52 ppm)

could be correlated to a bridgehead Al-C*H* environment (each integrated to 2H) in the respective spectra, implying the formation of the [1+4] cycloaddition product. A similar product was previously identified from the reaction of compound **3.21** and anthracene.[50]

(a)

(b)

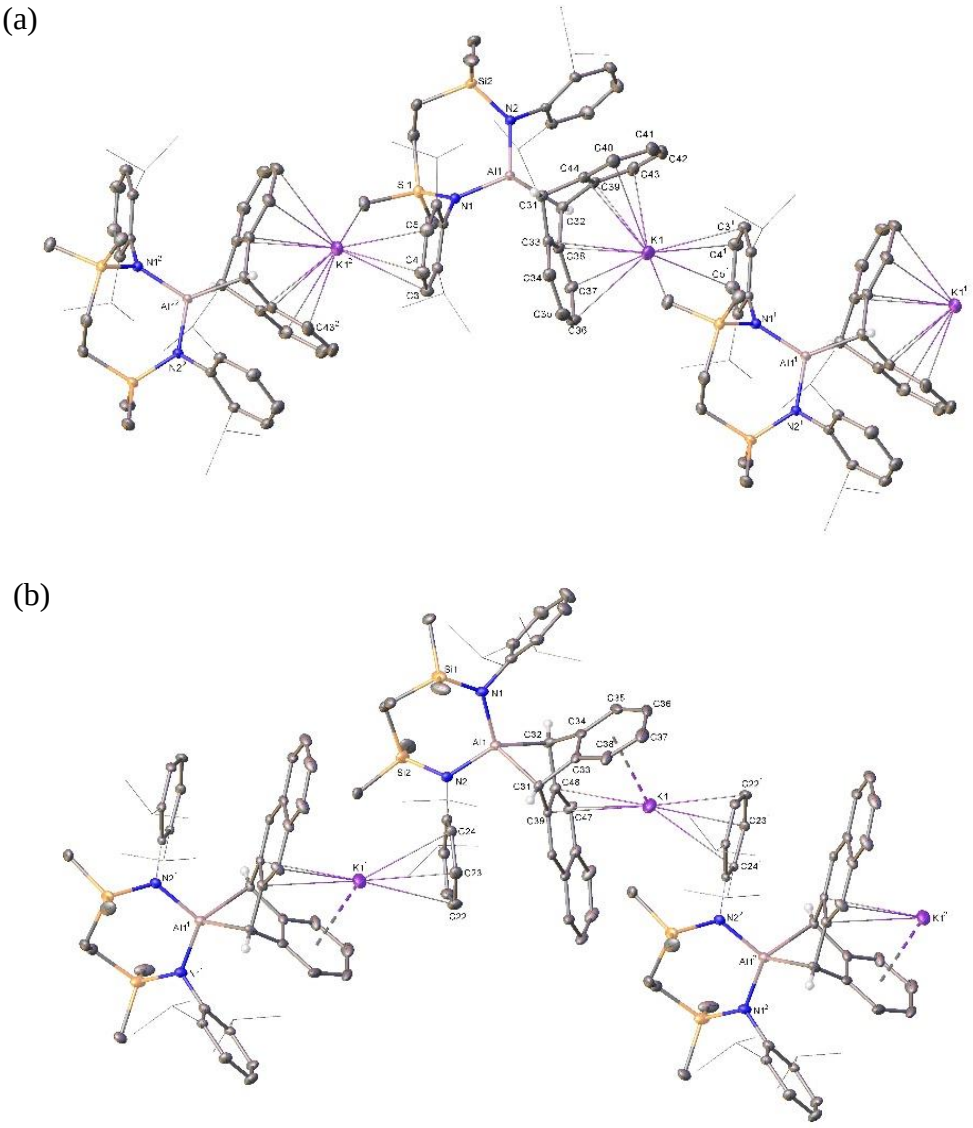

Figure 3. 14 : Displacement ellipsoid plots (30 % probability) of sections of the polymeric structures of (a) compound **3.33**. Symmetry operations to generate equivalent atoms, [1]1/2-X,-1/2+Y,1/2-Z; [2]1/2-X,1/2+Y,1/2-Z. (b) compound **3.34**. Symmetry operations to generate equivalent atoms, [1]1-X,1-Y,1/2+Z; [2]1-X,1-Y, -1/2+Z. Hydrogen atoms in both molecules (except those on C31 and C32) and solvent molecules have been removed and isopropyl groups are shown as wireframes for clarity.

This deduction was confirmed by the X-ray diffraction analyses conducted on colourless single crystals of **3.33** and **3.34**, disclosing the reaction products of **3.12** and polyaromatics were indeed the corresponding [1+4] cycloaddition species (**Figure 3.14**, **Table 3.3**). This outcome is further emphasised by the alternating C-C bond lengths found in the Al-bridged six-membered rings of **3.33** and **3.34** (**3.33**, C31-C33, 1.507(2) Å, C33-C38, 1.410(2) Å, C38-

C32, 1.504(2) Å, C32-C44, 1.508(2) Å, C44-C39, 1.413(2) Å, C39-C31, 1.502(2) Å; **3.34**, C31-C33, 1.494(4) Å, C33-C34, 1.393(5) Å, C34-C32, 1.497(5) Å, C32-C48, 1.504(4) Å, C48-C39, 1.425(4) Å, C39-C31, 1.494(4) Å). Both compounds **3.33** and **3.34** again feature polymeric structures arising from the K^+-arene interactions in the solid state, consistent with the low solubility of the molecules in non-coordinating hydrocarbon solvents.

	3.33	**3.34**	**3.36**	**3.37**
Al1-N1	1.8937(12)	1.884(2)	1.8238(17)	1.8910(18)
Al1-N2	1.8925(12)	1.896(2)	1.8415(17)	1.8852(17)
Al1-C31	2.0977(15)	2.092(3)	2.070(2)	2.0108(19)
Al1-C32	2.0778(15)	2.120(3)	2.071(2)	2.0144(19)[a]
N1−Al1−N2	111.65(5)	111.13(11)	118.17(8)	112.63(8)
N1−Al1−C31	108.75(6)	109.98(12)	124.23(8)	115.38(8)
N2−Al1−C32	108.29(6)	107.41(11)	110.93(8)	117.12(8)[b]
C31-Al1-C32	75.89(6)	74.76(12)	42.02(8)	90.75(8)[c]

Table 3. 3 : Selected bond lengths (Å) and angles (°) of compounds **3.33**, **3.34**, **3.36**, **3.37**. [a]Al1-C34; [b] N2-Al1-C31; [c]C31-Al1-C34.

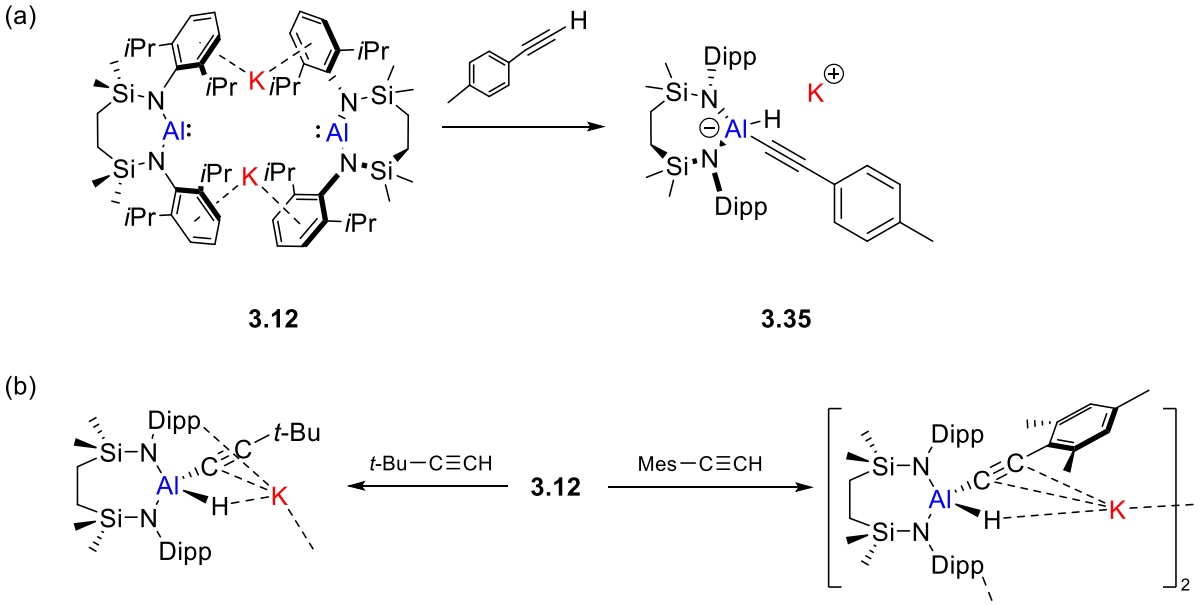

Scheme 3. 23 : Reactivity of **3.12** towards terminal alkynes: (a) Reaction of **3.12** with *p*-tolylacetylene (b) Reaction of **3.12** towards acetylenes described in Dr Shere's thesis.[51]

To shed further light on the reactivity of [{SiN^{Dipp}}AlK]$_2$ (**3.12**), its behaviour was assessed towards various organic molecules. Inspired by the recent reports of the reaction between [{^{Dipp}BDI}Al] (**3.1**) and alkenes, as well as the anionic Al(I) centred reactivity of **3.7** towards ethene;[52,53] 1-hexene and *p*-tolylacetylene were selected as representative terminal alkene and alkyne reagents, to react with compound **3.12**. Although the reaction mixture between **3.12** and 1-hexene displayed a colour change to colourless when it was kept at 110 ˚C for more than 7 days, the reaction mixture provided multiple species which were unidentifiable and inseparable by NMR spectroscopy or by fractional recrystallisation, plausibly due to the poor selectivity induced by the harsh reaction conditions. In contrast, treatment of *p*-tolylacetylene with **3.12** induced the instantaneous and quantitative formation of one species (**3.35**), which could be unambiguously characterised *in-situ* by its ^{1}H and ^{13}C NMR spectra to be the C-H activation product [({SiN^{Dipp}}Al)(H)(CC*p*-tolyl)K] (**3.35**) (**Figure 3.15**, **Scheme 3.23a**). Although compound **3.35** was not structurally characterised, this assignment can be verified by the analogous reactivity of **3.12** towards other acetylenes described in the thesis of Dr Shere formerly of the Hill Group (**Scheme 3.23b**).[51]

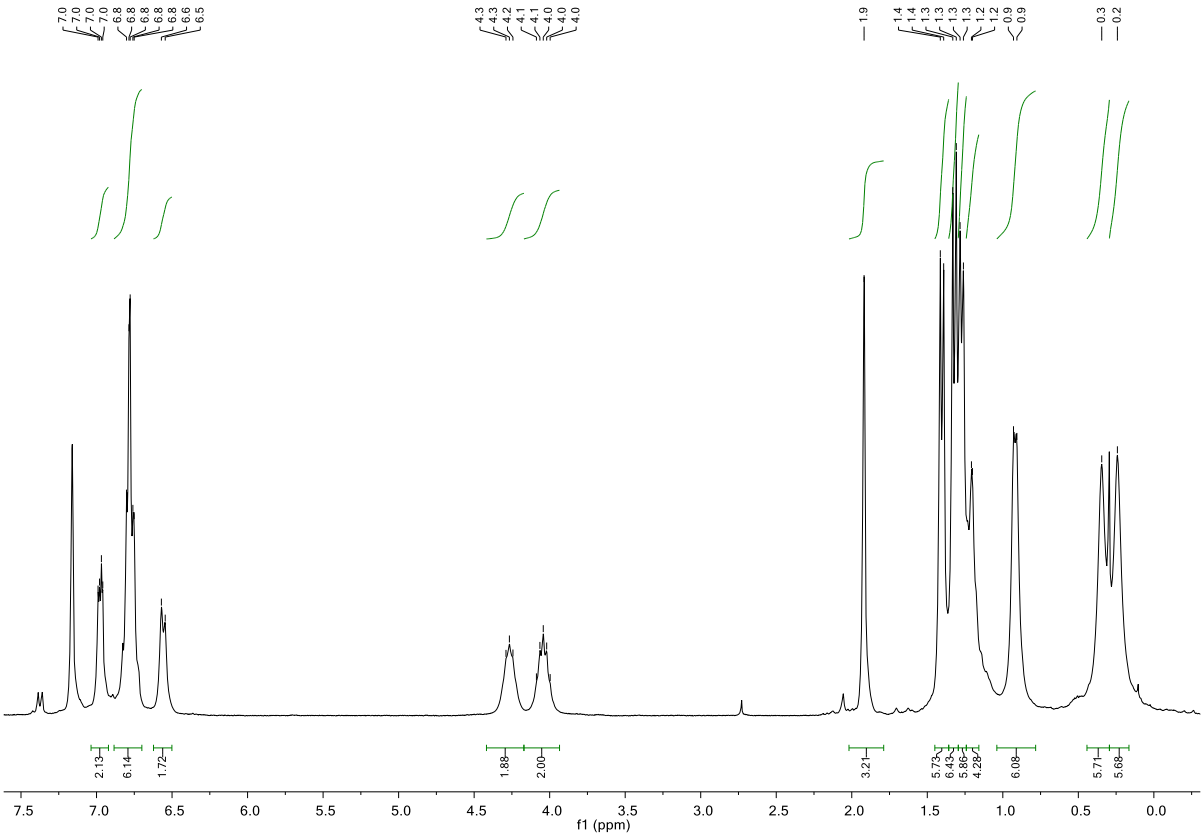

Figure 3. 15 : The *in-situ* recorded ^{1}H NMR (300 MHz, 298 K, C_6D_6) spectrum of compound **3.35**.

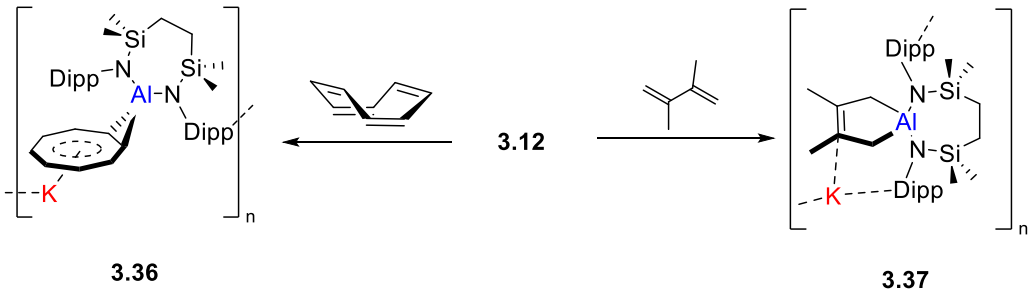

3.36 **3.37**

Scheme 3. 24 : Reaction of [{SiN^{Dipp}}AlK]$_2$ (**3.12**) with COT and 2,3-dimethylbutadiene.

The reactivity of [{SiN^{Dipp}}AlK]$_2$ (**3.12**) was also assessed by its treatment with conjugated unsaturated organic substrates. Similar to the reaction of **3.7** with 1,3,5,7-cyclooctatetraene (COT), a formal 2-electron reduction of the cyclooctatetraene was observed when reacting **3.12** with COT, giving [({SiN^{Dipp}}Al)(COT)K] (**3.36**, **Scheme 3.24**) as the reaction product.[25] Although the solid state strucutre of **3.36** merits no detailed discussion, it is consistent with the assignments of the bridging planar COT^{2-} dianion and the +III oxidation state to the group 13 centre in the [{SiN^{Dipp}}Al] unit (**Figure 3.16a**, **Table 3.3**). In addition, reminiscent of the behaviour of [{OSiN^{Dipp}}Al(COT)K] (reaction product of **3.7** with COT), compound **3.26** was found to be unstable in high polarity solvents (d_8-THF), hampering its

NMR spectroscopic characterisation. In a contrast to the COT^{2-} derivative of **3.7**, further treatment of **3.36** with 18-crown-6 only resulted in compound decomposition and an intractable reaction mixture.

Contrary to the high reactivity of compound **3.36**, treatment of 2,3-dimethylbutadiene with **3.12** provided a stable compound, **3.37** (**Scheme 3.24**), enabling full spectroscopic characterisation. The reaction mixture of **3.12** and two molar equivalents of 2,3-dimethylbutadiene in d_6-benzene was observed to undergo a gradual decolourisation at ambient temperature over the course of three days, whereupon complete conversion of **3.12** was inferred from the ^{1}H NMR spectrum along with compound **3.37** being observed to crystallise from the solution as colourless crystals. Despite its low solubility in aromatic solvents, NMR characterisation of **3.37** could be conducted in the more coordinating and more polar solvent d_8-THF, and the ^{1}H NMR spectrum of **3.37** displayed one set of methine resonances of the isopropyl group and one $SiMe_2$ environment in the $\{SiN^{Dipp}\}$ ligand backbone, as well as one methyl chemical shift from the organic moiety, consistent with a C_2 symmetry across the $[\{SiN^{Dipp}\}Al]$ seven-membered chelate in the solution.

This observation was rationalised by the X-ray diffraction analysis performed on a colourless single crystal of **3.37 (Figure 3.17**, **Table 3.3)** , identifying it to be the [1+4] cycloaddition product, a reactivity redolent of compound **3.1** towards conjugated organic substrates.[27] Compound **3.37** exhibits a polymeric structure arising from the cation-π interactions in the solid state, reflecting the low solubility in the arene solvents. The Al-C separations (avg. 2.011 Å) in **3.37** were observed to be longer in comparison to those (Al-C, avg. 1.9636 Å) in the related cycloaddition product originated from compound **3.1**, plausibly due to the significant cation-π association in compound **3.37**, which in turn resulted in weaker Al-C bonds.

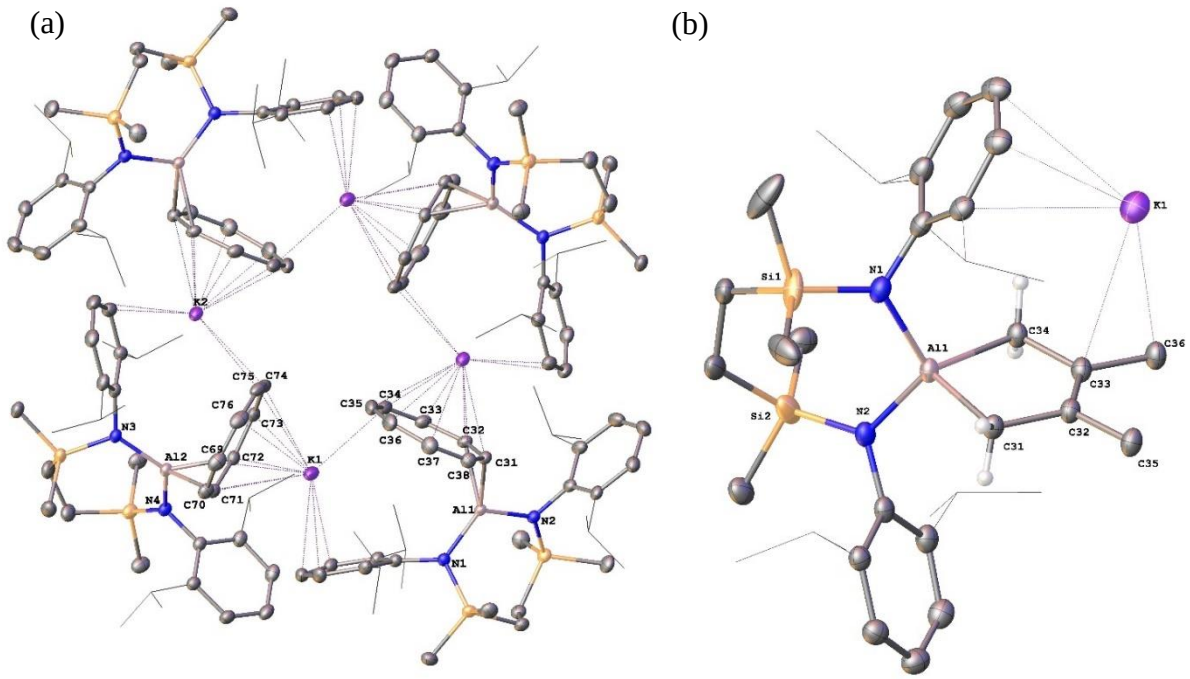

Figure 3. 16 : Displacement ellipsoid plots (30 % probability) of (a) the tetrameric aggregate of compound **3.36**. Symmetry operations to generate equivalent atoms, [1]1-X, -Y,1-Z; [2]1-X,1-Y,2-Z. (b) compound **3.37**. Symmetry operations to generate equivalent atoms, [1]1-X,1/2+Y,3/2-Z; [2]1-X, -1/2+Y,3/2-Z. Hydrogen atoms in both molecules (expect those attached to C31 and C34 in **3.37**) and solvent molecules have been removed for clarity. *iso*-propyl groups are shown as wireframe for clarity.

" There should be some butadiene in the box, I literally used it yesterday." – L. J. Morris, 2019.

3.5 Diverse Reactivity of [{SiN^{Dipp}}AlK]$_2$ Towards Ketones

Intrigued by the reactivity of [{SiN^{Dipp}}AlK]$_2$ (**3.12**) towards the various organic molecules described in **Section 3.3** and **3.4**, the study of compound **3.12** was then extended to its activation of heteroatom-containing organic molecules. In a parallel investigation to the reactivity of **3.12** towards organic nitriles (RCN) documented in Dr Shere's Ph.D. thesis,[51] the behaviour of compound **3.12** towards ketones was scrutinised.

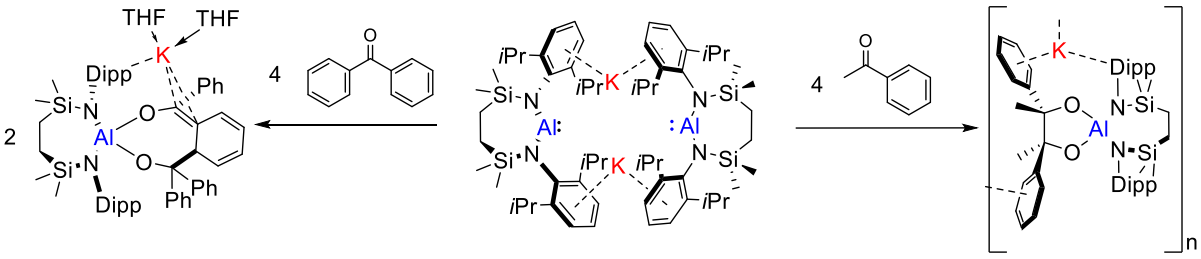

3.38 **3.12** **3.39**

Scheme 3. 25 : Reaction of **3.12** towards benzophenone and acetophenone.

Although an Al(I) centred reactivity towards C=O functional groups has previously been reported for the reaction of [{^{Dipp}BDI}Al] and benzophenones,[54] anionic low oxidation state aluminium(I) centred behaviour towards ketones was investigated at the start of this project. In this vein, compound **3.12** was treated with four molar equivalents of benzophenone. The reaction mixture resulted in a bright yellow oil and a colourless supernatant, from which the addition of a few drops of tetrahydrofuran provided a homogeneous yellow solution. The X-ray crystallographic analysis conducted on a single crystal obtained from the solution revealed that the product from the reaction was not a symmetrical tetraphenylpinacolate derivative analogous to that obtained from the reaction between **3.1** and benzophenone. Rather, the resultant molecule, [K(THF)$_2$][({SiN^{Dipp}}Al)-κ^2-O,O'-{OC$^{Ph}_2$C^{H}(CH=CHCH=CH)C=C^{Ph}O}] (**3.38**), is a molecular, spirocyclic aluminate comprising two seven-membered heterocycles (Al1–N1–Si1–C15–C16–Si2–N2 and Al1–O1–C31–C32–C33–C34–O2) (**Scheme 3.25**, **Figure 3.18a**, **Table 3.4**). The essential charge balance was maintained with cationic K1, which is encapsulated by an enolate-like (C33–C34–O2) subunit, a polyhapto-coordinated *N*-Dipp substituent and two molecules of THF.

" This benzophenone is premium." – D. B. Kennedy, 2020.

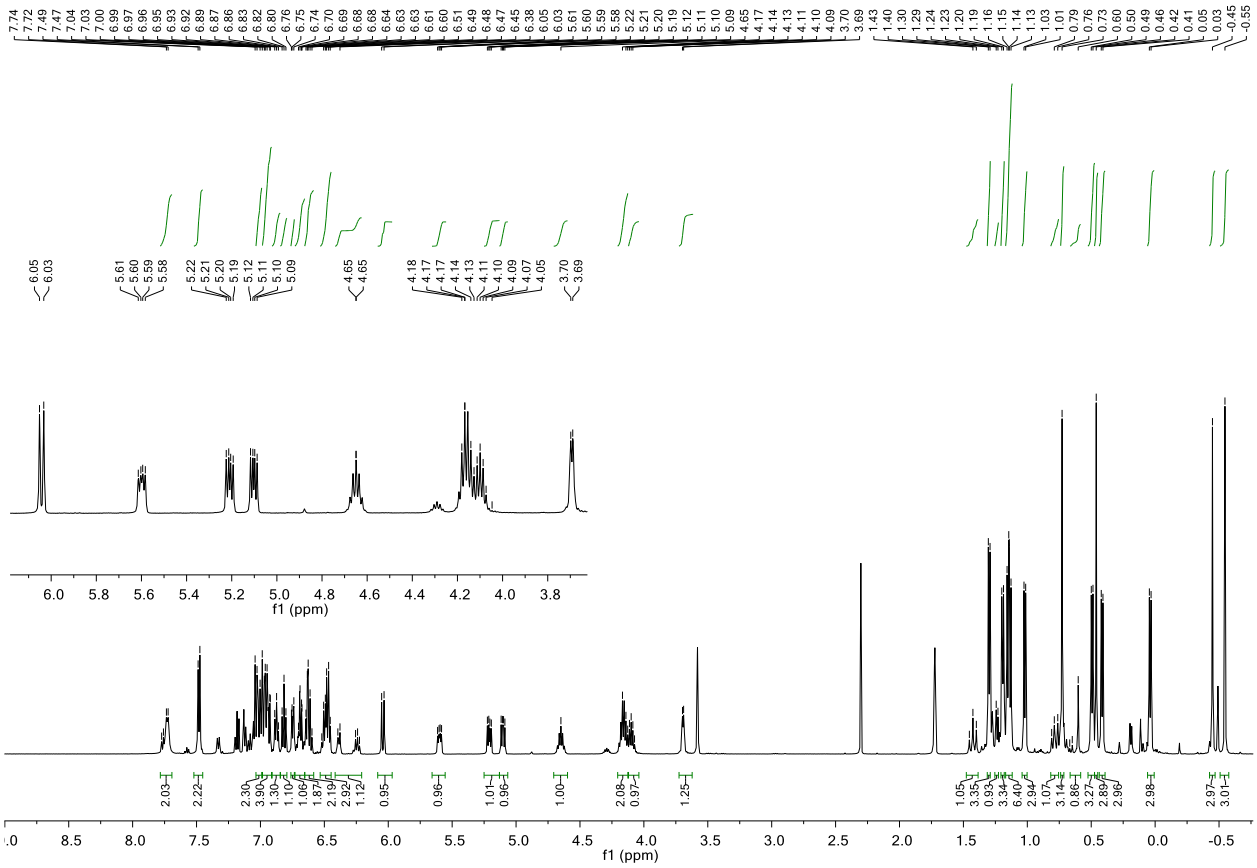

Figure 3. 17 : ^{1}H NMR (500 MHz, 298 K, d_8-THF) spectrum of **3.38**.

Although, like the reaction of **3.1** with benzophenone, the structure of **3.38** represents an Al(I) mediated reductive coupling product of benzophenone, C–C bond formation has occurred between a single ketyl carbon and an *ortho*-phenyl carbon of a second benzophenone moiety, resulting in a dearomatised six-membered carbocycle. In concordance with the assignment of a now formal +III oxidation state of the aluminium centre, the Al-N distances (avg. 1.883 Å) in **3.38** are noticeably shorter than those in **3.12** (avg. 1.892 Å). On the other hand, the alternating long (C32–C33 1.529(3), C32–C47 1.516(3) and C48–C49 1.453(4) Å) and short (C47–C48 1.335(4), C49–C50 1.346(4) Å) C–C bonds evidently denote a dienic structure to the dearomatised unit of **3.38**. This distinctive structure was further verified by the ^{1}H NMR spectrum of **3.38** obtained in d_8-THF (**Figure 3.17**), where the individual resonances characteristic of the dearomatized ring at δ 6.04, 5.60, 5.21, 5.10 and 3.69 ppm can be found and respectively assigned to the individual protons on the carbon atoms identified in the solid–state structure as C50, C47, C48, C49 and C32. In agreement with the loss of mirror plane in the {SiN^{Dipp}}-backbone observed in the solid-state structure, four discriminated SiMe peaks at d 0.73, 0.46, –0.45, –0.55 ppm, each 3H by relative integration, were also found in the ^{1}H NMR spectrum of compound **3.38**.

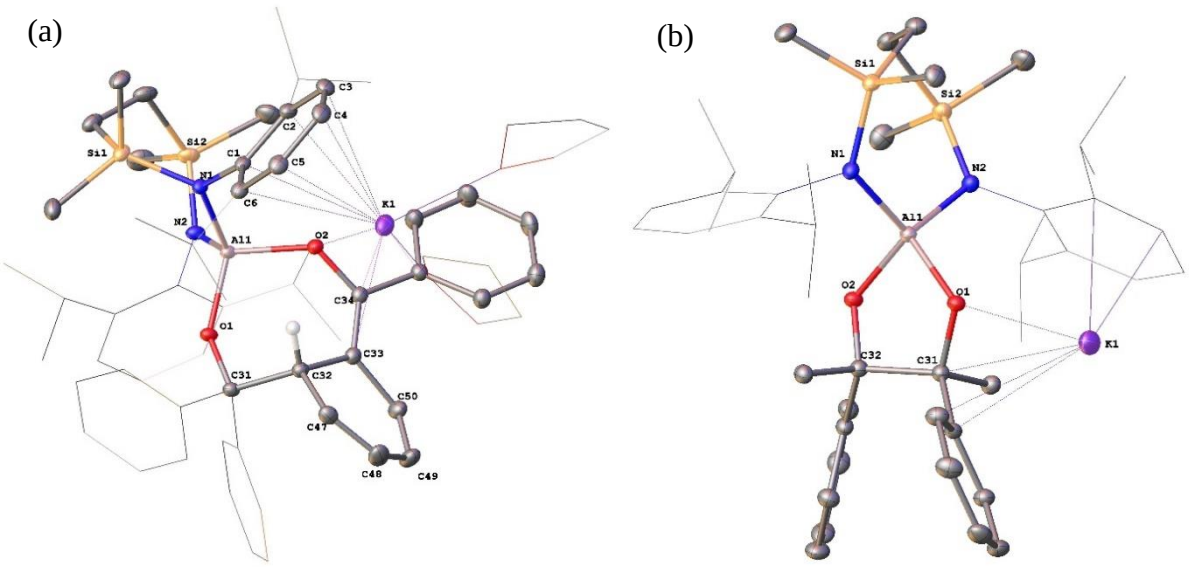

Figure 3. 18 : Displacement ellipsoid (30% probability) plots of (a) compound **3.38** and (b) compound **3.39**. For purposes of clarity, hydrogen atoms (except the hydrogen attached to C32 in **3.38**) are omitted, and selected aryl and iso-propyl substituents, solvent molecules are shown as wireframe.

[{SiN^{Dipp}}AlK]$_2$ (**3.12**) was then treated with four molar equivalents of acetophenone, where the decolourisation of the initial bright yellow solution and the precipitation of the product (**3.39**) as a colourless powder was observed (**Scheme 3.25**). Although the solution characterisation of compound **3.39** was hampered by its low solubility, its identification was facilitated by the X-ray diffraction analysis performed on a single crystal obtained from slow cooling of reactions performed at 60 ˚C, where the reaction mixture can be prepared as a solution either in *d*$_6$-benzene or toluene (**Figure 3.18b**, **Table 3.4**). While the Al-N (1.8705(15), 1.8855(15) Å) and Al-O (1.8008(12) and 1.7700(12) Å) separations found in compound **3.39** are again commensurate with oxidation to Al(III), the reaction provides a more conventional reductive ketyl C–C coupling between the previous carbonyl carbon centres, which is strongly reminiscent to the reaction between **3.1** and benzophenones.[54] The poor solubility of **3.39** can also be rationalised by its polymeric structure propagated through a combination of intra- and intermolecular polyhapto-potassium-arene associations arising from the phenyl and *N*-Dipp substituents.

	3.38	3.39	3.40	3.41[i]
Al1-N1	1.8934(18)	1.8705(15)	1.8779(14)	1.9003(17)
Al1-N2	1.8729(19)	1.8855(15)	1.8722(13)	1.9083(14)
Al1-O1	1.7477(15)	1.8008(12)	1.7329(13)	1.7509(15)
Al1-O2	1.7962(16)	1.7700(12)	-	2.0195(19)[e]
O1-C31	1.400(2)	1.437(2)	1.348(2)	1.421(3)
C31-C32	1.596(3)[a]	1.607(2)	1.338(3)	1.571(3)[f]
C32-O2	1.353(3)[b]	1.408(2)	1.518(3)[c]	-
N1−Al1−N2	109.56(8)	111.67(7)	111.71(6)	115.11(7)
O1-Al-O2	105.11(7)	91.52(6)	-	114.35(8)[g]
N1-Al1-O1	121.15(8)	117.00(6)	107.12(6)	111.13(8)
N2-Al1-O2	116.07(8)	113.65(6)	114.23(6)	99.95(7)[h]

Table 3. 4 : Selected bond lengths (Å) and angles (°) of compounds **3.38 ─ 3.41**. [a]C32–C33 1.529(3), C33–C34 1.362(3); [b]C34-O2; [c]C31-C35; [d]N2-Al1-O1; [e]Al1-C30; [f]unaffected C-C single bond; [g]O1-Al1-C30; [h] N2-Al1-C30; [i]The C31 in **3.41**: O1–C31–C36 110.45(17), O1–C31–C32,109.02(18), C32–C31–C36 118.93(18).

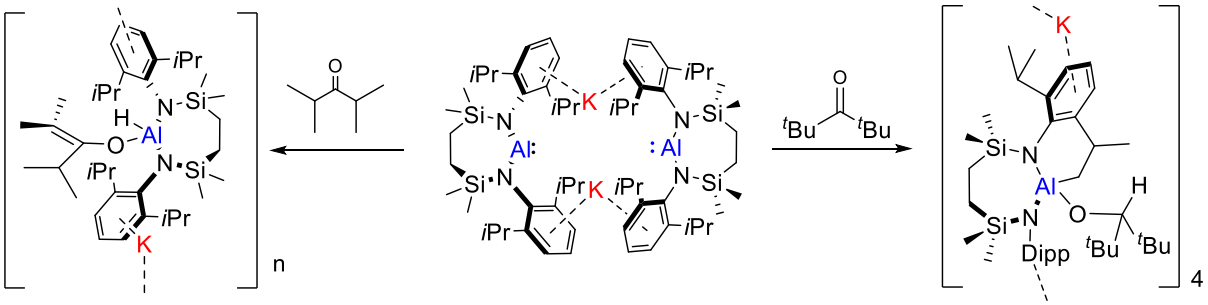

3.40 **3.12** **3.41**

Scheme 3. 26 : Synthesis of compounds **3.40** and **3.41**.

To shed further light on how the reductive reactivity of compound **3.12** is affected by the identity of the ketone reagent, it was then introduced to 2,4-dimethyl-3-pentanone. Colourless single crystals were obtained as the product (**3.40**) from a reaction mixture in d_6 -benzene heated at 60 ˚C for eight hours (**Scheme 3.26**). The subsequent X-ray analysis disclosed the identity of the product to be another polymeric species, the potassium (hydrido)(carboxyl)diamidoaluminate (**3.40**, **Figure 3.19**, **Table 3.4**). Compound **3.40** represents a formal oxidative addition of an enolisable *iso*-propyl methine proton of 2,4-dimethyl-3-pentanone at the aluminium centre of **3.12**. This inference was supported by the C31–C32 (1.338(3) Å) and C31–C35 (1.518(3) Å) distances that are strongly indicative of the enolate formulation in the structural data of **3.40**. This feature was also evident from the solution state characterisation of **3.40**, where a diagnostic ^{13}C resonance at 94.7 ppm could be assigned to the newly formed tertiary sp^2 (C32) carbon in the enolate-unit.

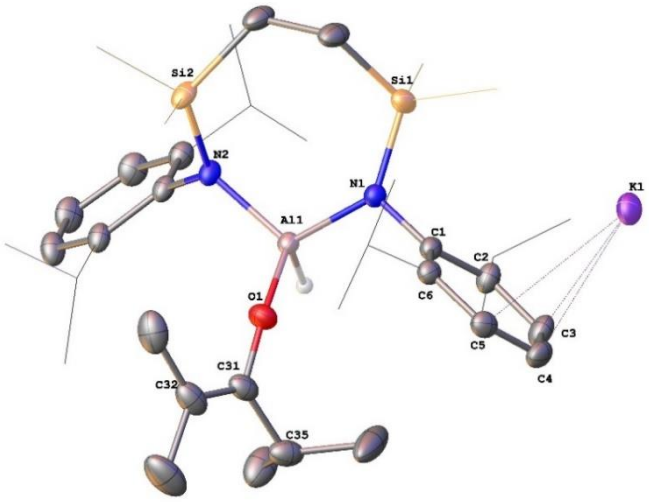

Figure 3. 19 : Displacement ellipsoid (30% probability) plot of a polymeric section of compound **3.40**. For purposes of clarity, most hydrogen atoms, disordered atoms and occluded benzene solvent are omitted, and selected methyl and iso-propyl substituents are shown as wireframe.

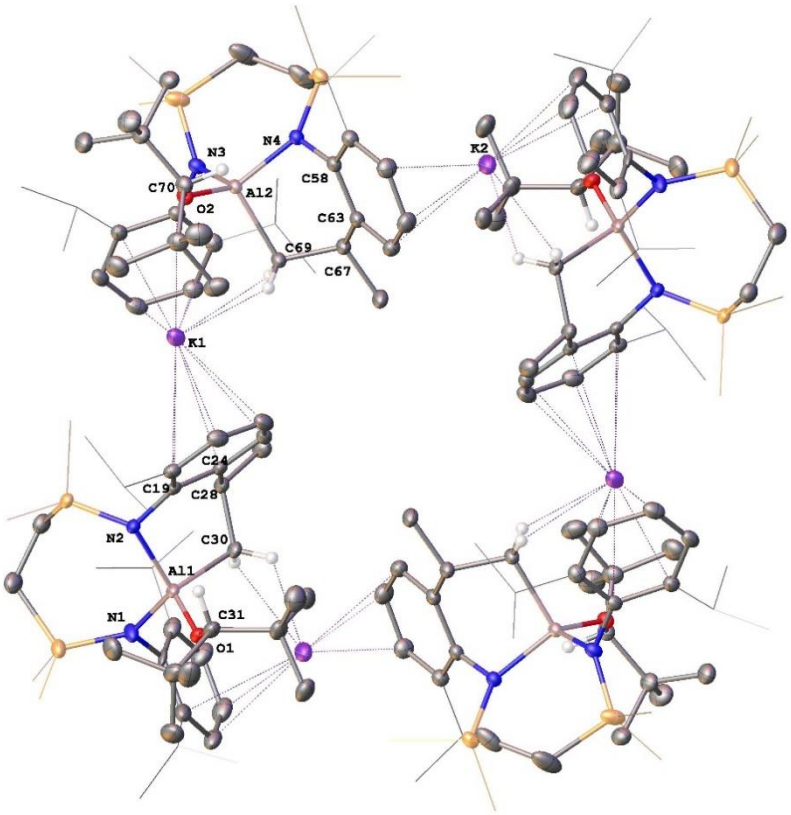

Figure 3. 20 : Displacement ellipsoid (30% probability) plot of the tetrameric aggregate of compound **3.41**. For purposes of clarity, most hydrogen atoms are omitted, and selected methyl and iso-propyl substituents are shown as wireframe.

Prompted by the formation of **3.40**, but to avoid the presence of a potentially reactive enolisable proton, 2,2,4,4-tetramethyl-3-pentanone was selected as a further ketone substrate to be reacted with **3.12**. Formation of compound **3.41** as colourless single crystals was observed when keeping the reaction mixture of **3.12** and 2,2,4,4-tetramethyl-3-pentanone in toluene for 12 hours at 60 ˚C. The resultant X-ray diffraction analysis identified **3.41** as a tetrameric potassium alkoxyaluminate, where the cyclotetrameric aggregation originated from a sequence of potassium–aryl interactions (**Figure 3.20**, **Table 3.4**). The 2,2,4,4-tetramethyl-3-pentanoxy substituent (Al1–O1, 1.7509(15) Å) has evidently resulted from the formal hydroalumination of 2,2,4,4-tetramethyl-3-pentanone, where the former sp^2 carbonyl carbon centre now adopts a tetrahedral geometry (O1–C31, 1.421(3)Å; O1–C31–C36 110.45(17)°, O1–C31–C32,109.02(18)°, C32–C31–C36 118.93(18)°). The hydrogen atom in this process can be deduced to have originated from the intramolecular C–H bond activation of an *iso*-propyl methyl group in the *N*-Dipp substituents, with the result that the fourth coordination site of the aluminium centre in the novel aluminate anion (**3.41**) is provided by a new (Al1–C30, 2.0195(19) Å) aluminium-methylene bond. Moreover, the molecular structure of **3.41** demonstrates that each molecular unit possesses two stereogenic centres (Al1 and C31), which

was reflected in the NMR spectroscopic characterisation of **3.41** conducted in d_8-THF (**Figure 3.21**). The ^{1}H NMR spectrum of **3.41** shows that there are two diastereomers, which, although inseparable, are clearly distinguishable. Most characteristically, two singlets at δ_H 3.63 ppm and 2.75 ppm may be unambiguously attributed to the Al–O–C*H* environments of each diastereomer, which was further verified by a ^{1}H–^{13}C HSQC experiment performed on **3.41**. The asymmetry of the {SiN^{Dipp}} backbone was also apparent in the four distinctive resonances assigned for the SiMe substituents (each relatively integrated to 3H) in the ^{1}H NMR spectrum.

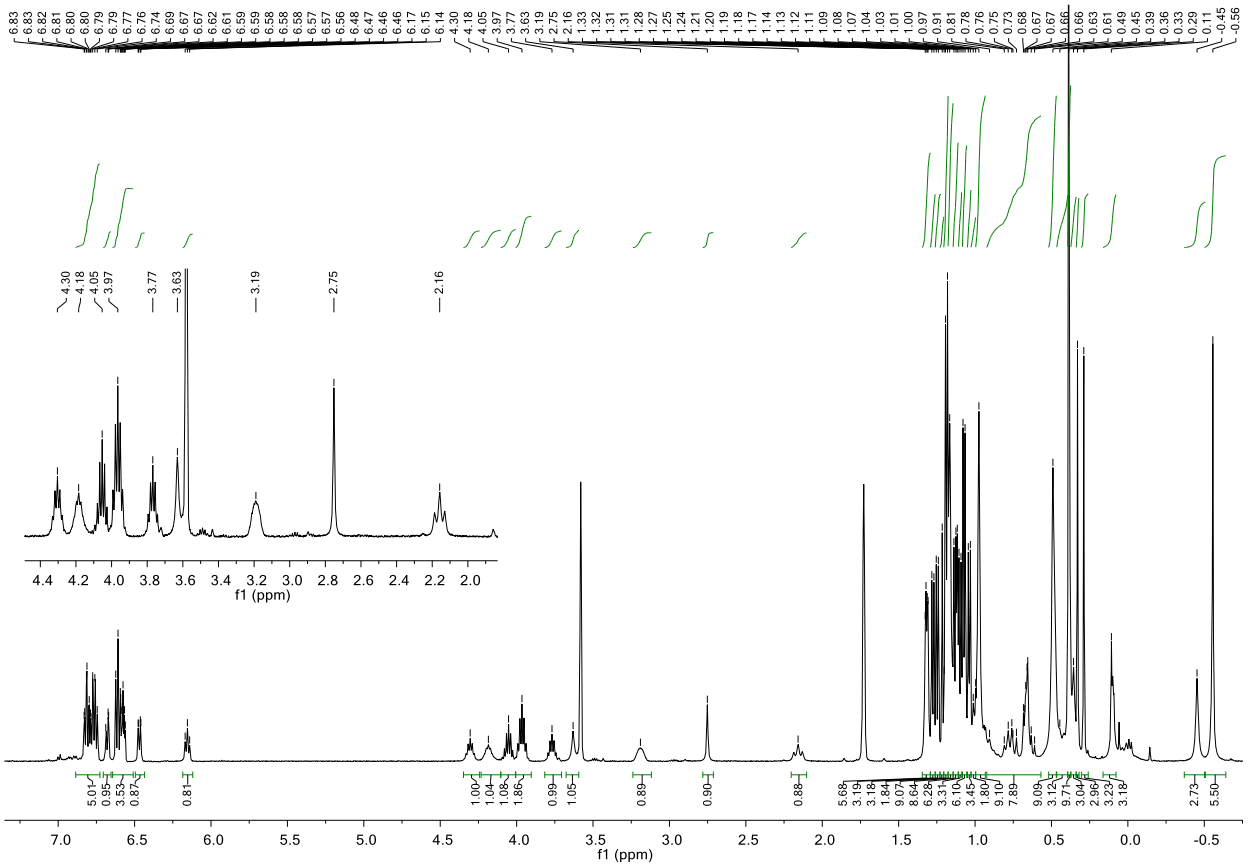

Figure 3. 21 : ^{1}H NMR (500 MHz, 298 K, d_8-THF) spectrum of **3.41**.

Although further in-situ monitoring of this process was precluded by the simultaneous formation and crystallisation of compound **3.41** under the applied reaction conditions, this reactivity is plausibly initiated through the coordination of a molecule of ketone to the aluminium centre of **3.12**. Previous studies of compound **3.5** have shown the augmented reductive Al(I) reactivity toward the C–C bonds of even benzene solvent that may be induced by abstraction of its potassium cations.[24] It is, thus, hypothesised that a similar disruption of the robust dimeric structure of **3.12** initiates the intramolecular oxidative addition of a C(sp^3)–H bond at the Al(I) centre, and the transiently formed hydridic Al–H bonds subsequently attack the carbonyl carbon, yielding the observed product **3.41**.

3.6 Potent Reducing Property of [{SiN^{Dipp}}AlK]$_2$ Towards p-block Substrates

As previously described in **Section 1.2**, the bisboryl-substituted stannylene (**1.11**) exhibits unprecedented reactivity in the class of stannylene molecules, which can be attributed to the decreased HOMO-LUMO gap in **1.11** originating from the interactions between the tin(II) centre with the adjacent boryl substituents. In a similar vein, anionic alumanyl supporting groups, being π-accepting and σ-donating ligands, may be anticipated to provide similar effects to that of boryls. Salt metathesis has been shown to be a feasible strategy in the preparation of boryl-substituted low oxidation state *p*-block species. Encouraged by the nucleophilic behaviour of [{SiN^{Dipp}}AlK]$_2$ demonstrated towards boron- and carbon-centred electrophiles (synthesis of **3.23–3.25, section 3.2**), the synthesis of [{SiN^{Dipp}}Al]-substituted low oxidation state p-block species (which are isoelectronic to singlet carbenes) was then investigated (**Figure 3.22**).

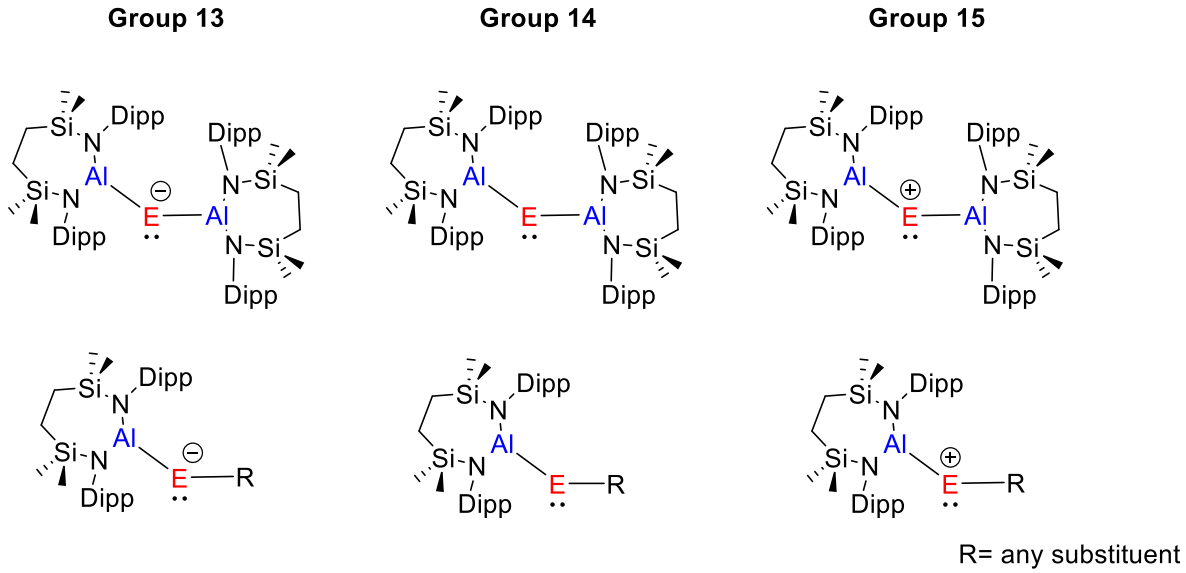

Figure 3. 22 : Proposed [{SiN^{Dipp}}Al]-substituted low oxidation state *p*-block molecules.

" These chemical bonds, they're too fragile." – Bibian O.-E., 2020.

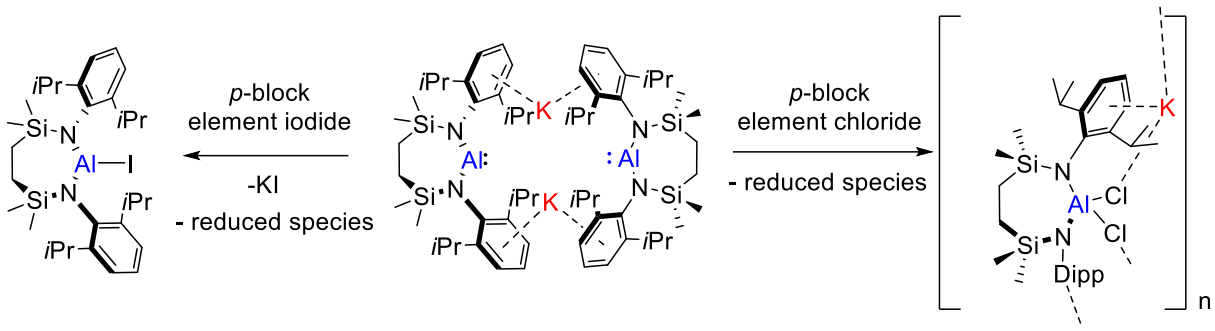

3.42 **3.12** **3.43**

Scheme 3. 27 : Reaction of **3.12** towards parent element halides in p-block.

Compound **3.12** was firstly treated with various parent *p*-block halides (BCl_3, $AlCl_3$, AlI_3, GaI_3, $InCl_3$, $GeCl_2$-dioxane, $SnCl_2$, SnI_4, PbI_2, PCl_3, $SbCl_3$, $BiCl_3$) as an initial approach to the proposed molecules depicted in **Figure 3.22**. In every case, formation of reduced *p*-block species was observed upon the introduction of **3.12**, plausibly either as metal deposition or the insoluble aggregation of unidentifiable low oxidation state element-halides. This deduction was subsequently supported by the identification of the formally oxidised product of **3.12**, as the related iodoalumane (**3.42**) or the potassium dichloroaluminate (**3.43**) (**Scheme 3.27**). The *in-situ* ^{1}H and ^{13}C NMR spectroscopic studies conducted on the crude reaction mixtures of **3.12** and the range of element iodides studied confirmed the production of **3.42** as the only soluble species by comparison to the reported spectra of the iodoalumane (**3.42**) (**Figure 3.23**). On the other hand, compound **3.43** was isolated by crystallisation from the filtrate of the reaction mixtures in benzene, facilitating its characterisation by both NMR spectroscopy and X-ray diffraction analysis (**Figure 3.24**). Like many derivatives of **3.12**, compound **3.43** features a polymeric structure propagated through intra- and intermolecular K^+ arene association and, in this case, K···Cl interactions. The significantly contracted Al-N distances (Al1-N1 1.8373(14) Å, Al1-N2 1.8428(15) Å) in **3.43** in comparison to those in compound **3.12** (Al-N, avg. 1.892 Å) clearly denote the oxidised aluminium centre in **3.43**, reflecting the reducing nature of compound **3.12** towards *p*-block halides.

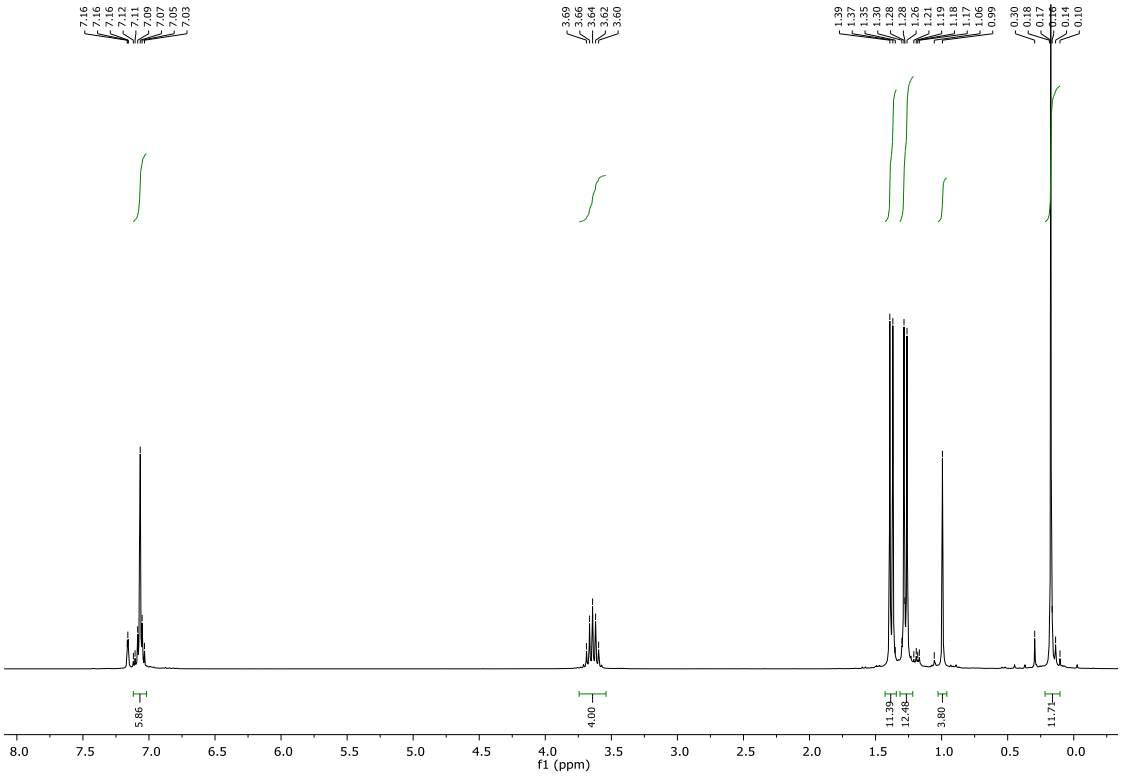

Figure 3. 23 : The *in-situ* generated ^{1}H NMR (500 MHz, 298 K, C_6D_6) spectrum of **3.42**.

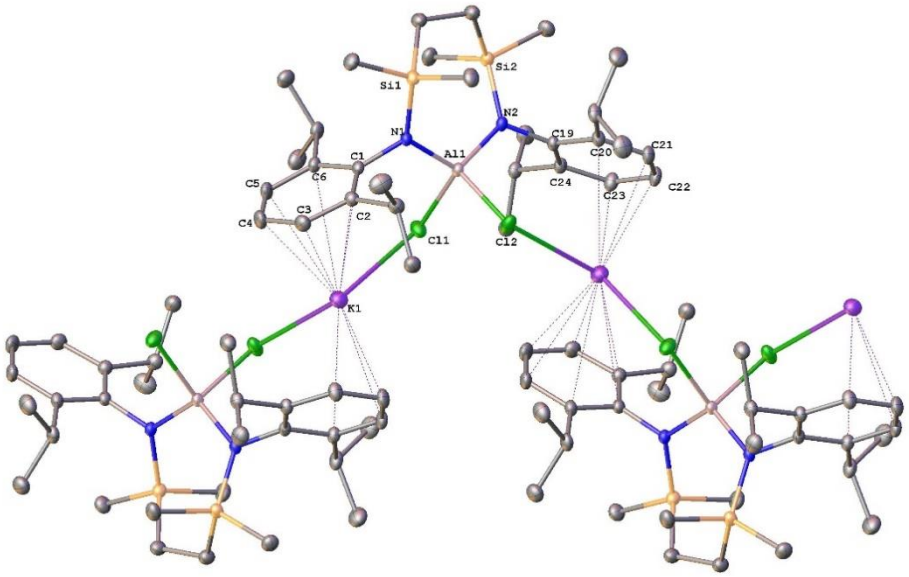

Figure 3. 24 : Displacement ellipsoid (30% probability) plot of a polymeric section of compound **3.43**. For purposes of clarity, most hydrogen atoms, disordered atoms and occluded benzene solvent are omitted. Selected Bond Distances (Å) and Bond Angles (°): Al1-N1 1.8373(14), Al1-N2 1.8428(15), Al1-Cl1 2.2034(6), Al1-Cl2 2.1960(6); N1-Al1-N2 116.75(6) N1-Al1-Cl1 107.70(5) N2-Al1-Cl2 107.80(5) Cl1-Al1-Cl2 98.54(3).

In light of the production of **3.42** and **3.43** under the applied reaction conditions, compound **3.12** was treated with more kinetically stabilised aluminium halide substrates, such that the potential products would display higher stability and continued solubility to allow their subsequent isolation. Interestingly, the reaction of **3.12** with either $[Cp^*AlCl_2]_2$ or $[Cp^*Al(OTf)_2]_2$ generates the reduced aluminium species $[Cp^*Al]_4$ regardless of the varying identity of the leaving group.[6] In a reaction between **3.12** and *N*-heterocyclic carbene-stabilised Cp^*AlCl_2, compound **3.44** ($[(\{SiN^{Dipp}\}AlCl_2)KCp^*_2K_2]_2$) was identified and characterised by X-ray diffraction analysis performed on a mechanically separated single crystal (**Figure 3.25**). In this reaction, the pentamethylcyclopentadienyl moiety is formally reduced and abstracted from the starting material by compound **3.12**. Although **3.44** is not representative of the entirety of the reaction, it still further reflects the potent reducing ability of **3.12** towards *p*-block substrates.

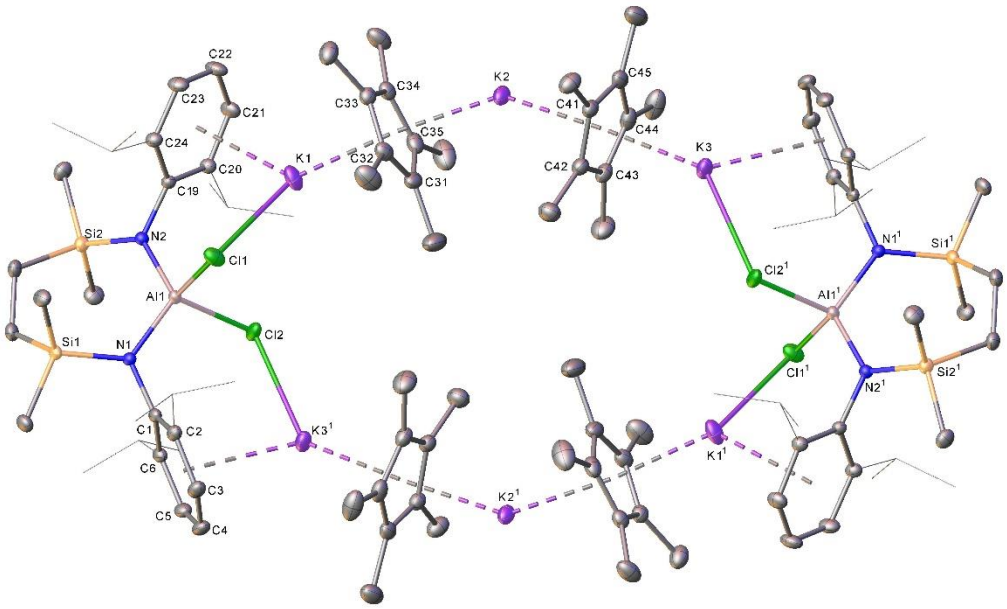

Figure 3. 25 : Displacement ellipsoid (30% probability) plot of a polymeric section of compound **3.44** ($[(\{SiN^{Dipp}\}AlCl_2)KCp^*_2K_2]_2$). For purposes of clarity, most hydrogen atoms, disordered atoms are omitted, and selected methyl and iso-propyl substituents are shown as wireframe. Selected Bond Distances (Å) and Bond Angles (°): Al1-N1, 1.8345(14); Al1-N2, 1.8454(14); Al1-Cl1, 2.1884(7); Al1-Cl2, 2.2018(6); C31-C32, 1.413(3); C32-C33, 1.413(3); C33-C34, 1.414(3); C34-C35, 1.406(3); C31-C35, 1.404(3); N1-Al1-N2, 118.07(6); N1-Al1-Cl1, 118.07(6); N2-Al1-Cl2, 111.64(5); Cl1-Al1-Cl2, 99.28(3).

Intrigued by the strongly reducing and homogeneous reactivity demonstrated by **3.12**, which can plausibly be attributed to the electropositive and high halogen affinity of the aluminium centre, it was then utilised as a reductant in the synthesis of various reported reduced main-group species. As depicted in **Scheme 3.28**, compound **3.12** can indeed be implemented

as a reductive halide abstractor in the preparation of low oxidation state *p*-block molecules, and its good solubility (well-dissolved in *n*-hexane) in comparison to conventional reducing agents (e.g. group 1 metals) may provide a potential further application of compound **3.12**.

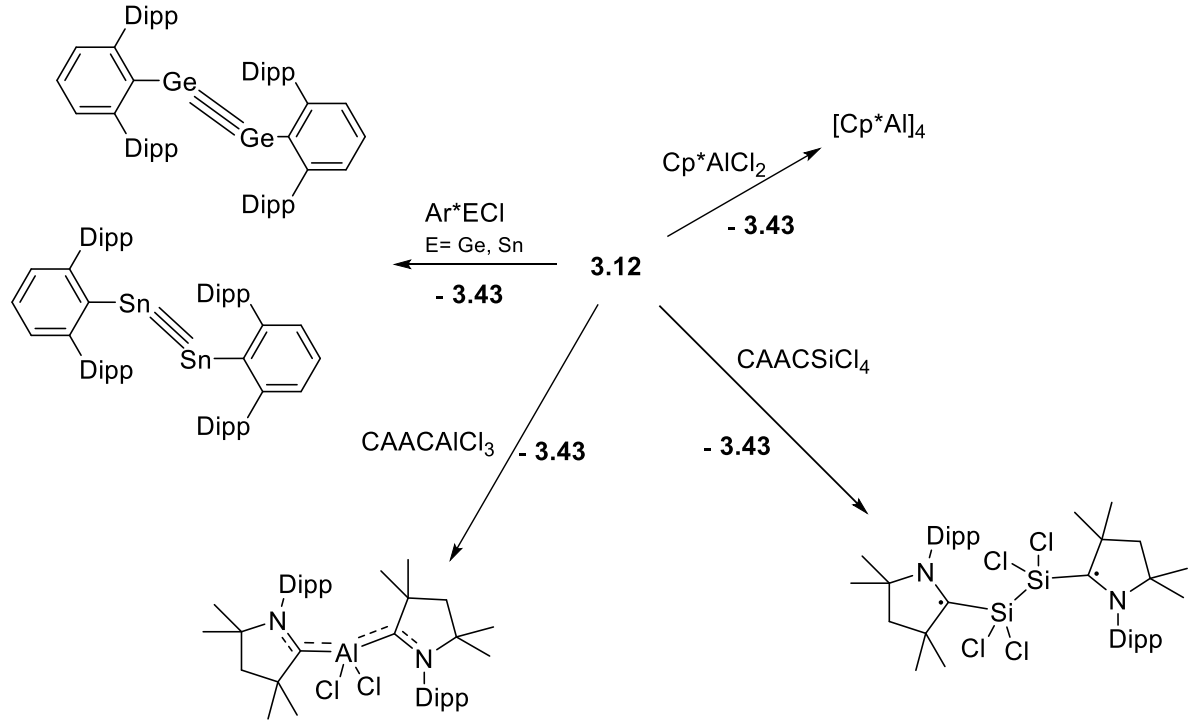

Scheme 3. 28 : Examples of known reduced *p*-block species prepared by reactions of **3.12** with respective high-oxidation precursors (where the identities of products were confirmed by respective unit-cell checks of obtained single crystals).[6,55-58]

3.7 Conclusion and Future Work

The reactivity of [{SiN^{Dipp}}AlK]$_2$ (**3.12**) has been extensively examined towards various organic small molecules. The newly prepared compound **3.12** with a formally anionic Al(I) centre demonstrates nucleophilicity and Lewis basicity alongside a potent reducing character, highlighting its low oxidation state aluminium centred nature. Oxidative addition across the Al(I) centre has been observed with a variety of organic molecules, even the relatively inert C-H bond of the benzene molecule. The Al(I) centred reactivity of **3.12** was also observed to vary with the precise structure within a specific subset of small molecule substrates, an observation which was especially denoted with its reactivity towards ketones. Although attempts to prepare lighter group 1 counterparts of **3.12** only provided the isolation of **3.28**, the rubidium and caesium analogues of **3.12** were successfully synthesised and assessed through their capability to activate benzene. This qualitative reactivity study indicated that a heavier counterion of the [{SiN^{Dipp}}Al] anion can result in a more rapid reaction towards organic molecules.

Although attempts to synthesise [{SiN^{Dipp}}Al]-substituted *p*-block low oxidation state molecules *via* salt metathesis were not successful, **3.12** has demonstrated its potential to be implemented as a potent homogeneous reducing reagent. On the other hand, the desired alumanyl supported *p*-block singlet carbene analogues may require a different synthetic route (e.g. oxidative addition), in that aluminium is one of the most electropositive elements in the *p*-block. A salt metathesis protocol with **3.12** for the generation of novel element-aluminium bond, however, might still be applicable for more electropositive elements.

"What a lovely molecule!" – M. F. Mahon

3.8 Experimental data

[({SiN^{Dipp}}AlBPh$_3$)K] (3.23)

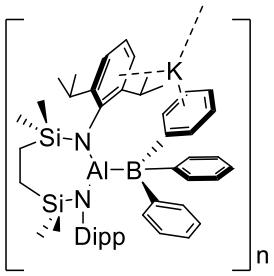

Inside a J-Young's tube, [{SiN^{Dipp}}AlK]$_2$ (**3.12**, 23 mg, 0.0205 mmol) was dissolved in 0.4 mL of d_6-benzene before the addition of BPh_3 (10mg, 0.041 mmol) into the clear bright yellow solution. Colourless solids crystallised from the reaction mixture inside the standing J Young's tube to afford the compound **3.23**, Yield 22 mg, 66.8%. Sample used for NMR spectra was prepared by collecting the crystals from the reaction mixture and washing with hexane. All volatiles were then removed *in vacuo* before being redissolved in deuterated chloroform. A single crystal suitable for crystallography was obtained from slow evaporation of the saturated toluene solution of the compound at ambient temperature. Anal. Calcd. for $C_{55}H_{73}AlBN_2Si_2K$ [**3.23**.C_7H_8] (895.26) C, 73.79; H, 8.22; N, 3.13; Found, C, 73.83; H, 8.28; N, 2.78. ^{1}H NMR (500 MHz, 298 K, $CDCl_3$) (With BPh_3 and solvent impurities) : δ 7.66 – 7.62 (m, 6H, B*Ph*$_3$), 7.59 – 7.54 (m, 3H, *p*-B*Ph*$_3$), 7.48-7.45 (m, 6H, B*Ph*$_3$), 7.07 – 7.00 (m, 6H, C_6H_3), 3.46 – 3.29 (sept, *J* = 6.9 Hz, 4H, C*H*Me$_2$), 1.18 (d, *J* = 6.9 Hz, 24H, CH*Me*$_2$), 0.58 (s, 4H, SiCH_2), 0.09 (s, 12H, Si*Me*$_2$). ^{13}C{^{1}H} NMR (126 MHz, 298 K, $CDCl_3$) δ 143.75, 143.55, 139.78 (Quaternary carbons for NC_6H_3 and B*Ph*$_3$), 138.6, 131.2, 127.4, (B*Ph*$_3$) 123.0, 122.8 (NC_6H_3), 28.1 (*C*HMe$_2$), 23.6 (CH*Me*$_2$), 9.5 (Si*C*H$_2$), -1.8 (Si*Me*$_2$). No ^{11}B resonance correlated to the LAl-*B*Ph$_3$ was observed (BPh_3 impurity observed).

[{SiN^{Dipp}}AlMe] (3.24)

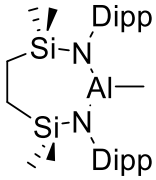

In a J-Young's tube, [{SiN^{Dipp}}AlK]$_2$ (**3.12**, 28 mg, 0.025 mmol) was dissolved in 0.4 mL of d_6-benzene before the addition of MeOTf (5.5 μL, 8.2 mg, 0.05 mmol) *via* a micropipette. The reaction mixture became colourless with the instantaneous formation of a white precipitate. NMR spectra were then recorded without further purification of the crude product, and the resonances were in good agreement with the previously reported data for [{SiN^{Dipp}}AlMe].[33, 34] ^{1}H NMR (500 MHz, 298 K, Benzene-d_6) δ 7.04 (m, 6H, C6*H*3), 3.75 (sept, *J* = 6.9 Hz, 4H, C*H*Me$_2$), 1.28 (d, *J* = 6.9 Hz,12H, CH*Me*$_2$), 1.19 (d, J = 6.9 Hz, 12H, CH*Me*$_2$), 1.05 (s, 4H, SiCH_2), 0.17 (s, 12H, Si*Me*$_2$), -1.08 (s, 3H, Al*Me*). ^{13}C{^{1}H} NMR (126 MHz, 298 K, benzene-d6): δ 145.7, 143.3, 124.5, 123.9(C_6H_3), 28.4, 24.9, 24.4 (*C*HMe$_2$ and CH*Me*$_2$), 13.4 (Si*C*H$_2$), 0.03 (Si*Me*$_2$). ^{13}C{^{1}H} NMR resonance for AlMe not observed.

[{SiN^{Dipp}}Al-(CH(CH=CH)$_2$C)=CPh$_2$] (3.25)

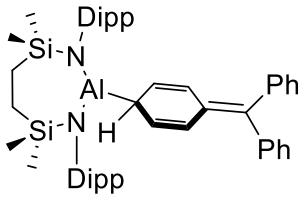

In a Young's NMR tube, [{SiN^{Dipp}}AlK]$_2$ (**3.12**, 5 mg, 0.014 mmol) was dissolved in 0.4 mL of d_8-toluene, [CPh_3][B(C_6F_5)$_4$] (24.7 mg, 0.027 mmol) was then added to the bright yellow solution**.** The reaction mixture demonstrated rapid colour changes from bright yellow to green to bright red then to light yellow within 10 minutes, and some colourless crystals were then observed. (The identity of the colourless crystal was confirmed by unit cell screening to be K[B(C_6F_5)$_4$].) The crude product was characterised by NMR spectroscopy without further purification and compound **3.25** was identified to be the major species. The solution was then filtered, slow evaporation of the toluene solution at room temperature afforded a colourless crystal suitable for X-ray crystallography. Yield 11 mg, 53.2%. No meaningful result was obtained for elemental analysis after multiple attempts. ^{1}H NMR (300 MHz, 298K, Toluene-d_8) δ 7.18-7.15 (m, 1H, Ar*H*), 7.15-7.12 (m, 2H, Ar*H*), 7.09-7.06 (m, 2H, C=C-Ar*H*), 7.06-7.04 (m, 1H, Ar*H*), 6.99-6.98 (m,

4H, Ar*H*), 6.95-6.90 (m, 6H, Ar*H*), 5.99 (dd, *J* = 10.4, 2.2 Hz, 2H, Al-CH-C*H*=CH), 4.39 (dd, *J* = 10.4, 4.3 Hz, 2H, Al-CH-CH=C*H*), 3.70 (sept, *J* = 6.9 Hz, 2H, C*H*Me$_2$), 2.85-2.82 (m, 1H, Al-C*H*-CH=CH), 1.28 (d, *J* = 6.9 Hz, 12H, CH*Me*$_2$), 1.25 (d, *J* = 6.9 Hz, 12H, CH*Me*$_2$), 0.99 (s, 4H, SiC*H*$_2$), 0.13 (s, 12H, Si*Me*$_2$). ^{13}C{^{1}H} NMR (75 MHz, 298 K, Toluene-*d*$_8$) δ 145.5 (*C*$_{sp2}$), 143.5 (*C*$_{sp2}$), 142.9 (*C*$_{sp2}$), 137.46 (*C*$_{sp2}$), 130.9 (*C*$_{sp2}$), 130.7 (*C*$_{sp2}$), 130.6 (*C*$_{sp2}$), 129.4 (*C*$_{sp2}$), 128.1 (*C*$_{sp2}$), 126.2 (*C*$_{sp2}$), 124.3 (*C*$_{sp2}$), 124.0 (*C*$_{sp2}$), 28.5 (*C*HMe$_2$), 4.9 (CH*Me*$_2$), 24.4 (CH*Me*$_2$), 13.5 (SiC*H*$_2$), -0.1 (Si*Me*$_2$). *13C resonance correlated to Al*C*H was not observed.

[{SiN^{Dipp}}AlAl{SiN^{Dipp}}] (3.26)

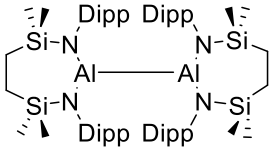

Inside a J-Young's tube, [{SiN^{Dipp}}AlK]$_2$ (**3.12**, 28 mg, 0.025 mmol) was dissolved in 0.4mL of deuterated benzene. 7,7,8,8-Tetracyanoquinodimethane (TCNQ, 10.2 mg, 0.05 mmol) was then added to the bright yellow solution. A blue precipitate was observed in the reaction mixture as the solution became pale yellow in colour. The solid was then removed by filtration and compound **3.26** was identified by X-ray crystallography as a colourless crystal selected from the mix of crystals obtained from slow evaporation of the benzene solution of the crude reaction mixture.

[{SiN^{Dipp}}Al(H)(Ph)K] (3.27)

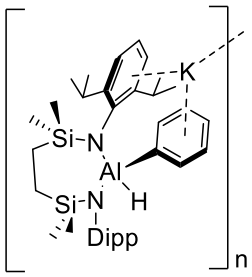

Inside a J-Young's tube, [({SiN^{Dipp}}Al)K]$_2$ (**3.12**, 28 mg, 0.025 mmol) was dissolved in 0.4 mL of benzene to afford a bright yellow solution. The reaction mixture was then kept at 110 ˚C for 14 days, during which a gradual decolourisation of the mixture was observed. After two weeks, colourless crystals were observed with the pale-orange hazy solution. The supernatant was then carefully decanted, colourless crystals were collected and washed with hexane (0.4 mL x 2) before removal of all volatiles to afford **3.27** as a colourless crystalline powder. Yield 24 mg, 75%. A single crystal suitable for X-ray crystallography was then picked from the obtained crystals. No meaningful result for elemental analyses was obtained after several attempts. ^{1}H NMR (400 MHz, 298 K, THF-*d*$_8$) δ 7.12 – 7.05 (m, 2H, *o*-C$_6$*H*$_5$), 6.83 – 6.77 (m, 2H, *p*-C$_6$*H*$_3$ on SiN^{Dipp}), 6.68 – 6.62 (m, 3H, Ar*H*), 6.63 – 6.57 (m, 4H, *m*-C$_6$*H*$_3$ on SiN^{Dipp}), 4.28 (sept, *J* = 6.9 Hz, 2H, C*H*Me$_2$ on SiN^{Dipp}), 3.94 (p, *J* = 6.9 Hz, 2H, C*H*Me$_2$ on SiN^{Dipp}), 1.17 (d, *J* = 6.9 Hz, 6H, CH*Me*$_2$ on SiN^{Dipp}), 1.14 (d, *J* = 6.9 Hz, 6H, CH*Me*$_2$ on SiN^{Dipp}), 1.07 (d, *J* = 6.9 Hz, 6H, CH*Me*$_2$ on SiN^{Dipp}), 1.03 – 0.93 (m, 4H, SiC*H*$_2$), 0.42 (d, *J* = 6.9 Hz, 6H, CH*Me*$_2$ on SiN^{Dipp}), 0.02 (s br, 12H, Si*Me*$_2$). ^{1}H resonance correlated to Al-*H* was not observed. ^{13}C{^{1}H} NMR (101 MHz, 298 K, THF-*d*$_8$) δ 151.4 (*i*-*C*$_6$H$_3$ on SiN^{Dipp}), 148.5 (*o*-*C*$_6$H$_3$ on SiN^{Dipp}), 148.0 (*o*-*C*$_6$H$_3$ on SiN^{Dipp}), 140.0 (*o*-*C*$_6$H$_5$), 125.8 (*m*-*C*$_6$H$_5$), 124.6 (*p*-*C*$_6$H$_5$), 123.5 (*m*-*C*$_6$H$_3$ on SiN^{Dipp}), 123.2 (*m*-*C*$_6$H$_3$ on SiN^{Dipp}), 121.3 (*p*-*C*$_6$H$_3$ on SiN^{Dipp}), 27.9 (*C*HMe$_2$), 27.9 (*C*HMe$_2$), 26.5 (CH*Me*$_2$), 26.4 (CH*Me*$_2$), 26.2 (CH*Me*$_2$), 26.0 (CH*Me*$_2$**)**, 16.2 (Si*C*H$_2$), 2.4 (Si*Me*$_2$), 1.7 (Si*Me*$_2$). ^{13}C resonance correlated to Al-*C* (*i*-*C*$_6$H$_5$) was not observed.

[{SiN^{Dipp}}AlNa({SiN^{Dipp}}Na$_2$)NaAl{SiN^{Dipp}}](3.28)

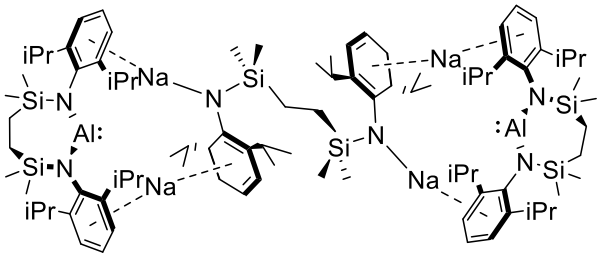

[{SiN^{Dipp}}AlI] (0.648 g, 1.0 mmol) and excess Na/NaCl (5 wt.%, 1.5 g) were charged to a Schlenk flask before addition of hexane (25 mL) into the vessel via cannula. The reaction mixture was then stirred for 3 days at room temperature, affording a pale-yellow solution with a grey suspension. The crude mixture was then filtered and concentrated

(to about 5 mL), and storage of the concentrated solution at -10 °C for 3 days afforded **3.28** as colourless crystalline powders in moderate yield (accounted by {SiN^{Dipp}}moiety). Yield 0.21 g, 77%. A single crystal suitable for X-ray diffraction was then picked from the batch of recrystallised solids. No meaningful result for elemental analysis was obtained after several attempts. The reaction was then repeated in a smaller scale for monitoring by NMR spectroscopy. In a J-Young's tube, [{SiN^{Dipp}}AlI] (16 mg, 0.025 mmol) was dissolved in C_6D_6 before addition of excess Na/NaCl (5 wt.%, 30 mg) to the colourless solution. The reaction mixture was then kept at 30 °C and continually shaken for 5 days. The ^{1}H NMR spectrum obtained in the small-scale reaction was virtually identical to that of the isolated sample, indicating exclusive formation of **3.28** under the applied reaction conditions. ^{1}H NMR (400 MHz, 298 K, Benzene-d_6) δ 7.05 (d_{app}, 4H, m-C$_6$*H*$_3$), 7.00 – 6.84 (m, 13H, C$_6$*H*$_3$), 6.72 (t_{app}, 1H, *p*-C$_6$*H*$_3$), 4.00 (sept, *J* = 6.8 Hz, 4H,C*H*Me$_2$), 3.87 – 3.68 (m, 8H, C*H*Me$_2$), 1.33 – 1.22 (m, 45H, CH*Me*$_2$), 1.19* (d, *J* = 6.8 Hz, CH*Me*$_2$), 1.18* (d, *J* = 6.8 Hz, 6H, CH*Me*$_2$), * overlapping doublets, 1.15 (s, 4H, SiC*H*$_2$), 1.13 (s, 8H, SiC*H*$_2$), 1.10 – 1.04 (m, 15H, CH*Me*$_2$), 0.26 – 0.12 (m, 36H, Si*Me*$_2$). ^{13}C{^{1}H} NMR (101 MHz, 298 K, Benzene-d_6) δ 148.2 (*i*-C$_6$H$_3$), 148.1 (*i*-C$_6$H$_3$), 145.7 (*o*-C$_6$H$_3$), 145.4 (*o*-C$_6$H$_3$), 123.9 (*m*-C$_6$H$_3$), 123.5 (*m*-C$_6$H$_3$), 123.4 (*p*-C$_6$H$_3$), 122.9 (*p*-C$_6$H$_3$), 28.7 (*C*HMe$_2$), 28.4 (*C*HMe$_2$), 27.9 (*C*HMe$_2$), 27.5 (*C*HMe$_2$), 25.6 (CH*Me*$_2$), 25.6 (CH*Me*$_2$), 25.1 (CH*Me*$_2$), 24.9 (CH*Me*$_2$), 24.7 (CH*Me*$_2$), 24.4 (CH*Me*$_2$), 24.2 (CH*Me*$_2$), 24.1 (CH*Me*$_2$), 14.6 (Si*C*H$_2$), 14.3 (Si*C*H$_2$), 14.2 (Si*C*H$_2$), 13.4 (Si*C*H$_2$), 1.5 (Si*Me*$_2$), 1.2 (Si*Me*$_2$), 0.0 (Si*Me*$_2$), -0.2 (Si*Me*$_2$).

[({SiN^{Dipp}}Al)Rb]$_2$ (3.29)

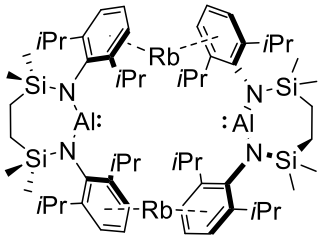

[{SiN^{Dipp}}AlI] (0.324 g, 0.500 mmol) and Rb metal (0.140 g, 1.655 mmol) was charged into a Schlenk flask, before hexane (30mL) was added *via* cannula. The reaction mixture was then stirred at 30 °C for 3 days, giving a bright yellow solution with a grey suspension. The mixture was then filtered through a cannula filter, and the bright yellow filtrate was collected and put under reduced pressure to remove all volatiles. [({SiN^{Dipp}}Al)Rb]$_2$ (**3.29**) was obtained as a bright yellow crystalline powder. Yield 0.290 g, 96%. Anal. Calcd. For $C_{60}H_{100}Al_2Rb_2N_4Si_4$ (**3.29**, 1212.48) C, 59.33; H, 8.30; N, 4.61 %. Found: C, 59.42; H, 8.46, N, 4.48 %. A single crystal suitable for X-ray diffraction characterisation was obtained by slow evaporation of a hexane solution of **3.29** at room temperature. ^{1}H NMR (500 MHz, 298 K, Benzene-d_6) δ 6.89 (d, *J* = 7.6 Hz, 4H, *m*-C$_6$*H*$_3$), 6.75 (t, *J* = 7.6 Hz, 2H, *p*-C$_6$*H*$_3$), 4.04 (sept, *J* = 6.9 Hz, 4H, C*H*Me$_2$), 1.30 (d, *J* = 6.9 Hz, 12H, CH*Me*$_2$), 1.13 (s, 4H, SiC*H*$_2$), 1.08 (d, *J* = 6.9 Hz, 12H, CH*Me*$_2$), 0.22 (s, 12H, Si*Me*$_2$). ^{13}C{^{1}H} NMR (126 MHz, 298 K, Benzene-d_6) δ 152.1 (*i*-C$_6$H$_3$), 149.1 (*o*-C$_6$H$_3$), 123.0 (*m*-C$_6$H$_3$), 122.1 (*p*-C$_6$H$_3$), 27.9 (*C*HMe$_2$), 25.0 (CH*Me*$_2$), 24.0 (CH*Me*$_2$), 14.4 (Si*C*H$_2$), 1.7 (Si*Me*$_2$). *hexane impurity observed within the sample.

[({SiN^{Dipp}}Al)Cs]$_2$ (3.30)

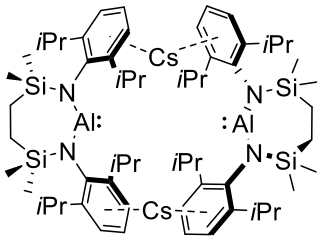

[{SiN^{Dipp}}AlI] (0.324 g, 0.500 mmol) and Cs metal (0.220 g, 1.655 mmol) was charged into a Schlenk Flask, before hexane (30mL) was added *via* cannula. The reaction mixture was then stirred at 30 °C for 2 hours followed by further stirring at room temperature for 2 days, giving a bright yellow solution with a grey suspension. The mixture was then filtered through a cannula filter, and the coloured filtrate was collected and put under reduced pressure to remove all volatiles. [({SiN^{Dipp}}Al)Cs]$_2$ (**3.30**) was obtained as a bright yellow crystalline powder. Yield 0.274 g, 86%. A single crystal suitable for X-ray diffraction characterisation was obtained by slow evaporation of a hexane solution of **3.30** at room temperature. Anal. Calcd. For

$C_{60}H_{100}Al_2Cs_2N_4Si_4$ (**3.30**, 1308.48) C, 55.03; H, 7.70; N, 4.28 %. Found: C, 54.86; H, 7.88, N, 4.10 %.^{1}H NMR (500 MHz, 298 K, Benzene-d_6) δ 6.87 (d, J = 7.5 Hz, 4H, m-C_6H_3), 6.72 (t, J = 7.5 Hz, 2H, p-C_6H_3), 4.12 (sept, J = 7.0 Hz, 4H, CHMe$_2$), 1.30 (d, J = 7.0 Hz, 12H, CHMe_2), 1.13† (s, 4H, SiCH_2), 1.13† (d, J = 7.0 Hz, 12H, CHMe_2) †overlapping peaks, 0.21 (s, 12H, SiMe_2). ^{13}C{^{1}H} NMR (126 MHz, 298 K, Benzene-d_6) δ 153.1 (i-C_6H_3), 149.1 (o-C_6H_3), 123.4 (m-C_6H_3) 122.0 (p-C_6H_3), 28.0 (CHMe$_2$), 24.9 (CHMe_2), 24.0 (CHMe_2), 14.4 (SiCH_2), 1.6 (SiMe_2). *hexane impurity observed within the sample.

[{SiN^{Dipp}}Al(H)(Ph)Rb] (3.31)

Inside a J-Young's tube, [({SiN^{Dipp}}Al)Rb]$_2$ (**3.29**, 30 mg, 0.025mmol) was dissolved with 0.4 mL of benzene to afford a bright yellow solution. The reaction mixture was then kept at 110 °C for 5 days, during which a gradual de-colourisation of the mixture was observed. After 5 days, colourless crystals were observed with the pale-orange hazy solution. The supernatant was then carefully decanted, colourless crystals were collected and washed with hexane (0.4 mL x 2) before removal of all volatiles, affording **3.31** as a colourless crystalline powder. Yield 23 mg, 67%. A single crystal suitable for X-ray crystallography was then picked from the obtained crystals. No meaningful result for elemental analysis was obtained after several attempts. ^{1}H NMR (400 MHz, 298 K, THF-d_8) δ 7.28 – 7.20 (m, 2H, o-C_6H_5), 6.85 – 6.87 (m, 2H, p-C_6H_3 on SiN^{Dipp}), 6.73 – 6.58 (m, 7H, ArH), 4.30 (sept, J = 6.8 Hz, 2H, CHMe$_2$), 3.93 (sept, J = 6.8 Hz, 2H, CHMe$_2$), 1.25 (d, J = 6.8 Hz, 6H, CHMe_2), 1.16 (d, J = 6.8Hz, 6H, CHMe_2), 1.08 (d, J = 6.8 Hz, 6H, CHMe_2), 1.04 – 0.94 (m, 4H, SiCH_2), 0.41 (d, J = 6.8 Hz, 6H, CHMe_2), 0.04 (s, 6H, SiMe_2), 0.03 (s, 6H, SiMe_2). ^{1}H resonance correlated to Al-H was not observed. ^{13}C{^{1}H} NMR (101 MHz, 298 K, THF-d_8) δ 151.4 (i-C_6H_3 on SiN^{Dipp}), 148.7 (o-C_6H_3 on SiN^{Dipp}), 148.2 (o-C_6H_3 on SiN^{Dipp}), 139.9 (o-C_6H_5), 126.3 (m-C_6H_5), 125.1 (p-C_6H_5), 123.7 (o-C_6H_3 on SiN^{Dipp}) , 123.5 (o-C_6H_3 on SiN^{Dipp}), 121.6 (p-C_6H_3 on SiN^{Dipp}), 27.9 (CHMe$_2$), 26.4 (CHMe_2), 26.3 (CHMe_2), 26.1(CHMe_2), 26.0 (CHMe_2), 16.1 (SiCH_2), 2.4 (SiMe_2), 1.6 (SiMe_2). ^{13}C resonance correlated to Al-C (i-C_6H_5) was not observed. hexane impurity observed within the sample.

[{SiN^{Dipp}}Al(H)(Ph)Cs] (3.32)

Inside a J-Young's tube, [({SiN^{Dipp}}Al)Cs]$_2$ (**3.30**, 33 mg, 0.025 mmol) was dissolved with 0.4 mL of benzene to afford a bright yellow solution. The reaction mixture was then kept at 110 °C for 12 hours, during which de-colourisation of the mixture and white precipitation was observed. The tube was then taken into glovebox, and 0.1 mL of toluene was added to the reaction mixture. The reaction mixture was then kept at 60 °C, affording single crystals suitable for X-ray diffraction analysis. The supernatant was then carefully decanted, the colourless crystals were collected and washed with hexane (0.4 mL x 2) before removal of all volatiles, affording **3.32** as a colourless crystalline powder. Yield 21 mg, 60%. ^{1}H NMR (400 MHz, 298 K, THF-d_8) δ 7.32 – 7.30 (m, 2H, o-C_6H_5), 6.88 – 6.86 (m, 2H, p-C_6H_3 on SiN^{Dipp}), 6.76 – 6.70 (m, 3H, m- and p-C_6H_5), 6.70 – 6.59 (m, 4H, m-C_6H_3 on SiN^{Dipp}), 4.32 (sept, J = 6.8 Hz, 2H, CHMe$_2$), 3.93 (sept, J = 6.8 Hz, 2H, CHMe$_2$), 1.28 (d, J = 6.8 Hz, 6H, CHMe_2), 1.17 (d, J = 6.9 Hz, 6H, CHMe_2), 1.09 (d, J = 6.8 Hz, 6H, CHMe_2), 1.05 – 0.94 (m, 4H, SiCH_2), 0.41 (d, J = 6.8 Hz, 6H, CHMe_2), 0.05 (s, 6H, SiMe_2), 0.02 (s, 6H, SiMe_2). ^{1}H resonance correlated to Al-H was not observed. ^{13}C{^{1}H} NMR (101 MHz, 298 K, THF-d_8) δ 151.6 (i-C_6H_3 on SiN^{Dipp}), 148.8 (o-C_6H_3 on SiN^{Dipp}), 148.4 (o-C_6H_3 on SiN^{Dipp}), 140.1 (o-C_6H_5), 129.2 (m-C_6H_5), 126.4 (p-C_6H_5), 125.3 (m-C_6H_3 on SiN^{Dipp}), 123.9 (m-C_6H_3 on SiN^{Dipp}), 121.8 (p-

C_6H_3 on SiN^{Dipp}), 28.0 (*C*HMe$_2$), 26.3 (CH*Me*$_2$), 26.2 (CH*Me*$_2$), 26.1 (CH*Me*$_2$), *plausibly one CH*Me*$_2$ peak merged with ^{13}C resonance of d_8-THF, 16.1 (Si*C*H$_2$), 2.4 (Si*Me*$_2$), 1.6 (Si*Me*$_2$). ^{13}C resonance correlated to Al-*C* (*i*-C_6H_5) was not observed. Hexane impurity observed within the sample.

[{SiN^{Dipp}}Al(C$_{14}$H$_{10}$)K] (3.33)

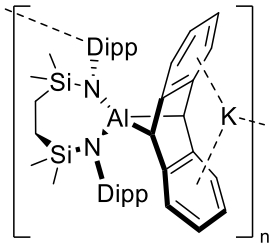

Inside a J-Young's tube, [{SiN^{Dipp}}AlK]$_2$ (**3.12**, 28 mg, 0.025 mmol) was dissolved in 0.4 mL of d_6-benzene before the addition of anthracene (9 mg, 0.05 mmol) into the clear bright yellow solution. The reaction mixture was then kept at 60 °C overnight and provided a colourless solution with white crystalline precipitates. The supernatant was then carefully decanted, colourless crystals were collected and washed with hexane (0.4 mL x 2) before removal of all volatiles, affording **3.33** as a colourless crystalline powder. Yield 26 mg, 70%. A single crystal suitable for X-ray crystallography was then picked from the obtained crystals. No meaningful result for elemental analysis was obtained after several attempts. ^{1}H NMR (500 MHz, 298 K, THF-d_8) δ 6.78 – 6.70 (m, 4H, *m*-C$_6$*H*$_3$), 6.67 – 6.59 (m, 2H, *p*-C$_6$*H*$_3$), 6.42 – 6.21 (m, 4H, Ar*H* on anthracene), 6.21 – 6.08 (m, 4H, Ar*H* on anthracene), 3.70 – 3.53 (m, 4H, C*H*Me$_2$, *overlapping with residual protio THF peak), 3.40 (s, 2H, AlC*H*), 1.21 (d, *J* = 6.7 Hz, 6H, CH*Me*$_2$), 1.17 (d, *J* = 6.7 Hz, 6H, CH*Me*$_2$), 1.02 (d, *J* = 6.5 Hz, 12H, CH*Me*$_2$), 0.89 (s br, 4H, SiC*H*$_2$), 0.12 – - 0.08 (m, 12H, Si*Me*$_2$). ^{13}C{^{1}H} NMR (126 MHz, 298 K, THF-d_8) δ 151.7 (*i*-C_6H_3), 150.3 (Ar*C* on anthracene), 145.7 (*o*-C_6H_3), 123.7 (*m*-C_6H_3), 122.3 (Ar*C* on anthracene), 121.6 (*p*-C_6H_3), 121.0 (Ar*C* on anthracene), 51.2 (Al*C*H), 28.9 (*C*HMe$_2$), 28.2 (CH*Me*$_2$), 23.1 (CH*Me*$_2$), 14.2 (Si*C*H$_2$), 4.1 (Si*Me*$_2$), 1.0 (Si*Me*$_2$). *residual anthracene was observed in both ^{1}H and ^{13}C NMR spectra.

[{SiN^{Dipp}}Al(C$_{18}$H$_{12}$)K] (3.34)

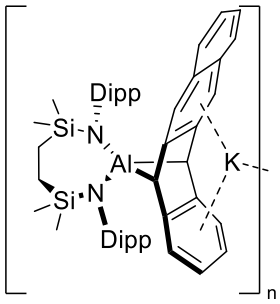

Inside a J-Young's tube, [{SiN^{Dipp}}AlK]$_2$ (**3.12**, 28 mg, 0.025 mmol) was dissolved in 0.4 mL of d_6-benzene before the addition of tetracene (11.5 mg, 0.05 mmol) into the clear bright yellow solution. The reaction mixture was then kept at 60 °C overnight to provide a colourless solution with white crystalline precipitates. The supernatant was then carefully decanted, colourless crystals were collected and washed with hexane (0.4 mL x 2) before removal of all volatiles, affording **3.34** as a colourless crystalline. Yield 30 mg, 76%. A single crystal suitable for X-ray crystallography was then picked from the obtained crystals. Anal. Calcd. For $C_{51}H_{65}AlKN_2Si_2$ (**3.34**. $(C_6H_6)_{0.5}$) C, 73.95; H, 7.91; N, 3.38 %. Found: C, 74.16; H, 7.31, N, 2.88 %. ^{1}H NMR (500 MHz, 298 K, THF-d_8) δ 7.31 – 7.03 (m, 2H, Ar*H*), 6.94 – 6.52 (m, 10H, Ar*H*), 6.30 (s, 2H, Ar*H*), 6.20 – 6.07 (m, 2H, Ar*H*), 3.75 – 3.60 (m, 4H, , C*H*Me$_2$), 3.52 (s, 2H, AlC*H*), 1.31 – 1.10 (m, 12H, , CH*Me*$_2$), 1.03 (d_{app}, 6H, CH*Me*$_2$), 0.94 – 0.92 (s br, 4H, SiC*H*$_2$), 0.92 – 0.83 (m, 6H, CH*Me*$_2$), 0.14 – –0.12 (s br, 12H, Si*Me*$_2$). ^{13}C{^{1}H} NMR (126 MHz, 298 K, THF-d_8) δ 145.7 (Ar*C*), 145.5 (Ar*C*), 132.0 (Ar*C*), 127.2 (Ar*C*), 123.7 (Ar*C*), 123.5 (Ar*C*), 122.3 (Ar*C*), 122.1 (Ar*C*), 121.6 (Ar*C*), 121.3 (Ar*C*), 117.6 (Ar*C*), 108.2 (Ar*C*), 50.9 (Al*C*H), 28.9 (*C*HMe$_2$), 28.3 (*C*HMe$_2$), 28.0 (CH*Me*$_2$), 26.4 (CH*Me*$_2$), 24.0 (CH*Me*$_2$), 23.1 (CH*Me*$_2$), 15.8 (Si*C*H$_2$), 4.0 (Si*Me*$_2$).

[({SiN^{Dipp}}Al)(H)(CC*p*-tolyl)K] (3.35)

In a J-Young's tube, [{SiN^{Dipp}}AlK]$_2$ (**3.12**, 28 mg, 0.025 mmol) was dissolved in 0.4 mL of d_6-benzene before the addition of 4-ethynyltoluene (5.5 μL, 8.2 mg, 0.05 mmol) *via* a micropipette to the bright yellow solution. The reaction mixture became colourless within 15

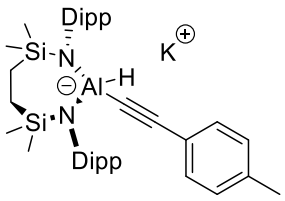

minutes of the addition of the acetylene and provided quantitative transformation of compound **3.35**. ^{1}H NMR (300 MHz, 298 K, Benzene-d_6) δ 7.04 – 6.90 (m, 2H, Ar*H* on p-tolyl), 6.84 – 6.70 (m, 6H, C_6H_3 on SiN^{Dipp}), 6.65 – 6.45 (m, 2H, Ar*H* on p-tolyl), 4.27 (sept, *J* = 6.9 Hz, 2H, C*H*Me$_2$), 4.04 (sept, *J* = 6.9 Hz, 2H, C*H*Me$_2$), 1.92 (s, 3H, CH_3 on p-tolyl), 1.40 (d, *J* = 6.9 Hz, 6H, CH*Me*$_2$), 1.32 (d, *J* = 6.9 Hz, 6H, CH*Me*$_2$), 1.27 (d, *J* = 6.9 Hz, 6H, CH*Me*$_2$), 1.21 (s, 4H, SiCH_2), 0.92 (d, *J* = 6.9 Hz, 6H, CH*Me*$_2$), 0.35 (s, 6H, Si*Me*$_2$), 0.24 (s, 6H, Si*Me*$_2$). ^{13}C{^{1}H} NMR (75 MHz, 298 K, Benzene-d_6) δ 159.0 (Al-C*C*), 150.6 (*i*-C_6H_3 on SiN^{Dipp}), 148.1 (*o*-C_6H_3 on SiN^{Dipp}), 147.9 (*o*-C_6H_3 on SiN^{Dipp}), 133.1 (Ar*C* on *p*-tolyl), 132.4 (Ar*C* on *p*-tolyl), 126.4 (Ar*C* on *p*-tolyl), 123.8 (*m*-C_6H_3 on SiN^{Dipp}), 123.1 (*m*-C_6H_3 on SiN^{Dipp}), 122.1 (*p*-C_6H_3 on SiN^{Dipp}), 27.8 (CH*Me*$_2$ on SiN^{Dipp}), 27.5 (CH*Me*$_2$ on SiN^{Dipp}), 26.4 (*C*HMe$_2$ on SiN^{Dipp}), 25.3 (CH*Me*$_2$ on SiN^{Dipp}), 24.9 (*C*H_3 on p-tolyl), 20.8 (CH*Me*$_2$ on SiN^{Dipp}), 15.0 (Si*C*H$_2$), 1.1 (Si*Me*$_2$), 0.8 (Si*Me*$_2$). The ^{1}H resonance to Al-*H* and ^{13}C resonance correlated to Al-*C*C was not observed.

[({SiN^{Dipp}}Al)(COT)K] (3.36)

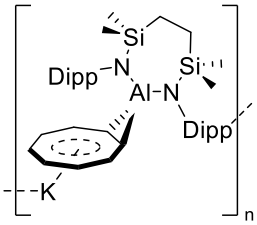

In a J-Young's tube, [{SiN^{Dipp}}AlK]2, (**3.12**, 28 mg, 0.025 mmol) was dissolved in 0.4 mL of d_6-benzene before the addition of COT (5.2 μL, 5.6 mg, 0.05 mmol) *via* a micropipette. The reaction mixture was then kept at ambient temperature overnight to afford a colourless solution with colourless crystalline powders. The supernatant was then carefully decanted, colourless crystals were collected and washed with hexane (0.4 mL x 2) before removal of all volatiles, affording **3.36** as a colourless crystalline powder. Yield 24 mg, 71%. Treatment of **3.36** with high polarity solvents or crown ethers resulted in degradation of the molecule.

[({SiN^{Dipp}}Al(C^{H_2}C^{Me})$_2$)K] (3.37)

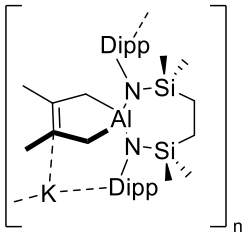

Inside a J-Young's tube, 2,3-dimethyl-1,3-butdiene (10 μL, 0.088 mmol) was dissolved in 0.4 mL of d_6-benzene before the addition of [{SiN^{Dipp}}AlK]$_2$ (**3.12**, 49.5 mg, 0.044 mmol) to afford a bright yellow reaction mixture. A ^{1}H NMR spectrum recorded right after the mixing of chemical exhibited no significant change. Colourless crystals were observed after the reaction mixture was left standing at ambient temperature for three days. A single crystal suitable for X-ray crystallography was picked from the crystalline solid, the benzene solution was then carefully decanted from the reaction mixture and the residual solid was washed with hexane (0.5 mL x 2) before removal of all volatiles under reduced pressure to afford compound **3.37** as white powder. Yield 35 mg, 62%. Anal. Calcd. For $C_{36}H_{60}AlKN_2Si_2$ (**3.37**, 643.14) C, 67.23; H, 9.40; N, 4.36 %. Found: C, 67.34; H, 9.17, N, 4.10 %. ^{1}H NMR (500 MHz, 298 K, THF-d_8) δ 6.77 (d, *J* = 7.5 Hz, 4H, *m*-C_6H_3), 6.64 (t, *J* = 7.5 Hz, 2H, *p*-C_6H_3), 4.18 (sept, *J* = 6.8 Hz, 4H, C*H*Me$_2$), 1.25 (s, 6H, AlCH$_2$C*Me*), 1.13 (d, *J* = 6.8 Hz, 12H, CH*Me*$_2$), 1.06 (d, *J* = 6.8 Hz, 12H, CH*Me*$_2$), 0.93 (s, 4H, SiCH_2), -0.11 (s, 12H, Si*Me*$_2$). *AlCH_2C^{Me} signal was not observed. ^{13}C{^{1}H} NMR (126 MHz, 298 K, THF-d_8) δ 152.2, 147.4, 134.0, (Quaternary carbons) 122.5(*m*-C_6H_3), 120.2(*p*-C_6H_3), 27.1 (*C*HMe$_2$), 26.0(CH*Me*$_2$), 25.6(CH*Me*$_2$), 23.0 (AlCH$_2$C*Me*), 15.1 (Si*C*H$_2$), 2.3 (Si*Me*$_2$). ^{13}C resonance correlated to Al*C*H$_2$C^{Me} was not observed.

[K(THF)$_2$][({SiN^{Dipp}}Al)-κ^2-O,O'-{OC^{Ph}2C^{H}(CH=CHCH=CH)C=C^{Ph}O}] (3.38)

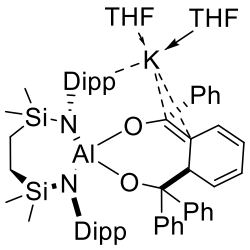

In a J Young's tube, [{SiN^{Dipp}}AlK]$_2$, (**3.12**, 28 mg, 0.025mmol), was dissolved in 0.4 mL of toluene before the addition of benzophenone (18mg, 0.10 mmol) to the bright yellow solution. The reaction mixture was then kept at 60 ˚C overnight to afford a colourless solution with a bright yellow oil. THF was then added to the reaction mixture to afford a homogeneous bright yellow solution. Bright yellow single crystals suitable for X-ray crystallography were then obtained by slow evaporation of the yellow solution at room temperature. Yield 37 mg, 80%. Anal. Calcd. For $C_{72}H_{101}AlKN_2Si_2O_6$ (**3.38**.(C_4H_8O)$_2$, 1211.86) C, 71.30; H, 8.39; N, 2.31 %. Found: C, 70.84; H, 8.06, N, 2.70 %. The recrystallised yellow crystalline solids were then collected and put under vacuum before being re-dissolved in *d*$_8$-THF for NMR characterisation. ^{1}H NMR (500 MHz, 298 K, THF-*d*$_8$) δ 7.78-7.69 (m, 2H, Ar*H*), 7.50-7.45 (m, 2H, Ar*H*), 7.04-6.99 (m, 2H, Ar*H*), 6.99-6.91 (m, 4H, Ar*H*), 6.91-6.84 (m, 1H, Ar*H*), 6.84-6.80 (m, 1H, Ar*H*), 6.78 – 6.73 (m, 1H, Ar*H*), 6.72 – 6.67 (m, 2H, Ar*H*), 6.66 – 6.58 (m, 2H, Ar*H*), 6.53-6.44 (m, 3H, Ar*H*), 6.43 – 6.17 (m, 1H, Ar*H*), 6.04 (d, *J* = 9.4 Hz, 1H, AlOC^{Ph}=CC*H*=CH), 5.60 (dd, J = 9.8, 5.3 Hz, 1H, AlOC^{Ph2}-CHC*H*=CH), 5.21 (dd, *J* = 9.8, 5.3 Hz, 1H, AlOC^{Ph2}-CHCH=C*H*), 5.10 (dd, *J* = 9.4, 5.3 Hz, 1H, AlOC^{Ph}=CCH=C*H*), 4.71-4.60 (m, 1H, C*H*Me$_2$), 4.24 – 4.03 (m, 3H, C*H*Me$_2$), 3.69 (d, *J* = 5.3 Hz, 1H, AlOC$_{Ph2}$-C*H*), 1.48-1.39 (m, 1H, SiC*H*$_2$) 1.30 (d, *J* = 6.7 Hz, 3H, CH*Me*$_2$), 1.25-1.22 (m, 1H, SiC*H*$_2$), 1.19 (d, *J* = 6.7 Hz, 3H, CH*Me*$_2$), 1.15 (d, *J* = 6.7 Hz, 3H, CH*Me*$_2$), 1.13 (d, *J* = 6.7 Hz, 3H, CH*Me*$_2$), 1.02 (d, *J* = 6.7 Hz, 3H, CH*Me*$_2$), 0.82 – 0.75 (m, 1H, SiC*H*$_2$), 0.73 (s, 3H, Si*Me*$_2$), 0.66-0.58 (m, 1H, SiC*H*$_2$), 0.49 (d, *J* = 6.7 Hz, 3H, m, 1H, CH*Me*$_2$), 0.46 (s, 3H, Si*Me*$_2$), 0.41 (d, *J* = 6.7 Hz, 3H, CH*Me*$_2$), 0.04 (d, *J* = 6.7 Hz, 3H, CH*Me*$_2$), -0.45 (s, 3H, Si*Me*$_2$), -0.55 (s, 3H, Si*Me*$_2$). ^{13}C{^{1}H} NMR (126 MHz, 298 K, THF-*d*$_8$) δ 162.2 (Al-O*C*^{Ph}=C), 153.7 (Ar*C*), 152.7 (Ar*C*), 152.4 (Ar*C*), 151.3 (Ar*C*), 150.5 (Ar*C*), 148.7 (Ar*C*), 147.6 (Ar*C*), 147.2 (Ar*C*), 147.1 (Ar*C*), 143.8 (Ar*C*), 135.7 (Ar*C*), 133.2 (Ar*C*), 132.9 (Ar*C*), 131.8 (Ar*C*), 131.4 (AlOC^{Ph2}-CH*C*H=CH) , 131.0 (Ar*C*), 130.7 (Ar*C*), 129.2 (Ar*C*), 129.0 (Ar*C*), 126.9 (Ar*C*), 126.9 (Ar*C*), 126.7 (Ar*C*), 126.2 (Ar*C*), 124.8 (Ar*C*), 124.7 (Ar*C*), 123.9 (Ar*C*), 123.8 (Ar*C*), 123.6 (Ar*C*), 123.5 (Ar*C*), 122.7 (AlOC^{Ph2}-CHCH=*C*H), 121.7 (Ar*C*), 121.6 (Ar*C*), 112.0 (AlOC^{Ph}=CCH=*C*H), 109.9 (AlOC^{Ph}=*C*), 87.0 (AlO*C*Ph$_2$), 54.0 (AlOC^{Ph2}-*C*H), 27.9 (C*H*Me$_2$), 27.9 (C*H*Me$_2$), 27.8 (C*H*Me$_2$), 27.8 (C*H*Me$_2$), 27.7 (CH*Me*$_2$), 27.6 (CH*Me*$_2$), 27.4 (CH*Me*$_2$), 27.0 (CH*Me*$_2$), 26.6 (CH*Me*$_2$), 26.3 (CH*Me*$_2$), 25.4 (CH*Me*$_2$), 24.8(CH*Me*$_2$), 15.1 (Si*C*H$_2$), 13.1 (Si*C*H$_2$), 5.0 (Si*Me*$_2$), 4.4 (Si*Me*$_2$), 2.8 (Si*Me*$_2$), 1.9 (Si*Me*$_2$).

[K({SiN^{Dipp}}Al)-κ^2-O,O'-(OCPhMe)$_2$] (3.39)

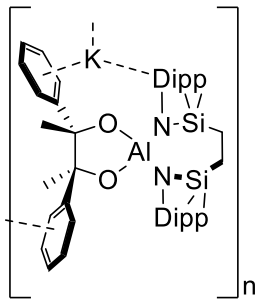

In a J Young's tube, [{SiN^{Dipp}}AlK]$_2$ (**3.12**, 28 mg, 0.025 mmol) was dissolved in 0.4 mL of *d*$_6$-benzene before the addition of acetophenone (11.5μL, 11.8mg, 0.10 mmol) *via* a micropipette. The resulting pale yellow reaction mixture was kept at 60 ˚C overnight to afford a colourless solution with colourless crystals. A single crystal suitable for X-ray crystallography was picked from the crystalline solid. The colourless solids were then collected, washed with hexane (0.5mL x 2), and dried under vacuum to give **3.39** as a colourless powder. Yield 29 mg, 72%. Synthesis was also conducted in toluene with the same result. Yield 30 mg, 74%. Anal. Calcd. For $C_{53}H_{74}AlKN_2Si_2O_2$ (**3.39**.C_7H_8) C, 71.25; H, 8.35; N, 3.14 %. Found: C, 70.72; H, 8.25; N, 2.86 %. The powder was dissolved in THF-*d*$_8$ for NMR characterisation. ^{1}H NMR (500 MHz, 298 K, THF-*d*$_8$) δ 7.85 – 7.15 (m, 2H, Ar*H* of AlOC*Ph*), 7.11 – 6.93 (d$_{app}$, 4H, *m*-C$_6$*H*$_3$), 6.92-6.77 (m, 8H, Ar*H* of AlOC*Ph*), 6.77-6.68 (t$_{app}$, 2H, *p*-C$_6$*H*$_3$), 4.19 (m , 4H, C*H*Me$_2$), 1.32 – 1.20 (m, 3H, AlOC*Me*Ph), 1.16 (d, *J* = 6.9 Hz, 6H,

CH*Me*$_2$), 1.13 (d, *J* = 6.9 Hz, 6H, CH*Me*$_2$), 1.08 (d, *J* = 6.9 Hz, 6H, CH*Me*$_2$), 1.06-0.98 (m, 3H, AlOC*Me*Ph), 0.96 (s, 4H, SiCH$_2$), 0.86 (d, J = 6.9 Hz, 6H CH*Me*$_2$), 0.03 (s, 6H, Si*Me*$_2$), -0.04 (s, 6H, Si*Me*$_2$). ^{13}C{^{1}H} NMR (126 MHz, 298 K, THF-*d*$_8$) δ 163.0 (Ar*C* of AlOCMe*Ph*), 160.6 (Ar*C* of AlOCMe*Ph*), 150.5 (Ar*C* of AlOCMe*Ph*), 148.7 (*i*-*C*$_6$H$_3$), 147.9 (Ar*C* of AlOCMe*Ph*), 143.6 (*o*-*C*$_6$H$_3$), 127.3 (Ar*C* of AlOCMe*Ph*), 126.9 (Ar*C* of AlOCMe*Ph*), 125.9 (*m*-*C*$_6$H$_3$), 123.4 (Ar*C* of AlOCMe*Ph*), 123.3 (Ar*C* of AlOCMe*Ph*), 121.5 (*p*-*C*$_6$H$_3$), 83.8 (AlO*C*), 28.0 (C*H*Me$_2$), 28.0 (C*H*Me$_2$), 26.7 (AlOC*Me*Ph), 26.1 (AlOC*Me*Ph), 25.8 (CH*Me*$_2$), 25.6 (CH*Me*$_2$), 24.2 (CH*Me*$_2$), 23.7 (CH*Me*$_2$), 15.9 (Si*C*H$_2$), 1.9 (Si*Me*$_2$), 1.6 (Si*Me*$_2$).

[K({SiN^{Dipp}}Al)(H)(OC(^{i}Pr)=CMe$_2$)] (3.40)

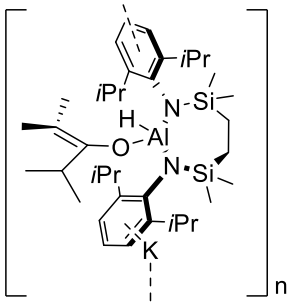

In a J Young's tube, [{SiN^{Dipp}}AlK]$_2$ (**3.12**, 28 mg, 0.025mmol) was dissolved in 0.4 mL of toluene before the addition of 2,4-dimethyl-3-pentanone (7.1 μL, 5.7 mg, 0.05 mmol) *via* a micropipette. The resulting bright yellow reaction mixture was kept at 60 ˚C overnight to afford a colourless solution with colourless crystals, single crystal suitable for X-ray crystallography was picked from the crystalline solid. The colourless solids were then collected, washed with hexane (0.5mL x 2), and dried under vacuum to give **3.40** as a colourless powder. Yield 30 mg, 89%. Anal. Calcd. For C$_{37}$H$_{64}$AlKN$_2$Si$_2$O (**3.40**) C, 65.82; H, 9.55; N, 4.15 %. Found: C, 64.76; H, 8.93, N, 3.92 %. ^{1}H NMR (500 MHz, 298 K, THF-*d*$_8$) δ 6.81 (d, *J* = 7.5 Hz, 4H, *m*-C$_6$*H*$_3$), 6.65 (t, *J* = 7.5 Hz, 2H, *p*-C$_6$*H*$_3$), 4.26 (sept, *J* = 6.5 Hz, 2H, C*H*Me$_2$ on SiN^{Dipp}), 4.20 (sept, *J* = 6.5 Hz, 2H, C*H*Me$_2$ on SiN^{Dipp}), 1.82 (sept, *J* = 7.2 Hz, 1H, OCC*H*Me$_2$), 1.33 (s$_{app}$, 6H, OCC*Me*$_2$), 1.17-1.14 (m, 12H, CH*Me*$_2$ on SiN^{Dipp}), 1.13 (d, *J* = 6.5 Hz, 6H, CH*Me*$_2$ on SiN^{Dipp}), 1.06 (d, *J* = 6.5 Hz, 6H, CH*Me*$_2$ on SiN^{Dipp}), 0.89 (s, br, 4H, SiC*H*$_2$), 0.40 (d, *J* = 7.2 Hz, 6H, OCCH*Me*$_2$), -0.05 (s, 6H, Si*Me*$_2$), -0.09 (s, 6H, Si*Me*$_2$). ^{1}H resonance correlated to Al*H* was not observed. ^{13}C{^{1}H} NMR (126 MHz, 298 K, THF-*d*$_8$) δ 155.7 (O*C*), 151.5 (*i*-*C*$_6$H$_3$), 148.8 (*o*-*C*$_6$H$_3$), 147.9 (*o*-*C*$_6$H$_3$), 123.3 (*m*-*C*$_6$H$_3$), 123.2 (*m*-*C*$_6$H$_3$), 121.2 (*p*-*C*$_6$H$_3$), 94.7 (OC*C*Me$_2$), 35.4 (OC*C*HMe$_2$), 29.0 (CH*Me*$_2$ on SiN^{Dipp}), 27.9 (C*H*Me$_2$ on SiN^{Dipp}), 27.8 (C*H*Me$_2$ on SiN^{Dipp}), 26.4 (CH*Me*$_2$ on SiN^{Dipp}), 26.0 (CH*Me*$_2$ on SiN^{Dipp}), 24.2 (CH*Me*$_2$ on SiN^{Dipp}), 21.2 (OCCH*Me*$_2$), 20.5 (OCC*Me*$_2$), 19.4 (OCC*Me*$_2$), 16.2 (Si*C*H$_2$), 2.4 (Si*Me*$_2$), -1.4 (Si*Me*$_2$).

C$_{39}$H$_{68}$AlKN$_2$Si$_2$O (3.41)

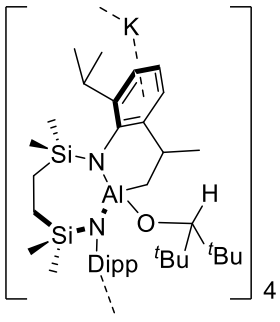

In a J Young's tube, [{SiN^{Dipp}}AlK]$_2$ (**3.12**, 28 mg, 0.025 mmol) was dissolved in 0.4 mL of toluene before the addition of 2,4-dimethyl-3-pentanone (8.6 μL, 7.1mg, 0.05 mmol) *via* a micropipette. The resulting bright yellow reaction mixture was kept at 60 ˚C overnight to afford a colourless solution with colourless crystals. A single crystal suitable for X-ray crystallography was picked from the crystalline solid. The colourless solids were then collected, washed with hexane (0.5 mL x 2), and dried under vacuum to give **3.41** as a colourless powder. Yield 28 mg, 83%. Anal. Calcd. For C$_{39}$H$_{68}$AlKN$_2$Si$_2$O (**3.41**) C, 66.01; H, 9.73; N, 3.98 %. Found: C, 65.97; H, 9.76, N, 3.74 %. NMR characterisation was undertaken with a mixture of diastereomers of compound **3.41**. ^{1}H NMR (500 MHz, 298 K, THF-*d*$_8$) δ 6.83 – 6.74 (m, 5H, Ar*H*), 6.69 – 6.67 (m, 1H, Ar*H*), 6.64 – 6.55 (m, 4H, , Ar*H*), 6.48– 6.46 (m, 1H, Ar*H*), 6.15 (t, *J* = 7.3 Hz, *p*-C$_6$*H*$_3$), 4.30 (sept, *J* = 6.8 Hz, 1H, C*H*Me$_2$), 4.18 (sept, *J* = 6.8 Hz, 1H, C*H*Me$_2$), 4.05 (sept, *J* = 6.8 Hz, 1H, C*H*Me$_2$), 3.97 (sept, *J* = 6.8 Hz, 2H, C*H*Me$_2$), 3.77 (sept, *J* = 6.8 Hz, 1H, C*H*Me$_2$), 3.63 (s, 1H, AlOC*H*), 3.19 (br, 1H, C*H*CH$_2$Al), 2.75 (s, 1H, AlOC*H*), 2.16 (t, *J* = 14.3 Hz, 1H, C*H*CH$_2$Al), 1.33 – 1.31 (m, 6H, CH*Me*$_2$), 1.28 (d, *J* = 6.8 Hz, 3H, CH*Me*$_2$), 1.25 (d, *J* = 6.8 Hz, 3H, CH*Me*$_2$), 1.21 (br, 2H, CHC*H*$_2$Al), 1.20 – 1.18 (m, 9H, CH*Me*$_2$), 1.17 (s br, 9H, C*Me*$_3$), 1.16 – 1.10 (m, 6H, CH*Me*$_2$),

1.10 (d, *J* = 6.8 Hz, 3H, CH*Me*$_2$), 1.07 (d, *J* = 6.7 Hz, 6H, CH*Me*$_2$), 1.04 (d, *J* = 6.8 Hz, 3H, CH*Me*$_2$), 1.02 – 1.00 (m, 2H, CHC*H*$_2$Al), 0.97 (s br, 9H, C*Me*$_3$), 0.91 – 0.59 (m, 8H, SiC*H*$_2$), 0.49 (s br, 9H, C*Me*$_3$), 0.45 (s, 3H, Si*Me*$_2$), 0.39 (s br, 9H, C*Me*$_3$), 0.36 (s, 3H, Si*Me*$_2$), 0.33 (s, 3H, Si*Me*$_2$), 0.29 (s, 3H, Si*Me*$_2$), 0.11 (s, 3H, Si*Me*$_2$), -0.45 (s, 3H, Si*Me*$_2$), -0.56 (s, 6H, Si*Me*$_2$). ^{13}C{^{1}H} NMR (126 MHz, 298 K, THF-*d*$_8$) δ 153.7 (*4*^{o} Ar*C*), 153.7 (*4*^{o} Ar*C*), 153.3 (*4*^{o} Ar*C*), 152.8 (*4*^{o} Ar*C*), 152.5 (*4*^{o} Ar*C*), 152.2 (*4*^{o} Ar*C*), 151.3 (*4*^{o} Ar*C*), 150.0 (*4*^{o} Ar*C*), 148.3 (*4*^{o} Ar*C*), 148.0(*4*^{o} Ar*C*), 147.7 (*4*^{o} Ar*C*), 145.4 (*4*^{o} Ar*C*), 123.7 (Ar*C*H), 123.6 (Ar*C*H), 123.4 (Ar*C*H), 123.1 (Ar*C*H), 122.9 (Ar*C*H), 122.7 (Ar*C*H), 122.0 (Ar*C*H), 121.4 (Ar*C*H), 121.3 (Ar*C*H), 121.1 (Ar*C*H), 120.7 (Ar*C*H), 119.7 (Ar*C*H), 87.2 (AlO*C*H), 84.0 (AlO*C*H), 39.5 (*C*Me$_3$), 39.2 (*C*Me$_3$), 38.9 (*C*Me$_3$), 38.5 (*C*Me$_3$), 36.8 (*C*HCH$_2$Al), 34.6 (*C*HCH$_2$Al), 32.1 (AlCH*C*H$_2$), 31.4 (C*Me*$_3$), 31.4 (C*Me*$_3$), 31.3 (C*Me*$_3$), 30.8 (C*Me*$_3$), 29.9 (AlCH*C*H$_2$), 29.0 (*C*HMe$_2$), 29.0 (*C*HMe$_2$), 28.4 (*C*HMe$_2$), 28.2 (*C*HMe$_2$), 27.7 (*C*HMe$_2$), 27.6 (CH*Me*$_2$), 27.4 (CH*Me*$_2$), 27.3 (CH*Me*$_2$), 27.3 (CH*Me*$_2$), 27.1 (CH*Me*$_2$), 27.1 (CH*Me*$_2$), 27.0 (CH*Me*$_2$), 27.0 (CH*Me*$_2$), 26.9 (CH*Me*$_2$), 26.8 (CH*Me*$_2$), 26.7 (CH*Me*$_2$), 26.7 (CH*Me*$_2$), 26.3 (CH*Me*$_2$), 26.0 (CH*Me*$_2$), 15.5 (Si*C*H$_2$), 15.4 (Si*C*H$_2$), 15.3 (Si*C*H$_2$), 15.0 (Si*C*H$_2$), 6.1 (Si*Me*$_2$), 4.8 (Si*Me*$_2$), 4.7 (Si*Me*$_2$), 3.7 (Si*Me*$_2$), 2.1 (Si*Me*$_2$), 1.0 (Si*Me*$_2$), 0.6 (Si*Me*$_2$), -0.6 (Si*Me*$_2$).

[{SiN^{Dipp}}AlI] (3.42)

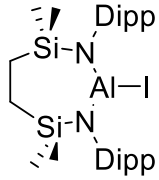

In a J-Young's tube, [{SiN^{Dipp}}AlK]$_2$ (**3.12**, 28 mg, 0.025 mmol) was dissolved in 0.4 mL of *d*$_6$-benzene before the addition of PbI$_2$ (23 mg, 0.05 mmol) to the bright yellow solution. The reaction mixture became colourless with the instantaneous precipitation of a grey metallic powder. NMR spectra were then recorded without further purification of this crude reaction mixture, and the resonances were in good agreement with the previously reported data for [{SiN^{Dipp}}AlI].[33, 34] ^{1}H NMR (500 MHz, 298 K, Benzene-*d*$_6$) δ 7.07 (m, 6H, C$_6$*H*$_3$), 3.64 (sept, J = 8.0 Hz, 4H,C*H*Me$_2$), 1.38 ((d, J = 8.0 Hz, 12H, CH*Me*$_2$), 1.27 (d, J = 8.0 Hz, 12H, CH*Me*$_2$), 1.00 (s, 4H, SiC*H*$_2$), 0.17 (s, 12H, Si*Me*$_2$).^{13}C{^{1}H} NMR (126 MHz, 298 K, C$_6$D$_6$): δ 145.5, 142.0, 125.2, 124.2 (Ar*C*), 28.9, 25.2, 24.6 (*C*HMe$_2$ and CH*Me*$_2$), 13.2 (Si*C*H$_2$), 0.15 (Si*Me*$_2$). This compound can also be observed in the reaction of **3.12** with various *p*-block element-iodides.

[({SiN^{Dipp}}Al)Cl$_2$K] (3.43)

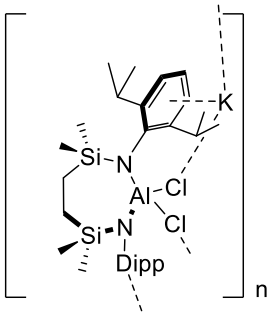

In a J-Young's tube, [{SiN^{Dipp}}AlK]$_2$ (**3.12**, 28 mg, 0.025 mmol) was dissolved in 0.4 mL of *d*$_6$-benzene before the addition of AlCl$_3$ (6.6 mg, 0.05 mmol) to the bright yellow solution. The reaction mixture instantly became colourless with white and black powder precipitates from the solution. Extra benzene (5mL) was then added to the reaction mixture, and the precipitates were filtered. The colourless filtrate was then collected and left at ambient temperature to afford **3.43** as colourless crystals. Yield 25 mg, 72%. No meaningful result for elemental analysis was obtained after several attempts. ^{1}H NMR (500 MHz, 298 K, THF-*d*$_8$) δ 6.92 (d, *J* = 7.5 Hz, 4H, *m*-C$_6$*H*$_3$), 6.77 (t, *J* = 7.5 Hz, 2H, *p*-C$_6$*H*$_3$), 4.12 (sept, *J* = 6.8 Hz, 4H, C*H*Me$_2$), 1.21 (d, *J* = 6.8 Hz, 12H, CH*Me*$_2$), 1.17 (d, *J* = 6.8 Hz, 12H, CH*Me*$_2$), 0.98 (s, 4H, SiC*H*$_2$), -0.01 (s, 12H, Si*Me*$_2$). ^{13}C{^{1}H} NMR (126 MHz, 298 K, THF-*d*$_8$) δ 149.1, 148.3, 124.0, 122.7(Ar*C*), 27.9 (*C*HMe$_2$), 26.7 (CH*Me*$_2$), 26.1(CH*Me*$_2$), 15.2 (Si*C*H$_2$), 1.9 (Si*Me*$_2$). This compound can also be prepared from the reaction of **3.12** with various *p*-block chlorides.

[({SiN^{Dipp}}AlCl$_2$)KCp*$_2$K$_2$] (3.44)

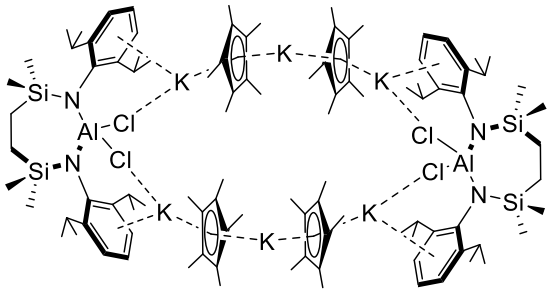

In a J-Young's tube, [{SiN^{Dipp}}AlK]$_2$ (**3.12**, 28 mg, 0.025 mmol) was dissolved in 0.4 mL of d_6-benzene before the addition of the [(NHC^{iPr})Cp*AlCl$_2$] (as depicted). The reaction mixture instantly turned colourless and provided crystalline solids, from which compound **3.44** could be mechanically separated and characterised.

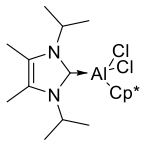

3.9 References

1. B. Rösch and S. Harder, *Chem Commun*, 2021, **57**, 9354-9365.
2. L. A. Freeman, J. E. Walley and R. J. Gilliard, *Nat Synth*, 2022, **1**, 439-448.
3. C. L. B. Macdonald, B. D. Ellis and A. Swidan, in *Encyclopedia of Inorganic and Bioinorganic Chemistry*, 2012, DOI: 10.1002/9781119951438.eibc0277.pub2.
4. M. P. Coles and M. J. Evans, *Chem Commun*, 2023, **59**, 503-519.
5. W. Klemm, E. Voss and K. Geiersberger, *Zeitschrift für anorganische Chemie*, 1948, **256**, 15-24.
6. C. Dohmeier, C. Robl, M. Tacke and H. Schnöckel, *Angew Chem Int Ed Engl*, 1991, **30**, 564-565.
7. C. Cui, H. W. Roesky, H.-G. Schmidt, M. Noltemeyer, H. Hao and F. Cimpoesu, *Angew Chem Int Ed*, 2000, **39**, 4274-4276.
8. J. Hicks, P. Vasko, J. M. Goicoechea and S. Aldridge, *Nature*, 2018, **557**, 92-95.
9. M. Tacke and H. Schnöckel, *Inorg Chem*, 1989, **28**, 2895-2896.
10. H. W. Roesky and S. S. Kumar, *Chem Commun*, 2005, 4027-4038.
11. L. Schebaum and P. Jutzi, *Cheminform*, 2003, **34**.
12. J. D. Gorden, A. Voigt, C. L. B. Macdonald, J. S. Silverman and A. H. Cowley, *J Am Chem Soc*, 2000, **122**, 950-951.
13. T. Chu, I. Korobkov and G. I. Nikonov, *J Am Chem Soc*, 2014, **136**, 9195-9202.
14. H. Zhu, J. Chai, H. Fan, H. W. Roesky, C. He, V. Jancik, H.-G. Schmidt, M. Noltemeyer, W. A. Merrill and P. P. Power, *Angew Chem Int Ed*, 2005, **44**, 5090-5093.
15. H. Zhu, R. B. Oswald, H. Fan, H. W. Roesky, Q. Ma, Z. Yang, H.-G. Schmidt, M. Noltemeyer, K. Starke and N. S. Hosmane, *J Am Chem Soc*, 2006, **128**, 5100-5108.
16. H. Sitzmann, M. F. Lappert, C. Dohmeier, C. Üffing and H. Schnöckel, *J Organometallic Chem*, 1998, **561**, 203-208.
17. A. Hofmann, T. Tröster, T. Kupfer and H. Braunschweig, *Chem Sci*, 2019, **10**, 3421-3428.
18. J. D. Queen, A. Lehmann, J. C. Fettinger, H. M. Tuononen and P. P. Power, *J Am Chem Soc*, 2020, **142**, 20554-20559.
19. X. Zhang and L. L. Liu, *Angew Chem Int Ed*, 2021, **60**, 27062-27069.
20. J. Hicks, A. Mansikkamäki, P. Vasko, J. M. Goicoechea and S. Aldridge, *Nat Chem*, 2019, **11**, 237-241.
21. M. M. D. Roy, J. Hicks, P. Vasko, A. Heilmann, A.-M. Baston, J. M. Goicoechea and S. Aldridge, *Angew Chem Int Ed*, 2021, **60**, 22301-22306.
22. J. T. Boronski, L. R. Thomas-Hargreaves, M. A. Ellwanger, A. E. Crumpton, J. Hicks, D. F. Bekiş, S. Aldridge and M. R. Buchner, *J Am Chem Soc*, 2023, **145**, 4408-4413.
23. C. McManus, J. Hicks, X. Cui, L. Zhao, G. Frenking, J. M. Goicoechea and S. Aldridge, *Chem Sci*, 2021, **12**, 13458-13468.
24. J. Hicks, P. Vasko, J. M. Goicoechea and S. Aldridge, *J Am Chem Soc*, 2019, **141**, 11000-11003.
25. R. J. Schwamm, M. D. Anker, M. Lein and M. P. Coles, *Angew Chem Int Ed*, 2019, **58**, 1489-1493.

26. R. J. Schwamm, J. R. Harmer, M. Lein, C. M. Fitchett, S. Granville and M. P. Coles, *Angew Chem Int Ed*, 2015, **54**, 10630-10633.
27. C. Bakewell, M. Garçon, R. Y. Kong, L. O'Hare, A. J. P. White and M. R. Crimmin, *Inorg Chem*, 2020, **59**, 4608-4616.
28. M. D. Anker and M. P. Coles, *Angew Chem Int Ed*, 2019, **58**, 13452-13455.
29. A. Heilmann, M. M. D. Roy, A. E. Crumpton, L. P. Griffin, J. Hicks, J. M. Goicoechea and S. Aldridge, *J Am Chem Soc*, 2022, **144**, 12942-12953.
30. M. J. Evans, M. G. Gardiner, M. D. Anker and M. P. Coles, *Chem Commun*, 2022, **58**, 5833-5836.
31. M. J. Evans, M. D. Anker, M. G. Gardiner, C. L. McMullin and M. P. Coles, *Inorg Chem*, 2021, **60**, 18423-18431.
32. T. X. Gentner, M. J. Evans, A. R. Kennedy, S. E. Neale, C. L. McMullin, M. P. Coles and R. E. Mulvey, *Chem Commun*, 2022, **58**, 1390-1393.
33. R. J. Schwamm, M. P. Coles, M. S. Hill, M. F. Mahon, C. L. McMullin, N. A. Rajabi and A. S. S. Wilson, *Angew Chem Int Ed*, 2020, **59**, 3928-3932.
34. R. J. Schwamm, M. S. Hill, H.-Y. Liu, M. F. Mahon, C. L. McMullin and N. A. Rajabi, *Chem Eur J*, 2021, **27**, 14971-14980.
35. S. Grams, J. Eyselein, J. Langer, C. Färber and S. Harder, *Angew Chem Int Ed*, 2020, **59**, 15982-15986.
36. S. Grams, J. Mai, J. Langer and S. Harder, *Dalton Trans*, 2022, **51**, 12476-12483.
37. G. Feng, K. L. Chan, Z. Lin and M. Yamashita, *J Am Chem Soc*, 2022, **144**, 22662-22668.
38. R. A. Jackson, A. J. R. Matthews, P. Vasko, M. F. Mahon, J. Hicks and D. J. Liptrot, *Chem Commun*, 2023, **59**, 5277-5280.
39. S. Kurumada, S. Takamori and M. Yamashita, *Nat Chem*, 2020, **12**, 36-39.
40. M. Kira, S. Ishida, T. Iwamoto and C. Kabuto, *J Am Chem Soc*, 1999, **121**, 9722-9723.
41. K. Koshino and R. Kinjo, *J Am Chem Soc*, 2020, **142**, 9057-9062.
42. J. Hicks, P. Vasko, J. M. Goicoechea and S. Aldridge, *Angew Chem Int Ed*, 2021, **60**, 1702-1713.
43. P. E. Romero, W. E. Piers, S. A. Decker, D. Chau, T. K. Woo and M. Parvez, *Organometallics*, 2003, **22**, 1266-1274.
44. Z. Yang, X. Ma, R. B. Oswald, H. W. Roesky, H. Zhu, C. Schulzke, K. Starke, M. Baldus, H.-G. Schmidt and M. Noltemeyer, *Angew Chem Int Ed*, 2005, **44**, 7072-7074.
45. A. Hofmann, C. Pranckevicius, T. Tröster and H. Braunschweig, *Angew Chem Int Ed*, 2019, **58**, 3625-3629.
46. M. Gomberg, *J Am Chem Soc*, 1900, **22**, 757-771.
47. W. Kaim and M. Moscherosch, *Coord Chem Rev*, 1994, **129**, 157-193.
48. R. Y. Kong and M. R. Crimmin, *J Am Chem Soc*, 2020, **142**, 11967-11971.
49. R. Y. Kong and M. R. Crimmin, *Angewandte Chemie International Edition*, 2021, **60**, 2619-2623.
50. K. Sugita, R. Nakano and M. Yamashita, *Chem Eur J*, 2020, **26**, 2174-2177.
51. H. Shere, PhD Thesis, *Alkaline Element Derivatives of Group 13-Centred Nucleophiles*, University of Bath, 2022.
52. C. Bakewell, A. J. P. White and M. R. Crimmin, *Chem Sci*, 2019, **10**, 2452-2458.

53. M. J. Evans, S. E. Neale, M. D. Anker, C. L. McMullin and M. P. Coles, *Angew Chem Int Ed*, 2022, **61**, e202117396.
54. C. Cui, S. Köpke, R. Herbst-Irmer, H. W. Roesky, M. Noltemeyer, H.-G. Schmidt and B. Wrackmeyer, *J Am Chem Soc*, 2001, **123**, 9091-9098.
55. B. Li, S. Kundu, A. C. Stückl, H. Zhu, H. Keil, R. Herbst-Irmer, D. Stalke, B. Schwederski, W. Kaim, D. M. Andrada, G. Frenking and H. W. Roesky, *Angew Chem Int Ed*, 2017, **56**, 397-400.
56. K. C. Mondal, B. Dittrich, B. Maity, D. Koley and H. W. Roesky, *J Am Chem Soc*, 2014, **136**, 9568-9571.
57. A. D. Phillips, R. J. Wright, M. M. Olmstead and P. P. Power, *J Am Chem Soc*, 2002, **124**, 5930-5931.
58. M. Stender, A. D. Phillips, R. J. Wright and P. P. Power, *Angew Chem Int Ed*, 2002, **41**, 1785-1787.

4. Application of an Al(I) Diamide: On the studies of group 11-[Al{SiN^{Dipp}}] Complexes

Capable of small-molecule activation and catalysis, transition metal complexes have long attracted considerable interests in organometallic chemistry.[1-3] Related species featuring unsupported transition metal-main group element bonds have also attracted significant attention in synthetic chemistry.[4,5] Historically, examples of this latter class of molecule comprising transition metal to group 13 element bonding, however, are relatively scarce. This may be attributed to the limited sources of group 13 centred nucleophiles, which may be ascribed to the more electropositive nature of atoms in the group. The past two decades, however, have witnessed noticeable advances in the field with numerous reports of unsupported boron- and gallium-bonded transition metal complexes.[6-21] The successful preparation of neutral Al(I) species has also facilitated the syntheses of a series of aluminium counterparts.[22]

As previously discussed in Chapter 3, recent years have seen a variety of reports of formally anionic aluminium(I) centred nucleophiles, several of which have provided access to further metal-aluminium bonded compounds. Aldridge and co-workers have demonstrated that the anionic aluminium nucleophile [{NON^{Dipp}}AlK]$_2$ (**3.5**) can provide access to novel gold-aluminium bonds *via* a salt metathesis with a phosphine-ligated gold halide.[23] Furthermore, [{SiN^{Dipp}}AlK]$_2$ (**3.12**) was reported to provide novel Mg-Al and Ca-Al chemical bonds through a similar displacement of KBPh$_4$,[24] this chapter will, therefore, describe a synthetic exploration of **3.12** to provide novel group 11 metal-Al bonded complexes and an assessment of their reactivity.

"Not all treasure is silver and gold, mate."

– Jack Sparrow, *Pirates of the Caribbean: The Curse of the Black Pearl,* 2003.

4.1 Organometallic Complexes Featuring Unsupported Metal – Aluminium Bonds

4.1.1 Implementation of neutral aluminium nucleophiles

Limited by the inherent electron-poor nature of the aluminium atom and the consequential lack of nucleophilic aluminium reagents, early examples of aluminium-bonded *d*-block complexes were prepared *via* the use of transition-metal centred nucleophiles, or through alkane elimination between an aluminium-alkyl and an acidic transition metal-hydride (**Scheme 4.1**).[25,26] There have been, however, numerous cases where Al-bonded *d*-block complexes were prepared by either a nucleophilic attack at the transition-metal centre or *via* oxidative addition across the aluminium of the neutral Al(I) compound [Al{η^5-(C_5Me_5)}]$_4$ ([Cp*Al]$_4$, **Scheme 4.2**).[27,28]

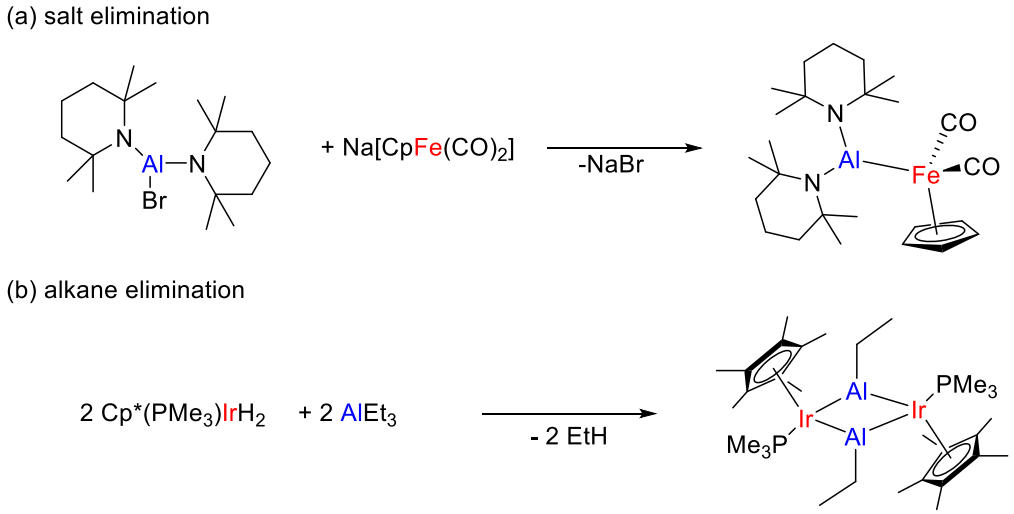

Scheme 4. 1 : Selected examples of synthetic routes to Al-transition metal complexes.[25,26]

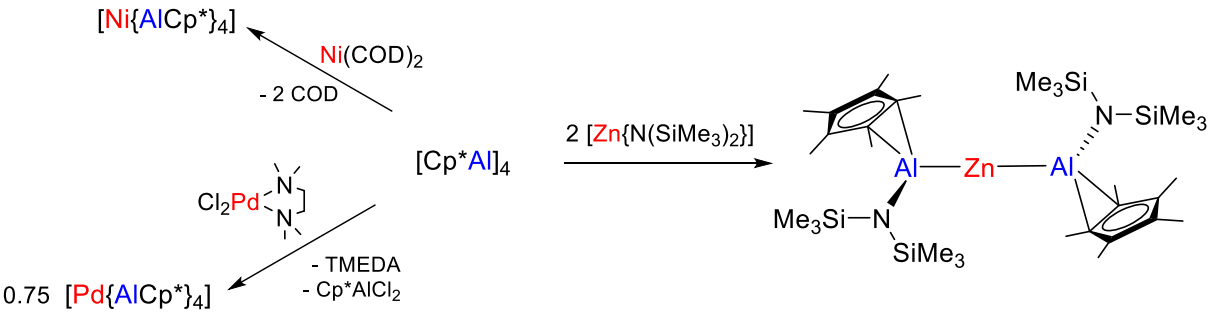

Scheme 4. 2 : Selected examples of synthesis of [Cp*Al] bonded transition metal complexes.[22,27,28]

The isolation of the well-defined monomeric aluminium(I) molecule [{^{Dipp}BDI}Al] (**3.1**, where ^{Dipp}BDI = CH(CMeNDipp)$_2$, Dipp = 2,6-diisopropylphenyl) facilitated further advances of a series of novel aluminium-supported transition metal complexes with interesting properties.[30] The synthesis of an Al-Pd complex (**4.1**) was reported to be feasible *via* a nucleophilic substitution type reaction between [Pd$_2${dvd}$_3$] (where dvd = 1,1,3,3-tetramethyl-1.3-divinyldisiloxnae) and [{^{Dipp}BDI}Al] (**3.1**).[21] [{dvd}Pd-Al{^{Dipp}BDI}] (**4.1**) was observed to undergo an equilibrium with a heterotrimetallic complex, [({dvd}Pd)$_2$(μ^2-Al{^{Dipp}BDI})], featuring a {Pd$_2$Al} core at room temperature (**Scheme 4.3a**). Although the dipalladium complex was not structurally characterised, its ^{1}H and ^{13}C{^{1}H} NMR spectra were unambiguously indicative of this configuration, and compound **4.1** could be quantitatively prepared through reaction of an excess amount (> 2.5 equiv) of [{^{Dipp}BDI}Al] (**3.1**) with [Pd$_2${dvd}$_3$], providing compound **4.1** as bright yellow crystals (Al1-Pd1 2.3702(10)Å, Al1-N1 1.906(3)Å, Al1-N2 1.912(3)Å; N1-Al1-N2 92.00(11)°, N1-Al1-Pd1 130.46(9)°, N2-Al1-Pd1 137.54(9)°). Later, Crimmin and co-workers reported a pair of multinuclear aluminium-supported palladium complexes which could be prepared by reacting [Pd(PCy$_3$)$_2$] with **3.1** or its related dihydride derivative [{^{Mes}BDI}AlH$_2$]. These reactions respectively provided the trimetallic complex [(PCy$_3$)Pd(Al{^{Dipp}BDI})$_2$] (**4.2**) and the tetrametallic hydride-bridged complex [((PCy$_3$)Pd)$_2$(μ^2-H)$_2$(Al{^{Mes}BDI})$_2$] (**4.3**) (**Scheme 4.3b**).[31] Although these intermetallic Al-Pd complexes are inherently different to the dinuclear heterobimetallic molecule **4.1**, the unsupported Al-Pd distances (Pd1-Al1 2.3621(13)Å, Pd1-Al2 2.3755(13)Å) in compound **4.2** were comparable to those measured in compound **4.1**. As [Pd(PCy$_3$)$_2$] catalyses the C-H activation of arene to provide new Al-C bonds under ambient conditions, **4.2** and **4.3** can be considered as the intermediates of the palladium-assisted Al-centred C-H activation of aromatic compounds. This supposition was further validated by DFT calculations and parallel reactions mediated by catalytic amounts of **4.2**.

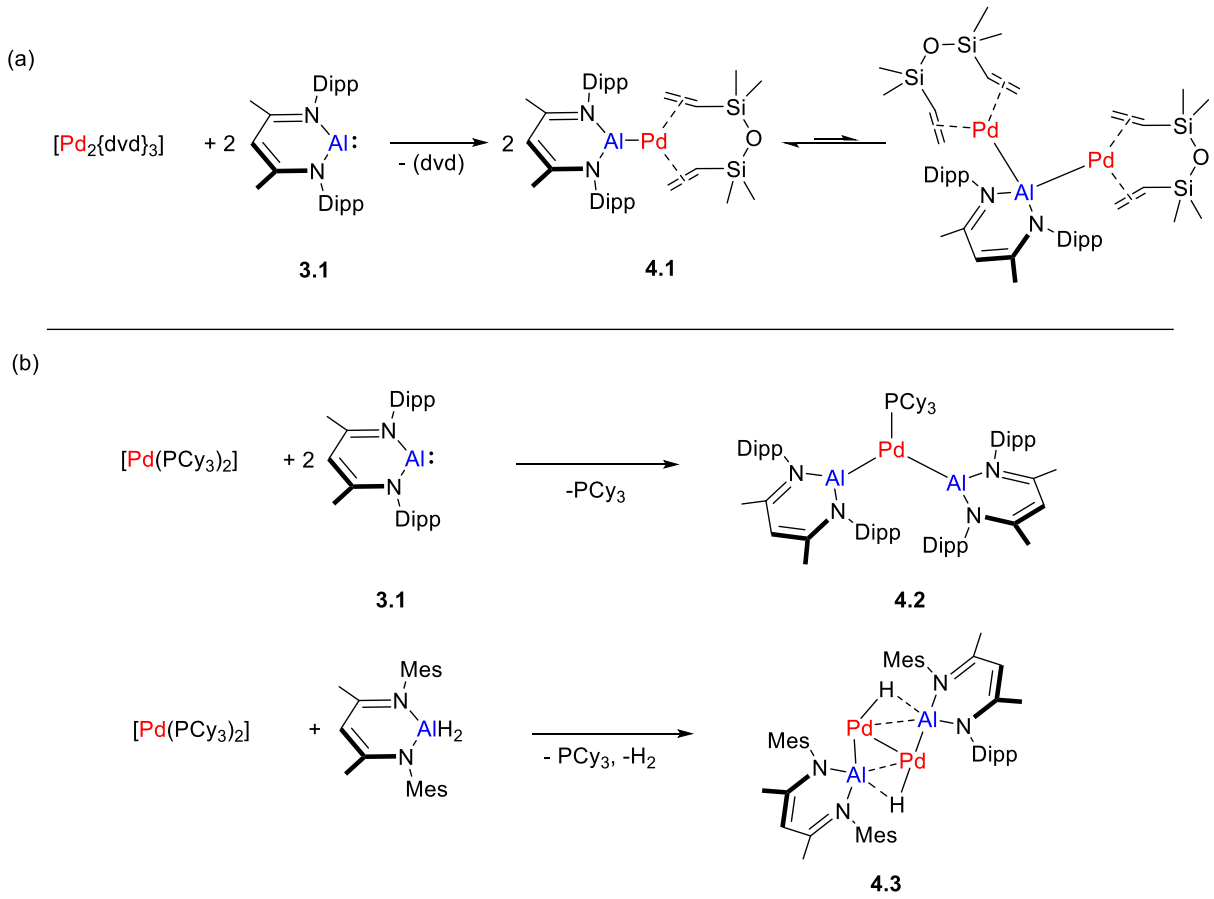

Scheme 4. 3 : Synthesis of {^{Dipp}BDI}Al-Pd complexes **4.1** – **4.3**.[21,31]

Recently, Power and co-workers expanded the class of [{^{Dipp}BDI}Al]-supported transition metal complexes to a bimetallic complex [{^{Dipp}BDI}Al-Cu{^{Mes}BDI}] (**4.4**) featuring an unsupported aluminium-copper bond (**Figure 4.1**).[32] Crystallographic and computational studies indicated that the metal-metal interaction is best considered as an Al(I) centre with a dative bond to a Cu(I) atom. Subsequent to the report of **4.4**, and in order to enhance an understanding of [{^{Dipp}BDI}Al]-coordinated *d*-block complexes, Crimmin and co-workers described a series of novel first-row transition metal complexes (**4.5** – **4.12**) featuring unsupported Al-metal bonds (**Figure 4.1**).[33] Similar to compound **4.4**, these molecules exhibited properties indicative of their formation as Al(I)-metal adducts, while the nucleophilic substitution type reactions of **3.1** with *d*-block substrates in the preparation of complexes **4.5** – **4.13** highlight the versatility of the synthetic strategy. Aluminium-iron complexes were also reported to be accessible through the treatment of phosphine-supported iron dibromide with related hydride derivatives of **3.1**. In these cases, subsequent magnesium reduction and bromine abstraction provided **4.13**, **4.14**, and **4.15**, respectively (**Scheme 4.4**).[34,35] Direct Al-Fe interactions were structurally and *in silico* characterised in these low-spin d^6 iron-aluminium complexes despite the presence of their auxiliary bridging hydride ligands, and they were

reported to be capable of conducting the *ortho*-C-H bond activation of pyridine derivatives, as well as the double deprotonation of acetonitrile.[34,35]

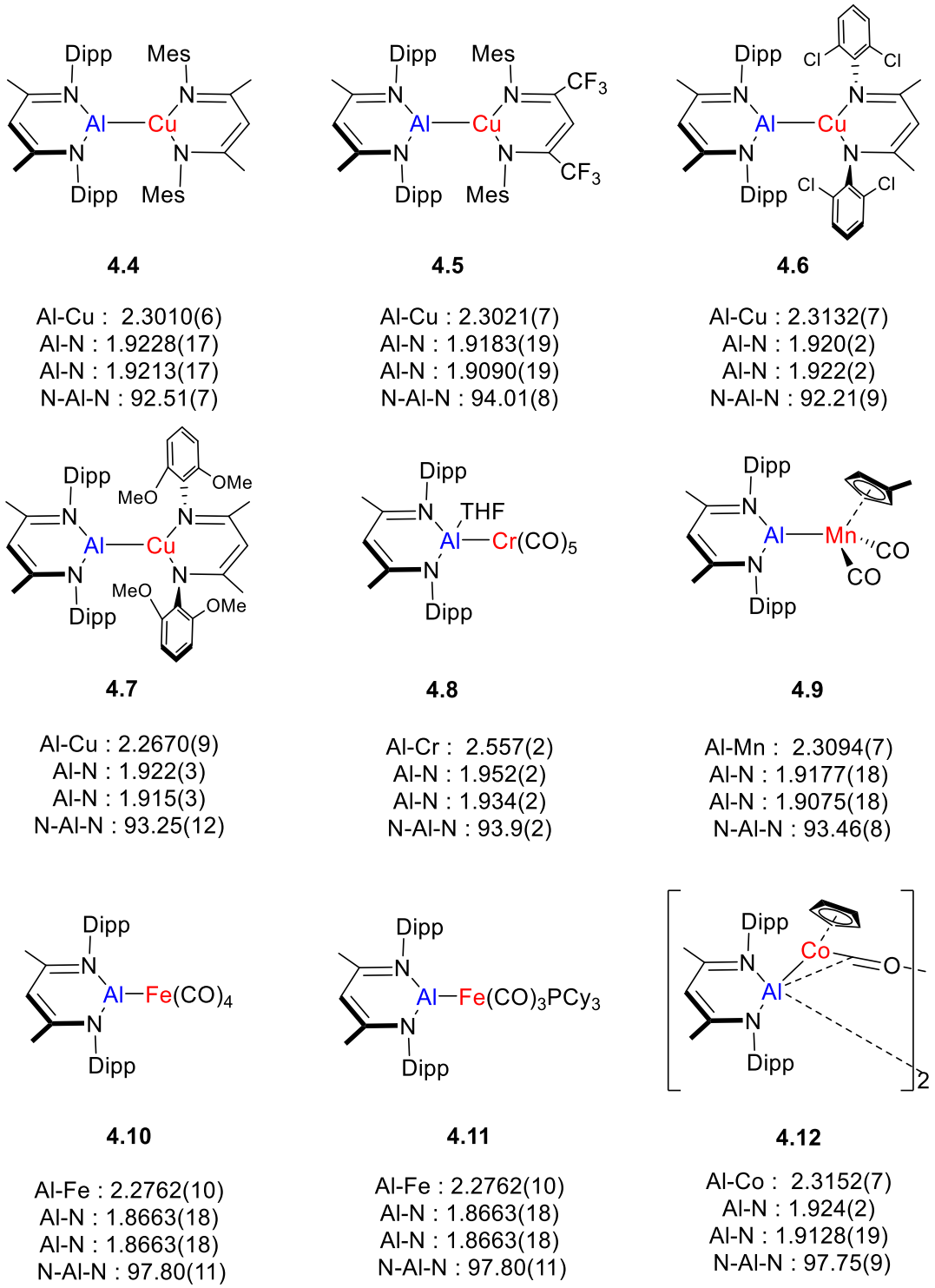

Figure 4. 1 : Selected Examples of [{^{Dipp}BDI}Al]- transition metal complexes **4.4** – **4.12** and their selected bond lengths (Å) and bond angles (°).[32,33]

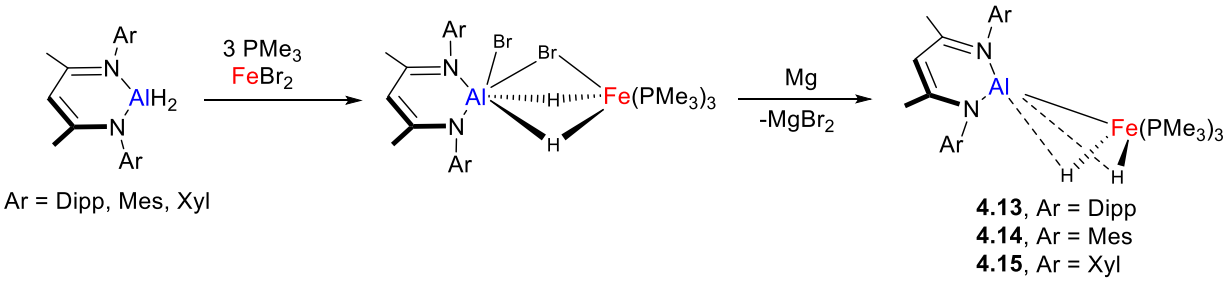

Scheme 4. 4 : Synthesis of iron-aluminium complexes **4.13** – **4.15**.[34,35]

Mono-substituted aluminium(I)-centred species have also recently been demonstrated to facilitate the synthesis of aluminium-coordinated transition metal complexes. Liu and co-workers prepared a base-free aluminylene, which, dependent on the identity of the *d*-block substrate, has exhibited nucleophilic behaviour towards the metal centre or oxidative insertion into the metal-element bond to provide the Al-metal bonded species (**4.16** – **4.17**, **Scheme 4.5a**).[36] Furthermore, a dialumene-benzene adduct, which can be considered as a dialumene during onward synthesis, has been utilised in the preparation of an aluminylene-platinum complex (**4.18**), where the Al-metal interaction is comparable to that in **4.16** (**Scheme 4.5b**).[37]

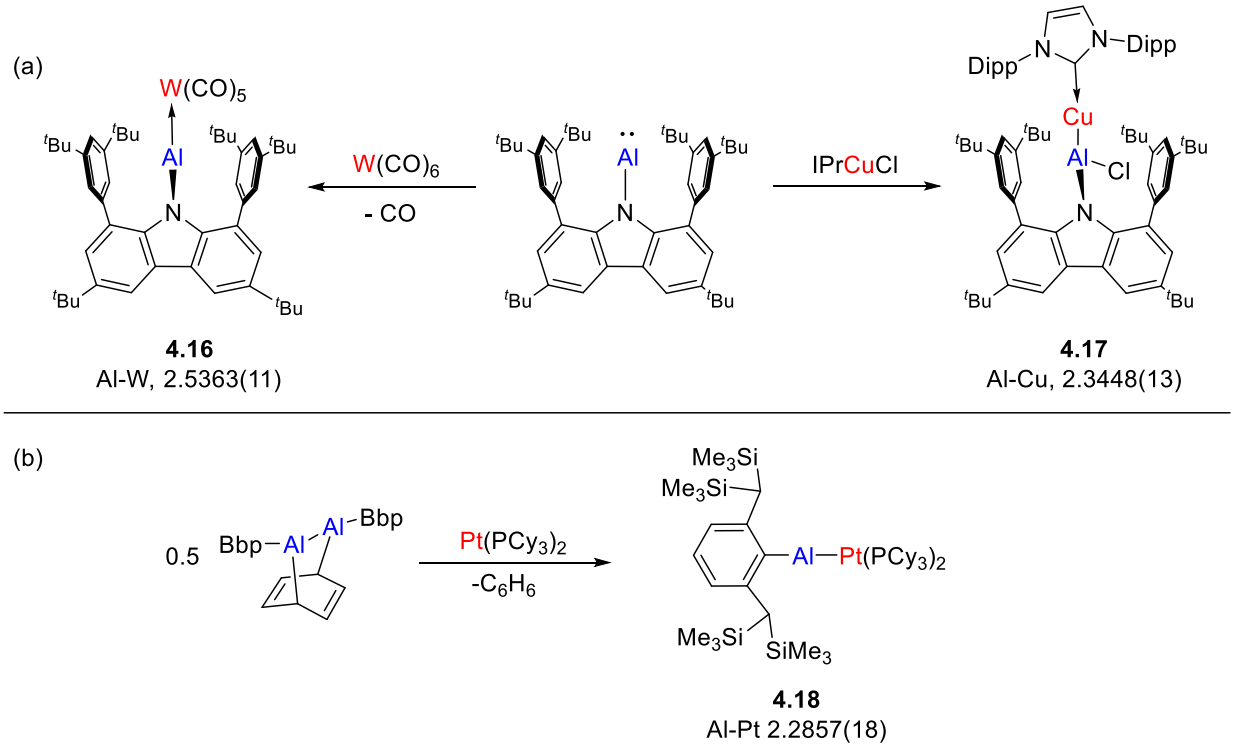

Scheme 4. 5 : Synthesis of compound **4.16** – **4.18** and their Al-metal bond lengths (Å).[36,37]

4.1.2 Implementation of anionic aluminium nucleophiles

There have been significant developments in formally anionic aluminium(I) centred molecules since the report of [{NON^{Dipp}}AlK]$_2$ (**3.5**),[38-40] and their application in providing new aluminium-substituted *d*-block complexes has emerged as a significant area of study.

Aldridge, Goicoechea, and co-workers demonstrated that **3.5** can be utilised in making the [{NON^{Dipp}}Al]-bonded gold complex (**4.19**) by treating a phosphine-ligated gold halide with **3.5** (**Scheme 4.6**).[23] The heterobimetallic complex [(^{t}Bu$_3$P)AuAl{NON^{Dipp}}] (**4.19**) was observed to exhibit gold-centred nucleophilic reactivity towards heteroallenes (**Scheme 4.6**), plausibly due to the more electropositive nature of the adjacent Al centre bonded to Au (Pauling electronegativity Au 2.54, Al 1.61). The unsupported Al-Au bond and almost linear P-Au-Al moiety (Al-Au, 2.402(3) Å, P-Au-Al, 167.47°) in **4.19** were unambiguously characterised by single-crystal X-ray diffraction analysis, while Al-N distances (avg. 1.902 Å) and the Al-O distance (2.046(8) Å) were indicative of a +III oxidation state assignment of the aluminium centre.

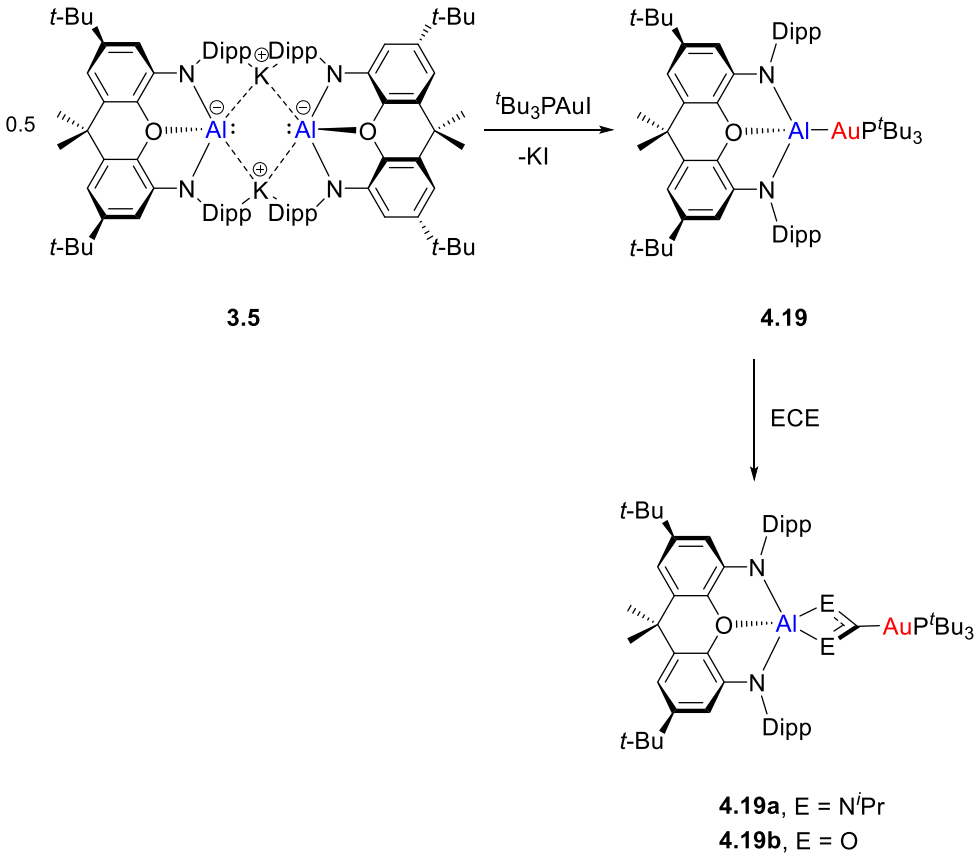

Scheme 4. 6 : Synthesis and Reactivity of [(^{t}Bu$_3$P)AuAl{NON^{Dipp}}] (**4.19**).[23]

Other [{NON^{Dipp}}Al]-substituted coinage metal complexes, [(^{t}Bu$_3$P)AgAl{NON^{Dipp}}] (**4.20**) and [(^{t}Bu$_3$P)CuAl{NON^{Dipp}}] (**4.21**), were also prepared *via* a similar synthetic salt elimination strategy (**Scheme 4.7**).[19] Although compounds **4.20** and **4.21** were not structurally characterised, their resultant NMR spectra and subsequent reactivity studies provided unambiguous evidence of the successful preparation of these molecules. Similar to **4.19**, compound **4.20** exhibits comparable Ag-centred nucleophilicity and provides the silver

counterparts (**4.20a** and **4.20b, Scheme 4.7a**) of **4.19a** and **4.19b** when reacted with carbodiimide and carbon dioxide at room temperature Reaction of **4.21** with carbodiimide also resulted in the copper analogues (**4.21a**) of **4.19a** (**Scheme 4.7b**). The copper counterpart (**4.21b**) of **4.19b**, however, was not observed even when the reaction of **4.19** with CO_2 was conducted at −78 °C. Rather, this reaction predominantly provided [(^{t}Bu$_3$P)Cu(OCO$_2$)Al{NON^{Dipp}}] (**4.21c**), where the mechanism of the metallo-carbonate (**4.21c**) formation was established by the stepwise transformation of **4.20b** to **4.20c** at elevated temperature (80 °C), to involve a CO extrusion from the first inserted CO_2 product followed by a subsequent insertion of CO_2 into the resultant oxo-bridged bimetallic species (**Scheme 4.7**).

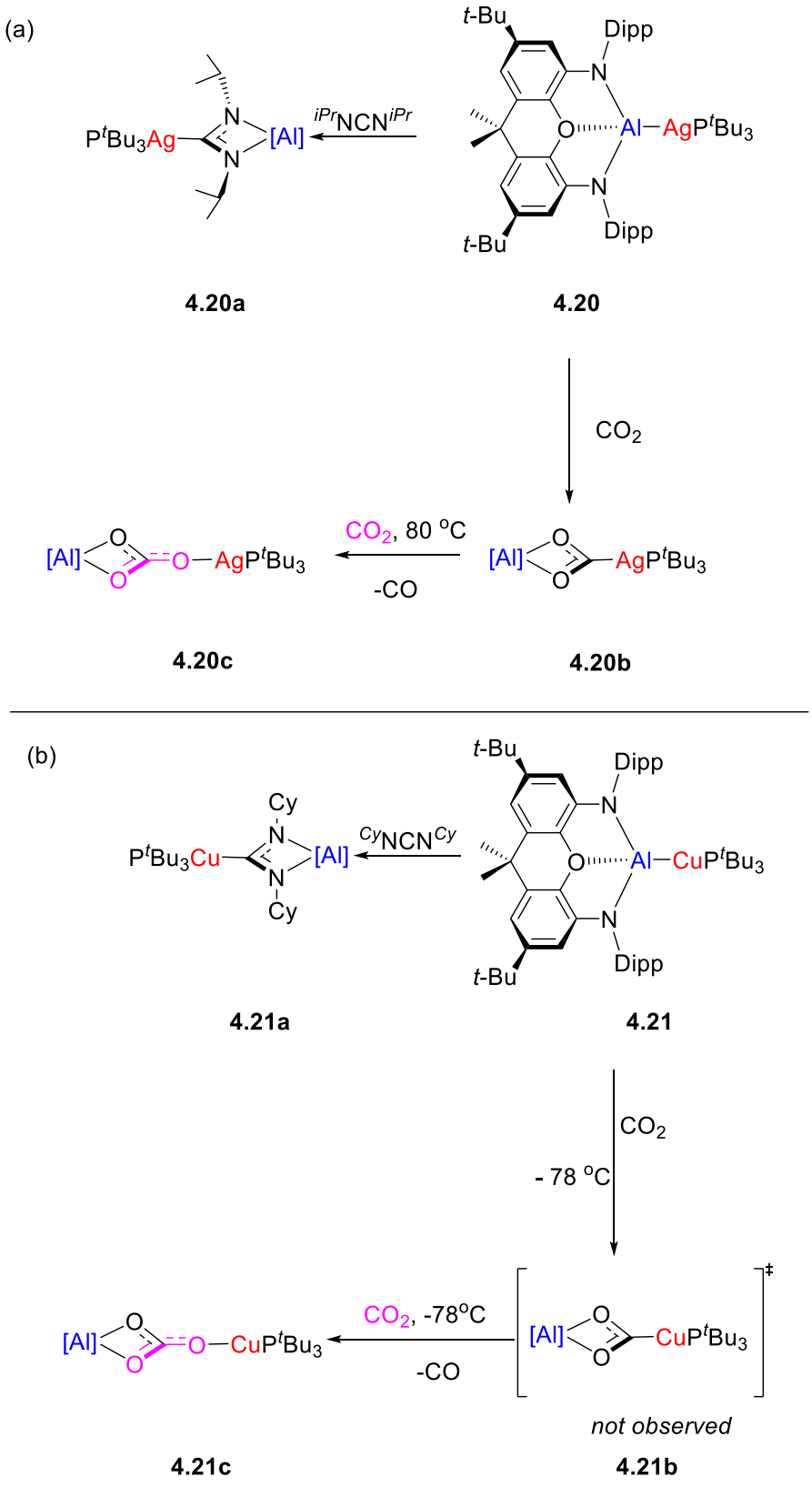

Scheme 4. 7 : Reactivity of [(^{t}Bu$_3$P)AgAl{NON^{Dipp}}] (**4.20**) and [(^{t}Bu$_3$P)CuAl{NON^{Dipp}}] (**4.21**).[19]

In order to probe the generality of the nucleophilic attack from the Al-centred nucleophile **3.5** in providing *d*-block element to aluminium chemical bonds, has also been reacted with the zinc-halide substrate [{^{Mes}BDI}ZnI], to provide the heterobimetallic complex [{^{Mes}BDI}ZnAl{NON^{Dipp}}] (**4.22**, **Scheme 4.8**).[41] The Al-Zn bond (2.4678(6) Å) and the structural data provided by the [Al{NON^{Dipp}}] unit (Al-N, 1.894(2), 1.911(2) Å; Al-O, 1.975(1) Å; N-Al-N, 127.2(1)°) in **4.22** suggested that the bimetallic interaction is best described as a metal-metal covalent bond. Treatment of **4.22** with CO_2 provided the dioxocarbene-zinc complex [{^{Mes}BDI}Zn(CO_2)Al{NON^{Dipp}}] (**4.22a**), which again implies a zinc-centred nucleophilicity (**Scheme 4.8**).

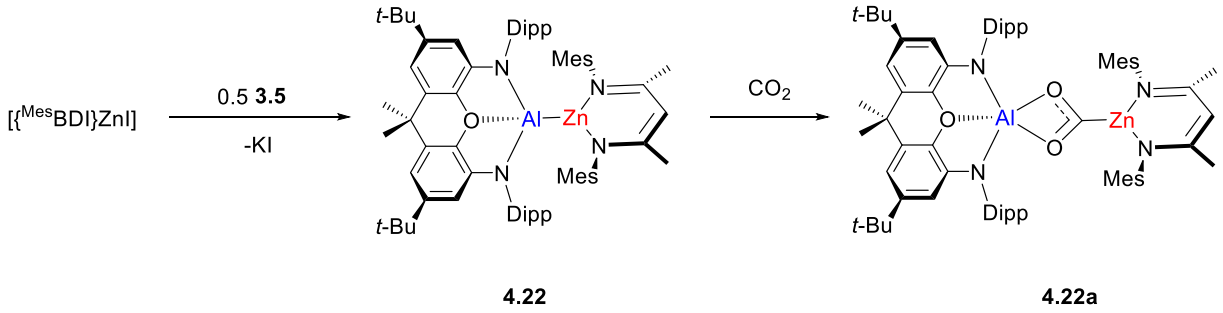

Scheme 4. 8 : Synthesis of **4.22** and its reaction with CO_2.

Inspired by the utilisation of the anionic aluminium nucleophile in the synthesis of **4.19**,[23] Yamashita and co-workers have investigated the synthetic potential of their recently reported potassium dialklyalumanyl **3.21** in providing novel Al-transition metal bonds.[42] When reacted with an yttrium electrophile, nucleophilic attack of **3.21** at the Y centre and salt metathesis ($KBPh_4$) provided the alumanylyttrium complex **4.23** (**Scheme 4.9a**).[43] Compound **4.23** features an unprecedented 2-centre-2-electron Al-Y bond (3.1870(8), 3.1942(8) Å) with Al adopting a trigonal planar geometry and Y in a trigonal bipyramidal configuration with two coordinating tetrahydrofuran molecules. The Al-C bond distances (avg. 2.035 Å) in **4.23** were found to be shorter than those (avg. 2.085 Å) in **3.21**, along with a wider C-Al-C (**4.23**, 93.81(11), 93.66(11)°; **3.21**, 90.40(5)°) angle. In contrast, the reaction of **3.21** with Ti(O^{i}Pr)$_4$ provided the one-electron reduction Ti(III) product (**4.24**), albeit a similar salt elimination (KO^{i}Pr) was observed (**Scheme 4.9b**),[44] highlighting the potent reducing behaviour of **3.21**.

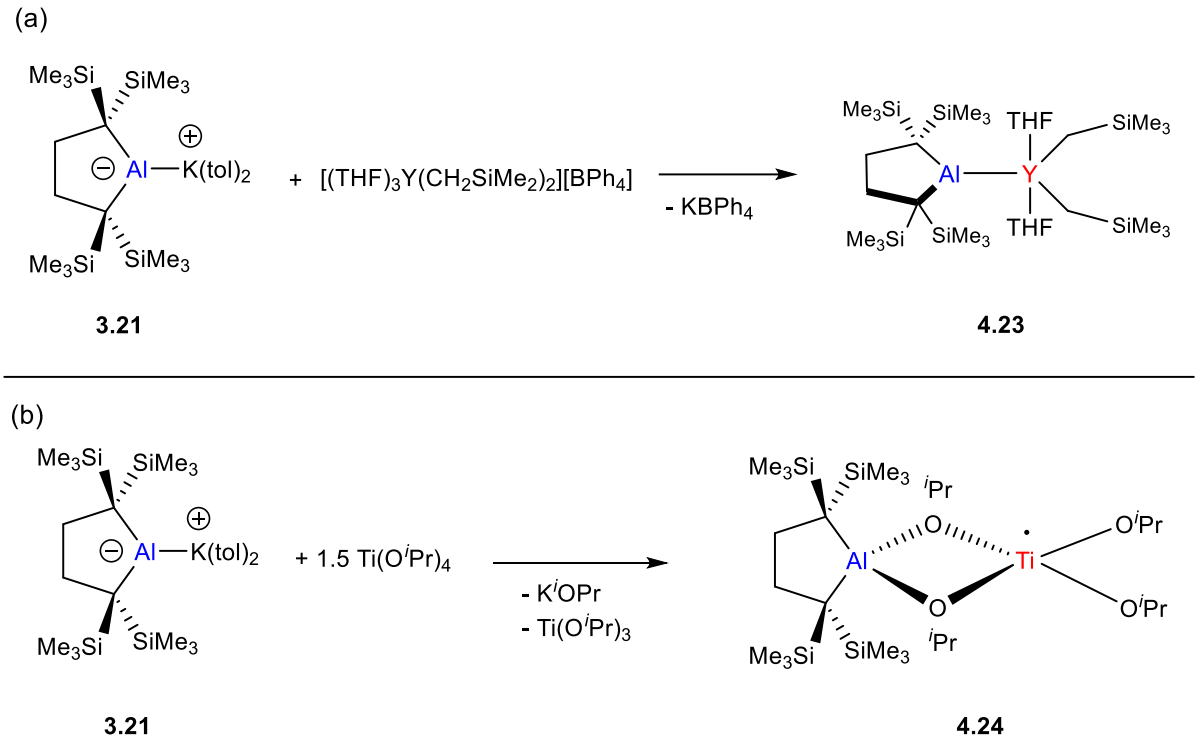

Scheme 4. 9 : Synthesis of bimetallic complexes **4.23** and **4.24**.[43,44]

Prompted by the strongly reducing reactivity of the dialkyl-substituted alumanyl (**3.21**) towards *d*-block substrates, Yamashita and co-workers prepared a cyclic potassium diamidoalumanyl (**3.19**). Reactions of **3.19** with various diamidoscandium-chlorides provided the respective Al-Sc complexes (**4.25** and **4.26**, **Scheme 4.10a**).[45] The metal-metal distances (**4.25**: 3.3095(5) Å; **4.26**: 3.018(1), 2.976(1) Å) in **4.25** and **4.26** were indicative of the ionic nature of the scandium-aluminium bonds, and the Al-N separations (**4.25**: avg. 1.838 Å; **4.26**: avg. 1.832 Å) in the bimetallic compounds were found to be slightly shorter to those (avg. 1.865 Å) in **3.19**. Compound **4.25** was observed to undergo intramolecular C-H activation at room temperature, whilst the relatively stable **4.26** was reported to be capable of activating a C-H bond of benzene and to mediate C-C coupling in presence of alkylhalides, denoting the unique reactivity of the Al-Sc bond (**Scheme 4.10b**).[45]

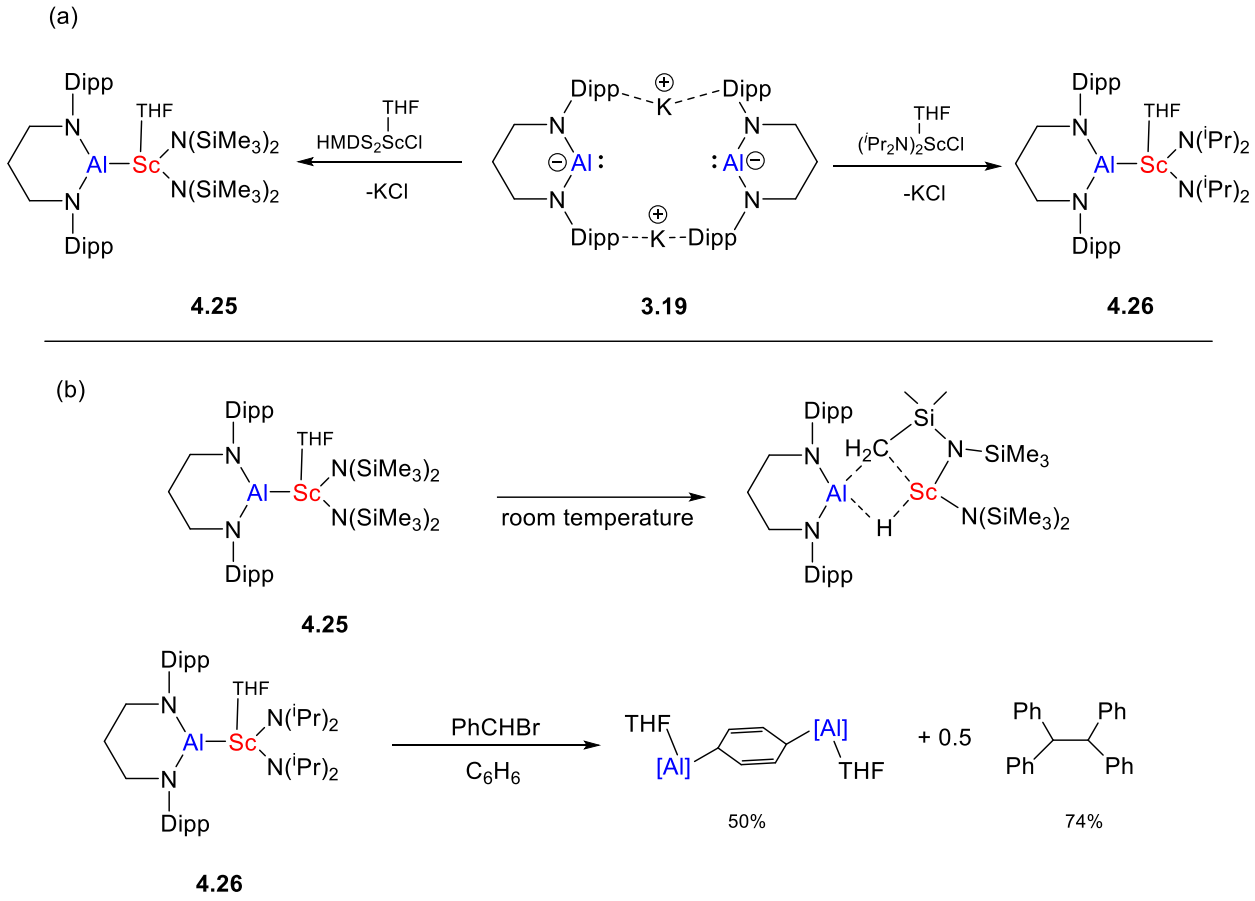

Scheme 4. 10 : Synthesis and Reactivity of Al-Sc complexes **4.25**, **4.26**.[45]

4.1.3 Implementation of the nucleophilic [{SiN^{Dipp}}AlK]$_2$ (**3.12**)

At the start of this project, Dr Schwamm in the Hill group had demonstrated that the generation of Mg-Al and Ca-Al bonds is viable through salt metathesis of **3.12** with the respective group 2 substrates.[24] In addition, nucleophilic behaviour towards electrophiles was observed to be a property of **3.12** (Section **3.2**). In this vein, reactions of [{SiN^{Dipp}}AlK]$_2$ (**3.12**) with *d*-block electrophiles to access [{SiN^{Dipp}}Al]-bonded transition metal complexes were identified as a viable entry point to further enhance an understanding and application of compound **3.12**. The resultant group 11 complexes will be the focus of this chapter.

4.2 Al-Cu Bonding in Carbene-Stabilised Cu-Al[{SiN^{Dipp}}] Complexes

4.2.1 Experimental Investigation of the Cu-Al{SiN^{Dipp}} Bonds

Inspired by the synthesis of **4.19** from the reaction of [{NON^{Dipp}}AlK]$_2$ (**3.5**) with phosphine coordinated gold-iodide (Scheme **4.6**), and to pursue the even more challenging Cu-centred nucleophilic behaviour (Pauling electronegativity Au 2.54, Cu 1.90, Al 1.61), an initial attempt to synthesise the Cu-Al bonded complex was conducted by the treatment of [{SiN^{Dipp}}AlK]$_2$ (**3.12**) with the Cu(I) chloride carbene adduct, [(NHC^{iPr})CuCl]. This protocol provided a predominant new species (**4.27**, **Scheme 4.11**). The ^{1}H NMR spectrum of **4.27** exhibited a 1 to 1 ratio of carbene to {SiN^{Dipp}}-ligand resonances, and its ^{13}C{^{1}H} NMR spectrum displayed a signal at δ 175.9 ppm, which was attributed to the carbene Cu–*C* environment.

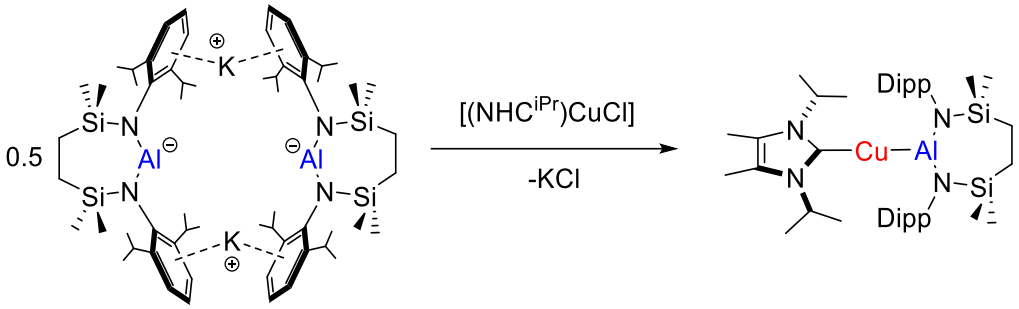

3.12 **4.27**

Scheme 4. 11 : Synthesis of [(NHC^{iPr})CuAl{SiN^{Dipp}}] (**4.27**).

This interpretation was verified by X-ray diffraction analysis conducted on a colourless crystal obtained from a methylcyclohexane solution, identifying **4.27** to be the carbene coordinated copper-alumanyl complex [(NHC^{iPr})CuAl{SiN^{Dipp}}] (Figure **4.2**). The two-coordinate copper in **4.27** exhibits an unsupported Al-Cu bond (2.3449(4) Å) and an almost linear bonding motif (C-Cu-Al: 178.85(4)°), where the Al-Cu distance is longer than all the terminal Al-Cu bonds (2.2670(9) – 2.3132(7) Å) in the reported bimetallic complexes **4.4** – **4.7**.[32,33] This observation may be rationalised by the transoid disposition of the potent sigma donating *N*-heterocyclic carbene.

"This copper-alumanyl really takes any ligands." – S. E. Neale, 2021.

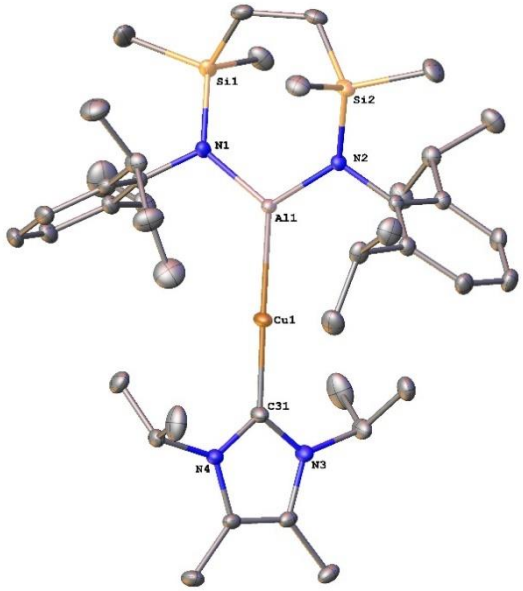

Figure 4. 2 : Displacement ellipsoid plot of compound **4.27**. Hydrogen atoms are omitted for clarity. Selected bond lengths (Å) and angles (°): Cu1-Al1 2.3449(4), Cu1-C31 1.9529(12), Al1-N1 1.8455(10), Al1-N2 1.8473(10), C31-Cu1-Al1 178.85(4), N1-Al1-N2 112.05(5), N1-Al1-Cu1 123.41(4), N2-Al1-Cu1 124.54(3).

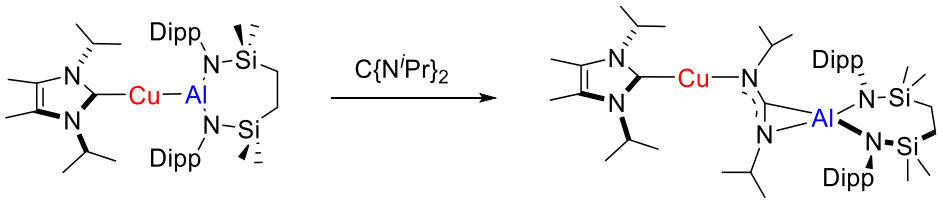

4.27 **4.28**

Scheme 4. 12 : Reaction of **4.27** with *N,N'*-diisopropylcarbodiimide.

To probe the nature of the Cu-Al bond in compound **4.27**, it was treated with *N,N'*-diisopropylcarbodiimide. The reaction resulted in a gradual consumption of the starting materials and formation of a single new species, **4.28** (**Scheme 4.12**), which, upon work-up, provided a ^{1}H NMR spectrum with broadened {SiN^{Dipp}} ligand environments, plausibly consistent with a restriction in conformation. Furthermore, the *i*-Pr methine resonances of the carbodiimide moiety were separated into two distinctive signals at δ_H 3.32 and 4.38 ppm, indicating the [Cu-μ^2-C{NiPr}$_2$-Al] unit is not the lighter analogue of that observed in compound **4.19a**.

Single crystal X-ray diffraction analysis of **4.28** confirmed the insertion of the diisopropylcarbodiimide into the Cu–Al bond and revealed the formation of a constrained three-membered AlCN (Al–C 1.9554(17), Al–N 1.8693(14), C–N 1.358(2) Å) metallacycle

(**Figure 4.3**). This newly formed three-membered heterocycle clearly denotes the side-on η^2-interaction between aluminium and a C=N bond of C{N^{i}Pr}$_2$, whilst the copper centre is ligated by a nitrogen atom of the CN_2 unit and the NHC^{iPr} (Cu–N6 1.8846(15) Å, Cu–C31 1.8959(18) Å).

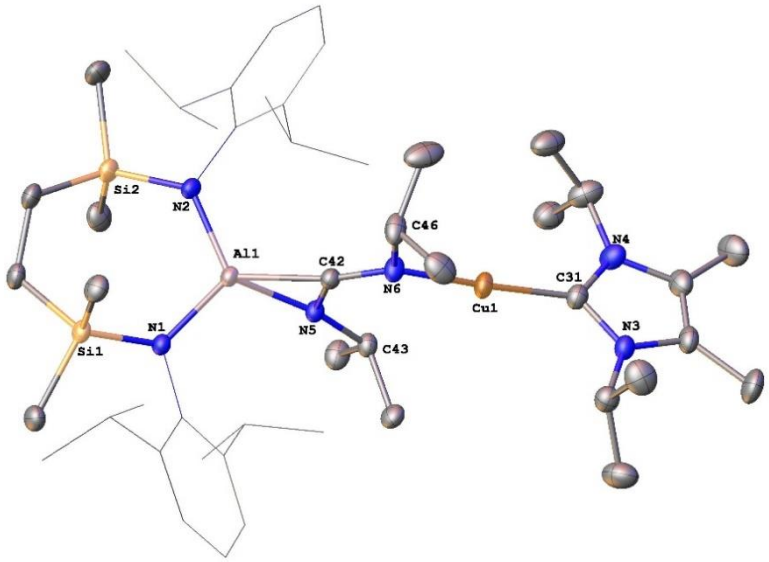

Figure 4. 3 : Displacement ellipsoid plot of compound **4.28** (30% probability ellipsoids). Dipp substituents are shown as wireframe and hydrogen atoms are omitted for clarity. Selected bond lengths (Å) and angles (°): Cu1-N6 1.8846(15), Cu1-C31 1.8959(18), Al1-N1 1.8425(14), Al1-N2 1.8411(14), Al1-N5 1.8693(14), Al1-C42 1.9554(17), N6-Cu1-C31 174.70(7), N1-Al1-N5 115.08(6).

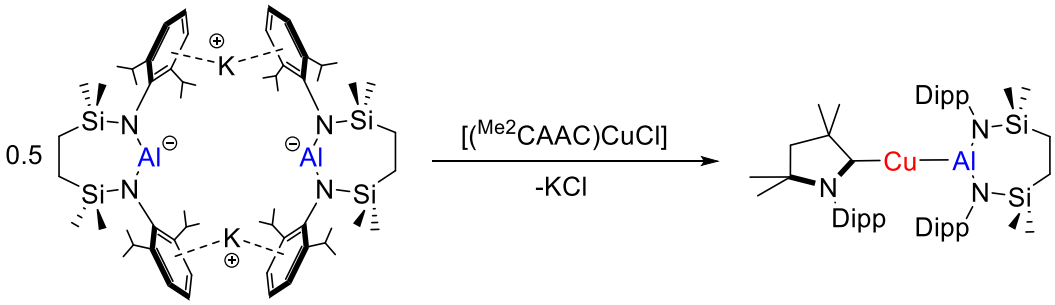

3.12 **4.29**

Scheme 4. 13 : Synthesis of [(^{Me2}CAAC)CuAl{SiN^{Dipp}}] (**4.29**).

In contrast to the coordinating arrangement provided by the central [μ-CN_2] moiety in **4.19a** (later **4.20a** and **4.21a**), the strucutre **4.28** is suggestive of a Cu$^{\delta+}$–Al$^{\delta-}$ bond polarity in the compound **4.27**, and the retention of Al-based nucleophilicity. To further enhance the potential of a Cu$^{\delta-}$–Al$^{\delta+}$ bond polarisation and Cu-centred nucleophilic reactivity, a more σ-donating and π-withdrawing carbene ^{Me2}CAAC (^{Me2}CAAC = 1-(2,6-diisopropylphenyl)-3,3,5,5-tetramethylpyrrolidin-2-ylidene) was implemented in the preparation of the copper-

alumanyl complex. Like **4.27**, compound **4.29** was synthesised by reacting [{SiN^{Dipp}}AlK]$_2$ (**3.12**) with the corresponding carbene Cu(I) chloride substrate, [(^{Me2}CAAC)CuCl] (**Scheme 4.13**). Reminiscent of the NMR spectroscopic characterisation of **4.27**, a one-to-one ratio of carbene to {SiN^{Dipp}}-ligand could be determined in the ^{1}H NMR spectrum of **4.29**, alongside a resonance at δ 144.9 ppm assigned to the Cu–$C_{carbene}$ environment in its ^{13}C{^{1}H} NMR spectrum.

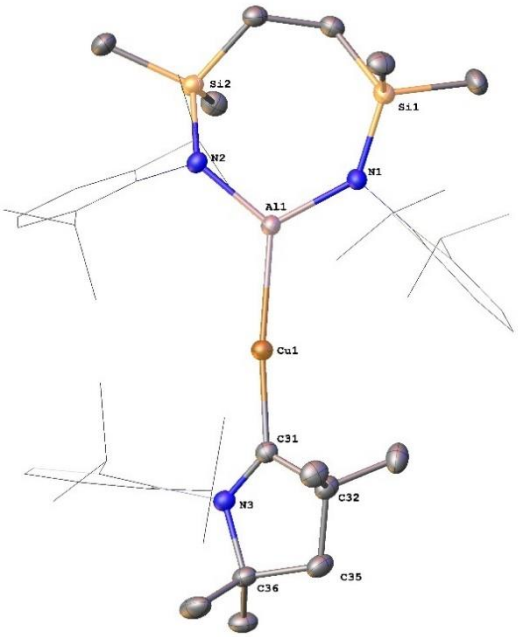

Figure 4. 4 : Displacement ellipsoid plot of compound **4.29** (30% probability ellipsoids). Dipp substituents are shown as wireframe and hydrogen atoms are omitted for clarity. Selected bond lengths (Å) and angles (°): Cu1-Al1 2.4028(7), Cu1-C31 1.964(2), Al1-N1 1.8668(18), Al1-N2 1.8546(18), C31-Cu1-Al1 173.42(6), N1-Al1-N2 110.96(8).

Structural characterisation of **4.29** was achieved by performing X-ray diffraction analysis on a colourless crystal obtained from a hexane solution (**Figure 4.4**), confirming it is indeed the ^{Me2}CAAC ligated copper-alumanyl complex [(^{Me2}CAAC)CuAl{SiN^{Dipp}}] (**4.29**). In a similar manner to the structure of **4.27**, the two-coordinate copper centre in **4.29** features a linear bonding motif (C-Cu-Al: 173.42(6)°), whilst the unsupported Al-Cu bond (2.4028(7) Å) is observed to be longer in comparison to the metal-metal separation (2.3449(4) Å) in **4.27**. Moreover, the Cu1-C31 distance (1.964(2) Å) in **4.29** is notably longer than that (1.9529(12) Å) in compound **4.27**. The elongation of both Al-Cu and Cu-$C_{carbene}$ bonds in **4.29** are suggested to be a likely consequence of the increased steric pressure across the molecule.

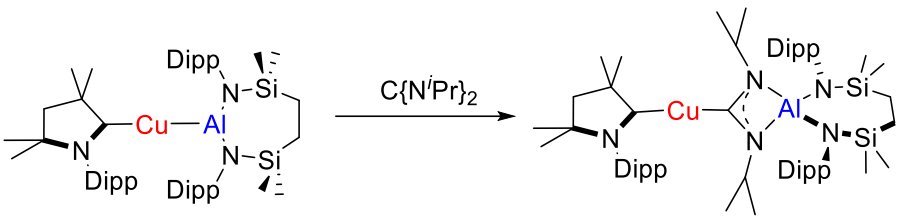

4.29 **4.30**

Scheme 4. 14 : Reaction of **4.29** with *N,N'*-diisopropylcarbodiimide.

Compound **4.29** was then reacted with *N,N'*-diisopropylcarbodiimide to investigate the behaviour of its Al-Cu bond. The reaction mixture of **4.29** and the carbodiimide reagent was observed to gradually transform into a new species (**4.30**) by ^{1}H NMR spectroscopy (**Scheme 4.14**). In a contrast to that of **4.28**, the ^{1}H NMR spectrum of **4.30** displayed a single sharp resonance at δ 3.37 ppm which could be assigned to the methine protons of the *i*Pr group in the carbodiimide. More diagnostically, a new low-field peak at δ 220.9 ppm was observed in the corresponding ^{13}C{^{1}H} NMR spectrum, which was strongly indicative of a copper-coordinated carbon centre.

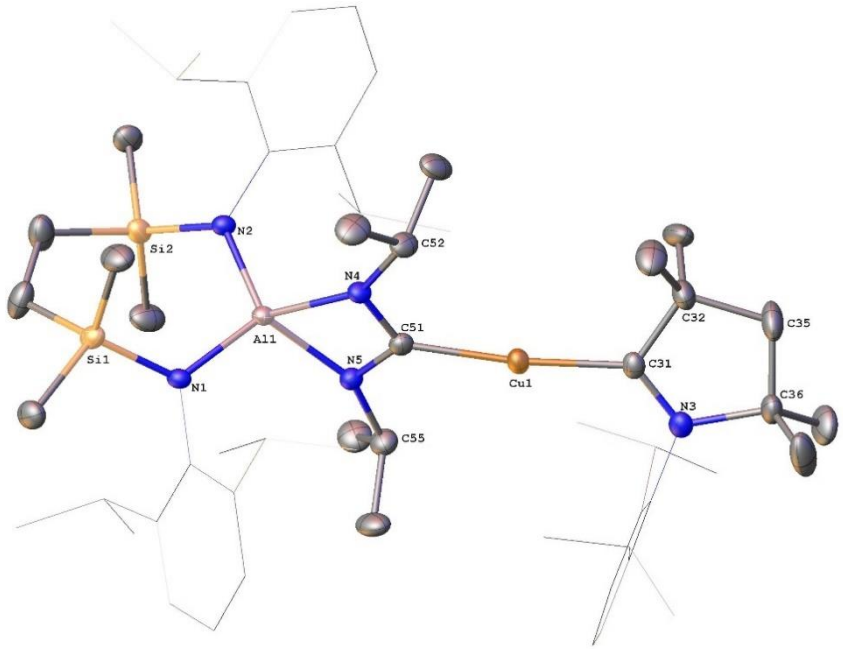

Figure 4. 5 : Displacement ellipsoid plot of compound **4.30** (30% probability ellipsoids). Dipp substituents are shown as wireframe and hydrogen atoms are omitted for clarity. Selected bond lengths (Å) and angles (°): Cu1-C31 1.919(3), Cu1-C51 1.960(3), Al1-N1 1.860(2), Al1-N2 1.862(2), Al1-N4 1.908(2), Al1-N5 1.923(2), C31-Cu1-C51 173.82(13).

This observation was subsequently authenticated by a single crystal X-ray diffraction analysis, disclosing that **4.30** recrystallised as a cupra-amidinate with the ^{Me2}CAAC-coordinated copper atom bonded to the CN_2 fragment at the central carbon atom (**Figure 4.5**).

The newly formed Cu1–C51 bond (1.960(3) Å) is longer than the carbene-copper interaction (C31–Cu1, 1.919(3) Å), while the two-substituted copper centre retains a linear structural arrangement (C31-Cu1-C51 173.82(13)°). The coordination sphere of the aluminium centre is completed by *N,N'*-bidentate binding from the carbodiimide unit, where essentially identical Al–N distances are observed (Al1–N4 1.908(2); Al1–N5 1.923(2) Å). In compound **4.30**, the CN_2 fragment is found to insert into the Al-Cu bond in a similar fashion to that of **4.19a** (and the later reported **4.20a** and **4.21a**), and the closely related Cu-*C*N_2 interaction (Cu1-C46, 1.952(4) Å) in **4.21a** is comparable to that in **4.30** (Cu1–C51, (1.960(3) Å).[19] The contrast in reaction products (**4.28** and **4.30**) obtained from insertion of *N,N'*-di-isopropylcarbodiimide into the Cu-Al bond of **4.27** and **4.29** suggests the apparent polarity of the bond can be modulated through adjustment of the identity of the co-ligand adjacent to the copper centre.

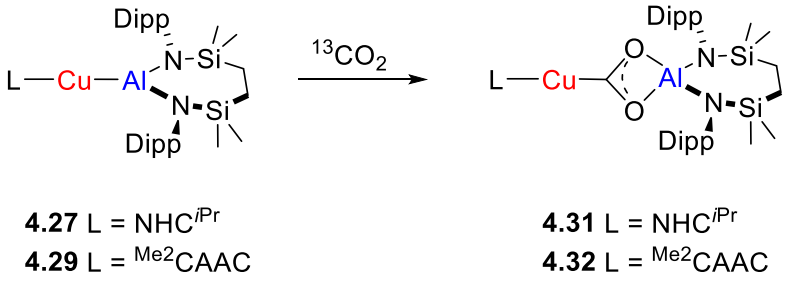

4.27 L = NHC^{iPr}
4.29 L = $^{Me2}CAAC$

4.31 L = NHC^{iPr}
4.32 L = $^{Me2}CAAC$

Scheme 4. 15 : Reaction of complexes **4.27** and **4.29** with $^{13}CO_2$.

To provide further experimental insight into the nature of the Cu-Al bonds, compounds **4.27** and **4.29** were reacted with $^{13}CO_2$. The individual reactions were spectroscopically monitored to undergo rapid transformations into compound **4.31** and **4.32**, respectively, upon the introduction of the gaseous reagent (**Scheme 4.15**). The ^{1}H NMR spectra of **4.31** and **4.32** each show a single set of peaks correlated to the respective carbene and the {SiN^{Dipp}} environments. In addition, the $^{13}C\{^{1}H\}$ NMR spectra each exhibit a single ^{13}C-enriched resonance at δ 236.2 (**4.31**, **Figure 4.6**) and 234.9 (**4.32**, **Figure 4.7**) ppm, which is strongly suggestive of closely related structures. These low-field carbon environments are characteristic of a Cu–*C*O_2 unit, and are comparable to the diagnostic peaks correlated to the related gold-metallacarboxylate (**4.19b**, 242.3 ppm),[23] and the later reported silver counterpart (**4.20b**, 220.2 ppm).[19] In a stark contrast to the observation that compound **4.20b** undergoes further transformation with CO_2 to a carbonate at elevated temperature, and the copper counterpart **4.21b** was not even observable at −78 °C,[19] compounds **4.31** and **4.32** displayed excellent thermal stability, with no evidence of further reaction even when heated to 60 °C under 2 atm. of $^{13}CO_2$ for 3 days.

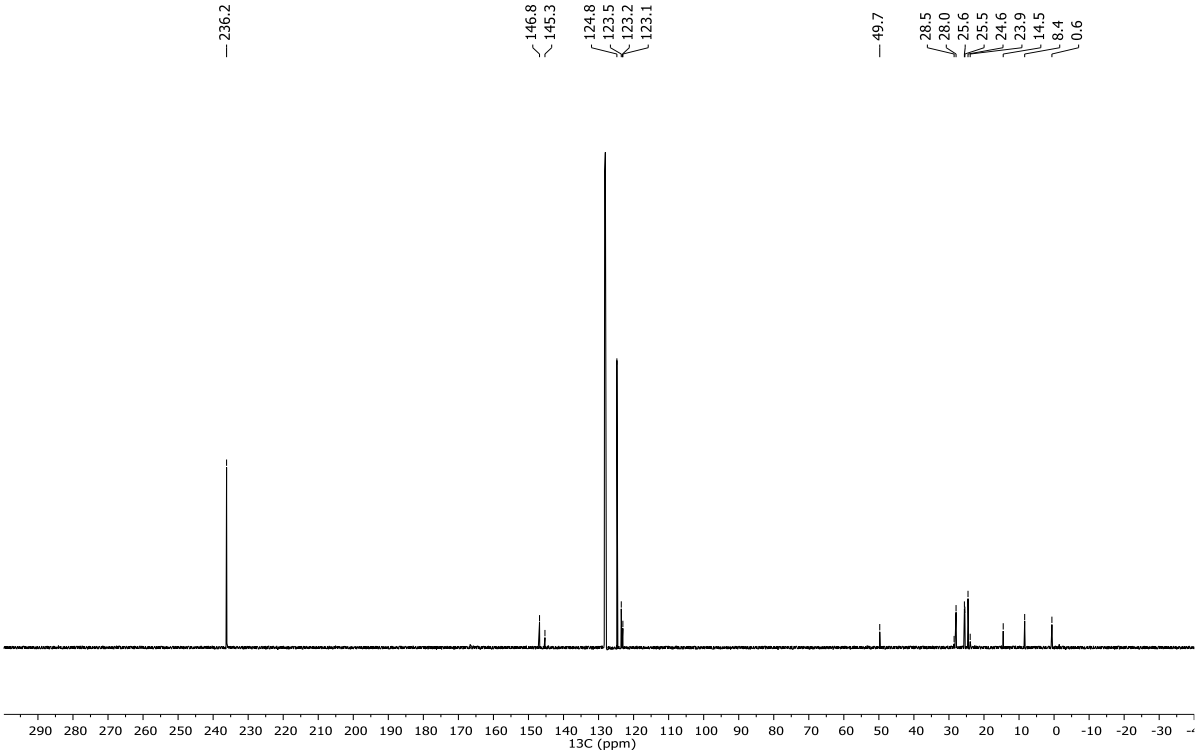

Figure 4. 6 : $^{13}C\{^{1}H\}$ NMR Spectrum of **4.31** (126 MHz, 298 K, C_6D_6).

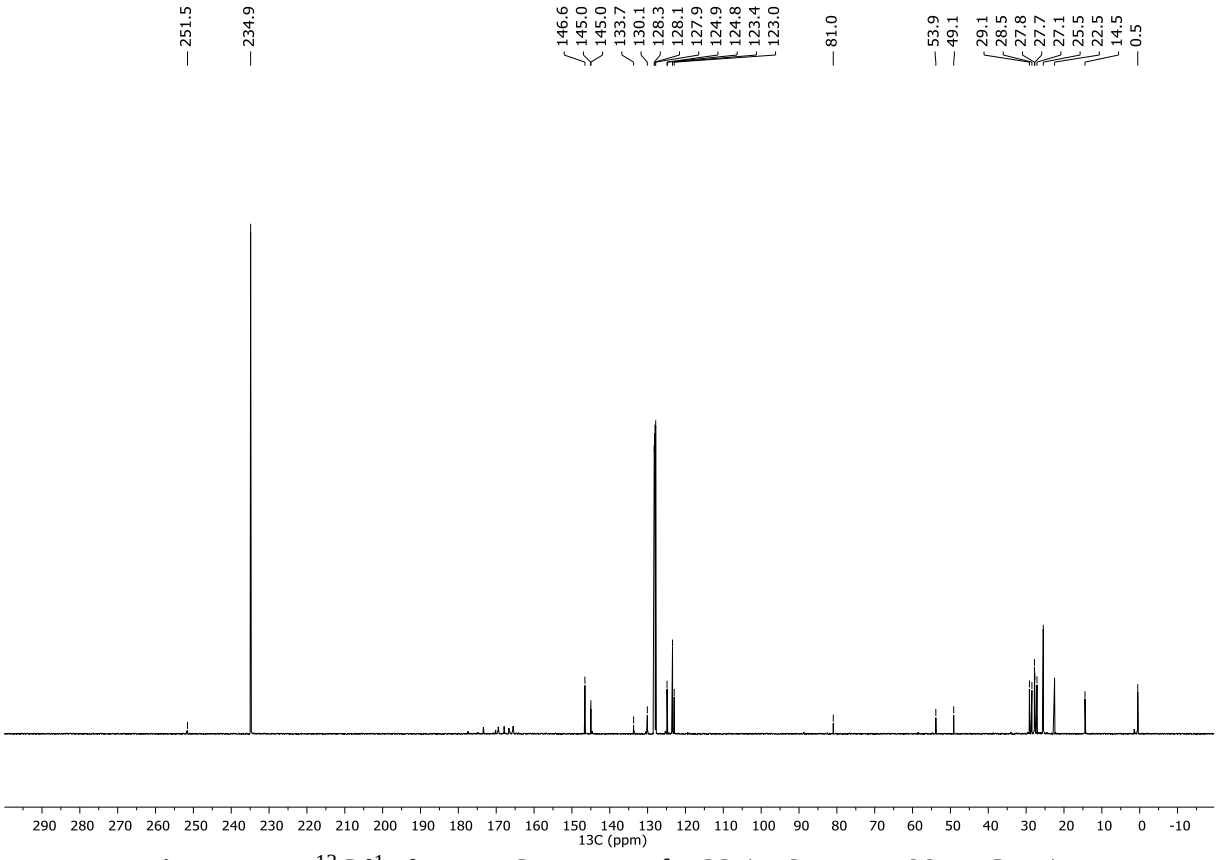

Figure 4. 7 : $^{13}C\{^{1}H\}$ NMR Spectrum of **4.32** (126 MHz, 298 K, C_6D_6).

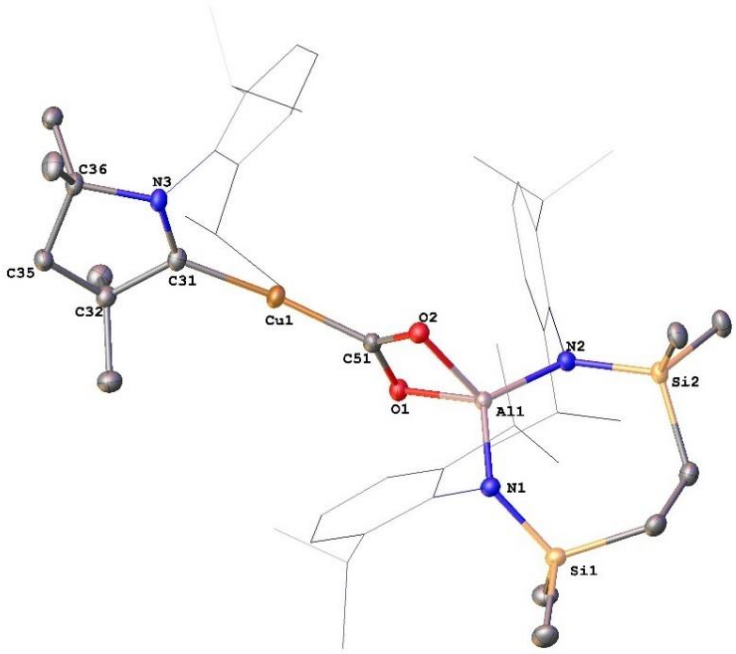

Figure 4. 8 : Displacement ellipsoid plot of compound **4.32** (30% probability ellipsoids). Dipp substituents are shown as wireframe and hydrogen atoms are omitted for clarity. Selected bond lengths (Å) and angles (°): Cu1-C31 1.894(2), Cu1-C51 1.902(2), Al1-O1 1.8563(16), Al1-O2 1.8405(17), Al1-N1 1.8096(19), Al1-N2 1.8125(18), C31-Cu1-C51 171.16(10), O2-Al1-O1 71.34(7).

The solid-state characterisation of **4.32** identified it to be a cupra-carboxylate species (**Figure 4.8**), while the closely related NMR spectra arising from **4.31**, are strongly suggestive of a similar configuration. The linear di-substituted copper centre (C31-Cu1-C51 171.16(10)°) in **4.32** bonds to the central μ-CO_2 unit through the central carbon atom, while its coordination sphere is completed by the ligation of the ^{Me2}CAAC. The aluminium centre is chelated by the two oxygen atoms with comparable Al-O distances (Al1-O1 1.8563(16), Al1-O2 1.8405(17) Å), and the Al-O and C-O distances [1.301(3), 1.307 (3)Å] are indicative of π-electron delocalisation over the entire {CO_2} fragment. Comparable to that of **4.30**, the Cu1-C51 distance [1.902(2) Å] is slightly longer than the carbene-copper interaction (Cu1-C31 1.894(2) Å).

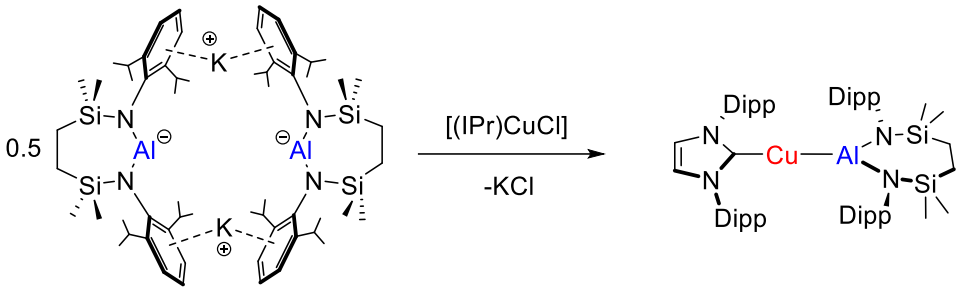

3.12 **4.33**

Scheme 4. 16 : Synthesis of [(IPr)CuAl{SiN^{Dipp}}] (**4.33**)

To further assess the impact of variations in the steric demands of the *N*-heterocyclic carbene (NHC) co-ligand, a carbene copper-alumanyl species analogous to compounds **4.27** and **4.29** but with the more bulky NHC, 1,3-bis(2,6-di-isopropylphenyl)imidazol-2-ylidene) (IPr), was then prepared. In a similar fashion to that of **4.27** and **4.29**, the [(IPr)CuAl{SiN^{Dipp}}] (**4.33**) was synthesised by treating the copper chloride carbene adduct, [(IPr)CuCl], with half a molar equivalent of [{SiN^{Dipp}}AlK]$_2$ (**Scheme 4.16**). Although attempts to obtain a crystal of **4.33** for X-ray diffraction analysis were not successful, its formation was unambiguously confirmed by the appearance of a series of resonances that were consistent with a 1:1 ratio of carbene to {SiN^{Dipp}} environments in the ^{1}H NMR spectrum (**Figure 4.9**), as well as a low-field resonance at δ = 185.1 ppm attributed to the carbenic Cu*C* environment in the ^{13}C{^{1}H} NMR spectrum.

"How about sterics?" – A. S. S. Wilson, 2020.

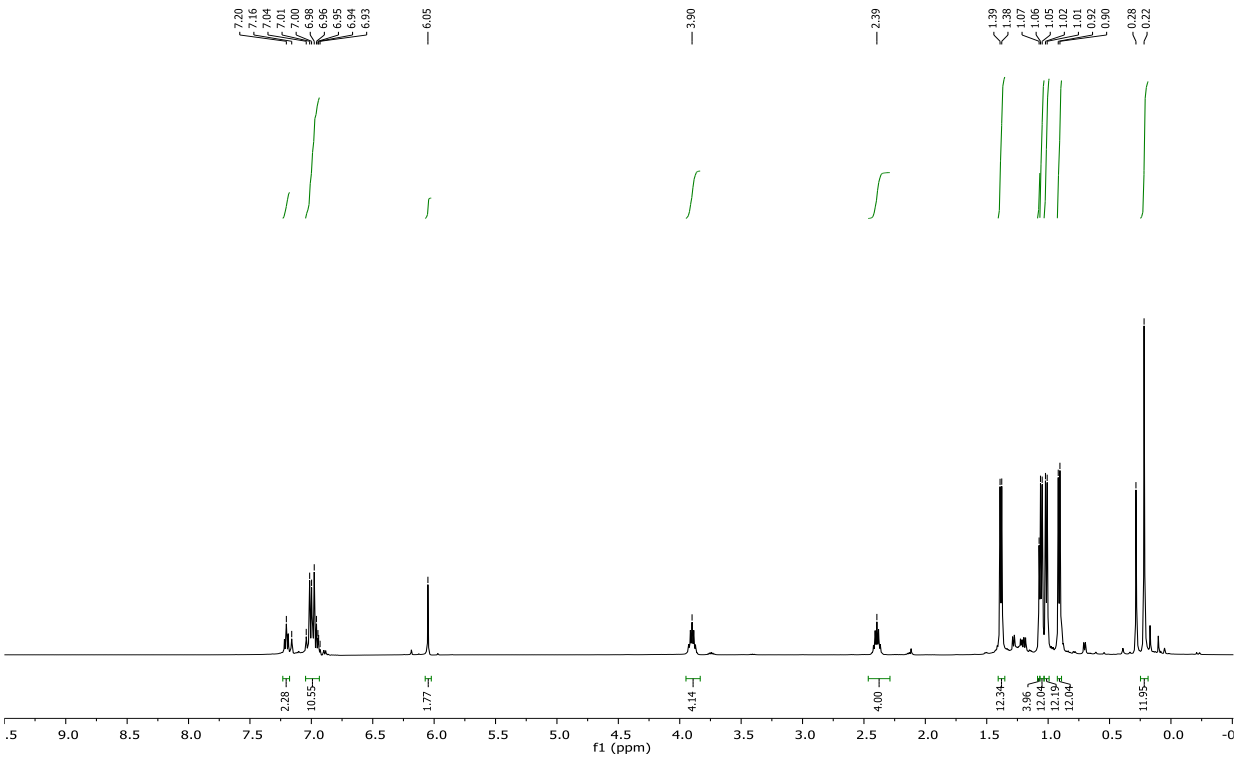

Figure 4. 9 : ^{1}H NMR spectrum of **4.33** (500 MHz, 298 K, C_6D_6).

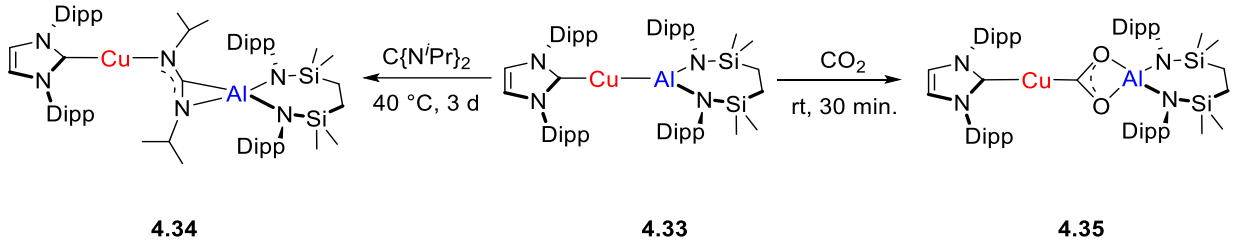

Scheme 4. 17 : Reactions of **4.33** with *N,N'*-diisopropylcarbodiimide and $^{13}CO_2$.

The nature of compound **4.33** was then assessed through its reactivity towards heteroallenes (**Scheme 4.17**). The reaction of **4.33** with *N,N'*-di-isopropylcarbodiimide and CO_2 gave a similar outcome as that previously observed for compound **4.27**. The reaction of **4.33** with carbodiimide resulted in the gradual consumption of both starting materials at 40 °C over the course of 3 days and exclusively yielded compound **4.34**, where the slow conversion may be a consequence of the more sterically hindered Cu-Al bond in **4.33**. In common with the observations of compound **4.28**, the ^{1}H NMR spectrum arising from **4.34**, which was obtained from the reaction of **4.33** with *N,N'*-di-isopropylcarbodiimide, indicated a significant level of asymmetry alongside limited conformational flexibility in compound **4.34** (**Figure 4.10**). The methine resonances of the *i*Pr groups in the [C{N^{i}Pr}$_2$] unit of compound **4.34** were found as two distinctive (each correlated to 1H by relative integration) multiplets at δ 3.38 and 2.99 ppm, and its ^{13}C{^{1}H} NMR spectrum did not exhibit any low field signals assignable to a

copper-coordinated *sp*-hybridised carbodiimide carbon (which is closely related to the ^{13}C environment observed at δ 220.9 ppm for the copper-coordinated [Cu-*C*{N^{i}Pr}$_2$] carbon in compound **4.30**). These observations are, thus, indicative of the configuration of compound **4.34** being reminiscent of the solid-state structure of **4.28** (as illustrated in Scheme **4.17**), and suggestive of the aluminium centre of **4.33** exhibiting a level of nucleophilic behaviour towards the carbodiimide.

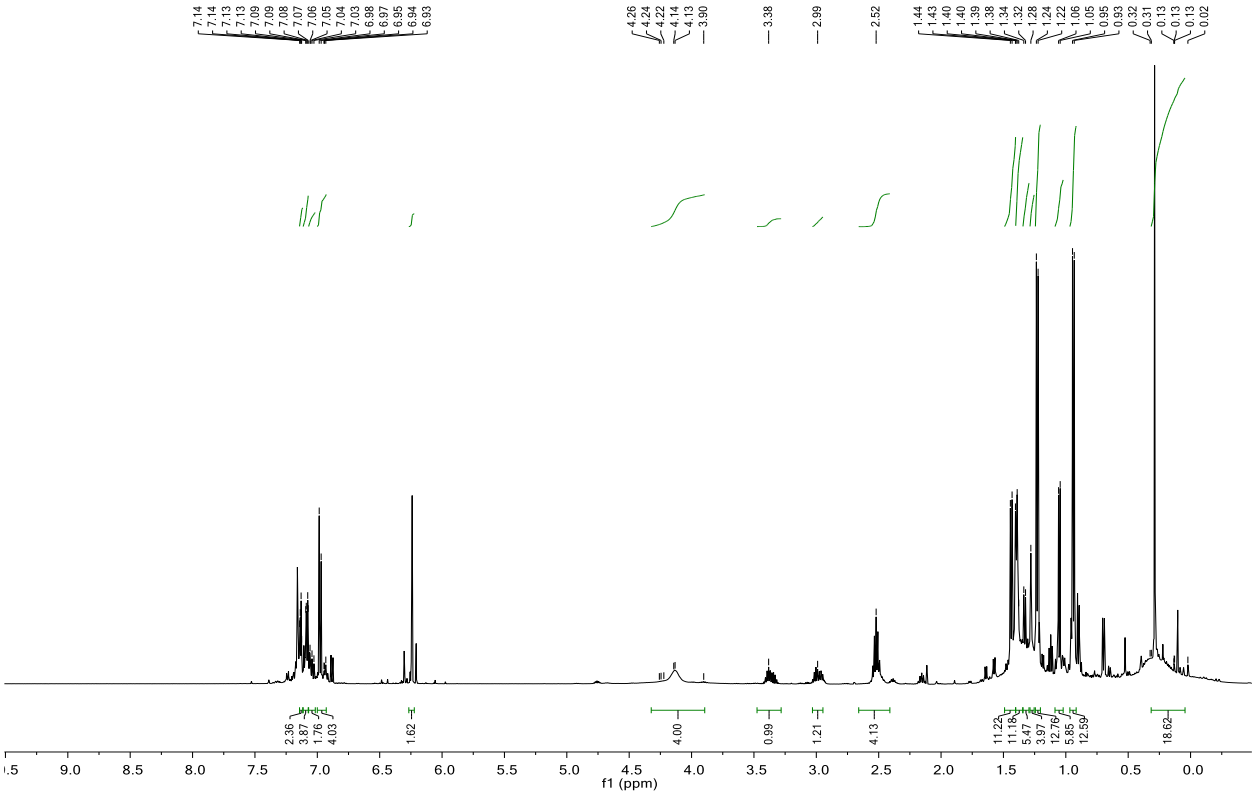

Figure 4. 10 : ^1H NMR spectrum of **4.34** (500 MHz, 298 K, C_6D_6).

The reaction of compound **4.33** with 2 atm. of $^{13}CO_2$ provided additional evidence of the similar nature of its Cu-Al bond to that of **4.27**, where a rapid conversion of **4.33** and CO_2 into a single new species (**4.35**) was observed within 30 minutes of the reaction. Although structural characterisation of **4.35** was hampered by an inability to obtain a suitable single crystal, the symmetrical environments observed in its ^1H NMR spectrum and the emergence of a single new ^{13}C-enriched peak (δ 234.0 ppm) in its $^{13}C\{^1H\}$ NMR spectrum (**Figure 4.11**) are clear indicators of the constitution of **4.35**. The latter low field ^{13}C peak is closely comparable to the diagnostic [Cu-*C*O$_2$] environments found in the respective $^{13}C\{^1H\}$ spectra provided by compound **4.31** (δ 236.2 ppm) and compound **4.32** (δ 234.9 ppm). As depicted in Figure **4.8**, the structure of compound **4.32** has been determined by single crystal X-ray crystallography to

comprise a linear [^{Me2}CAAC-Cu-{CO_2}] unit, and the solution-state data of **4.35** are, therefore, strongly indicative that a similar structure may be ascribed to compound **4.35** (Scheme **4.17**).

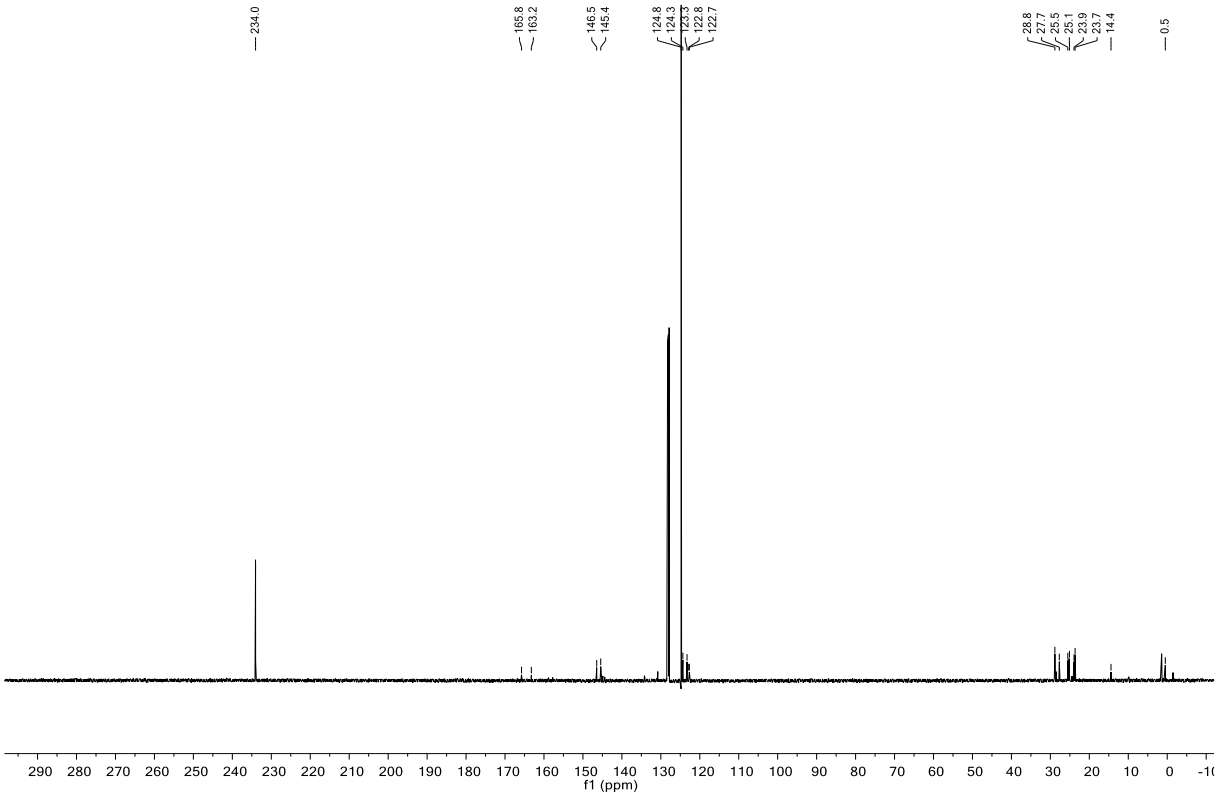

Figure 4. 11 : $^{13}C\{^{1}H\}$ NMR Spectrum of **4.35** (126 MHz, 298 K, C_6D_6).

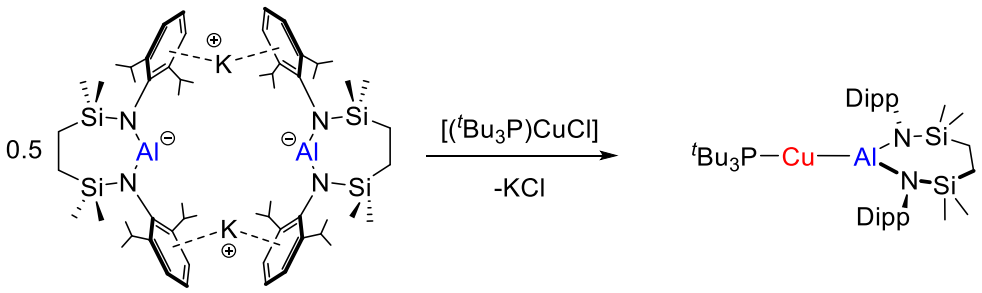

3.12 **4.36**

Scheme 4. 18 : Synthesis of [(^{t}Bu$_3$P)CuAl{SiN^{Dipp}})] (**4.36**)

From the results of the reaction of **4.33** with representative heteroallenes, it can be inferred that moderation of the steric environment associated with the *N*-heterocyclic carbene co-ligand exerts only a limited influence on the reactivity of the {(NHC)Cu-Al} bond. Prompted by these observations and the latest report of [(^{t}Bu$_3$P)CuAl{NON^{Dipp}}] (**4.21**), the copper chloride phosphine adduct, [(^{t}Bu$_3$P)CuCl], was reacted with half a molar equivalent of [{SiN^{Dipp}}AlK]$_2$ (**3.12**) in order to scrutinise the relative influence of alumanyl and co-ligand identity (**Scheme 4.18**). This reaction cleanly yielded the proposed phosphine-supported copper alumanyl,

[(^{t}Bu$_3$P)CuAl{SiN^{Dipp}})] (**4.36, Scheme 4.18**), and its ^{1}H NMR spectrum displayed one phosphine environment per each {SiN^{Dipp}} unit while its ^{31}P NMR spectrum comprised a single resonance at δ 43.9 ppm. This ^{31}P peak is only slightly downfield in comparison to that reported for [(^{t}Bu$_3$P)CuAl{NON^{Dipp}}] (**4.21**, δ 38.3 ppm),[19] suggesting only a marginal perturbation to the phosphorus and, by extension, the copper environments.

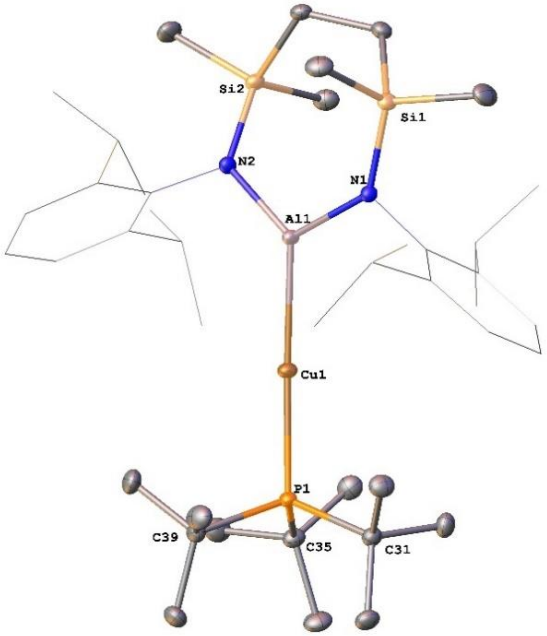

Figure 4. 12 : Displacement ellipsoid plot of compound **4.36** (30% probability ellipsoids). Dipp substituents are shown as wireframe and hydrogen atoms are omitted for clarity. Selected bond lengths (Å) and angles (°): Cu1-Al1 2.3755(3), Cu1-P1 2.2807(3), Al1-N1 1.8457(10), Al1-N2 1.8490(10); P1-Cu1-Al1 175.879(14), N1-Al1-Cu1 120.28(3), N2-Al1-Cu1 127.11(3), N1-Al1-N2 112.24(4).

These observations and the structure of **4.36** were then verified by an X-ray diffraction analysis performed on a single crystal of **4.36** grown from a hexane solution (**Figure 4.12**). Although the structural data of the closely related **4.21** were not available for comparison, the Cu1-Al1 bond length (2.3755(3) Å) of **4.36** was measured to be between the analogous Cu-Al interactions in compound **4.27** (2.3449(4) Å) and compound **4.29** (2.4028(7) Å), whilst the P1-Cu1-Al1 unit (175.879(14) °) exhibits a similar configuration as the essentially linear C31-Cu1-Al1 bonding motifs observed in the carbene stabilised copper-alumanyl complexes (**4.27**, 178.85(4)°; **4.29**, 173.42(6)°).

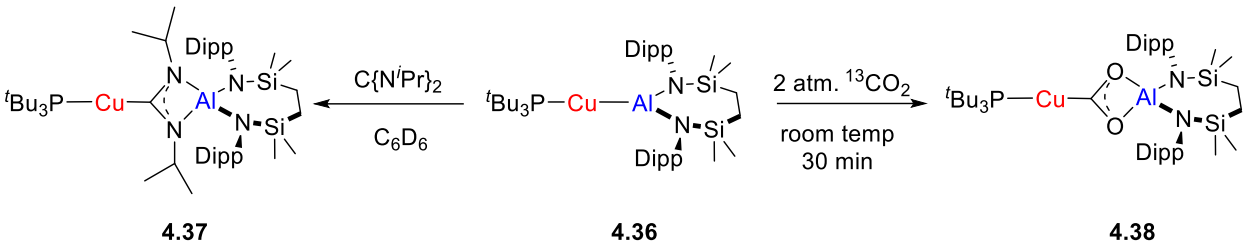

Scheme 4. 19 : Reaction of **4.36** with *N,N'*-diisopropylcarbodiimide and $^{13}CO_2$.

As the carbene-stabilised copper-alumanyl derivatives (**4.27**, **4.29**, **4.33**) provided a variable outcome in their reactions with *N,N'*-di-isopropylcarbodiimide, which was tentatively attributed to the relative σ-basicity and π-acidity of the carbene co-ligands, compound **4.36** was then treated with the carbodiimide reagent (**Scheme 4.19**). The ^{1}H NMR spectrum of the single predominant product (**4.37**) obtained from the reaction exhibits a 1:1:1 ratio of the P^{t}Bu$_3$, carbodiimide, and {SiN^{Dipp}} ligand environments, confirming the insertion of the *N,N'*-diisopropylcarbodiimide into compound **4.36**. In addition, the highly symmetrical configuration of **4.37** could be inferred from its ^{1}H NMR spectrum, indicating the conformation of the [C{N^{i}Pr}$_2$] unit in compound **4.37** is strongly reminiscent of that in compound **4.30** (and comparable to those in **4.19a**, **4.20a 4.21a**). This was further supported by the emergence of a low field peak (δ 218.0 ppm) in the $^{13}C\{^{1}H\}$ NMR spectrum, which could be attributed to the Cu-coordinated *sp*-hybridised carbon centre of [C{N^{i}Pr}$_2$]. Indicative of closely comparable electronic environments of the phosphorus, the $^{31}P\{^{1}H\}$ NMR spectrum of **4.37** displayed a single chemical shift at δ 59.8 ppm, which is also effectively identical to that reported for [(^{t}Bu$_3$P)Cu{C(NCy)$_2$}Al{NON^{Dipp}}] (**4.21a**, δ 59.6 ppm).

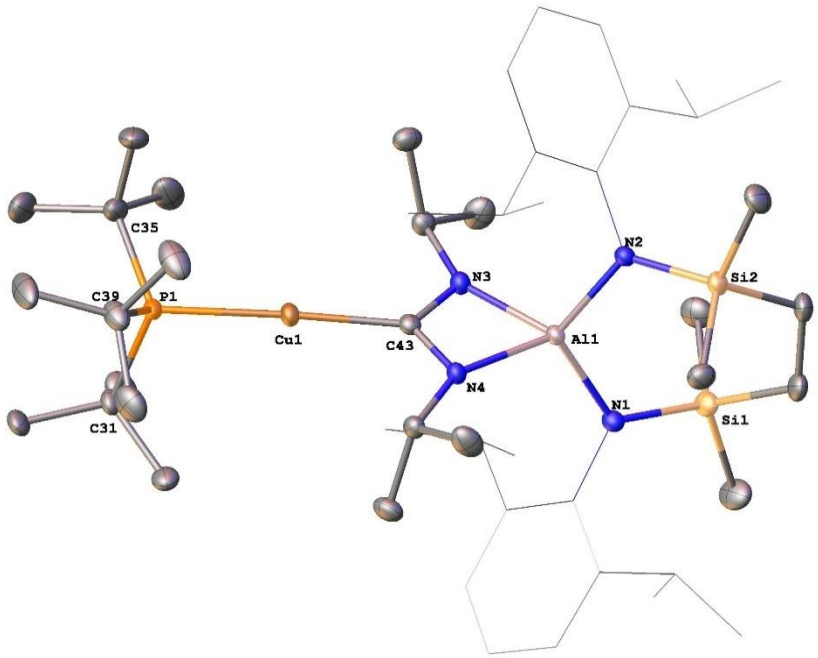

Figure 4. 13 : Displacement ellipsoid plot of compound **4.37** (30% probability ellipsoids). Dipp substituents are shown as wireframe and hydrogen atoms are omitted for clarity. Selected bond lengths (Å) and angles (°): Cu1-C43 1.9383(15), Cu1-P1 2.2095(4), Al1-N1 1.8654(13), Al1-N2 1.8620(13), Al1-N3 1.9091(13), Al1-N4 1.9096(13), C43-N5 1.346(2), C42-N6 1.343(2); P1-Cu1-C43 177.73(4), N1-Al1-N2 113.32(6), N1-Al1-N3 122.64(6), N1-Al1-N4 112.16(6), N2-Al1-N3 110.72(6) N2-Al1-N4 122.14(6), N3-C43-N4 108.75(13).

These interpretations of the solution-state data were subsequently confirmed by the X-ray diffraction analysis conducted on a single crystal of **4.37** obtained from a hexane solution (**Figure 4.13**). The solid-state characterisation demonstrated that the copper coordination geometry in compound **4.37** is, as observed in **4.30** and **4.21a**, close to linear (C43-Cu1-P1 177.73(4)°). In addition, the C-Cu-P unit of [(^{t}Bu$_3$P)Cu{C(N^{i}Pr)$_2$}Al{SiN^{Dipp}}] (**4.37**) is broadly comparable to that reported for [(^{t}Bu$_3$P)Cu{C(NCy)$_2$}Al{NON^{Dipp}}] (**4.21a**) despite the variations in the substituents of carbodiimide and the aluminium supporting backbone. The Cu1-P1 (2.2095(4) Å) and Cu1-C43 (1.9383(15) Å) bond distances of **4.37** are only marginally altered in comparison to the analogous distances in **4.21a** (Cu-P 2.2163(13); Cu-C 1.952(4) Å).[19] The maintenance of the nucleophilicity of the copper centre in **4.36** through the introduction of the tri-*tert*butyl-phosphine was, therefore, confirmed by the formation and detailed characterisation of **4.37**.

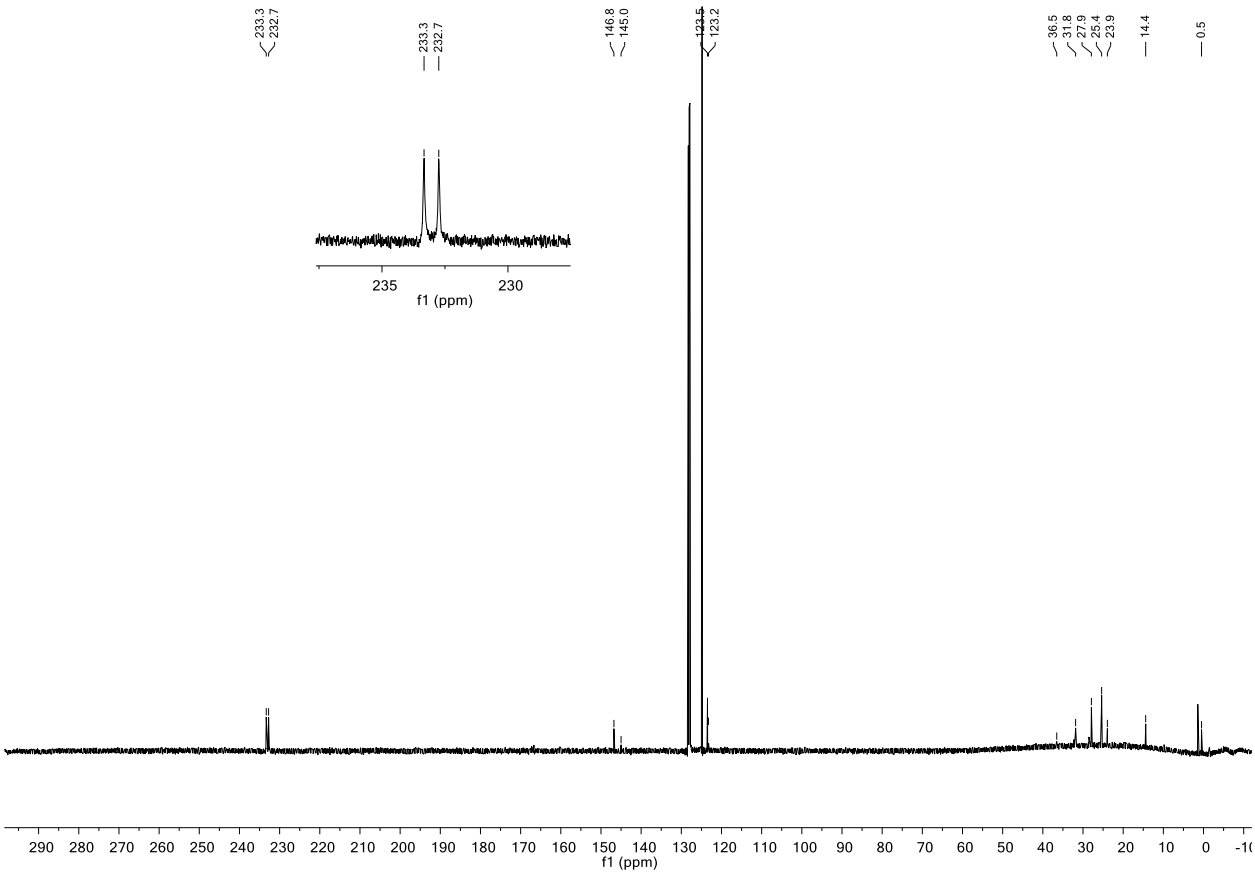

Figure 4. 14 : $^{13}C\{^{1}H\}$ NMR Spectrum of **4.38** (126 MHz, 298 K, C_6D_6).

Compound **4.36** was also observed to react rapidly with $^{13}CO_2$ to provide compound **4.38** as the predominant product (**Scheme 4.19**), which was readily identified *via* its characteristic low field doublet chemical shift (δ 233.1 ppm, $^{2}J_{PC}$ = 73.9 Hz) in its $^{13}C\{^{1}H\}$ NMR spectrum (**Figure 4.15**), as a dioxocarbene-coordinated copper complex analogous to compounds **4.31**, **4.32** and **4.35**. Moreover, a nearly identical electronic environment to the copper centre of [(^{t}Bu$_3$P)Cu{CO$_2$}Al{SiN^{Dipp}}] (**4.38**) its structurally characterised diaminocarbene-copper analogue (**4.37**), was evident from the similarity in their phosphorus chemical shifts, each of which appeared at δ 59.8 ppm in the respective $^{31}P\{^{1}H\}$ NMR spectra.

A single crystal of compound **4.38** could not be obtained due to its slow decomposition in solution at room temperature, which was be most clearly reflected in its $^{31}P\{^{1}H\}$ NMR spectrum through the appearance of further signals at 62.5 and 66.0 ppm over the course of a few weeks. Heating of this solution with the maintenance of the atmosphere of CO_2 overnight at 60 °C resulted in the complete disappearance of the ^{31}P NMR signal assigned to compound **4.38** and the emergence of a single copper phosphine species (**4.39**) observed as a resonance at δ 62.1 ppm. This chemical shift is almost identical to that observed in Aldridge and co-workers' spontaneously formed carbonate, [(^{t}Bu$_3$P)Cu{CO$_3$}Al{NON^{Dipp}}] (**4.21c**, δ 62.5 ppm).[19]

Moreover, the disappearance of the {Cu*C*O$_2$} signal at 233.1 ppm after heating of **4.38** and the emergence of new sharp resonances at δ 166.7, 168.4 and 176.7 ppm in the corresponding $^{13}C\{^1H\}$ NMR spectrum are reminiscent of that arising from the {O$_3$*C*} environment of **4.21c** (δ 170 ppm). Although attempts to isolate a pure sample of the new species were not successful, compound **4.39** was, thus, assigned as the analogous copper carbonate, [(^{t}Bu$_3$P)Cu{CO$_3$}Al{SiN^{Dipp}}] (**Scheme 4.20**). On this basis, the further new species apparent at δ 66.0 ppm in the room temperature ^{31}P NMR spectrum of **4.38** is tentatively attributed to the oxo derivative, [(^{t}Bu$_3$P)CuOAl{SiN^{Dipp}}] (**4.38a**), which is closely related to the {Al-O-Cu}-bridged intermediate implicated computationally, but not spectroscopically identified, in Aldridge, Frenking and co-workers' analysis of the formation of [(^{t}Bu$_3$P)Cu{CO$_3$}Al{NON^{Dipp}}] (**4.21c**).[19]

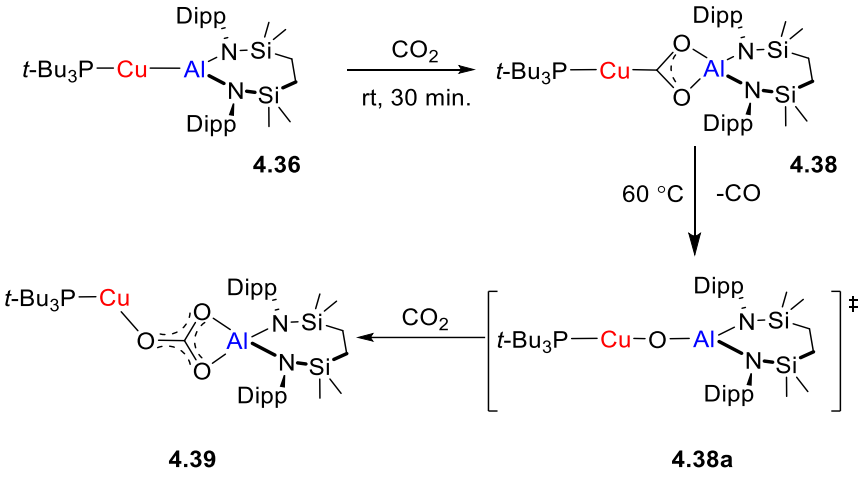

Scheme 4. 20 : Synthesis and proposed further transformation of **4.38** under CO$_2$.

4.3.2 Computational Investigation of the Cu-Al Bonds

The four dissimilar L–Cu–[Al] complexes [(NHC^{iPr})CuAl{SiN^{Dipp}}] (**4.27**), [(^{Me2}CAAC)CuAl{SiN^{Dipp}}] (**4.29**), [(^{t}Bu$_3$P)CuAl{SiN^{Dipp}}] (**4.36**), and [(^{t}Bu$_3$P)CuAl{NON^{Dipp}}] (**4.21**) were also investigated *in silico* by Dr Neale and Dr M^{c}Mullin. The identity of both the co-ligand and the alumanyl backbone was found to impact the electronic behaviour of the Cu centre in a variety of ways. Although correlated QTAIM analyses indicated that all Cu–Al BCPs (Bond Critical Point) possess similar electron densities and Laplacians, subtle changes to the computed atomic charges arise across these complexes. Whereas the Cu atom in **4.29** bears the least negative charge (q_{Cu} = −0.202), the effect of co-ligand identity is highlighted by the profound change in q_{Cu} observed upon changing from NHC^{iPr} in **4.27** (q_{Cu} = −0.323) to P^{t}Bu$_3$ in **4.36** (q_{Cu} = −0.403). These findings are consistent

with the Al-centred nucleophilicity towards carbodiimide observed in compound **4.27**. Conversely, a negligible difference is calculated in q_{Cu} between **4.36** and **4.21** (q_{Cu} = −0.406), where the [Al{SiN^{Dipp}}] supporting group is exchanged for [Al{NON^{Dipp}}]. This latter observation implies that the identity of the co-ligand plays a much larger role in determining the Cu centre's electronic structure and potential nucleophilicity than the nature of the alumanyl group. On the other hand, the alteration in q_{Al} between **4.27** (+1.887) and **4.21** (+1.851) is more noticeable than the change in q_{Cu}, indicating that the [Al{NON^{Dipp}}]-bonded Cu centre is more likely to exhibit a higher degree of nucleophilic behaviour.

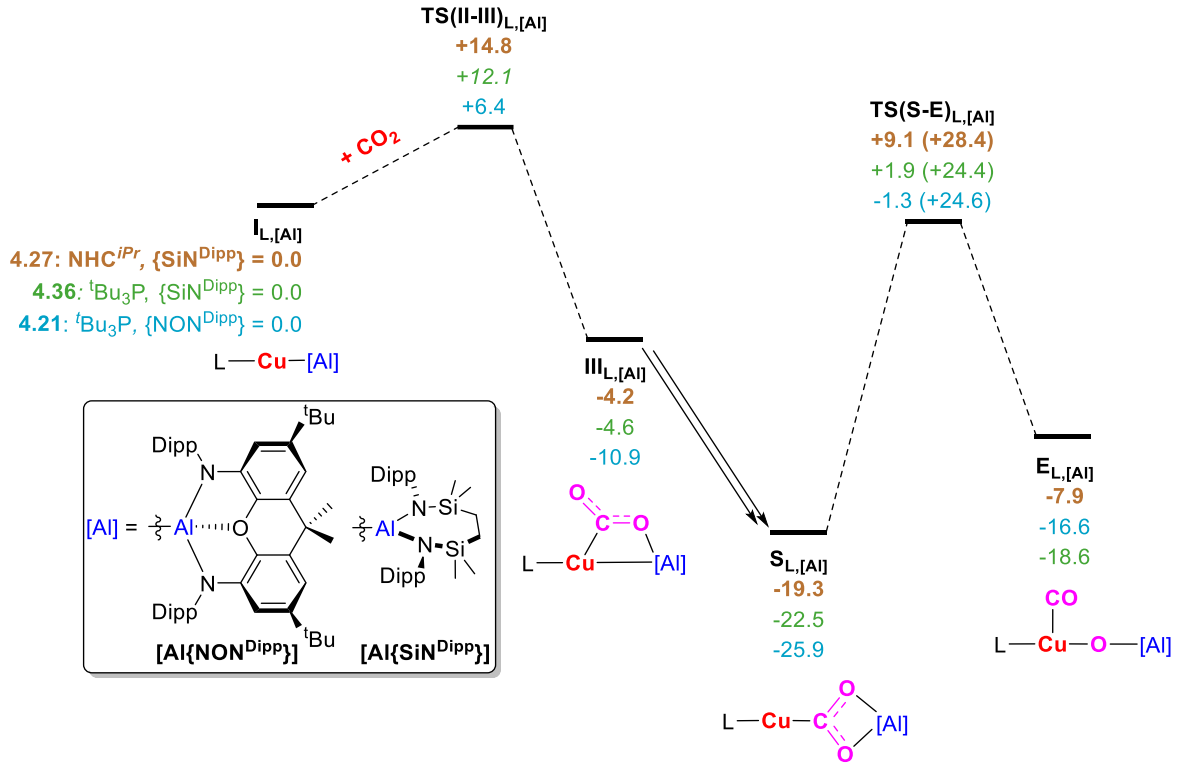

Figure 4. 15 : Computed (at the BP86-D3BJ,benzene/BS2//BP86/BS1 level) free energy profile (kcal mol^{-1}) of CO_2 addition, dioxocarbene formation, and subsequent CO extrusion for L-Cu-[Al] complexes **4.27** (copper brown, bold), **4.36** (green) and **4.21** (teal). Energetic spans of CO extrusion reported in parenthesis are from the preceding adducts, **S**$_L$,[Al].

Intrigued by the contrasting stability of the dioxocarbene derivatives (**4.31**, **4.32**, **4.38**, **4.21b**) resulting from the reactions of respective copper-alumanyl complexes (**4.27**, **4.29**, **4.36**, **4.21**) with CO_2 appears to be modulated by the identity of the co-ligand as well as the {NON^{Dipp}} and {SiN^{Dipp}} alumanyl backbone environments, the thermodynamics of formation of the dioxocarbene derivatives and the mechanisms of subsequent CO extrusion were computed for **4.27**, **4.36**, and **4.21**. **Figure 4.15** summarises the kinetics and thermodynamics of both CO_2 addition and CO extrusion from the three corresponding dioxocarbene adducts.

While the disparity in the kinetic barriers toward CO_2 addition between **4.36** (+12.1 kcal/mol) and **4.27** (+14.8 kcal/mol) is relatively minor, addition is kinetically more facile for **4.21** with a smaller barrier (+6.4 kcal/mol). This observation suggested that the nature of the alumanyl has a larger influence over the kinetics of electrophile addition than the identity of the co-ligand. The previously discussed QTAIM analyses of compounds **4.27**, **4.36**, and **4.21,** have highlighted that the adjustment to the backbone of the alumanyl group results in only minor modulation of the Cu–Al BCP and q_{Cu}, and a modest change to q_{Al}. On this basis, therefore, it is implied that the backbone influence could be more of a steric effect in nature. On the other hand, the energetic span of CO extrusion is notably higher for the system derived from **4.27** (+28.4 kcal/mol) than for **4.36** (+24.4 kcal/mol). This is in concordance with the observable CO extrusion reactivity from **4.38** at 60 °C and the contrasting excellent thermal stability of **4.30**, highlighting the more significant influence from the co-ligand over this onwards reactivity from the dioxocarbene species.

4.3 Carbene Stabilised Heavier Group 11-[Al{SiN^{Dipp}}] Complexes

4.3.1 Experimental Investigation of the group 11 metal (Ag,Au)-Al{SiN^{Dipp}} bonds

With the results described in **Section 4.2** in hand, and the insights obtained from the reactions of [(IPr)CuAl{SiN^{Dipp}}] (**4.33**) with heteroallenes such that steric demands in the carbene co-ligands have limited influence on the reactivity of the Al-Cu bond, reactions of [{SiN^{Dipp}}AlK]$_2$ (**3.12**) were performed with NHC^{iPr} adducts of both AgCl and AuCl (**Scheme 4.21**). In both cases, overnight reactions in hexane gave the respective carbene-coordinated silver and gold alumanyl derivatives (**4.40**, **4.41**) as colourless solids.

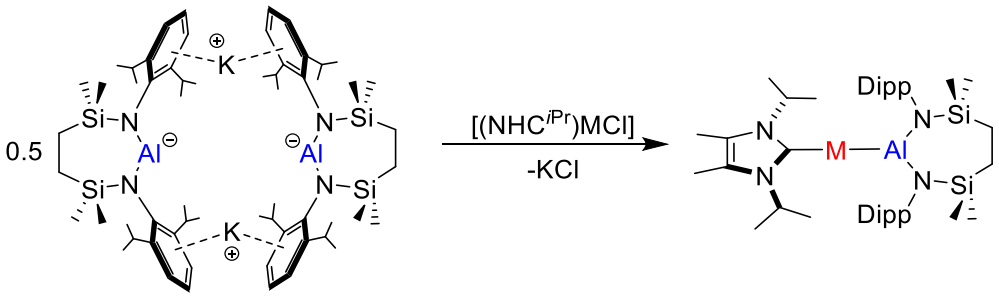

Scheme 4. 21 : Synthesis of [(NHC^{iPr})AgAl{SiN^{Dipp}}] (**4.40**) and [(NHC^{iPr})AuAl{SiN^{Dipp}}] (**4.41**).

Both of the ^{1}H NMR spectra of compounds **4.40** and **4.41** were strongly comparable to that of their copper analogue, [(NHC^{iPr})CuAl{SiN^{Dipp}}] (**4.27**), where respective spectra displayed a 1 to 1 ratio of the carbene and the {SiN^{Dipp}} environments. On the other hand, the carbenic carbon resonances in the heavier group 11 [(NHC^{iPr})MAl{SiN^{Dipp}}] complexes (**4.40**, **4.41**) were found to be at much lower field (**4.40**, δ = 230.5; **4.41**, δ = 216.1 ppm) in comparison to that of the *C*-donor chemical shift of **4.27** (δ 175.9 ppm). These chemical shift values are also significantly downfield compared to those reported for the relevant chloride starting materials [(NHC^{iPr})MCl] (δ M = Ag: 172.3; M = Au: 166.0 ppm).[46,47]

" You're collecting these coinage bois like infinity stones." – H. T. W. Shere, 2021.

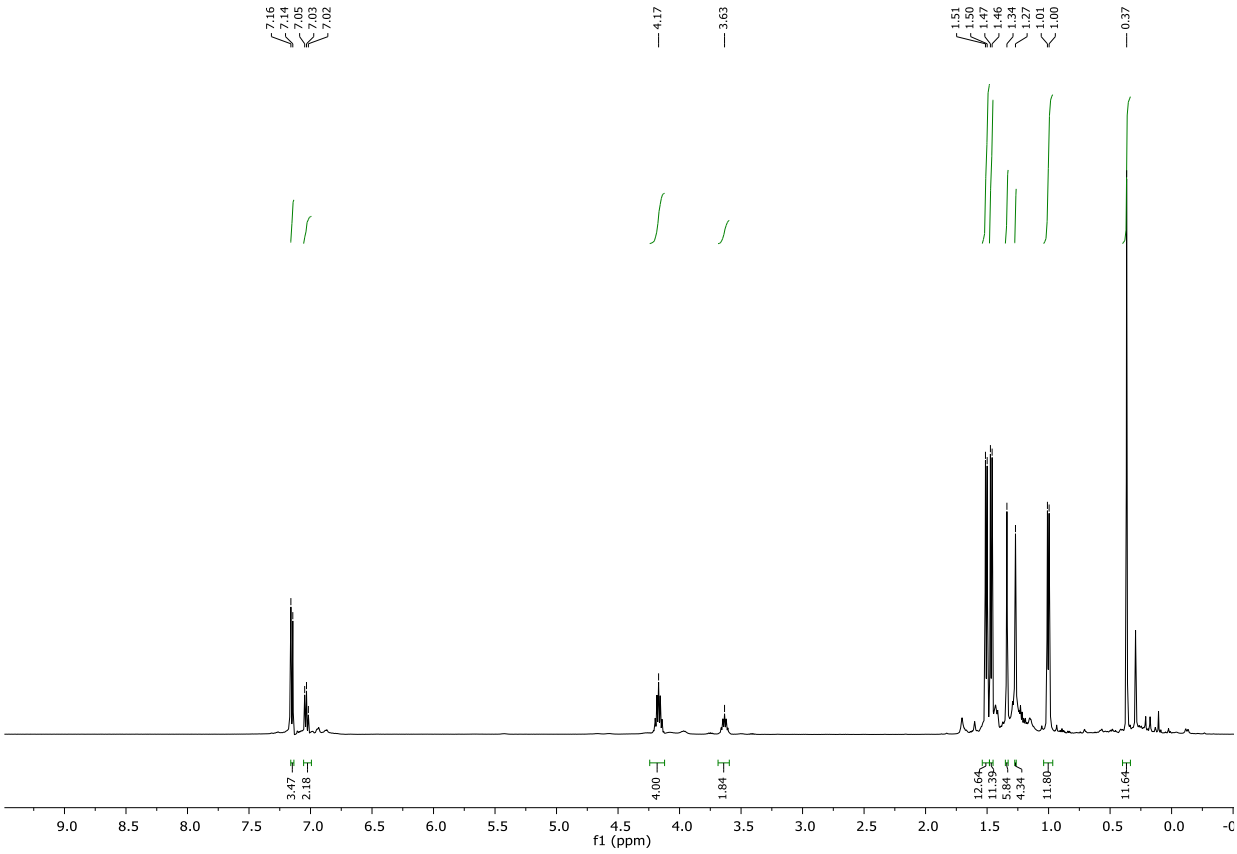

Figure 4. 16 : ^{1}H NMR Spectrum of **4.40** (500 MHz, 298 K, C_6D_6).

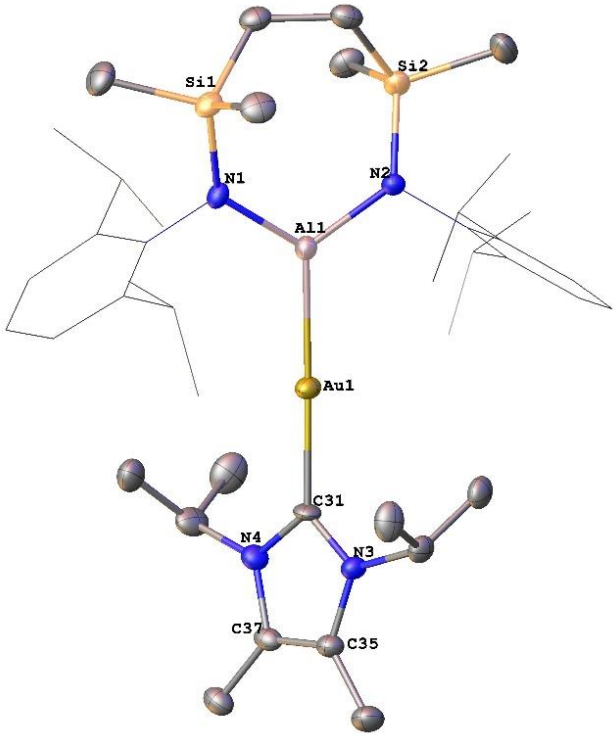

Figure 4. 17 : Displacement ellipsoid plot of compound **4.41** (30% probability ellipsoids). Dipp substituents are shown as wireframe and hydrogen atoms are omitted for clarity.

Although analytically pure bulk samples of compound **4.40** were available for further studies (**Figure 4.16**), all attempts to obtain single crystals were unsuccessful. On the other hand, a colourless single crystal of **4.41** suitable for X-ray diffraction analysis was grown by slow evaporation of a methylcyclohexane solution (**Figure 4.17**, **Table 4.1**). The structural characterisation of the compound **4.41** revealed a gold coordination sphere comprising solely its interaction with the NHC$^{i\text{Pr}}$ and the [Al{SiN$^{\text{Dipp}}$}] moiety, where the C31-Au1-Al1 angle approaches linearity (178.3(2)°). In comparison to the Au-Al distance (2.402(3) Å) in [(^{t}Bu$_3$P)AuAl{NON$^{\text{Dipp}}$}] (**4.19**),[23] compound **4.41** features a significantly contracted Au-Al bond (2.094(7) Å), while the C31-Au1 separation in **4.41** is only marginally elongated compared to that (Au-C 1.996(9) Å) measured in [(NHC$^{i\text{Pr}}$)AuCl].

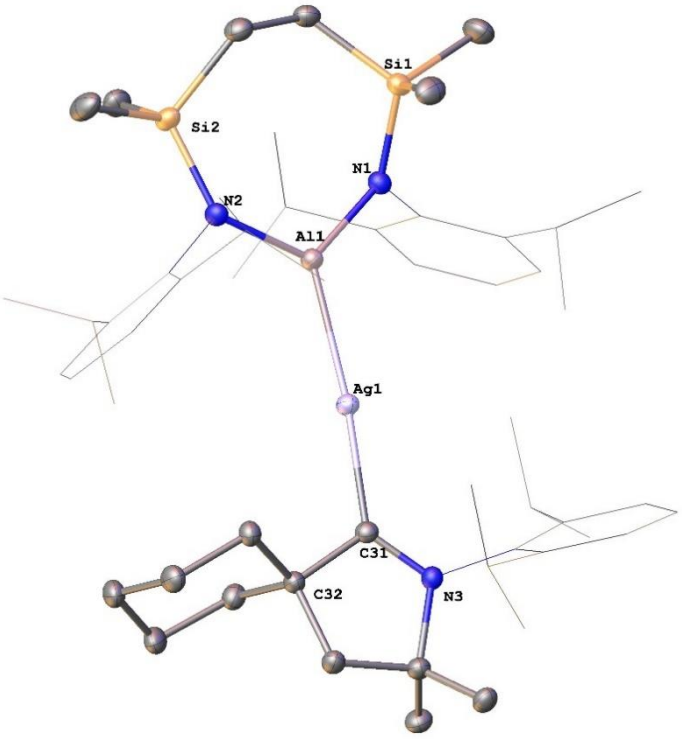

Figure 4. 18 : Displacement ellipsoid plot of [($^{\text{Cy}}$CAAC)AgAl{SiN$^{\text{Dipp}}$}] (**4.42**) (30% probability ellipsoids). Dipp substituents are shown as wireframe and hydrogen atoms are omitted for clarity. Selected bond lengths (Å) and angles (°): Ag1-Al1 2.4694(6), Ag1-C31 2.182(2), Al1-N1 1.8526(18), Al1-N2 1.8484(18); C31-Ag1-Al1 171.13(6), N1-Al1-Ag1 124.91(6), N2-Al1-Ag1 121.48(6).

In contrast to the smooth production of compounds **4.40** and **4.41** from the reaction of [{SiN$^{\text{Dipp}}$}AlK]$_2$ (**3.12**) with [(NHC$^{i\text{Pr}}$)AgCl] and [(NHC$^{i\text{Pr}}$)AuCl], respectively, attempts to synthesise the heavier analogues of [($^{\text{Me2}}$CAAC)CuAl{SiN$^{\text{Dipp}}$}] (**4.29**) were not successful. All attempted reactions of either [($^{\text{Me2}}$CAAC)AgCl] or [($^{\text{Me2}}$CAAC)AuCl] with compound **3.12** resulted in a complex mixture of products and precipitation of grey metallic powder which

plausibly originated from reduction of the group 11 metals. Analogous attempted synthesis of silver and gold complexes was then repeated with the more sterically encumbered cyclic (alkyl)(amino)carbene, ^{Cy}CAAC (^{Cy}CAAC = 2-[2,6-di-isopropylphenyl]-3,3-dimethyl-2-azaspiro[4.5]dec-1-ylidene). Although these attempted reactions generally presented a similar outcome, the reaction of [(^{Cy}CAAC)AgCl] with **3.12** in C_6D_6 enabled the identification of the silver alumanyl derivative, [(^{Cy}CAAC)AgAl{SiN^{Dipp}}] (**4.42**), by X-ray diffraction analysis performed on a colourless single crystal mechanically separated from the crude reaction mixture (**Figure 4.18**). Although further studies of **4.42** were hampered by the unavailability of a pure bulk sample, the structural characterisation of **4.42** represents the first solid-state authentication of a silver-aluminium bond (2.4694(6) Å). Compound **4.42** exhibits a *pseudo*-linear 2-coordinated silver environment (C31-Ag1-Al1 171.13(6)°) provided by the carbenic carbon and the aluminium donor atoms, which is strongly reminiscent of the bonding motif observed at the coinage metal centres of compounds **4.27**, **4.29**, and **4.41**.

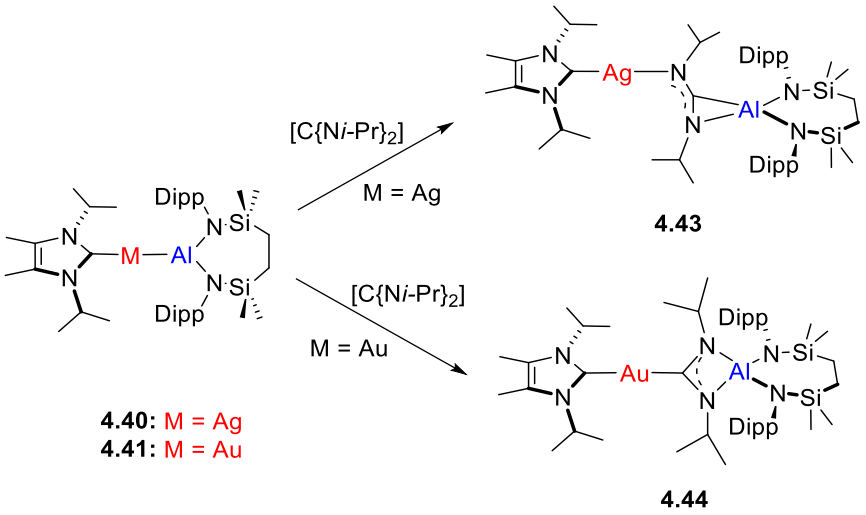

Scheme 4. 22 : Synthesis of **4.43** and **4.44**.

To shed light onto the effect of the identity of the group 11 metal on the reactivity of the M-Al bonds, **4.40** (M = Ag) and **4.41** (M = Au) were then treated with *N*,*N*′-di-isopropylcarbodiimide. In both cases, the reaction mixtures were observed to provide the respective products, **4.43** and **4.44**, within a few hours at room temperature (**Scheme 4.22**) The ^{1}H and ^{13}C{^{1}H} NMR spectra of compound **4.43** were closely comparable to that of **4.28**, such that the methine resonances in the [C{N^{i}Pr}$_2$] unit were separated into two distinct (each 1H by relative integration) multiplets at δ 3.46 and 4.34 ppm, strongly indicative of an unsymmetrical insertion regiochemistry. In contrast, the ^{1}H NMR spectrum of compound **4.44** featured only a single set of closely related methine environments arising from the inserted

carbodiimide. These solution-state data of compounds **4.43** and **4.44** are, therefore, strongly suggestive that these molecules exhibit contrasting carbodiimide insertion regiochemistry.

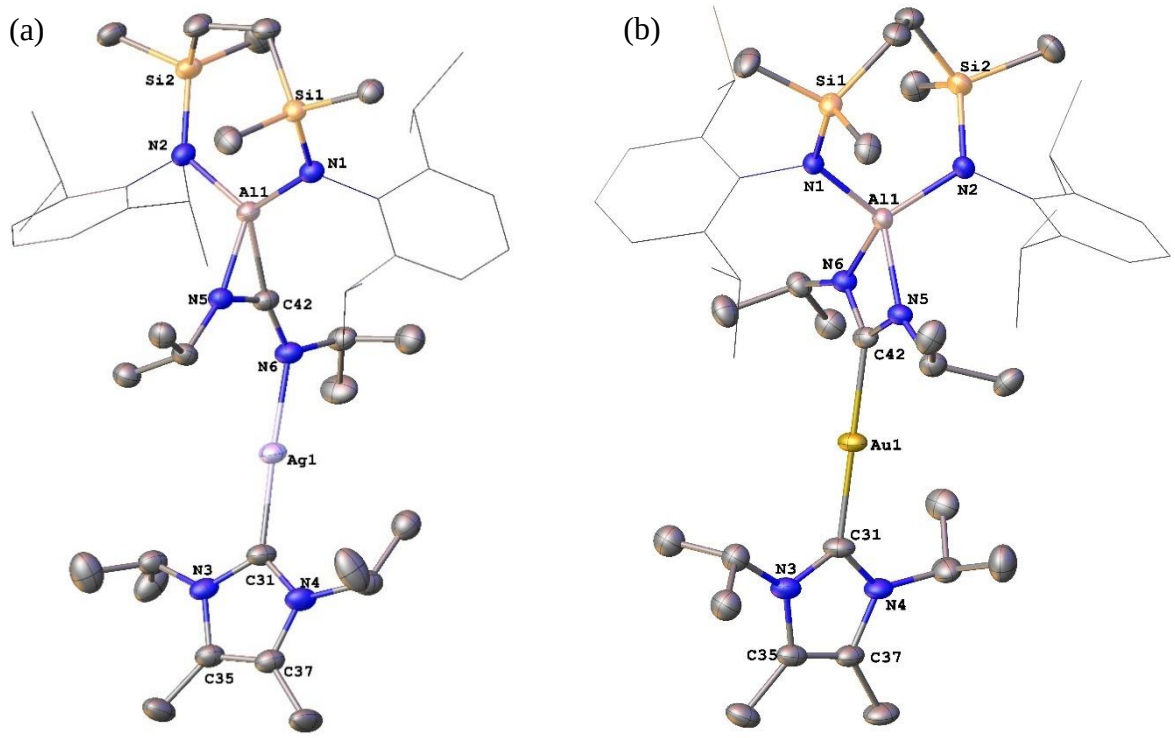

Figure 4. 19 : Displacement ellipsoid plots (30% probability ellipsoids) of (a) compound **4.43** (b) compound **4.44**. Dipp substituents are shown as wireframe and hydrogen atoms are omitted for clarity.

The deduction made from the NMR spectra was later verified by X-ray diffraction analyses performed on colourless single crystals of compounds **4.43** and **4.44**, which were isolated by slow evaporation of methylcyclohexane solutions (**Figure 4.19**, **Table 4.1**). In both cases, the asymmetric units constitute two very similar molecules and the discussion will, therefore, be confined to the Ag1- and Au1-containing molecules. The silver centre in the structure of **4.43** is coordinated by NHC$^{i\text{Pr}}$ and a single nitrogen atom of the [C{N^{i}Pr}$_2$] fragment (Ag1–C31 2.078(5) Å, Ag1–N6 2.087(4) Å), whilst the aluminium coordination sphere is satisfied by a side-on η^2-interaction with the C42–N5 bond of the [C{N^{i}Pr}$_2$] unit. The resultant three-membered AlCN metallacycle is closely realted to that found in compound **4.28** (**4.43**, Al1–C42 1.948(5) Å, Al1–N5 1.853(4)Å, C42–N5 1.362(6) Å; **4.28**, (Al1–C42 1.9554(17), Al1–N5 1.8693(14), C42–N5 1.358(2) Å). On the other hand, structural characterisation identified compound **4.44** as an aura-amidinate, where the NHC$^{i\text{Pr}}$-ligated gold centre is bound to the former carbodiimide unit fragment through its central carbenic carbon atom. The Au1-C42 distance of **4.44** [2.046(3) Å] is essentially identical to that (2.058(10) Å) reported for [(^{t}Bu$_3$P)Au(C{N^{i}Pr}$_2$)Al{NON$^{\text{Dipp}}$}] (**4.19a**) despite the dissimilar carbene co-

ligand in **4.44**. Consistent with its assignment as a delocalised aura-amidinate, the [C{N^{i}Pr}$_2$] unit interacts with the aluminium centre in a *N*,*N*′-bidentate fashion, with essentially identical Al–N distances (Al1–N5 1.913(2) Å, Al1–N6 1.904(2) Å), which are also closely comparable with those found in compounds **4.30** and **4.37** (**4.30**, Al1-N4 1.908(2) Å, Al1-N5 1.923(2) Å; **4.37**, Al1-N3 1.9091(13) Å, Al1-N4 1.9096(13) Å).

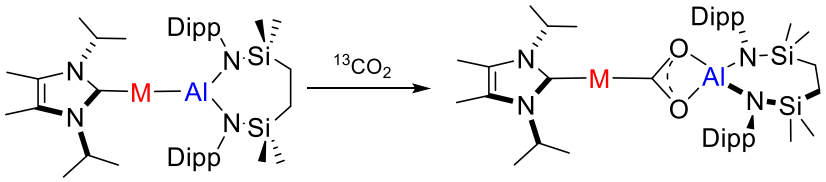

4.40: M = Ag
4.41: M = Au

4.45: M = Ag
4.46: M = Au

Scheme 4. 23 : Reactions of **4.40** and **4.41** with $^{13}CO_2$

	4.27[a]	**4.41**[c]	**4.28**[a]	**4.43**[b]	**4.44**[c]
M1-C42	2.3449(4)[d]	2.369(2)[h]	1.8846(15)[l]	2.087(4)[q]	2.046(3)
M1-C31	1.9529(12)	2.094(7)	1.8959(18)	2.078(5)	2.058(3)
Al1-N1	1.8455(10)	1.827(6)	1.8425(14)	1.842(5)	1.849(2)
Al1-N2	1.8473(10)	1.828(6)	1.8411(14)	1.854(4)	1.839(2)
Al1-N5	-	-	1.8693(14)	1.853(4)	1.913(2)
Al1-N6	-	-	1.9554(17)[m]	1.948(5)[m]	1.904(2)
C42-N5	-	-	1.358(2)	1.362(6)	1.364(4)
C42-N6	-	-	1.319(2)	1.315(6)	1.335(3)
C31-M1-C42	178.85(4)[e]	178.3(2)[i]	174.70(7)[n]	174.9(2)[r]	179.41(12)
N1-Al1-N2	112.05(5)	115.0(3)	112.63(6)	114.80(19)	110.37(10)
N1-Al1-N5	123.41(4)[f]	122.8(2)[j]	115.08(6)	115.52(19)[s]	123.61(10)
N1-Al1-N6	-	-	127.95(7)[o]	124.22(19)[t]	111.62(10)
N2-Al1-N5	124.54(3)[g]	122.2(2)[k]	125.43(7)	121.54(19)[u]	113.24(10)
N2-Al1-N6	-	-	116.68(7)[p]	118.8(2)[v]	123.65(10)
N5-C42-N6	-	-	126.50(15)	127.7(5)	108.4(2)

Table 4. 1 : Selected bond lengths (Å) and angles (°) for compounds **4.27**, **4.41**, **4.28**, **4.43**, and **4.44**. [a] M= Cu, [b] M= Ag, [c] M=Au, [d] Cu1-Al1, [e] C31-Cu1-Al1, [f] N1-Al1-Cu1, [g] N2-Al1-Cu1, [h] Au1-Al1, [i] C31-Au1-Al1, [j] N1-Al1-Au1, [k] N2-Al1-Au1, [l] Cu1-N6, [m] Al1-C42, [n] C31-Cu1-N6, [o] N1-Al1-C42, [p] N2-Al1-C42, [q] Ag1-N6; [r] C31-Ag1-N6, [s] N2-Al1-N5, [t] N2-Al1-C42, [u] N1-Al2-N5, [v] N1-Al1-C41.

Treatment of compounds **4.40** and **4.41** with 2 atm. of $^{13}CO_2$ gave quantitative conversion to the respective new species, **4.45** and **4.46**, within 30 minutes at room temperature (**Scheme 4.23**). Although a single crystal of neither compound could be obtained, the assignments of their solution-state configurations were unambiguous. As described in **Section 4.2** for the copper dioxocarbene derivatives (**4.31**, **4.32**, **4.35**, **4.38**), the appearance of low field ^{13}C-enriched resonances in their respective $^{13}C\{^1H\}$ NMR spectra at δ 240.4 (**4.45**) and 239.1 (**4.46**) ppm is diagnostic of the formation of the respective silver and gold analogues, [(NHC^{iPr})M(CO_2)Al{SiN^{Dipp}}] (**4.45**, M = Ag; **4.46**, M = Au; **Figure 4.20** and **4.21**). Furthermore, the dioxocarbene environments are found to be redolent of those reported for the analogous coinage metal-bonded {$^{13}CO_2$} environments in [(NHC^{iPr})M(CO_2)Al{NON^{Dipp}}] (**4.20b**, δ 220.2, **4.19b**, δ 242.3 ppm). Also, as shown in **Figure 4.20**, the {CO_2} environment in compound **4.45** resonated as two doublets resulting from the coupling to the naturally abundant I = ½ ^{109}Ag (48.2%) and ^{107}Ag (51.8%) isotopes ($^1J^{109}_{Ag\text{-}C}$ = 252.6, $^1J^{107}_{Ag\text{-}C}$ = 218.9 Hz).

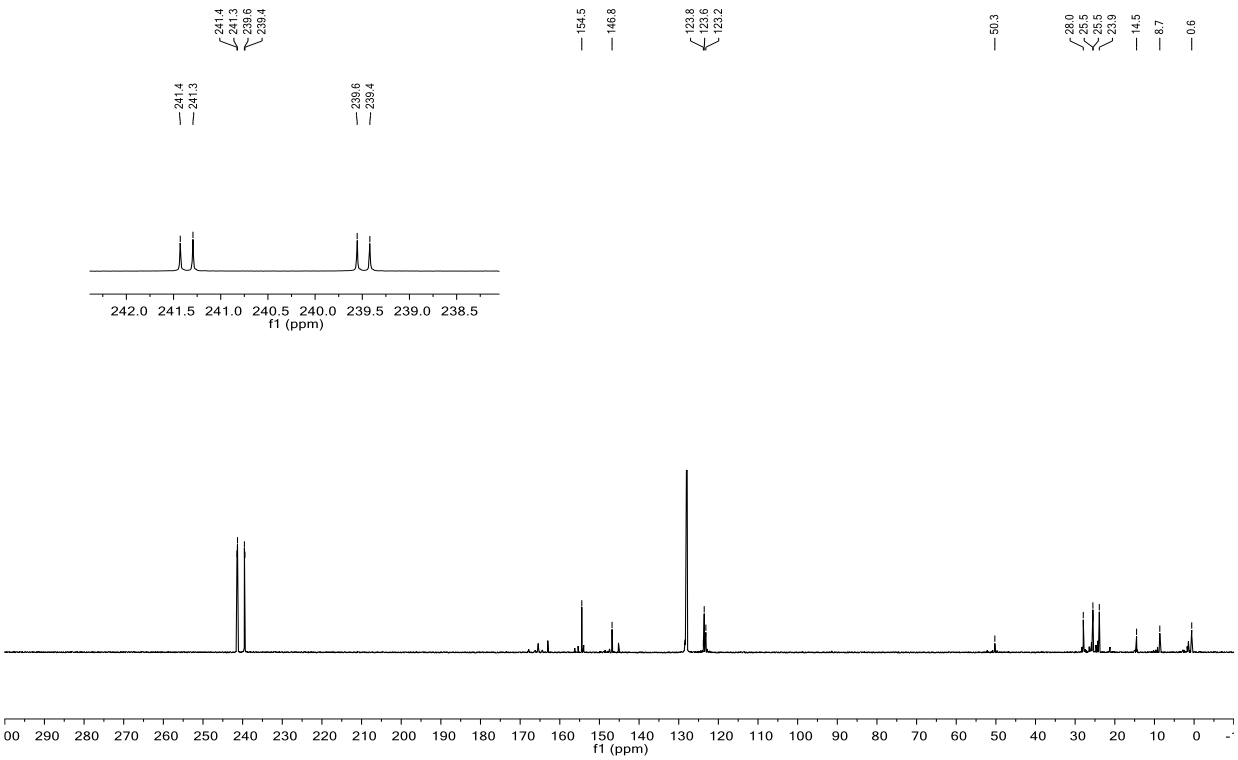

Figure 4. 20 : $^{13}C\{^1H\}$ NMR Spectrum of **4.45** (126 MHz, 298 K, C_6D_6).

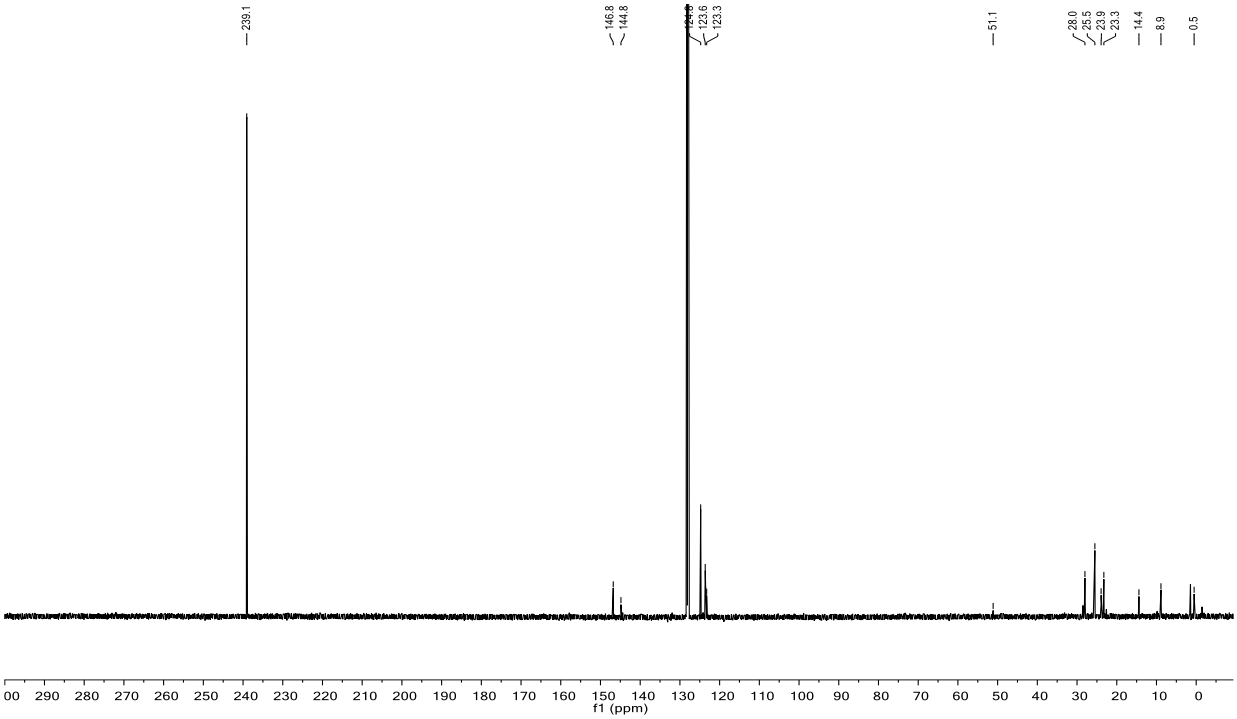

Figure 4. 21 : $^{13}C\{^{1}H\}$ NMR Spectrum of **4.46** (126 MHz, 298 K, C_6D_6).

4.3.3 Computational Assessment of the group 11 metal–Al Bonds

With these synthetic insights in hand, the electronic structures of [(NHC^{iPr})CuAl{SiN^{Dipp}}] (**4.27**), [(NHC^{iPr})CuAl{SiN^{Dipp}}] (**4.40**), [(NHC^{iPr})CuAl{SiN^{Dipp}}] (**4.41**) were also probed with QTAIM analysis by Dr Neale and Dr M^{c}Mullin to discern how the identities of the group 11 element perturb the nature of the M–Al bond.

Complex	BCP (A–B)	ρ(r)	$\nabla^2\rho(r)$	H(r)	DI(A|B)	q_A	q_B	Δq (A-B)
4.27	Cu–Al	0.061	−0.045	−0.030	0.752	−0.323	+1.817	−2.140
	Cu–C	0.105	0.275	-0.039	0.734		+0.622	−0.9445
4.40	Ag–Al	0.060	−0.028	−0.029	0.719	−0.428	+1.874	−2.302
	Ag–C	0.086	0.214	-0.025	0.665		+0.670	−1.098
4.41	Au–Al	0.066	0.049	-0.029	0.618	−0.720	+2.080	−2.800
	Au–C	0.105	0.209	−0.037	0.799		+0.702	−1.422

Table 4. 2 : Selected BCP and atomic QTAIM data for **4.27**, **4.40**, and **4.41** computed at the BP86/BS2//BP86/BS1 level of theory. Electron density units are in *e* bohr^{-3} and energy units are in Hartrees.

The electron densities associated with the M–Al BCPs are largely consistent across the group 11 [(NHC^{iPr})MAl{SiN^{Dipp}}] complexes ($\rho(r)$ = 0.061 (**4.27**), 0.060 (**4.40**), 0.066 (**4.41**) *e* bohr^{-3}). Futhermore, the total energy density, *H(r),* is negative in each case, indicating comparable stabilising M–Al interactions in all three cases. The associated Laplacians [$\nabla^2\rho(r)$ = −0.045 (**4.27**), −0.028 (**4.40**) and +0.049 (**4.41**) *e* bohr^{-3}], however, imply that, while the

nature of the Cu–Al and Ag–Al bonds bear a significant level of covalency, the Au–Al interaction is non-covalent with a contraction of $\rho(r)$ towards each nucleus. The atomic charges, q_{Cu} = −0.323 (**4.27**), q_{Ag} = −0.428 (**4.40**) and q_{Au} −0.720 (**4.41**), indicate that Au is more electronegative in nature and thus lends itself to enhanced nucleophilic reactivity, a supposition that is also reinforced by the respective reaction product obtained from the reactions with *N,N'*-di-isopropylcarbodiimide (**4.27 → 4.28**; **4.40 → 4.43**; **4.41 → 4.44**). This is also supported by inspection of the Natural Localised Molecular Orbitals *via* NBO analysis, and the respective atomic contributions to each M–Al bonding orbital. While **4.27** [51.0% on Al and 45.5% on Cu] and **4.40** [53.1% on Al and 43.2% on Ag] have the Al atom as the main contributor, this is reversed in **4.41** [41.8% on Al and 55.5% on Au], indicative of Au being the more significant contributor to the NLMO and, therefore, suggestive of a greater degree of $M^{\delta-}$–$Al^{\delta+}$ polarisation in [(NHC^{iPr})AuAl{SiN^{Dipp}}] (**4.41**) in comparison to its lighter analogues (**4.27** and **4.40**).

4.4 Conclusion and Future Work

Salt metathesis protocols with the aluminium(I) centred nucleophile [{SiN^{Dipp}}AlK]$_2$ (**3.12**) in the generation of novel element-aluminium bonds have been demonstrated to be feasible for all the non-radioactive group 11 elements, and the nature of the resultant ligand-stabilised metal-alumanyl complexes ([(NHC^{iPr})CuAl{SiN^{Dipp}}](**4.27**), [(^{Me2}CAAC)CuAl{SiN^{Dipp}}](**4.29**), [(IPr)CuAl-{SiN^{Dipp}}](**4.33**), [(^{t}Bu$_3$P)CuAl{SiN^{Dipp}})] (**4.36**), [(NHC^{iPr})AgAl{SiN^{Dipp}}](**4.40**), [(NHC^{iPr})AuAl{SiN^{Dipp}}](**4.41**)) have been readily assessed through their reactivity towards heteroallenes. In addition, although the study of [(^{Cy}CAAC)AgAl{SiN^{Dipp}}] (**4.42**) was limited by the difficulty in obtaining a pure bulk sample, it has provided the first solid-state verification of an Ag-Al bond.

Further Investigation of the synthesised group 11-alumanyl complexes is to be conducted to further shed light on the properties and potential applications of these novel group 11-alumanyl complexes. For example, an extensive study in Cu-Al bond mediated terminal alkyne transformations has been conducted (**II. Publications as a Result of this Thesis**). More generally, as discussed in this chapter, [{SiN^{Dipp}}AlK]$_2$ (**3.12**) indeed provides a convenient synthon for the generation of Al-coordinated species which display unconventional behaviour. It is, thus, anticipated that future research will yield a much wider array of [Al{SiN^{Dipp}}]-bonded species from across the *d*-block and even the *f*-block of metals.

"It'd be nice to start doing some f-block chemistry." – M. S. Hill

4.5 Experimental Data

[(NHC^{iPr})CuAl{SiN^{Dipp}}](4.27)

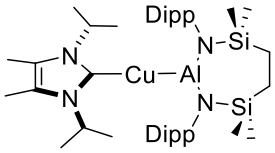

A solution of *N,N'*-diisopropyl-4,5-dimethyl-2-ylidene (NHC^{iPr}, 0.166 g, 0.912 mmol) in toluene (10 mL) was added to a Schlenk flask containing CuCl (0.090 g, 0.912 mmol). After stirring for 2 hours at room temperature, a solution of [{SiN^{Dipp}}AlK]$_2$ (**3.12**, 0.505 g, 0.455 mmol) in toluene (10 mL) was added to the stirring suspension, and the resulting brown hazy reaction mixture was then stirred at room temperature overnight. Removal of the volatiles *in vacuo*, followed by extraction into hexane and filtration gave a clear, colourless solution. Removal of the hexane solvent *in vacuo* gave a colourless powder of **4.27**. Colourless crystals of **4.27** were isolated from a saturated methylcyclohexane solution stored at -30 °C for 24 hours. Yield 0.61 g, 89%. Anal Calc'd for $C_{41}H_{70}AlCuN_4Si_2$ (**4.27** (C_7H_{14})$_{0.5}$, *814.12*): C, 65.52; H, 9.64; N, 6.87 %. Found: C, 65.49; H, 9.21; N, 6.51 %. ^{1}H NMR (500 MHz, 298 K, Benzene-d_6): δ 7.14 (d, 4H, J = 7.6 Hz, *m*-C_6H_3), 7.03 (t, 2H, J = 7.6 Hz, *p*-C_6H_3), 4.21 (sept, 4H, J = 6.9 Hz, C*H*Me$_2$ on SiN^{Dipp}), 3.55 (sept, 2H, J = 6.8 Hz, C*H*Me$_2$ on NHC^{iPr}) 1.49 – 1.46 (m, 24H, CH*Me$_2$* on SiN^{Dipp}), 1.29 (s, 6H, NC*Me*), 1.27 (s, 4H, CH_2Si), 0.99 (d, 12H, J = 6.8 Hz, CH*Me$_2$* on NHC^{iPr}), 0.35 (s, 12H, Si*Me$_2$*). ^{13}C{^{1}H} NMR (126 MHz, 298 K, Benzene-d_6) δ 175.9 (Cu*C* of NHC^{iPr}), 147.4 (*i*-C_6H_3), 147.1 (*o*-C_6H_3), 123.2 (*m*-C_6H_3), 122.8 (*p*-C_6H_3), 49.7 (*C*HMe$_2$ on NHC^{iPr}), 35.7 (N*C*Me), 28.3 (*C*HMe$_2$ on SiN^{Dipp}), 26.3, 24.5* (CH*Me$_2$* on SiN^{Dipp} and NHC^{iPr}), 14.4 (*C*H$_2$Si), 8.6 (NC*Me*), 1.2 (Si*Me$_2$*). *two overlapping resonances.

[(NHC^{iPr})Cu-κ^1-*N*-({N^{i}Pr}C{N^{i}Pr})-κ^2-*C,N'*-Al{SiN^{Dipp}}](4.28)

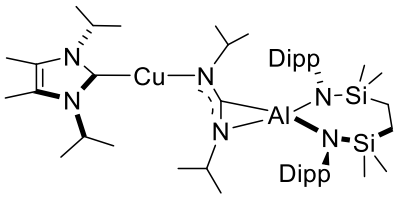

Inside a J Young's tube, [(NHC^{iPr})CuAl{SiN^{Dipp}}](**4.27**, 25 mg, 0.033 mmol) was dissolved in 0.4 mL of C_6D_6. *N,N'*-diisopropylcarbodiimide (5 μL, 0.033mmol) was then added *via* micropipette. No significant change was observed in the ^{1}H NMR spectrum within one hour of the mixing of the starting materials. The reaction mixture was then left at room temperature overnight, forming compound **4.28** in quantitative yields (determined by ^{1}H NMR). The benzene solution was then put under reduced pressure to remove all volatiles giving **4.28** as a white solid. Crystals suitable for X-ray crystallography were obtained by slow evaporation of a hexane solution of **4.28** at room temperature. Yield 20 mg, 69%. Anal Calc'd for $C_{51}H_{91}AlCuN_6Si_2$ (**4.28**.(C_6H_{14})$_{0.5}$, *935.04*): C, 65.51; H, 9.81; N, 8.99 %. Found: C, 65.66; H, 9.79; N, 8.66 %. ^{1}H NMR (500 MHz, 298 K, Benzene-d_6) δ 7.26 – 7.22 (m, 4H, *m*-C_6H_3 on SiN^{Dipp}), 7.15 – 7.11 (m, 2H, *p*- C_6H_3 on SiN^{Dipp}), 4.46 – 4.17 (m, 7H, C*H*Me$_2$ on SiN^{Dipp} and NC*H*Me$_2$), 3.36-3.27 (m, 1H, NC*H*Me$_2$ of carbodiimide), 1.60 (d, 6H, J = 6.8 Hz, CH*Me$_2$* on SiN^{Dipp}), 1.57-1.53 (m, 6H, CH*Me$_2$*, CH*Me$_2$* on SiN^{Dipp}) 1.53-1.48 (m, 12H, CH*Me$_2$*, CH*Me$_2$* on SiN^{Dipp}), 1.39-1.33 (m, 4H, SiCH_2) 1.35 (s, 6H, NC*Me*), 1.29-1.19 (m, 6H, NCH*Me$_2$* on carbodiimide) , 1.13 (d, J = 7.0 Hz, 12H, NCH*Me*2 on NHC), 1.03-0.89 (m, 6H, NCH*Me$_2$* of carbodiimide), 0.54 - 0.25 (br, 12H, Si*Me$_2$*). ^{13}C{^{1}H} NMR (126 MHz,298 K, Benzene-d_6) δ 146.8 (*i*-C_6H_3),146.6 (*o*-C_6H_3), 124.0 (Cu*C*), 123.7 (*m*-C_6H_3), 122.7 (*p*-C_6H_3), 57.6 (N*C*HMe$_2$ of carbodiimide), 52.2 (N*C*HMe$_2$ on NHC^{iPr}), 44.9 (N*C*HMe$_2$ of carbodiimide), 32.0 (CH*Me$_2$*), 28.1 (CH*Me$_2$*), 28.0 (*C*HMe$_2$), 27.6 (*C*HMe$_2$), 26.5 (CH*Me*2), 26.3 (CH*Me*2), 25.9 (CH*Me*2), 23.2 (NCH*Me$_2$* on NHC^{iPr}), 15.1 (Si*C*H$_2$), 9.0 (NC*Me*), 1.98 (Si*Me*2); ^{13}C resonance correlated to Al-*C*N$_2$ not observed.

[(^{Me2}CAAC)CuAl{SiN^{Dipp}}] (4.29)

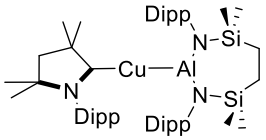

A solution of [{SiN^{Dipp}}AlK]$_2$ (**3.12,** 0.560 g, 0.500 mmol) in hexane (20 mL) was added dropwise into a stirring suspension of {^{Me2}CAAC}CuCl (0.384 g, 1 mmol) in hexane (30 mL) at room temperature. The mixture was stirred for 12 hours before filtering. The colourless filtrate was then collected, and all volatiles were removed *in vacuo* yielding **4.29** as a colourless solid. Yield 0.688 g, 79%. Colourless crystals suitable for X-ray crystallography were obtained by slow evaporation of a hexane solution of **4.29** at room temperature. No meaningful result was obtained for elemental analysis after multiple attempts. ^{1}H NMR (500 MHz, 298 K, Benzene-d_6) δ 7.14 – 7.09 (m, 4H, *m*-C$_6$*H*$_3$ on SiN^{Dipp}), 7.09 – 7.03 (m, 3H, *p*-C$_6$*H*$_3$ on SiN^{Dipp} and ^{Me2}CAAC), 6.89 (d, 2H, J = 7.8 Hz, *m*-C$_6$*H*$_3$ on ^{Me2}CAAC), 4.05 (sept, 4H, J = 6.9 Hz, C*H*Me$_2$ on SiN^{Dipp}), 2.40 (sept, 2H, J = 6.8 Hz, C*H*Me$_2$ on ^{Me2}CAAC), 1.43, 1.26 (d, 12H, J = 6.9 Hz, CH*Me*$_2$ on SiN^{Dipp}), 1.19 (s, 2H, CMe$_2$C*H*$_2$CMe$_2$), 1.14 (s, 4H, SiC*H*$_2$), 1.02 (d, 6H, J = 6.8 Hz, CH*Me*$_2$ on ^{Me2}CAAC), 0.85 (d, 6H, J = 6.8 Hz, CH*Me*$_2$ on ^{Me2}CAAC), 0.81 (s, 6H, C*Me*$_2$), 0.68 (s, 6H, NC*Me*$_2$CH$_2$ on ^{Me2}CAAC), 0.27 (s, 12H, Si*Me*$_2$). ^{13}C{^{1}H} NMR (126 MHz, 298 K, Benzene-d_6) δ 147.0 (*i*-*C*$_6$H$_3$ on SiN^{Dipp}), 146.8 (*o*-*C*$_6$H$_3$ on SiN^{Dipp}), 144.9 (*i*-*C*$_6$H$_3$ on ^{Me2}CAAC), 134.5 (*o*-*C*$_6$H$_3$ on ^{Me2}CAAC), 129.4 (*p*-*C*$_6$H$_3$ on ^{Me2}CAAC), 124.61 (*m*-*C*$_6$H$_3$ on ^{Me2}CAAC), 123.4 (*m*-*C*$_6$H$_3$ on SiN^{Dipp}), 122.7 (*p*-*C*$_6$H$_3$ on SiN^{Dipp}), 80.6 (N*C*Me$_2$CH$_2$), 55.7 (*C*Me$_2$CH$_2$CMe$_2$), 50.1 (CMe$_2$*C*H$_2$CMe$_2$), 29.1 (*C*HMe$_2$ on ^{Me2}CAAC), 28.9 (CH*Me*$_2$ on ^{Me2}CAAC), 28.7 (NC*Me*$_2$CH$_2$), 28.2 (*C*HMe$_2$ on SiN^{Dipp}), 27.3 (CH*Me*$_2$ on ^{Me2}CAAC), 26.4 (CH*Me*$_2$ on SiN^{Dipp}), 24.5 (CH*Me*$_2$ on SiN^{Dipp}), 22.5 (CH*Me*$_2$ on ^{Me2}CAAC), 14.66 (Si*C*H$_2$), 1.6 (Si*Me*$_2$); Cu*C* not observed.

[(^{Me2}CAAC)Cu-κ^1-*C*-(C{N^{i}Pr}$_2$)-κ^2-*N,N'*-Al{SiN^{Dipp}}] (4.30)

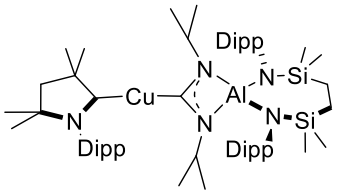

Inside a J Young's tube, [(^{Me2}CAAC)CuAl{SiN^{Dipp}}] (**4.29**, 43.5 mg, 0.05 mmol) was dissolved in 0.4 mL of C$_6$D$_6$, *N,N'*-diisopropylcarbodiimide (7.8 μL, 0.05 mmol) was then added *via* a micropipette. No significant change was observed within one hour of the mixing of the starting materials by ^{1}H NMR spectroscopy. The reaction mixture was then left at room temperature overnight, cleanly forming the inserted product. The benzene solution was then put under reduced pressure to remove all volatiles giving **4.30** as white solid. Crystals suitable for X-ray crystallography were obtained by slow evaporation of a hexane solution of **4.30** at room temperature. Yield 36 mg, 72%. Anal Calc'd for C$_{57}$H$_{95}$AlCuN$_5$Si$_2$ (**4.30**, *997.12*): C, 68.66; H, 9.60; N, 7.02 %. Found: C, 68.68; H, 9.42; N, 6.82 %. ^{1}H NMR (500 MHz, 298 K, Benzene-d_6) δ 7.24-7.18 (m, 4H, *m*-C$_6$*H*$_3$ on SiN^{Dipp}), 7.14 – 7.08 (m, 2H, *p*-C$_6$*H*$_3$ on SiN^{Dipp}), 6.98 (t, 1H, J = 7.7 Hz, *p*-C$_6$*H*$_3$ on ^{Me2}CAAC), 6.84 (d, 2H, J = 7.7 Hz, *m*-C$_6$*H*$_3$ on ^{Me2}CAAC), 4.47 – 4.13 (m, 4H, C*H*Me$_2$ on SiN^{Dipp}), 3.57 – 3.19 (m, 2H, NC*H*Me$_2$), 2.54-2.43 (m, 2H, C*H*Me$_2$ on ^{Me2}CAAC), 1.51 – 1.37 (m, 30H, CH*Me*$_2$ on SiN^{Dipp} and NCH*Me*$_2$), 1.27 (s, 2H, CMe$_2$C*H*$_2$CMe$_2$ on ^{Me2}CAAC), 1.17 (d, J = 6.6 Hz, 2H, CH*Me*$_2$ on ^{Me2}CAAC), 1.10 (s, 4H, SiC*H*$_2$), 1.05 (d, 6H, J = 6.9 Hz, NCH*Me*$_2$), 1.02 (d, 6H, J = 6.6 Hz, CH*Me*$_2$ on ^{Me2}CAAC), 0.78 (br s, 12H, C*Me*$_2$ on ^{Me2}CAAC), 0.52-0.21 (br, 12H, Si*Me*$_2$). ^{13}C{^{1}H} NMR (126 MHz, 298 K, Benzene-d_6) δ 253.8 (Cu*C*), 220.9 (Cu*C*N$_2$) , 149.7 (*i*-*C*$_6$H$_3$ on SiN^{Dipp}), 146.8 (*o*-*C*$_6$H$_3$ on SiN^{Dipp}), 144.8 (*i*-*C*$_6$H$_3$ on ^{Me2}CAAC), 135.2 (*o*-*C*$_6$H$_3$ on ^{Me2}CAAC), 129.9 (*p*-*C*$_6$H$_3$ on ^{Me2}CAAC), 125.1 (*m*-*C*$_6$H$_3$ on ^{Me2}CAAC) 124.1 (*m*-*C*$_6$H$_3$ on SiN^{Dipp}), 122.5 (*p*-*C*$_6$H$_3$ on SiN^{Dipp}), 81.0 (N*C*Me$_2$CH$_2$), 54.9 (*C*Me$_2$CH$_2$), 51.9 (N*C*HMe$_2$), 49.9 (CMe$_2$*C*H$_2$CMe$_2$), 29.2 (*C*HMe$_2$), 29.0 (C*Me*$_2$ on CAAC), 28.1 (Si*C*H$_2$) , 27.7, 26.9, 26.7, 26.7, 26.6, 26.5, 24.8, 23.0 (CH*Me*$_2$), 15.2 (Si*C*H$_2$), 4.1 (Si*Me*$_2$).

[(NHC^{iPr})Cu-κ^1-*C*-(CO$_2$)-κ^2-*O,O'*-Al{SiN^{Dipp}}] (4.31)

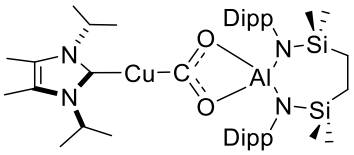

[(NHC^{iPr})CuAl{SiN^{Dipp}}] (**4.27**, 25 mg, 0.033 mmol) was dissolved in 0.4 mL of C_6D_6 inside a J Young's tube. The solution was then degassed by three cycles of freeze-pump-thaw before the tube was charged with 2 atm. of $^{13}CO_2$. Full Conversion of the starting material was determined by ^{1}H and ^{13}C NMR spectra within 30 minutes of the addition of the CO_2 to the solution. The benzene solution was then put under reduced pressure to remove all volatiles to give **4.31** as a colourless waxy solid. Yield 22 mg, 82%. No meaningful result was obtained for elemental analysis after multiple attempts. ^{1}H NMR (500 MHz, 298 K, Benzene-d_6) δ 7.18 (d, 4H, J = 7.6 Hz, m-C$_6H_3$), 7.07 (t, 2H, J = 7.6 Hz, p-C$_6H_3$), 4.23 (sept, 4H, J = 6.8 Hz, CHMe$_2$ on SiN^{Dipp}), 3.51 (sept, 2H, J = 6.8 Hz, NCHMe$_2$ on NHC^{iPr}), 1.60 (d, 12H, J = 6.8 Hz, CHMe_2 on SiN^{Dipp}), 1.48 (d, 12H, J = 6.8 Hz, CHMe_2 on SiN^{Dipp}), 1.30 (s, 4H, SiCH_2), 1.21 (s, 6H, NCMe), 1.03 (d, 12H, J = 6.8 Hz, NCHMe_2), 0.40 (s, 12H, SiMe_2). ^{13}C{^{1}H} NMR (126 MHz, 298 K, Benzene-d_6) δ 236.2 (CuCO2), 146.9 (o-C_6H$_3$), 145.3 (i-C_6H$_3$), 123.5 (m-C_6H$_3$ on SiN^{Dipp}), 123.2 (CuC), 123.1 (p-C_6H$_3$ on SiN^{Dipp}), 49.8 (NCHMe$_2$), 28.0, 25.6, 25.5 (CCHMe$_2$), 24.6 (NCHMe_2), 14.5 (SiCH$_2$), 8.4 (NCMe), 0.6 (SiMe_2); Resonance at 124.8 corresponding to residual $^{13}CO_2$ was observed.

[(Me2CAAC)Cu-κ^1-*C*-(CO$_2$)-κ^2-*O,O'*-Al{SiN^{Dipp}}] (4.32)

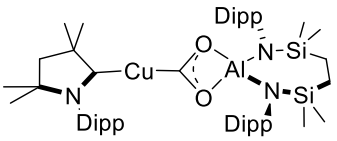

[(^{Me2}CAAC)CuAl{SiN^{Dipp}}] (**4.29**, 43.5 mg, 0.05 mmol) was dissolved in 0.4 mL of C_6D_6 inside a J Young's tube. The solution was then degassed by three cycles of freeze-pump-thaw before the tube was charged with 2 atm. of $^{13}CO_2$. Full conversion of the starting material was determined by ^{1}H and ^{13}C NMR spectra within 30 minutes of the addition of the CO_2 to the solution. The benzene solution was then put under reduced pressure to remove all volatiles giving **4.32** as a colourless solid. Crystals suitable for analysis by X-ray crystallography were obtained by slow evaporation of a hexane solution at room temperature. Yield 31 mg, 68%. No meaningful result was obtained for elemental analysis after multiple attempts. ^{1}H NMR (500 MHz, 298 K, Benzene-d_6) δ 7.14 – 7.08 (m, 5H, m-C$_6H_3$ on SiN^{Dipp} and p-C$_6H_3$ on ^{Me2}CAAC), 7.07 – 7.02 (m, 2H, p-C$_6H_3$ on SiN^{Dipp}), 6.92 (d, 2H, J = 7.8 Hz, m-C$_6H_3$ on ^{Me2}CAAC), 4.05 (p, 4H, J = 6.9 Hz, CHMe$_2$ on SiN^{Dipp}), 2.33 (sept, 2H, J = 6.8 Hz, CHMe$_2$ on ^{Me2}CAAC), 1.42 (d, 12H, J = 6.9 Hz, CHMe_2 on SiN^{Dipp}), 1.35 (d, 12H, J = 6.9 Hz, CHMe_2 on SiN^{Dipp}), 1.23 (s, 4H, SiCH_2), 1.17 (s, 2H, CMe$_2$CH_2CMe$_2$), 1.03 (d, 6H, J = 6.8 Hz, CHMe_2 on ^{Me2}CAAC), 0.99 (d, 6H, J = 6.8 Hz, CHMe_2 on ^{Me2}CAAC), 0.84 (s, 6H, CMe_2CH$_2$CMe$_2$), 0.66 (s, 6H, NCMe_2CH$_2$), 0.33 (s, 12H, SiMe_2). ^{13}C{^{1}H} NMR (126 MHz, , 298 K, Benzene-d_6) δ 251.6 (CuC), 234.9 (CuCO$_2$), 146.6 (i-C$_6H_3$ on SiN^{Dipp}), 145.0, 145.0 (o-C$_6H_3$ on SiN^{Dipp} and i-C$_6H_3$ on ^{Me2}CAAC), 133.7 (o-C$_6H_3$ on ^{Me2}CAAC), 130.1 (p-C$_6H_3$ on ^{Me2}CAAC), 124.9 (m-C$_6H_3$ on ^{Me2}CAAC), 123.4 (m-C$_6H_3$ on SiN^{Dipp}), 122.97 (p-C$_6H_3$ on SiN^{Dipp}), 81.0 (NCMe$_2$CH$_2$), 53.9 (CMe$_2$CH$_2$CMe$_2$), 49.1 (CMe$_2$$CH_2CMe_2$, 29.1 (CH$Me_2$ on ^{Me2}CAAC), 28.5 (NCMe_2CH$_2$), 27.8 (CHMe_2 on SiN^{Dipp}), 27.7 (CMe_2CH$_2$CMe$_2$), 27.1 (CHMe_2 on ^{Me2}CAAC), 25.5 (CHMe2 on SiN^{Dipp}), 22.5 (CHMe_2 on ^{Me2}CAAC), 14.5 (SiCH$_2$), 0.5 (SiMe_2); Resonance at 124.8 corresponds to residual $^{13}CO_2$, only impurities at 165-175ppm, no correlation with proton observed in ^{1}H-^{13}C HSQC, HMBC, plausibly ^{13}C labelled minor impurities.

[(IPr)CuAl{SiN^{Dipp}}] (4.33)

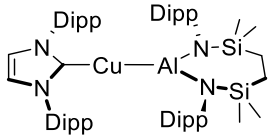

A solution of *N,N'*-bis{diisopropylphenyl}-2-ylidene (IPr, 0.388 g, 1.00 mmol) in toluene (25 mL) was added to a Schlenk flask containing CuCl (0.099 g, 1.00 mmol). After stirring for 3 days at room temperature, the solution was put under vacuum to remove all volatiles and afford an off-white solid. A solution of [{SiN^{Dipp}}AlK]$_2$ (**3.12**, 0.560 g, 0.500 mmol) in hexane (40 mL) was then added to the Schlenk flask, affording a pale-yellow reaction mixture. The resulting mixture was then left stirring at room temperature overnight before filtering. The colourless filtrate was then collected, and all volatiles were removed *in vacuo* yielding **4.33** as an off-white solid. Yield 0.751 g, 77%. No meaningful result was obtained for elemental analysis after multiple attempts. ^{1}H NMR (500 MHz, 298 K, Benzene-*d*$_6$) δ 7.20 (t, *J* = 7.8 Hz, 2H, *p*-C$_6$*H*$_3$ on IPr), 7.05 – 6.94 (m, 10H, C$_6$*H*$_3$ on IPr and SiN^{Dipp}), 6.05 (s, 2H, NC*H* on IPr), 3.90 (sept, *J* = 6.9 Hz, 4H, C*H*Me$_2$ on SiN^{Dipp}), 2.39 (sept, *J* = 6.9 Hz, 4H, , C*H*Me$_2$ on IPr), 1.38 (d, *J* = 6.9 Hz, 12H, CH*Me*$_2$ on SiN^{Dipp}), 1.07 (s, 4H, SiC*H*$_2$), 1.06 (d, *J* = 6.9 Hz, 12H, CH*Me*$_2$ on SiN^{Dipp}), 1.01 (d, *J* = 6.9 Hz, 12H, CH*Me*$_2$ on IPr), 0.91 (d, *J* = 6.9 Hz, 12H, CH*Me*$_2$ on IPr), 0.22 (s, 12H, Si*Me*$_2$). ^{13}C{^{1}H} NMR (126 MHz, 298 K, Benzene-*d*$_6$) δ 185.1 (Cu*C*$_{carbene}$),146.9 (*C*$_6$H$_3$ on SiN^{Dipp}), 146.3 (*C*$_6$H$_3$ on SiN^{Dipp}), 145.1 (*C*$_6$H$_3$ on IPr), 136.0 (*C*$_6$H$_3$ on IPr), 130.1 (*C*$_6$H$_3$), 124.5 (*C*$_6$H$_3$ on IPr), 123.3 (*C*$_6$H$_3$ on SiN^{Dipp}), 123.0 (N*C*H on IPr), 122.5 (*C*$_6$H$_3$), 28.9 (*C*HMe$_2$ on IPr), 28.2 (*C*HMe$_2$ on SiN^{Dipp}), 25.8 (CH*Me*$_2$ on SiN^{Dipp}), 24.5 (CH*Me*$_2$ on IPr), 24.3 (CH*Me*$_2$ on IPr), 24.1 (CH*Me*$_2$ on SiN^{Dipp}), 14.6 (Si*C*H$_2$), 1.6 (Si*Me*$_2$).

[(IPr)Cu-κ^1-*N*-({N^{i}Pr}C{N^{i}Pr})-κ^2-*C,N'*-Al{SiN^{Dipp}}](4.34)

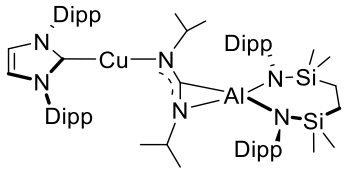

Inside a J Young's tube, [(IPr)CuAl{SiN^{Dipp}}] (**4.33**, 48.5 mg, 0.05 mmol) was dissolved in 0.4 mL of C$_6$D$_6$, N,N'-diisopropylcarbodiimide (7.8 μL, 0.05mmol) was then added via a micropipette. No significant change was observed in the ^{1}H NMR spectrum when the reaction mixture was left at room temperature overnight. The reaction mixture was then kept at 40 °C, and quantitative conversion into compound **4.34** was determined by ^{1}H NMR spectroscopy after 3 days. ^{1}H NMR (500 MHz, 298 K, Benzene-d$_6$) δ 7.14 – 7.12 (m, 2H, p-C$_6$H$_3$), 7.10-7.08 (m, 4H, m-C$_6$H$_3$), 7.06 – 7.02 (m, 2H, p-C$_6$H$_3$), 6.98 (d$_{app}$, 4H, m-C$_6$H$_3$), 4.13 (s, 2H, NCH on IPr), 4.26-3.90(m, 4H, CHMe$_2$ on SiN^{Dipp}), 3.38 (sept, J = 6.9 Hz, 1H, NCHMe$_2$ on carbodiimide) 2.99 (sept, J = 6.9 Hz, 1H, NCHMe$_2$ on carbodiimide), 2.52 (sept, J = 6.8 Hz, 4H, CHMe$_2$ on IPr), 1.44-1.43 (m, 12H, CHMe$_2$ on SiN^{Dipp}), 1.42 – 1.36 (m, 12H, CHMe$_2$ on SiN^{Dipp}), 1.33 (d, J = 6.9 Hz, 6H, NCHMe$_2$ on carbodiimide), 1.28 (s, 4H, SiCH$_2$), 1.23 (d, J = 6.9 Hz, 12H, CHMe$_2$ on IPr), 1.05 (d, J = 6.9 Hz, 6H, NCHMe$_2$ on carbodiimide), 0.94 (d, J = 6.8 Hz, 12H CHMe$_2$ on IPr), 0.33 – 0.02 (s, br, 12H, SiMe$_2$) *SiMe$_2$ peak overlapping with the grease. ^{13}C{^{1}H} NMR (126 MHz, 298 K, Benzene-d$_6$) δ 182.1 (CuC$_{carbene}$), 149.6 (i-C$_6$H$_3$), 148.4 (i-C$_6$H$_3$), 146.7 (o-C$_6$H$_3$), 146.4(o-C$_6$H$_3$), 145.3(o-C$_6$H$_3$), 135.7 (o-C$_6$H$_3$), 130.7 (m-C$_6$H$_3$), 128.4 (m-C$_6$H$_3$), 124.6 (m-C$_6$H$_3$) 123.7 (p-C$_6$H$_3$), 123.6 (p-C$_6$H$_3$) , 123.4 (NCH on IPr), 122.5 (m-C$_6$H$_3$), 58.0 (NCHMe$_2$ on carbodiimide), 45.9 (NCHMe$_2$ on carbodiimide), 44.4 ((NCHMe$_2$ on carbodiimide), 28.9 (CHMe$_2$ on IPr), 27.8 (CHMe$_2$ on SiN^{Dipp}), 27.4 (NCHMe$_2$ on carbodiimide), 26.2 (CHMe$_2$ on SiN^{Dipp}), 26.1 (CHMe$_2$ on SiN^{Dipp}), 24.8 (CHMe$_2$ on IPr), 23.8 (CHMe$_2$ on IPr), 15.1 (SiCH$_2$), 1.4 (SiMe$_2$). ^{13}C resonance correlated to AlCN not observed.

[(NHC^{iPr})Cu-κ^1-*C*-(CO$_2$)-κ^2-*O,O'*-Al{SiN^{Dipp}}] (4.35)

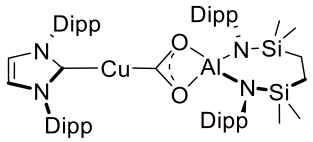

[(IPr)CuAl{SiN^{Dipp}}] (**4.33**, 25 mg, 0.026 mmol),was dissolved in 0.4 mL of C_6D_6 inside a J Young's tube. The solution was then degassed by three cycles of freeze-pump-thaw before the tube was charged with 2 atm of $^{13}CO_2$. Full Conversion of the starting material was determined by ^{1}H and ^{13}C NMR spectra within 30 minutes of the addition of the CO_2 to the solution. No meaningful result was obtained for elemental analysis after multiple attempts. ^{1}H NMR (500 MHz, 298 K, Benzene-d_6) δ 7.25-7.22 (m, 2H, *p*-C$_6$*H*$_3$), 7.12 – 7.08 (m, 2H, *p*-C$_6$*H*$_3$), 7.04-7.01 (m, 8H, *m*-C$_6$*H*$_3$), 6.09 (s, 2H, NC*H*), 3.95 (sept, *J* = 6.8 Hz, 4H,C*H*Me$_2$ on SiN^{Dipp}), 2.24 (sept, *J* = 6.9 Hz, 4H, C*H*Me$_2$ on IPr), 1.41 (d, *J* = 6.8 Hz, 12H, CH*Me*$_2$ on SiN^{Dipp}), 1.20 (s, 4H, SiC*H*$_2$), 1.13 (d, *J* = 6.8 Hz, 12H, CH*Me*$_2$ on SiN^{Dipp}), 1.06 (d, *J* = 6.9 Hz, 12H CH*Me*$_2$ on IPr), 1.01 (d, *J* = 6.9 Hz, 12H CH*Me*$_2$ on IPr), 0.29 (s, 12H, Si*Me*$_2$)*overlapping with grease. ^{13}C{^{1}H} NMR (126 MHz, 298 K, Benzene-d_6) δ 234.0 (Cu*C*O$_2$), 165.8 (*i*-*C*$_6$H$_3$), 163.2 (*i*-*C*$_6$H$_3$), 146.5 (*o*-*C*$_6$H$_3$), 145.4 (*o*-*C*$_6$H$_3$), 124.3 (*m*-*C*$_6$H$_3$), 123.3 (*m*-*C*$_6$H$_3$), 122.8 (*p*-*C*$_6$H$_3$), 122.7 (*p*-*C*$_6$H$_3$), 28.8 (*C*HMe$_2$), 27.7 (*C*HMe$_2$), 25.5 (CH*Me*$_2$), 25.1 (CH*Me*$_2$), 23.9 (CH*Me*$_2$), 23.7 (CH*Me*$_2$), 14.4 (Si*C*H$_2$), 0.5 (Si*Me*$_2$) ^{13}C resonance correlated to Cu$C_{carbene}$ was not observed.

[(*t*Bu$_3$P)CuAl{SiN^{Dipp}})] (4.36)

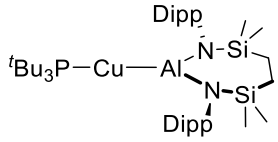

Hexane (25 mL) was cannula transferred into a Schlenk flask charged with the mixture of tri-*tert*butyl-phosphine (P^{t}Bu$_3$, 0.200 g, 1.00 mmol), CuCl (0.100 g, 1.00 mmol), and [{SiN^{Dipp}}AlK]$_2$ (**3.12**, 0.560 g, 0.500 mmol). The resulting pale-yellow reaction mixture was left stirring overnight before filtering. The colourless filtrate was then collected, and all volatiles were removed *in vacuo* yielding **4.36** as a white solid. Yield 0.620 g, 79%. Colourless crystals suitable for X-ray crystallography were obtained by slow evaporation of a hexane solution at room temperature. Anal Calc'd for $C_{42}H_{77}AlCuN_2PSi_2$ (**4.36**, 787.76) C, 64.04; H, 9.85; N, 3.56 %. Found: C, 63.85; H, 9.96; N, 3.69 %. ^{1}H NMR (500 MHz, 298 K, Benzene-d_6) δ 6.94 (d, *J* = 7.9 Hz, 4H, *m*-C$_6$*H*$_3$), 6.82 (t, *J* = 7.9 Hz, 2H, *p*-C$_6$*H*$_3$), 3.85 (sept, *J* = 6.9 Hz, 4H, C*H*Me$_2$), 1.29 (d, *J* = 6.9 Hz, 12H, CH*Me*$_2$), 1.24 (d, *J* = 6.9 Hz, 12H, CH*Me*$_2$), 1.01 (s, 4H, SiC*H*$_2$), 0.69 (d, $^3J_{PH}$ = 12.1 Hz, 27H, PC*Me*$_3$), 0.19 (s, 12H, Si*Me*$_2$). ^{13}C{^{1}H} NMR (126 MHz, 298 K, Benzene-d_6) δ 146.7, 145.7 (*i*- and *o*- *C*$_6$H$_3$), 123.2 (*m*-*C*$_6$H$_3$), 122.7 (p-C$_6$H$_3$), 32.7 (d, $^1J_{PC}$ = 13.2Hz, PCMe$_3$), 32.2 (d, $^2J_{PC}$ = 6.4 Hz, PCMe$_3$), 28.6 (*C*HMe$_2$), 26.0 (CH*Me*$_2$), 24.3 (CH*Me*$_2$), 14.4 (Si*C*H$_2$), 1.6 (Si*Me*$_2$). ^{31}P NMR (202 MHz, 298 K, Benzene-d_6) δ 43.9.

[(*t*Bu$_3$P)Cu-κ^1-*C*-(C{N*i*Pr}$_2$)-κ^2-*N,N'*-Al{SiN^{Dipp}}] (4.37)

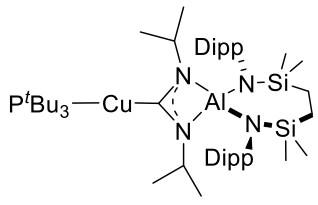

Inside a J Young's tube, [(*t*Bu$_3$P)CuAl{SiN^{Dipp}})] (**4.36**, 38.5 mg, 0.05 mmol) was dissolved in 0.4 mL of C_6D_6, *N,N'*-diisopropylcarbodiimide (7.8 μL, 0.05 mmol) was then added via a micropipette. Total transformation was observed after the reaction mixture was left at room temperature for overnight. The benzene solution was then put under vacuum to remove all volatiles giving **4.37** as a waxy colourless solid. Colourless crystals suitable for X-ray crystallography were obtained by slow evaporation of a hexane solution at room temperature. Yield 35 mg, 77%. Anal Calc'd for $C_{49}H_{91}AlCuN_4PSi_2$ (**4.37**,913.97) C, 64.39; H, 10.04; N, 6.13 %. Found: C, 64.01; H, 9.93; N, 6.24 %. ^{1}H NMR (500 MHz, 298 K, Benzene-d_6) δ 7.24 (d, *J* = 7.6 Hz, 4H, *m*-C$_6$*H*$_3$), 7.13 (t, *J* = 7.6 Hz, 2H, *p*-C$_6$*H*$_3$), 4.62-4.07 (m, 4H, C*H*Me$_2$), 3.68-3.60 (m, 2H, NC*H*Me$_2$), 1.65 – 1.32 (m, 30H, CH*Me*$_2$ on SiN^{Dipp} and CN$^{iPr}{}_2$), 1.30 – 1.21 (m, 4H, SiC*H*$_2$), 0.97 (d, $^3J_{PH}$ = 12.5 Hz, 27H, PC*Me*$_3$), 0.64 – -0.16 (m, 12H, SiMe$_2$). ^{13}C{^{1}H} NMR (126 MHz, Benzene-d_6) δ 218.0 (Cu*C*N$^{iPr}{}_2$), 149.1, 147.1 (*i*- and *o*-*C*$_6$H$_3$), 123.8 (*m*-*C*$_6$H$_3$), 122.2 (p-*C*$_6$H$_3$),

51.8 (N*C*HMe$_2$), 36.4 (d, $^1J_{PC}$ = 9.6 Hz, P*C*Me$_3$) 31.6 (d, $^2J_{PC}$ = 5.5 Hz, PC*Me*$_3$), 26.4 (*C*HMe$_2$), 25.8, 22.6 (CH*Me*$_2$ on N^{Dipp} and CN$^{iPr}{}_2$), 14.7 (Si*C*H$_2$), 1.0 (Si*Me*$_2$). ^{31}P NMR (202 MHz, 298 K, Benzene-d_6) δ 59.8.

[(^{t}Bu$_3$P)Cu-κ^1-*C*-(CO$_2$)-κ^2-*O,O'*-Al{SiN^{Dipp}}] (4.38)

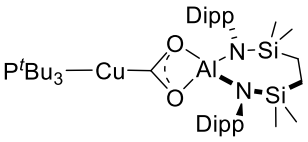

[(^{t}Bu$_3$P)CuAl{SiN^{Dipp}})] (**4.36**, 25 mg, 0.032 mmol) was dissolved in 0.4 mL of C$_6$D$_6$ inside a J Young's tube. The solution was then degassed by three cycles of freeze-pump-thaw before the tube was charged with 2 atm of ^{13}CO$_2$. Full conversion of the starting material was determined by ^{1}H and ^{13}C NMR spectra within 30 minutes of the addition of the CO$_2$ to the solution. The benzene solution was then put under reduced pressure to remove all volatiles giving **4.38** as an off-white solid. Yield 20 mg, 77%. No meaningful result was obtained for elemental analysis after multiple attempts. ^{1}H NMR (500 MHz, 298 K, Benzene-d_6) δ 7.14-7.10 (m, 4H, *m*-C$_6$*H*$_3$), 7.04-6.98 (m, 2H, *p*-C$_6$*H*$_3$), 4.15 (sept, *J* = 6.9 Hz, 4H, C*H*Me$_2$), 1.53 (d, *J* = 6.9 Hz, 12H, CH*Me*$_2$), 1.44 (d, *J* = 6.9 Hz, 12H, CH*Me*$_2$), 1.27 (s, 4H, SiC*H*$_2$), 0.80 (d, $^3J_{PH}$ = 12.9 Hz, 27H, C*Me*$_3$), 0.37 (s, 12H, Si*Me*$_2$). ^{13}C{^{1}H} NMR (126 MHz, 298 K, Benzene-d_6) δ 233.1 (d, $^2J_{PC}$ = 73.9 Hz, Cu*C*O$_2$) 146.8 (*o*-*C*$_6$H$_3$), 145.0 (*i*-*C*$_6$H$_3$), 123.5 (*m*-*C*$_6$H$_3$), 123.2 (*p*-*C*$_6$H$_3$), 36.4 (*C*Me$_3$), 31.9 (C*Me*$_3$), 27.9 (*C*HMe$_2$), 25.4 (CH*Me*$_2$), 25.4 (CH*Me*$_2$), 14.4 (Si*C*H$_2$), 0.5 (Si*Me*$_2$). ^{31}P{^{1}H} NMR (202 MHz, 298 K, Benzene-d_6) δ 59.8.

4.38a and 4.39

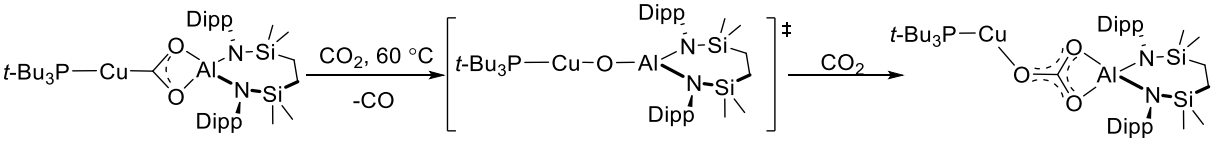

4.38 **4.38a** **4.39**

The d_6-benzene solution of **25** was kept at room temperature for three days, no significant change was observed by ^{1}H or ^{13}C{^{1}H} spectroscopy (observation of an emergence of a minor peak at δ 66.0 ppm in ^{31}P NMR spectrum). The sample was then kept at 60 °C overnight, and monitored by NMR spectroscopy. Further transformation was observed, especially with the disappearance of ^{13}C resonance at 233.1 (Cu*C*O$_2$) ppm and the emergence of new sharp ^{13}C resonances at 166.7, 168.4, 176.7 ppm; also in in ^{31}P NMR spectrum, the peak at 59.8 ppm was observed to decrease in intensity alongside the emergence of a new peak at 62.1 ppm.

[(NHC^{iPr})AgAl{SiN^{Dipp}}] (4.40)

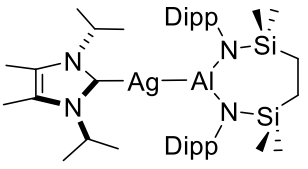

Hexane (25 mL) was cannula transferred into a foil wrapped Schlenk flask containing *N,N'*-diisopropyl-4,5-dimethyl-2-ylidene (NHC^{iPr}, 0.180 g, 1.00 mmol) and AgCl (0.143 g, 1.00 mmol). After the suspension was stirred for 3 days at 40 °C, a solution of [{SiN^{Dipp}}AlK]$_2$ (**3.12**, 0.560 g, 0.500 mmol) in hexane (20 mL) was added to the stirring white suspension, and the resulting pale yellow reaction mixture was stirred at room temperature overnight before filtering. The colourless filtrate was then collected, and all volatiles were removed *in vacuo* yielding **4.40** as an off-white solid. Yield 0.528 g, 65%. Anal Calc'd for C$_{41}$H$_{70}$AlAgN$_4$Si$_2$ (**4.40**, 810.06) C, 60.79; H, 8.71; N, 6.92 %. Found: C, 60.04; H, 8.32; N, 6.63 %. ^{1}H NMR (500 MHz, 298 K, Benzene-d_6) δ 7.16-7.14 (m, 4H, *m*-C$_6$*H*$_3$), 7.06 – 6.99 (m, 2H, *p*-C$_6$*H*$_3$), 4.17 (sept, *J* = 6.9 Hz, 4H, C*H*Me$_2$ on SiN^{Dipp}), 3.63 (sept, *J* = 6.7 Hz, 2H, NC*H*Me$_2$ on NHC^{iPr}), 1.51 (d, *J* = 6.9 Hz, 12H, CH*Me*$_2$ on SiN^{Dipp}), 1.47 (d, *J* = 6.9 Hz, 12H, CH*Me*$_2$ on SiN^{Dipp}), 1.34 (s, 6H, NC*Me*), 1.27 (s, 4H, SiC*H*$_2$), 1.00 (d, *J* = 6.7 Hz, 12H, NCH*Me*$_2$ on NHC^{iPr}), 0.37 (s, 12H, Si*Me*$_2$). ^{13}C{^{1}H} NMR (126 MHz, 298 K,

Benzene-d_6) δ 230.5 (Ag$C_{carbene}$). 147.4(*o*-C_6H_3), 146.6 (*i*-C_6H_3), 123.1 (*m*-C_6H_3), 122.8 (*p*-C_6H_3), 122.5 (N*C*Me), 49.7 (N*C*HMe$_2$ on NHC^{iPr}), 28.3 (*C*HMe$_2$ on SiN^{Dipp}), 26.0 (CH*Me*$_2$ on SiN^{Dipp}), 24.7 (CH*Me*$_2$ on SiN^{Dipp}), 24.2 (NCH*Me*$_2$ on NHC^{iPr}), 14.3 (Si*C*H$_2$), 8.7 (NC*Me*), 1.3 (Si*Me*$_2$).

[(NHC^{iPr})AuAl{SiN^{Dipp}}] (4.41)

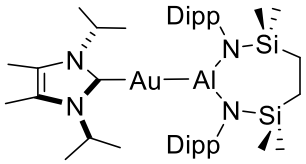

Hexane (30 mL) was cannula transferred into a Schlenk flask charged with *N,N'*-diisopropyl-4,5-dimethyl-2-ylidene (NHC^{iPr}, 0.180 g, 1.00 mmol) and Me$_2$SAuCl (0.295 g, 1.00 mmol). After the suspension was stirred for 3 days at 40 °C, all the volatiles were removed under vacuum, and hexane (20 mL) was added to the residue to afford a pale-yellow suspension. A solution of [{SiN^{Dipp}}AlK]$_2$ (**3.12**, 0.560 g, 0.500 mmol) in hexane (30 mL) was then added to the stirring suspension, and the resulting light-brown reaction mixture was stirred at room temperature overnight before filtering. The pale-yellow filtrate was then collected, and all volatiles were removed *in vacuo*, giving **4.41** as a light brown fine powder. Yield 0.617 g, 69%. Colourless crystals suitable for X-ray crystallography were obtained by slow evaporation of a methylcyclohexane solution at room temperature. No meaningful result was obtained for elemental analysis after multiple attempts. ^{1}H NMR (500 MHz, 298 K, Benzene-d_6) δ 7.15 – 7.13 (m, 4H, *m*-C$_6H_3$), 7.04 – 6.98 (m, 2H, *p*-C$_6H_3$), 4.15 (sept, *J* = 6.9 Hz, 4H, C*H*Me$_2$ on SiN^{Dipp}), 3.84 (sept, *J* = 6.9 Hz, 2H, C*H*Me$_2$ on NHC^{iPr}), 1.57 (d, *J* = 6.9 Hz, 12H, CH*Me*$_2$ on SiN^{Dipp}), 1.47 (d, *J* = 6.9 Hz, 12H, CH*Me*$_2$ on SiN^{Dipp}), 1.33 (s, 6H, NC*Me*), 1.24 (s, 4H, SiC*H*$_2$), 1.07 (d, *J* = 6.9 Hz, 12H, CH*Me*$_2$ on NHC^{iPr}), 0.35 (s, 12H, Si*Me*$_2$). ^{13}C{^{1}H} NMR (126 MHz, 298 K, Benzene-d_6) δ 216.1 (Au$C_{carbene}$) 147.3 (*o*-C_6H_3), 146.3 (*i*-C_6H_3), 123.1 (*m*-C_6H_3), 123.0 (*p*-C_6H_3), 122.7 (N*C*Me), 50.1 (N*C*HMe$_2$ on NHC), 28.4 (*C*HMe$_2$ on SiN^{Dipp}), 26.0 (CH*Me*$_2$ on SiN^{Dipp}), 24.7 (CH*Me*$_2$ on SiN^{Dipp}), 23.5 (NCH*Me*$_2$ on NHC^{iPr}), 14.2 (Si*C*H$_2$), 9.1 (NC*Me*), 1.1 (Si*Me*$_2$).

[(^{Cy}CAAC)AgAl{SiN^{Dipp}}] (4.42)

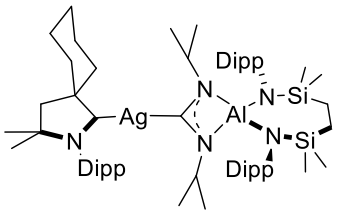

Inside a J-Young's tube, ^{cy}CAACAgCl (23.5 mg, 0.05 mmol) was added to the C_6D_6 solution of [{SiN^{Dipp}}AlK]$_2$ (**3**) (28 mg, 0.025 mmol) to afford a pale-yellow reaction mixture. compound **4.42** was then identified by X-ray crystallography as a colourless crystal selected from the mix of crystals obtained from slow evaporation of the benzene solution of the crude reaction mixture.

[(NHC^{iPr})Ag-κ^1-*N*-({N^{i}Pr}C{N^{i}Pr})-κ^2-*C,N'*-Al{SiN^{Dipp}}](4.43)

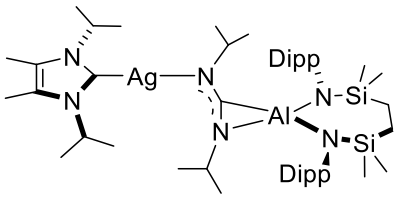

Inside a J Young's tube, [(NHC^{iPr})AgAl{SiN^{Dipp}}] (**4.40**, 40.5 mg, 0.05 mmol) was dissolved in 0.4 mL of C_6D_6, *N,N'*-diisopropylcarbodiimide (7.8 μL, 0.05 mmol) was then added via a micropipette. ^{1}H NMR suggested a slow conversion of the starting materials into a new species within 30 min. Quantitative transformation was observed after the reaction mixture was left at room temperature for 4 hours, cleanly forming a single new species. The benzene solution was then put under vacuum to remove all volatiles giving **4.43** as a colourless solid. Colourless crystals suitable for X-ray crystallography were obtained by slow evaporation of a methylcyclohexane solution at room temperature. Yield 34 mg, 73%. No meaningful result for elemental analysis was obtained after several attempts. ^{1}H NMR (500 MHz, 298 K, Benzene-d$_6$) δ 7.26-7.24 (m, 4H, m-C$_6H_3$), 7.16 – 7.11 (m, 2H, p-C$_6H_3$), 4.56 – 4.48 (m, 1H, NCHMe$_2$ on carbodiimide), 4.41 – 4.27 (m, 4H, CHMe$_2$ on SiN^{Dipp}), 4.06 (sept, *J* = 6.9 Hz, 2H, NCHMe$_2$ on NHC^{iPr}), 3.51 – 3.42 (m, 1H, NCHMe$_2$ on carbodiimide), 1.63 (d, *J* = 6.8 Hz, 6H,

$CHMe_2$ on SiN^{Dipp}), 1.56 (m, 6H, $CHMe_2$ on SiN^{Dipp}), 1.53-1.48 (m, 12H, $CHMe_2$ on SiN^{Dipp}), 1.40-1.35 (br, 4H, $SiCH_2$), 1.34 (s, 6H, NCMe), 1.09 (d, J = 6.9 Hz, 12H, $NCHMe_2$ on NHC^{iPr}), 1.01 – 0.91 (m, 6H, $NCHMe_2$ on carbodiimide) 0.91-0.77 (m, 6H, $NCHMe_2$ on carbodiimide), 0.52 – 0.31 (br, 12H, $SiMe_2$). $^{13}C\{^1H\}$ NMR (126 MHz, 298 K, Benzene-d_6) δ 200.0 ($AgC_{carbene}$) 148.6 (i-C_6H_3), 147.0 (o-C_6H_3), 146.5 (o-C_6H_3), 123.9 (m-C_6H_3), 123.6 (p-C_6H_3), 122.6 (NCMe), 57.8 ($NCHMe_2$ on carbodiimide), 52.0 ($NCHMe_2$ on NHC^{iPr}), 42.5 ($NCHMe_2$ on carbodiimide), 28.2 ($NCHMe_2$ on carbodiimide), 28.1 ($CHMe_2$ on SiN^{Dipp}), 27.6 ($CHMe_2$ on SiN^{Dipp}), 26.5 ($CHMe_2$ on SiN^{Dipp}), 26.4 ($CHMe_2$ on SiN^{Dipp}), 26.1 ($CHMe_2$ on SiN^{Dipp}), 25.9 ($NCHMe_2$ on carbodiimide), 23.2 ($NCHMe_2$ on NHC^{iPr}), 15.2 ($SiCH_2$) , 9.0 (NCMe), 2.0 ($SiMe_2$); ^{13}C resonance correlated to Al-CN_2 was not observed.

[(NHC^{iPr})Au-κ^1-*C*-($C\{N^iPr\}_2$)-κ^2-*N,N'*-Al{SiN^{Dipp}}](4.44)

Inside a J Young's tube, [(NHC^{iPr})AuAl{SiN^{Dipp}}] (**4.41**, 45.0 mg, 0.05 mmol) was dissolved in 0.4 mL of C_6D_6, *N,N'*-diisopropylcarbodiimide (7.8 μL, 0.05 mmol) was then added *via* a micropipette. Quantitative transformation was observed after the reaction mixture was left at room temperature for an hour, cleanly forming a single new single species. The benzene solution was then put under vacuum to remove all volatiles giving **4.44** as an off white solid. Colourless crystals suitable for X-ray crystallography were obtained by slow evaporation of a methylcyclohexane solution at room temperature. Yield 38 mg, 74%. Anal Calc'd for $C_{48}H_{84}AlAuN_6Si_2$ (**4.44**, 1025.36) C, 56.23; H, 8.26; N, 8.20 %. Found: C, 56.05; H, 8.00; N, 8.25 %. ^1H NMR (500 MHz, 298 K, Benzene-d_6) δ 7.31-7.24 (m, 4H, *m*-C_6H_3), 7.18-7.14 (m, 2H, *p*-C_6H_3, overlapping with C_6D_6), 4.61- 4.34 (m, 4H, C*H*Me_2 on SiN^{Dipp}), 4.34- 4.22 (m, 2H, C*H*Me_2 on carbodiimide) 4.04 (sept, J = 6.8 Hz, 2H, C*H*Me_2 on NHC^{iPr}), 1.67 – 1.60 (m, 12H, CH*Me*$_2$ on SiN^{Dipp}), 1.60-1.58 (m, 4H, SiC*H*$_2$) 1.54-1.45 (m, 12H, CH*Me*$_2$ on SiN^{Dipp}), 1.33 (s, 6H, NC*Me*), 1.22 (d, J = 6.8 Hz, 12H, CH*Me*$_2$ on NHC^{iPr}), 0.87 (d_{app}, 12H, CH*Me*$_2$ on carbodiimide) 0.85-0.73 (br, 6H, Si*Me*$_2$), 0.28 - −0.24 (br, 6H, Si*Me*$_2$). $^{13}C\{^1H\}$ NMR (126 MHz, 298 K, Benzene-d_6) δ 220.5 (Au*C* on NHC^{iPr}), 157.9, 149.5 (*i*- and *o*- C_6H_3), 124.2 (N*C*Me), 123.8 (*m*-C_6H_3), 122.7 (*p*-C_6H_3), 51.6 (*C*HMe_2 on carbodiimide), 51.2 (*C*HMe_2 on NHC^{iPr}), 35.7 (*C*HMe_2 on SiN^{Dipp}), 26.8 (CH*Me*$_2$ on SiN^{Dipp}), 26.7 (CH*Me*$_2$ on SiN^{Dipp}), 23.1 (CH*Me*$_2$ on carbodiimide), 22.9 (CH*Me*$_2$ on NHC^{iPr}), 15.1 (Si*C*H_2), 9.1 (NC*Me*), 1.4 (Si*Me*$_2$). ^{13}C resonance correlated to the Au*C* on carbodiimide not observed.

[(NHC^{iPr})Ag-κ^1-*C*-(CO_2)-κ^2-*O,O'*-Al{SiN^{Dipp}}] (4.45)

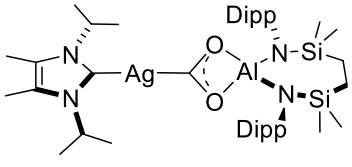

[(NHC^{iPr})AgAl{SiN^{Dipp}}] (**4.40**, 25 mg, 0.031 mmol) was dissolved in 0.4 mL of C_6D_6 inside a J Young's tube. The solution was then degassed by three cycles of freeze-pump-thaw before the tube was charged with 2 atm of $^{13}CO_2$. Quantitative conversion of the starting material was determined by ^1H and ^{13}C NMR spectra within 30 minutes of the addition of the CO_2 to the solution. The benzene solution was then put under reduced pressure to remove all volatiles giving **4.45** as an off-white waxy solid. Yield 19 mg, 71%. No meaningful result was obtained for elemental analysis after multiple attempts. ^1H NMR (500 MHz, 298 K, Benzene-d_6) δ 7.18 (d, J = 7.6 Hz, 4H, *m*-C_6H_3), 7.07 (t, J = 7.6 Hz, 2H, *p*-C_6H_3), 4.22 (sept, J = 6.9 Hz, 4H, C*H*Me_2 on SiN^{Dipp}), 3.63 (sept, J = 6.8 Hz, 2H, C*H*Me_2 on NHC^{iPr}), 1.60 (d, J = 6.9 Hz, 12H, CH*Me*$_2$ on SiN^{Dipp}), 1.47 (d, J = 6.9 Hz, 12H, CH*Me*$_2$ on SiN^{Dipp}), 1.30 (s, 4H, SiC*H*$_2$), 1.24 (s, 6H, NC*Me*), 0.99 (d, J = 6.8 Hz, 12H, CH*Me*$_2$ on NHC^{iPr}), 0.39 (s, br, 12H, Si*Me*$_2$). $^{13}C\{^1H\}$ NMR (126 MHz, 298 K, Benzene-d_6) δ 240.4 (2xd, $J_{^{109}Ag-C}$ = 252.6, $J_{^{107}Ag-C}$ = 218.9 Hz, Ag*C*O_2), 154.5 (*i*-C_6H_3), 146.8 (*o*-C_6H_3),

123.8 (*m*-C_6H_3), 123.6 (*p*-C_6H_3), 123.1 (N*C*Me), 50.3 (N*C*HMe$_2$ on NHC^{iPr}), 27.9 (*C*HMe$_2$ on SiN^{Dipp}), 25.5 (CH*Me*$_2$ on SiN^{Dipp}), 25.5 (CH*Me*$_2$ on SiN^{Dipp}), 23.9 (NCH*Me*$_2$ on NHC^{iPr}), 14.5 (Si*C*H$_2$), 8.7 (NC*Me*), 0.6 (Si*Me*$_2$). ^{13}C resonance correlated to Ag*C*$_{carbene}$ was not observed.

[(NHC^{iPr})Au-κ^1-*C*-(CO$_2$)-κ^2-*O,O'*-Al{SiN^{Dipp}}] (4.46)

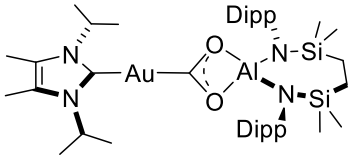

[(NHC^{iPr})AuAl{SiN^{Dipp}}] (**4.41**,, 25 mg, 0.028 mmol) was dissolved in 0.4 mL of C_6D_6 inside a J Young's tube. The solution was then degassed by three cycles of freeze-pump-thaw before the tube was charged with 2 atm of $^{13}CO_2$. Quantitative conversion of the starting material was determined by ^{1}H and ^{13}C NMR spectra within 30 minutes of the addition of the CO_2 to the solution. The benzene solution was then put under reduced pressure to remove all volatiles giving **4.46** as an off-white waxy solid. Yield 20 mg, 78%. Anal Calc'd for $C_{42}H_{70}AlAuN_4Si_2O_2$ (**4.46**, 943.17) C, 53.49; H, 7.48; N, 5.94 %. Found: C, 52.95; H, 8.07; N, 5.38 %. ^{1}H NMR (500 MHz, 298 K, Benzene-d_6) δ 7.20-7.19 (m, 4H, *m*-C_6H_3), 7.11 – 7.08 (m, 2H, *p*-C_6H_3), 4.21 (sept, *J* = 6.8 Hz, 4H, C*H*Me$_2$ on N^{Dipp}), 3.92 (sept, *J* = 7.2 Hz, 2H, C*H*Me$_2$ on NHC), 1.62 (d, *J* = 6.8 Hz, 12H, CH*Me*$_2$ on N^{Dipp}), 1.47 (d, *J* = 6.8 Hz, 12H, CH*Me*$_2$ on N^{Dipp}), 1.29 (s, 4H, SiC*H*$_2$), 1.20 (s, 6H, NC*Me*), 1.09 (d, *J* = 7.2 Hz, 12H, CH*Me*$_2$ on NHC), 0.39 (s, br, 12H, Si*Me*$_2$). ^{13}C{^{1}H} NMR (126 MHz, 298 K, Benzene-d_6) δ 239.1 (Au*C*O$_2$), 146.8 (*i*-C_6H_3), 144.8 (*o*-C_6H_3), 124.8 (*m*-C_6H_3), 123.6 (*p*-C_6H_3), 123.3 (N*C*Me), 51.1 (N*C*HMe$_2$ on NHC), 28.0 (*C*HMe$_2$ on N^{Dipp}), 25.5 (CH*Me*$_2$ on N^{Dipp}), 23.9 (CH*Me*$_2$ on N$^{Dipp)}$, 23.2 (NCH*Me*$_2$ on NHC), 14.4 (Si*C*H$_2$), 8.9 (N*C*Me), 0.5 (Si*Me*$_2$). ^{13}C resonance correlated to Au*C*$_{carbene}$ was not observed.

4.6 References

1. B. H. Cornils, W. *Applied homogeneous catalysis with organometallic compounds*, Wiley-VCH, Weinheim, 1996.
2. F. A. Cotton, Wilkinson, G., Murillo, C. A. & Bochmann, M. *Advanced Inorganic Chemistry 6th ed*, Wiley-Interscience, Hoboken, NJ, 1999.
3. W. Tolman, *Activation of Small Molecules*, Wiley-VCH, Weinheim, 2006.
4. M. J. Taylor, *Metal-to-Metal Bonded States of the Main Group Elements*, Academic Press, London, 1975.
5. J. F. Berry and C. C. Lu, *Inorg Chem*, 2017, **56**, 7577-7581.
6. D. L. Kays and S. Aldridge, T. B. Marder and Z. Lin, in *Contemporary Metal Boron Chemistry I: Borylenes, Boryls, Borane σ-Complexes, and Borohydrides*, eds. Springer Berlin Heidelberg, Berlin, Heidelberg, 2008, pp. 29-122.
7. A. Suzuki, X. Guo, Z. Lin and M. Yamashita, *Chem Sci*, 2021, **12**, 917-928.
8. J. H. Muessig, D. Prieschl, A. Deißenberger, R. D. Dewhurst, M. Dietz, J. O. C. Jiménez-Halla, A. Trumpp, S. R. Wang, C. Brunecker, A. Haefner, A. Gärtner, T. Thiess, J. Böhnke, K. Radacki, R. Bertermann, T. B. Marder and H. Braunschweig, *J Am Chem Soc*, 2018, **140**, 13056-13063.
9. H. Braunschweig, A. Damme, R. D. Dewhurst, T. Kramer, S. Östreicher, K. Radacki and A. Vargas, *J Am Chem Soc*, 2013, **135**, 2313-2320.
10. D. S. Laitar, P. Müller and J. P. Sadighi, *J Am Chem Soc*, 2005, **127**, 17196-17197.
11. T. Higashi, S. Kusumoto and K. Nozaki, *Angew Chem Int Ed*, 2021, **60**, 2844-2848.
12. C. M. Zinser, F. Nahra, L. Falivene, M. Brill, D. B. Cordes, A. M. Z. Slawin, L. Cavallo, C. S. J. Cazin and S. P. Nolan, *Chem Commun*, 2019, **55**, 6799-6802.
13. L. Koren-Selfridge, I. P. Query, J. A. Hanson, N. A. Isley, I. A. Guzei and T. B. Clark, *Organometallics*, 2010, **29**, 3896-3900.
14. C. Brunecker, M. Arrowsmith, J. H. Müssig, J. Böhnke, A. Stoy, M. Heß, A. Hofmann, C. Lenczyk, C. Lichtenberg, J. Ramler, A. Rempel and H. Braunschweig, *Dalton Trans*, 2021, **50**, 3506-3515.
15. S. Aldridge, R. J. Calder, A. Rossin, A. A. Dickinson, D. J. Willock, C. Jones, D. J. Evans, J. W. Steed, M. E. Light, S. J. Coles and M. B. Hursthouse, *J Chem Soc, Dalton Trans*, 2002, 2020-2026.
16. Y. Segawa, M. Yamashita and K. Nozaki, *Angew Chem Int Ed*, 2007, **46**, 6710-6713.
17. T. M. Horsley Downie, R. S. C. Charman, J. W. Hall, M. F. Mahon, J. P. Lowe and D. J. Liptrot, *Dalton Trans*, 2021, **50**, 16336-16342.
18. A. Kempter, C. Gemel and R. A. Fischer, *Inorg Chem*, 2005, **44**, 163-165.
19. C. McManus, J. Hicks, X. Cui, L. Zhao, G. Frenking, J. M. Goicoechea and S. Aldridge, *Chem Sci*, 2021, **12**, 13458-13468.
20. C. Jones, D. P. Mills, R. P. Rose, A. Stasch and W. D. Woodul, *J Organometallic Chem*, 2010, **695**, 2410-2417.
21. A. Kempter, C. Gemel and R. A. Fischer, *Chem Eur J*, 2007, **13**, 2990-3000.
22. Y. Liu, J. Li, X. Ma, Z. Yang and H. W. Roesky, *Coord Chem Rev*, 2018, **374**, 387-415.

23. J. Hicks, A. Mansikkamäki, P. Vasko, J. M. Goicoechea and S. Aldridge, *Nat Chem*, 2019, **11**, 237-241.
24. R. J. Schwamm, M. P. Coles, M. S. Hill, M. F. Mahon, C. L. McMullin, N. A. Rajabi and A. S. S. Wilson, *Angew Chem Int Ed*, 2020, **59**, 3928-3932.
25. J. T. Golden, T. H. Peterson, P. L. Holland, R. G. Bergman and R. A. Andersen, *J Am Chem Soc*, 1998, **120**, 223-224.
26. B. N. Anand, I. Krossing and H. Nöth, *Inorg Chem*, 1997, **36**, 1979-1981.
27. B. Buchin, T. Steinke, C. Gemel, T. Cadenbach and R. A. Fischer, *Zeitschrift für anorganische und allgemeine Chemie*, 2005, **631**, 2756-2762.
28. J. Weßing, C. Göbel, B. Weber, C. Gemel and R. A. Fischer, *Inorg Chem*, 2017, **56**, 3517-3525.
29. C. Dohmeier, C. Robl, M. Tacke and H. Schnöckel, *Angew Chem Int Ed Engl*, 1991, **30**, 564-565.
30. C. Cui, H. W. Roesky, H.-G. Schmidt, M. Noltemeyer, H. Hao and F. Cimpoesu, *Angew Chem Int Ed*, 2000, **39**, 4274-4276.
31. T. N. Hooper, M. Garçon, A. J. P. White and M. R. Crimmin, *Chem Sci*, 2018, **9**, 5435-5440.
32. K. L. Mears, C. R. Stennett, E. K. Taskinen, C. E. Knapp, C. J. Carmalt, H. M. Tuononen and P. P. Power, *J Am Chem Soc*, 2020, **142**, 19874-19878.
33. R. Y. Kong and M. R. Crimmin, *Dalton Trans*, 2021, **50**, 7810-7817.
34. N. Gorgas, A. J. P. White and M. R. Crimmin, *J Am Chem Soc*, 2022, **144**, 8770-8777.
35. B. Stadler, N. Gorgas, A. J. P. White and M. R. Crimmin, *Angew Chem Int Ed*, 2023, **62**, e202219212.
36. X. Zhang and L. L. Liu, *Angew Chem Int Ed*, 2021, **60**, 27062-27069.
37. K. Nagata, T. Agou and N. Tokitoh, *Angew Chem Int Ed*, 2014, **53**, 3881-3884.
38. J. Hicks, P. Vasko, J. M. Goicoechea and S. Aldridge, *Nature*, 2018, **557**, 92-95.
39. J. Hicks, P. Vasko, J. M. Goicoechea and S. Aldridge, *Angew Chem Int Ed*, 2021, **60**, 1702-1713.
40. M. P. Coles and M. J. Evans, *Chem Commun*, 2023, **59**, 503-519.
41. M. M. D. Roy, J. Hicks, P. Vasko, A. Heilmann, A.-M. Baston, J. M. Goicoechea and S. Aldridge, *Angew Chem Int Ed*, 2021, **60**, 22301-22306.
42. S. Kurumada, S. Takamori and M. Yamashita, *Nat Chem*, 2020, **12**, 36-39.
43. K. Sugita and M. Yamashita, *Chem Eur J*, 2020, **26**, 4520-4523.
44. K. Sugita and M. Yamashita, *Organometallics*, 2020, **39**, 2125-2129.
45. G. Feng, K. L. Chan, Z. Lin and M. Yamashita, *J Am Chem Soc*, 2022, **144**, 22662-22668.
46. P. de Frémont, N. M. Scott, E. D. Stevens, T. Ramnial, O. C. Lightbody, C. L. B. Macdonald, J. A. C. Clyburne, C. D. Abernethy and S. P. Nolan, *Organometallics*, 2005, **24**, 6301-6309.
47. P. de Frémont, N. M. Scott, E. D. Stevens and S. P. Nolan, *Organometallics*, 2005, **24**, 2411-2418.

5. General Experimental Procedures

5.1 General Synthetic Notes

All manipulations were carried out using standard Schlenk line and glovebox techniques under an inert atmosphere of argon. NMR experiments were conducted in J Youngs tap NMR tubes prepared and sealed in a glovebox. NMR spectra were collected on a Bruker AV-300 (300 MHz) spectrometer, a Bruker AV-400 (400 MHz) spectrometer, or an Agilent ProPulse spectrometer operating at 500 MHz and at a temperature of 298 K unless stated otherwise. The spectra were referenced relative to residual protio solvent resonances. Elemental analysis was performed externally by Elemental Microanalysis Ltd., Okehampton, Devon, UK. For each compound at least three attempts were made to acquire satisfactory elemental analysis results (i.e. within ±0.5% of the expected C, H and N content). Solvents (toluene, hexane, diethyl ether) used were dried by passage through a commercially available (Innovative Technologies) solvent purification system under argon or utilising potassium/benzophenone (THF, methylcyclohexane) and stored over 4 Å molecular sieves. Deuterated solvents (d_8-toluene, C_6D_6, d_8-THF) were purchased from Sigma-Aldrich Ltd., dried over a potassium mirror before vacuum distilling under argon and storing over molecular sieves. Di-*n*-butylmagnesium (1.0 M solution in *n*-heptane), quinuclidine, TEMPO, diphenylacetylene, methyl triflate, TCNQ; lecture bottles of H_2, D_2, ^{13}CO, $^{13}CO_2$ were purchased from Sigma-Aldrich Ltd. and used without further purification. Anthracene, tetracene, triphenyl-borane, $[\{CH_2SiMe_2\}_2Cl_2]$, ketones, was purchased from Sigma-Aldrich Ltd. and purified by sublimation/distillation under vacuum before use. Other starting materials were synthesised according to literature conditions (see **Chapter 2 – 4**, and references contained therein).

5.2 Crystallographic Analysis

Single crystal X-ray diffraction data for all compounds were collected on a Supernova, EosS2 diffractometer using Cu-Kα (λ = 1.54184 Å) radiation or Mo Kα (λ = 0.71073 Å). The crystals were maintained at 150(2) K during data collection. Dr Mary Mahon assisted in the processing and finalisation of the crystallographic data. All structures were solved using Olex2 and refined with the ShelXL suite of programs using Least Squares minimization.[1]

1. O. V. Dolomanov, L. J. Bourhis, R. J. Gildea, J. A. Howard and H. Puschmann, *J Appl Crys*, 2009, **42**, 339-341.

	2.24-benzene	**2.24**-toluene	**2.25**
Empirical formula	$C_{36}H_{56}MgN_2Si_2$	$C_{37}H_{58}MgN_2Si_2$	$C_{148}H_{232}Mg_4N_8Na_4Si_8$
Formula weight	597.31	611.34	2537.32
Temperature / K	150.00(10)	150.00(10)	150.01(16)
Crystal system	monoclinic	monoclinic	triclinic
Space group	$P2_1$	$P2_1$	P-1
a / Å	9.2966(1)	9.2699(1)	19.7481(3)
b / Å	19.0191(1)	18.9358(2)	19.9460(3)
c / Å	10.5858(1)	10.6928(1)	20.2316(4)
α / °	90	90	77.123(2)
β / °	105.119(1)	102.036(1)	79.366(2)
γ / °	90	90	89.5220(10)
Volume / Å^3	1806.92(3)	1835.68(3)	7630.8(2)
Z	2	2	2
ρ_{calc} / g/cm^3	1.098	1.106	1.104
μ / mm^{-1}	1.236	1.227	0.147
F(000)	652.0	668.0	2760.0
Crystal size / mm^3	0.301 × 0.187 × 0.161	0.222 × 0.164 × 0.121	0.548 × 0.373 × 0.27
Radiation	CuKα (λ = 1.54184)	CuKα (λ = 1.54184)	MoKα (λ = 0.71073)
2θ range for data collection / °	8.652 to 146.24	8.456 to 146.094	5.838 to 56.564
Index ranges	$-11 \le h \le 11$, $-20 \le k \le 23$, $-12 \le l \le 13$	$-11 \le h \le 10$, $-23 \le k \le 21$, $-13 \le l \le 13$	$-26 \le h \le 26$, $-22 \le k \le 26$, $-26 \le l \le 26$
Reflections collected	20760	21713	84001
Independent reflections	6080 [R_{int} = 0.0354, R_{sigma} = 0.0330]	6441 [R_{int} = 0.0433, R_{sigma} = 0.0467]	37247 [R_{int} = 0.0439, R_{sigma} = 0.1025]
Data / restraints / parameters	6080/67/462	6441/2/396	37247/462/2279
Goodness-of-fit on F^2	1.011	1.029	1.003
Final R indexes [I >= 2σ (I)]	R_1 = 0.0415, wR_2 = 0.1108	R_1 = 0.0468, wR_2 = 0.1222	R_1 = 0.0575, wR_2 = 0.1240
Final R indexes [all data]	R_1 = 0.0420, wR_2 = 0.1117	R_1 = 0.0477, wR_2 = 0.1237	R_1 = 0.1134, wR_2 = 0.1510
Largest diff. peak/hole / e. Å^{-3}	0.76/-0.29	0.52/-0.28	0.78/-0.40
Flack parameter	0.040(15)	0.02(2)	-

	2.26	**2.27**	**2.28**
Empirical formula	$C_{86}H_{134}Mg_2N_4O_2Si_4$	$C_{30}H_{50}MgN_2Si_2$	$C_{120}H_{156}Mg_2N_6Na_2Si_4$
Formula weight	1416.94	519.21	1889.46
Temperature / K	150.00(10)	150.00(10)	150.01(10)
Crystal system	monoclinic	monoclinic	monoclinic
Space group	$P2_1/c$	$P2_1/n$	$P2_1/n$
a / Å	18.4111(1)	17.1366(2)	19.88519(15)
b / Å	24.2048(1)	9.8013(1)	20.70181(18)
c / Å	20.3155(1)	20.3055(2)	27.6936(2)
α / °	90	90	90
β / °	103.599(1)	113.2580(10)	95.8273(8)
γ / °	90	90	90
Volume / Å^3	8799.53(8)	3133.38(6)	11341.44(16)
Z	4	4	4
ρ_{calc} / g/cm^3	1.070	1.101	1.107
μ / mm^{-1}	1.101	1.356	1.034
F(000)	3096.0	1136.0	4080.0
Crystal size / mm^3	0.2 × 0.17 × 0.115	0.165 × 0.156 × 0.106	0.284 × 0.102 × 0.057
Radiation	Cu Kα (λ = 1.54184)	Cu Kα (λ = 1.54184)	Cu Kα (λ = 1.54184)
2θ range for data collection / °	7.304 to 146.006	8.662 to 146.002	7.17 to 151.052
Index ranges	$-22 \le h \le 16$, $-30 \le k \le 29$, $-25 \le l \le 25$	$-21 \le h \le 21$, $-10 \le k \le 12$, $-25 \le l \le 25$	$-24 \le h \le 24$, $-25 \le k \le 25$, $-34 \le l \le 33$
Reflections collected	123836	42736	26999
Independent reflections	17517 [R_{int} = 0.0500, R_{sigma} = 0.0317]	6253 [R_{int} = 0.0437, R_{sigma} = 0.0261]	26999 [R_{int} = 0.0664, R_{sigma} = 0.0591]
Data / restraints / parameters	17517/154/943	6253/0/328	26999/368/1372
Goodness-of-fit on F^2	1.017	1.033	0.916
Final R indexes [I >= 2σ (I)]	R_1 = 0.0365, wR_2 = 0.0915	R_1 = 0.0354, wR_2 = 0.0960	R_1 = 0.0474, wR_2 = 0.1052
Final R indexes [all data]	R_1 = 0.0439, wR_2 = 0.0968	R_1 = 0.0396, wR_2 = 0.0996	R_1 = 0.0724, wR_2 = 0.1125
Largest diff. peak/hole / e. Å^{-3}	0.32/-0.22	0.30/-0.23	0.24/-0.25
Flack parameter	-	-	-

	2.29	**2.31**	**2.32**
Empirical formula	$C_{48}H_{83}MgN_3Na_2Si_3$	$C_{66}H_{106}Mg_2N_4Na_2OSi_4$	$C_{74}H_{110}Mg_2N_4Na_2Si_4$
Formula weight	856.73	1178.50	1262.61
Temperature / K	150.00(10)	150.00(10)	150.00(10)
Crystal system	triclinic	monoclinic	monoclinic
Space group	P-1	I2/a	$P2_1/n$
a / Å	10.4759(3)	23.3563(4)	9.8837(1)
b / Å	12.0459(4)	14.3910(2)	22.4079(1)
c / Å	23.1083(8)	21.1181(3)	33.1579(2)
α / °	76.271(3)	90	90
β / °	78.238(3)	105.484(2)	93.601(1)
γ / °	69.189(3)	90	90
Volume / Å^3	2624.90(16)	6840.59(19)	7329.08(9)
Z	2	4	4
ρ_{calc} / g/cm^3	1.084	1.144	1.144
μ / mm^{-1}	0.152	0.160	1.353
F(000)	936.0	2560.0	2736.0
Crystal size / mm^3	0.53 × 0.391 × 0.144	0.328 × 0.285 × 0.141	0.202 × 0.081 × 0.051
Radiation	Mo Kα (λ = 0.71073)	Mo Kα (λ = 0.71073)	Cu Kα (λ = 1.54184)
2θ range for data collection / °	5.922 to 60.634	6.476 to 60.82	7.892 to 146.096
Index ranges	$-14 \le h \le 14$, $-16 \le k \le 17$, $-32 \le l \le 32$	$-31 \le h \le 32$, $-20 \le k \le 20$, $-29 \le l \le 29$	$-12 \le h \le 9$, $-27 \le k \le 27$, $-41 \le l \le 40$
Reflections collected	45674	56107	96648
Independent reflections	13937 [R_{int} = 0.0357, R_{sigma} = 0.0456]	9474 [R_{int} = 0.0239, R_{sigma} = 0.0178]	14574 [R_{int} = 0.0389, R_{sigma} = 0.0252]
Data / restraints / parameters	13937/116/564	9474/72/397	14574/0/799
Goodness-of-fit on F^2	1.027	1.042	1.024
Final R indexes [I >= 2σ (I)]	R_1 = 0.0466, wR_2 = 0.1096	R_1 = 0.0333, wR_2 = 0.0859	R_1 = 0.0380, wR_2 = 0.1021
Final R indexes [all data]	R_1 = 0.0700, wR_2 = 0.1213	R_1 = 0.0414, wR_2 = 0.0905	R_1 = 0.0429, wR_2 = 0.1064
Largest diff. peak/hole / e. Å^{-3}	0.60/-0.33	0.32/-0.24	0.36/-0.32
Flack parameter	-	-	-

	2.33	**2.34**	**3.23**
Empirical formula	$C_{88}H_{126}Mg_2N_4Na_2Si_4$	$C_{65}H_{107}Mg_2N_4Na_2O_2Si_4$	$C_{48}H_{65}AlBKN_2Si_2$
Formula weight	1446.88	1183.50	803.09
Temperature / K	150.01(10)	150.00(10)	150.01(10)
Crystal system	monoclinic	monoclinic	monoclinic
Space group	$P2_1/c$	I2/a	$P2_1/n$
a / Å	25.5518(5)	23.4040(4)	14.7608(4)
b / Å	13.2671(2)	15.2673(3)	16.1650(5)
c / Å	24.6303(4)	40.5655(6)	19.7217(5)
α / °	90	90	90
β / °	94.791(2)	99.641(2)	100.406(3)
γ / °	90	90	90
Volume / Å^3	8320.5(2)	14290.0(4)	4628.4(2)
Z	4	8	4
ρ_{calc} / g/cm^3	1.155	1.100	1.153
μ / mm^{-1}	1.253	1.377	1.928
F(000)	3136.0	5144.0	1728.0
Crystal size / mm^3	0.156 × 0.135 × 0.04	0.232 × 0.115 × 0.085	0.089 × 0.048 × 0.013
Radiation	Cu Kα (λ = 1.54184)	CuKα (λ = 1.54184)	CuKα (λ = 1.54184)
2θ range for data collection / °	7.514 to 145.948	7.664 to 145.994	6.914 to 136.486
Index ranges	$-30 \le h \le 31$, $-16 \le k \le 15$, $-23 \le l \le 30$	$-28 \le h \le 25$, $-18 \le k \le 18$, $-46 \le l \le 50$	$-17 \le h \le 17$, $-19 \le k \le 16$, $-23 \le l \le 22$
Reflections collected	43508	38609	33245
Independent reflections	16375 [R_{int} = 0.0535, R_{sigma} = 0.0710]	14060 [R_{int} = 0.0290, R_{sigma} = 0.0314]	8370 [R_{int} = 0.0686, R_{sigma} = 0.0635]
Data / restraints / parameters	16375/610/1045	14060/113/814	8370/3/519
Goodness-of-fit on F^2	1.055	1.025	1.017
Final R indexes [I >= 2σ (I)]	R_1 = 0.0742, wR_2 = 0.1870	R_1 = 0.0380, wR_2 = 0.0998	R_1 = 0.0520, wR_2 = 0.1246
Final R indexes [all data]	R_1 = 0.0994, wR_2 = 0.2022	R_1 = 0.0456, wR_2 = 0.1053	R_1 = 0.0804, wR_2 = 0.1398
Largest diff. peak/hole / e. Å^{-3}	0.54/-0.46	0.25/-0.23	0.37/-0.26
Flack parameter	-	-	-

	3.25	**3.26**	**3.27**
Empirical formula	$C_{49}H_{65}AlN_2Si_2$	$C_{66}H_{106}Al_2N_4Si_4$	$C_{36}H_{56}AlKN_2Si_2$
Formula weight	765.19	1121.86	639.08
Temperature / K	150.00(10)	150.00(10)	150.00(10)
Crystal system	monoclinic	monoclinic	monoclinic
Space group	$P2_1/c$	I2/a	$P2_1/c$
a / Å	10.3005(1)	23.6172(2)	11.7099(4)
b / Å	34.6564(3)	13.6850(1)	12.9316(5)
c / Å	12.8827(1)	22.0608(2)	25.0396(8)
α / °	90	90	90
β / °	98.702(1)	113.771(1)	98.151(3)
γ / °	90	90	90
Volume / Å^3	4545.90(7)	6525.19(10)	3753.4(2)
Z	4	4	4
ρ_{calc} / g/cm^3	1.118	1.142	1.131
μ / mm^{-1}	1.140	1.411	2.257
F(000)	1656.0	2448.0	1384.0
Crystal size / mm^3	0.402 × 0.315 × 0.205	0.287 × 0.179 × 0.123	0.129 × 0.071 × 0.035
Radiation	CuKα (λ = 1.54184)	CuKα (λ = 1.54184)	Cu Kα (λ = 1.54184)
2θ range for data collection / °	5.1 to 146.2	7.646 to 146.282	7.132 to 146.8
Index ranges	$-11 \leq h \leq 12$, $-36 \leq k \leq 43$, $-15 \leq l \leq 14$	$-28 \leq h \leq 29$, $-16 \leq k \leq 16$, $-26 \leq l \leq 27$	$-14 \leq h \leq 14$, $-15 \leq k \leq 15$, $-30 \leq l \leq 25$
Reflections collected	61867	32466	20520
Independent reflections	9058 [R_{int} = 0.0492, R_{sigma} = 0.0258]	6472 [R_{int} = 0.0315, R_{sigma} = 0.0226]	7414 [R_{int} = 0.0479, R_{sigma} = 0.0552]
Data / restraints / parameters	9058/0/520	6472/0/355	7414/129/442
Goodness-of-fit on F^2	1.022	1.044	1.039
Final R indexes [I >= 2σ (I)]	R_1 = 0.0441, wR_2 = 0.1190	R_1 = 0.0348, wR_2 = 0.0948	R_1 = 0.0600, wR_2 = 0.1521
Final R indexes [all data]	R_1 = 0.0480, wR_2 = 0.1232	R_1 = 0.0364, wR_2 = 0.0963	R_1 = 0.0775, wR_2 = 0.1668
Largest diff. peak/hole / e. Å^{-3}	0.38/-0.33	0.30/-0.37	0.55/-0.40
Flack parameter	-	-	-

	3.28	**3.29**	**3.30**
Empirical formula	$C_{51}H_{87}AlN_3Na_2Si_3$	$C_{66}H_{114}Al_2N_4Rb_2Si_4$	$C_{66}H_{114}Al_2Cs_2N_4Si_4$
Formula weight	899.46	1300.87	1395.75
Temperature / K	150.00(10)	150.00(10)	150.00(10)
Crystal system	triclinic	monoclinic	monoclinic
Space group	P-1	$P2_1/c$	$P2_1/c$
a / Å	10.51871(18)	16.7763(3)	17.0215(4)
b / Å	13.1772(3)	17.3329(3)	17.2252(6)
c / Å	21.5875(5)	26.5344(4)	26.7216(8)
α / °	105.1605(19)	90	90
β / °	93.2082(16)	101.481(2)	101.274(3)
γ / °	101.1801(16)	90	90
Volume / Å^3	2815.20(10)	7561.3(2)	7683.6(4)
Z	2	4	4
ρ_{calc} / g/cm^3	1.061	1.143	1.207
μ / mm^{-1}	1.319	1.418	1.071
F(000)	982.0	2776.0	2920.0
Crystal size / mm^3	0.26 × 0.105 × 0.065	0.471 × 0.349 × 0.162	0.267 × 0.155 × 0.092
Radiation	Cu Kα (λ = 1.54184)	Mo Kα (λ = 0.71073)	Mo Kα (λ = 0.71073)
2θ range for data collection / °	7.118 to 145.744	6.648 to 60.792	6.644 to 60.584
Index ranges	$-13 \leq h \leq 9$, $-16 \leq k \leq 16$, $-25 \leq l \leq 26$	$-23 \leq h \leq 23$, $-24 \leq k \leq 22$, $-36 \leq l \leq 36$	$-22 \leq h \leq 22$, $-23 \leq k \leq 21$, $-35 \leq l \leq 30$
Reflections collected	25761	94208	45340
Independent reflections	11065 [R_{int} = 0.0332, R_{sigma} = 0.0455]	20530 [R_{int} = 0.0434, R_{sigma} = 0.0450]	19683 [R_{int} = 0.0291, R_{sigma} = 0.0480]
Data / restraints / parameters	11065/0/561	20530/178/829	19683/201/785
Goodness-of-fit on F^2	1.031	1.030	1.043
Final R indexes [I >= 2σ (I)]	R_1 = 0.0535, wR_2 = 0.1382	R_1 = 0.0412, wR_2 = 0.0828	R_1 = 0.0402, wR_2 = 0.0810
Final R indexes [all data]	R_1 = 0.0635, wR_2 = 0.1460	R_1 = 0.0703, wR_2 = 0.0925	R_1 = 0.0654, wR_2 = 0.0901
Largest diff. peak/hole / e. Å^{-3}	0.73/-0.39	0.42/-0.40	0.52/-0.47
Flack parameter	-	-	-

	3.31	**3.32**	**3.33**
Empirical formula	$C_{72}H_{112}Al_2N_4Rb_2Si_4$	$C_{72}H_{112}Al_2Cs_2N_4Si_4$	$C_{47}H_{63}AlKN_2Si_2$
Formula weight	1370.91	1465.79	778.25
Temperature / K	150.00(10)	150.01(10)	150.00(10)
Crystal system	triclinic	triclinic	monoclinic
Space group	P-1	P-1	$P2_1/n$
a / Å	11.7623(4)	11.8376(4)	12.5845(2)
b / Å	13.0073(3)	13.0926(3)	19.7751(2)
c / Å	24.9819(4)	25.0313(3)	17.6105(2)
α / °	90.4636(15)	90.330(1)	90
β / °	98.128(2)	98.135(2)	92.079(1)
γ / °	91.451(2)	91.695(3)	90
Volume / Å^3	3782.26(15)	3838.56(16)	4379.66(10)
Z	2	2	4
ρ_{calc} / g/cm^3	1.204	1.268	1.180
μ / mm^{-1}	2.811	8.522	2.025
F(000)	1456.0	1528.0	1676.0
Crystal size / mm^3	0.191 × 0.091 × 0.034	0.129 × 0.086 × 0.035	0.101 × 0.08 × 0.061
Radiation	Cu Kα (λ = 1.54184)	Cu Kα (λ = 1.54184)	Cu Kα (λ = 1.54184)
2θ range for data collection / °	7.594 to 145.71	7.548 to 146.97	8.332 to 145.934
Index ranges	$-14 \leq h \leq 14$, $-15 \leq k \leq 16$, $-30 \leq l \leq 30$	$-14 \leq h \leq 14$, $-16 \leq k \leq 12$, $-30 \leq l \leq 30$	$-15 \leq h \leq 15$, $-24 \leq k \leq 24$, $-17 \leq l \leq 21$
Reflections collected	16692	18379	32074
Independent reflections	16692 [R_{int} = twinned, R_{sigma} = 0.0639]	18379 [R_{int} = twinned, R_{sigma} = 0.0472]	8688 [R_{int} = 0.0358, R_{sigma} = 0.0334]
Data / restraints / parameters	16692/0/790	18379/0/790	8688/0/509
Goodness-of-fit on F^2	0.887	0.875	1.053
Final R indexes [I >= 2σ (I)]	R_1 = 0.0354, wR_2 = 0.0745	R_1 = 0.0297, wR_2 = 0.0607	R_1 = 0.0370, wR_2 = 0.0937
Final R indexes [all data]	R_1 = 0.0521, wR_2 = 0.0776	R_1 = 0.0426, wR_2 = 0.0628	R_1 = 0.0447, wR_2 = 0.0988
Largest diff. peak/hole / e. Å^{-3}	0.65/-0.41	0.80/-0.57	0.40/-0.30
Flack parameter	-	-	-

	3.34	**3.36**	**3.37**
Empirical formula	$C_{48}H_{62}AlKN_2Si_2$	$C_{82}H_{122}Al_2K_2N_4Si_4$	$C_{39}H_{63}AlKN_2Si_2$
Formula weight	789.25	1408.35	682.17
Temperature / K	150.00(10)	150.00(10)	150.01(10)
Crystal system	orthorhombic	triclinic	monoclinic
Space group	$Pna2_1$	P-1	$P2_1/c$
a / Å	22.2792(7)	10.6934(2)	16.2988(2)
b / Å	10.8361(4)	19.9911(4)	13.0306(2)
c / Å	18.1317(5)	20.5625(4)	19.2783(3)
α / °	90	98.974(2)	90
β / °	90	101.821(2)	106.855(2)
γ / °	90	99.771(2)	90
Volume / Å^3	4377.3(2)	4156.33(15)	3918.50(11)
Z	4	2	4
ρ_{calc} / g/cm^3	1.198	1.125	1.156
μ / mm^{-1}	0.231	2.082	2.190
F(000)	1696.0	1524.0	1484.0
Crystal size / mm^3	0.174 × 0.137 × 0.089	0.19 × 0.097 × 0.046	0.133 × 0.064 × 0.044
Radiation	Mo Kα (λ = 0.71073)	CuKα (λ = 1.54184)	CuKα (λ = 1.54184)
2θ range for data collection / °	6.908 to 60.79	5.736 to 146.528	5.666 to 146.198
Index ranges	-31 ≤ h ≤ 21, -14 ≤ k ≤ 15, -23 ≤ l ≤ 25	-8 ≤ h ≤ 13, -24 ≤ k ≤ 24, -25 ≤ l ≤ 25	-19 ≤ h ≤ 20, -16 ≤ k ≤ 16, -23 ≤ l ≤ 13
Reflections collected	43516	55794	28730
Independent reflections	11290 [R_{int} = 0.0347, R_{sigma} = 0.0390]	16471 [R_{int} = 0.0589, R_{sigma} = 0.0589]	7814 [R_{int} = 0.0405, R_{sigma} = 0.0382]
Data / restraints / parameters	11290/19/519	16471/159/959	7814/23/494
Goodness-of-fit on F^2	1.031	1.052	1.029
Final R indexes [I >= 2σ (I)]	R_1 = 0.0459, wR_2 = 0.1043	R_1 = 0.0664, wR_2 = 0.1634	R_1 = 0.0523, wR_2 = 0.1380
Final R indexes [all data]	R_1 = 0.0585, wR_2 = 0.1108	R_1 = 0.0753, wR_2 = 0.1752	R_1 = 0.0602, wR_2 = 0.1456
Largest diff. peak/hole / e. Å^{-3}	0.50/-0.34	0.88/-0.46	0.39/-0.69
Flack parameter	0.025(13)	-	-

	3.38	**3.39**	**3.40**
Empirical formula	$C_{64}H_{86}AlKN_2O_4Si_2$	$C_{46}H_{66}AlKN_2O_2Si_2$	$C_{40}H_{67}AlKN_2OSi_2$
Formula weight	1069.60	801.26	714.21
Temperature / K	150.01(10)	150.00(10)	150.00(10)
Crystal system	monoclinic	orthorhombic	orthorhombic
Space group	Cc	Pbca	Pbcn
a / Å	21.7511(4)	22.4043(4)	20.3555(1)
b / Å	13.3392(2)	17.8222(3)	23.0087(1)
c / Å	20.8348(3)	22.5974(5)	18.3408(1)
α / °	90	90	90
β / °	101.877(2)	90	90
γ / °	90	90	90
Volume / Å^3	5915.64(17)	9023.0(3)	8589.98(7)
Z	4	8	8
ρ_{calc} / g/cm^3	1.201	1.180	1.105
μ / mm^{-1}	1.686	2.012	2.035
F(000)	2304.0	3456.0	3112.0
Crystal size / mm^3	0.102 × 0.071 × 0.037	0.137 × 0.028 × 0.024	0.209 × 0.163 × 0.104
Radiation	Cu Kα (λ = 1.54184)	Cu Kα (λ = 1.54184)	Cu Kα (λ = 1.54184)
2θ range for data collection / °	7.822 to 144.238	7.448 to 146.122	7.54 to 145.934
Index ranges	$-26 \leq h \leq 26$, $-16 \leq k \leq 12$, $-21 \leq l \leq 25$	$-27 \leq h \leq 24$, $-18 \leq k \leq 21$, $-27 \leq l \leq 27$	$-24 \leq h \leq 25$, $-28 \leq k \leq 23$, $-22 \leq l \leq 22$
Reflections collected	15239	30723	112622
Independent reflections	7932 [R_{int} = 0.0209, R_{sigma} = 0.0332]	8870 [R_{int} = 0.0464, R_{sigma} = 0.0455]	8574 [R_{int} = 0.0487, R_{sigma} = 0.0212]
Data / restraints / parameters	7932/2/683	8870/0/512	8574/42/470
Goodness-of-fit on F^2	1.035	1.015	1.022
Final R indexes [I >= 2σ (I)]	R_1 = 0.0281, wR_2 = 0.0720	R_1 = 0.0386, wR_2 = 0.0875	R_1 = 0.0443, wR_2 = 0.1260
Final R indexes [all data]	R_1 = 0.0295, wR_2 = 0.0731	R_1 = 0.0571, wR_2 = 0.0959	R_1 = 0.0471, wR_2 = 0.1289
Largest diff. peak/hole / e. Å^{-3}	0.24/-0.21	0.31/-0.25	0.97/-0.56
Flack parameter	0.027(7)	-	-

	3.41	**3.43**	**3.44**
Empirical formula	$C_{39}H_{68}AlKN_2OSi_2$	$C_{33}H_{53}AlCl_2KN_2Si_2$	$C_{53}H_{83}AlCl_2K_3N_2Si_2$
Formula weight	703.21	670.93	1019.57
Temperature / K	150.00(10)	150.01(10)	150.01(10)
Crystal system	monoclinic	monoclinic	monoclinic
Space group	C2/c	$P2_1/c$	$P2_1/c$
a / Å	44.6873(10)	15.3831(2)	24.4279(2)
b / Å	12.4327(1)	12.8992(1)	13.2094(1)
c / Å	37.5655(8)	18.7156(2)	17.8959(2)
α / °	90	90	90
β / °	127.202(3)	102.246(1)	94.940(1)
γ / °	90	90	90
Volume / Å^3	16623.8(7)	3629.23(7)	5753.16(9)
Z	16	4	4
ρ_{calc} / g/cm^3	1.124	1.228	1.177
μ / mm^{-1}	2.094	3.680	3.755
F(000)	6144.0	1436.0	2188.0
Crystal size / mm^3	0.112 × 0.068 × 0.057	0.134 × 0.128 × 0.036	0.11 × 0.077 × 0.026
Radiation	Cu Kα (λ = 1.54184)	CuKα (λ = 1.54184)	Cu Kα (λ = 1.54184)
2θ range for data collection / °	7.522 to 146.568	5.88 to 146.206	7.264 to 140.144
Index ranges	-53 ≤ h ≤ 55, -15 ≤ k ≤ 15, -46 ≤ l ≤ 46	-19 ≤ h ≤ 18, -14 ≤ k ≤ 16, -22 ≤ l ≤ 23	-29 ≤ h ≤ 28, -10 ≤ k ≤ 16, -21 ≤ l ≤ 21
Reflections collected	156548	50552	39537
Independent reflections	16566 [R_{int} = 0.0535, R_{sigma} = 0.0266]	7246 [R_{int} = 0.0445, R_{sigma} = 0.0288]	10901 [R_{int} = 0.0358, R_{sigma} = 0.0345]
Data / restraints / parameters	16566/499/1030	7246/0/382	10901/0/590
Goodness-of-fit on F^2	1.019	1.022	1.018
Final R indexes [I >= 2σ (I)]	R_1 = 0.0414, wR_2 = 0.1008	R_1 = 0.0370, wR_2 = 0.0995	R_1 = 0.0357, wR_2 = 0.0904
Final R indexes [all data]	R_1 = 0.0512, wR_2 = 0.1066	R_1 = 0.0411, wR_2 = 0.1028	R_1 = 0.0455, wR_2 = 0.0962
Largest diff. peak/hole / e. Å^{-3}	0.60/-0.46	0.50/-0.47	0.74/-0.39
Flack parameter	-	-	-

	4.27	**4.28**	**4.29**
Empirical formula	$C_{48}H_{84}AlCuN_4Si_2$	$C_{51}H_{91}AlCuN_6Si_2$	$C_{50}H_{81}AlCuN_3Si_2$
Formula weight	863.89	934.99	870.87
Temperature / K	150.00(10)	150.00(10)	150.00(10)
Crystal system	monoclinic	triclinic	orthorhombic
Space group	$P2_1/n$	P-1	$P2_12_12_1$
a / Å	9.8859(1)	9.9857(3)	13.5166(1)
b / Å	18.7781(1)	16.5218(5)	19.1988(1)
c / Å	27.8353(2)	17.1986(4)	19.7555(1)
α / °	90	90.874(2)	90
β / °	96.8140(10)	90.617(2)	90
γ / °	90	104.471(3)	90
Volume / Å^3	5130.80(7)	2746.80(14)	5126.60(5)
Z	4	2	4
ρ_{calc} / g/cm^3	1.118	1.130	1.128
μ / mm^{-1}	1.457	1.406	1.459
F(000)	1880.0	1018.0	1888.0
Crystal size / mm^3	0.293 × 0.202 × 0.149	0.286 × 0.24 × 0.136	0.241 × 0.209 × 0.183
Radiation	CuKα (λ = 1.54184)	CuKα (λ = 1.54184)	CuKα (λ = 1.54184)
2θ range for data collection / °	5.69 to 146.308	5.14 to 146.412	6.42 to 143.34
Index ranges	$-11 \le h \le 12$, $-20 \le k \le 23$, $-34 \le l \le 34$	$-11 \le h \le 12$, $-19 \le k \le 20$, $-20 \le l \le 21$	$-16 \le h \le 16$, $-23 \le k \le 20$, $-24 \le l \le 24$
Reflections collected	67476	35272	61131
Independent reflections	10232 [R_{int} = 0.0266, R_{sigma} = 0.0171]	10974 [R_{int} = 0.0313, R_{sigma} = 0.0295]	10028 [R_{int} = 0.0434, R_{sigma} = 0.0263]
Data / restraints / parameters	10232/0/525	10974/41/601	10028/0/534
Goodness-of-fit on F^2	1.031	1.040	1.026
Final R indexes [I >= 2σ (I)]	R_1 = 0.0294, wR_2 = 0.0759	R_1 = 0.0435, wR_2 = 0.1208	R_1 = 0.0274, wR_2 = 0.0748
Final R indexes [all data]	R_1 = 0.0314, wR_2 = 0.0777	R_1 = 0.0467, wR_2 = 0.1242	R_1 = 0.0282, wR_2 = 0.0755
Largest diff. peak/hole / e. Å^{-3}	0.26/-0.24	0.92/-0.50	0.26/-0.17
Flack parameter	-	-	-0.015(7)

	4.30	**4.32**	**4.36**
Empirical formula	$C_{63}H_{109}AlCuN_5Si_2$	$C_{51}H_{81}AlCuN_3O_2Si_2$	$C_{42}H_{77}AlCuN_2PSi_2$
Formula weight	1083.25	914.88	787.72
Temperature / K	150.00(10)	150.01(10)	150.01(10)
Crystal system	monoclinic	monoclinic	monoclinic
Space group	$P2_1$	$P2_1$	$P2_1/n$
a / Å	16.7744(1)	12.4775(1)	12.4581(1)
b / Å	10.1320(1)	16.0721(1)	16.1906(1)
c / Å	19.3730(2)	14.3837(1)	23.0546(1)
α / °	90	90	90
β / °	101.104(1)	111.948(1)	96.251(1)
γ / °	90	90	90
Volume / Å^3	3230.96(5)	2675.44(4)	4622.56(5)
Z	2	2	4
ρ_{calc} / g/cm^3	1.113	1.136	1.132
μ / mm^{-1}	1.252	1.450	1.876
F(000)	1184.0	988.0	1712.0
Crystal size / mm^3	0.24 × 0.14 × 0.078	0.211 × 0.174 × 0.098	0.209 × 0.191 × 0.158
Radiation	CuKα (λ = 1.54184)	CuKα (λ = 1.54184)	Cu Kα (λ = 1.54184)
2θ range for data collection / °	5.368 to 144.258	6.626 to 142.634	7.716 to 146.316
Index ranges	$-20 \leq h \leq 20$, $-12 \leq k \leq 12$, $-22 \leq l \leq 23$	$-15 \leq h \leq 10$, $-19 \leq k \leq 19$, $-17 \leq l \leq 17$	$-15 \leq h \leq 11$, $-19 \leq k \leq 19$, $-28 \leq l \leq 28$
Reflections collected	68468	31439	58911
Independent reflections	12722 [R_{int} = 0.0463, R_{sigma} = 0.0308]	9949 [R_{int} = 0.0383, R_{sigma} = 0.0386]	9195 [R_{int} = 0.0272, R_{sigma} = 0.0176]
Data / restraints / parameters	12722/36/667	9949/1/561	9195/0/463
Goodness-of-fit on F^2	1.064	1.035	1.018
Final R indexes [I >= 2σ (I)]	R_1 = 0.0397, wR_2 = 0.1052	R_1 = 0.0283, wR_2 = 0.0734	R_1 = 0.0271, wR_2 = 0.0712
Final R indexes [all data]	R_1 = 0.0412, wR_2 = 0.1068	R_1 = 0.0290, wR_2 = 0.0741	R_1 = 0.0286, wR_2 = 0.0724
Largest diff. peak/hole / e. Å^{-3}	0.51/-0.27	0.37/-0.35	0.32/-0.28
Flack parameter	-0.021(16)	0.011(8)	-

	4.37	**4.41**	**4.42**
Empirical formula	$C_{42}H_{77}AlCuN_2PSi_2$	$C_{48}H_{84}AlAuN_4Si_2$	$C_{53}H_{85}AgAlN_3Si_2$
Formula weight	787.72	997.31	955.26
Temperature / K	150.01(10)	150.00(10)	150.00(10)
Crystal system	monoclinic	monoclinic	orthorhombic
Space group	$P2_1/n$	$P2_1/n$	Pbca
a / Å	12.4581(1)	9.9421(2)	17.8026(3)
b / Å	16.1906(1)	18.8454(5)	20.9308(3)
c / Å	23.0546(1)	27.7494(9)	28.5781(4)
α / °	90	90	90
β / °	96.251(1)	96.781(3)	90
γ / °	90	90	90
Volume / Å^3	4622.56(5)	5162.8(3)	10648.8(3)
Z	4	4	8
ρ_{calc} / g/cm^3	1.132	1.283	1.192
μ / mm^{-1}	1.876	6.208	3.884
F(000)	1712.0	2080.0	4096.0
Crystal size / mm^3	0.209 × 0.191 × 0.158	0.135 × 0.080 × 0.060	0.182 × 0.106 × 0.044
Radiation	Cu Kα (λ = 1.54184)	CuKα (λ = 1.54184)	CuKα (λ = 1.54184)
2θ range for data collection / °	7.716 to 146.316	7.95 to 146.308	7.216 to 146.282
Index ranges	$-15 \le h \le 11$, $-19 \le k \le 19$, $-28 \le l \le 28$	$-12 \le h \le 12$, $-23 \le k \le 23$, $-34 \le l \le 34$	$-21 \le h \le 21$, $-12 \le k \le 25$, $-35 \le l \le 35$
Reflections collected	58911	14179	38287
Independent reflections	9195 [R_{int} = 0.0272, R_{sigma} = 0.0176]	14179 [R_{int} = 0.0790, R_{sigma} = 0.0721]	10516 [R_{int} = 0.0470, R_{sigma} = 0.0436]
Data / restraints / parameters	9195/0/463	14179/0/525	10516/0/559
Goodness-of-fit on F^2	1.018	0.898	1.023
Final R indexes [I >= 2σ (I)]	R_1 = 0.0271, wR_2 = 0.0712	R_1 = 0.0662, wR_2 = 0.1585	R_1 = 0.0374, wR_2 = 0.0946
Final R indexes [all data]	R_1 = 0.0286, wR_2 = 0.0724	R_1 = 0.0988, wR_2 = 0.1739	R_1 = 0.0450, wR_2 = 0.1008
Largest diff. peak/hole / e. Å^{-3}	0.32/-0.28	1.83/-1.09	0.60/-0.98
Flack parameter	-	-	-

	4.43	**4.44**
Empirical formula	$C_{96}H_{168}Ag_2Al_2N_{12}Si_4$	$C_{106.5}H_{189}Al_2Au_2N_{12}Si_4$
Formula weight	1872.47	2197.94
Temperature / K	150.01(10)	150.00(10)
Crystal system	orthorhombic	monoclinic
Space group	$Pna2_1$	$P2_1/c$
a / Å	24.3646(2)	14.9232(1)
b / Å	10.9273(1)	31.7335(1)
c / Å	39.1524(3)	26.0764(1)
α / °	90	90
β / °	90	91.103(1)
γ / °	90	90
Volume / $Å^3$	10423.91(15)	12346.6(1)
Z	4	4
ρ_{calc} / g/cm^3	1.193	1.182
μ / mm^{-1}	3.973	5.245
F(000)	4016.0	4608.0
Crystal size / mm^3	0.171 × 0.09 × 0.054	0.106 × 0.068 × 0.047
Radiation	CuKα (λ = 1.54184)	CuKα (λ = 1.54184)
2θ range for data collection / °	7.6 to 142.748	7.32 to 147.01
Index ranges	$-29 \leq h \leq 29$, $-13 \leq k \leq 13$, $-48 \leq l \leq 42$	$-17 \leq h \leq 18$, $-39 \leq k \leq 35$, $-31 \leq l \leq 32$
Reflections collected	121205	172051
Independent reflections	15006 [R_{int} = 0.0531, R_{sigma} = 0.0364]	24603 [R_{int} = 0.0529, R_{sigma} = 0.0320]
Data / restraints / parameters	15006/115/1201	24603/8/1118
Goodness-of-fit on F^2	1.045	1.026
Final R indexes [I >= 2σ (I)]	R_1 = 0.0571, wR_2 = 0.1422	R_1 = 0.0318, wR_2 = 0.0809
Final R indexes [all data]	R_1 = 0.0591, wR_2 = 0.1454	R_1 = 0.0362, wR_2 = 0.0837
Largest diff. peak/hole / e. $Å^{-3}$	2.82/-0.85	0.97/-1.21
Flack parameter	0.035(7)	-

6. Miscellaneous Structures

This Chapter contains selected molecules that have been prepared from the species described within this thesis. These structures further demonstrate the chemistry of the compounds utilised in the project, albeit they do not fit in with the main content of the thesis.

Figure 6.1 is the structure of the dilithium salt of the $[SiN^{Dipp}]^{2-}$ diamide ligand. The solid-state data highlight the flexibility of this 6-membered chelating backbone, which contributed to the cation-arene interactions and the dimeric structures of $[\{SiN^{Dipp}\}MgNa]_2$ (**2.25**) and $[\{SiN^{Dipp}\}AlK]_2$ (**3.12**). **Figures 6.2** and **6.3** represent the outcome of attempts to exploit the $[\{SiN^{Dipp}\}Mg]$ (**2.24**) in the preparation of $\{SiN^{Dipp}\}$-supported *d*- and *f*-block molecules. While the reaction of **2.24** with $ZnCl_2$ gave the 14-membered macrocyclic zinc-diamide, $[\{SiN^{Dipp}\}Zn]_2$ (**Figure 6.2**), treatment of **2.24** with YbI_2 provided a heterotrinuclear species, $[\{SiN^{Dipp}\}Mg\text{-}IYbI\text{-}Mg\{SiN^{Dipp}\}]$ (**Figure 6.3**). Although respective reactions of $[CpMo(CO)_3]_2$ with$[\{SiN^{Dipp}\}MgNa]_2$ (**2.25**) and $[\{SiN^{Dipp}\}AlK]_2$ (**3.12**) resulted in diverse Mo-environments, the products highlight the reducing nature of **2.25** and **3.12** (**Figure 6.4** and **6.5**). Treatment of **3.12** with $[(NHC^{iPr})Rh(COD)Cl]$ gave the hydride-bridging heterobimetallic complex shown in **Figure 6.6**, where the KCl elimination in the synthesis of the molecule is indicative of a salt metathesis process.

"Be rude not to." – Common saying.

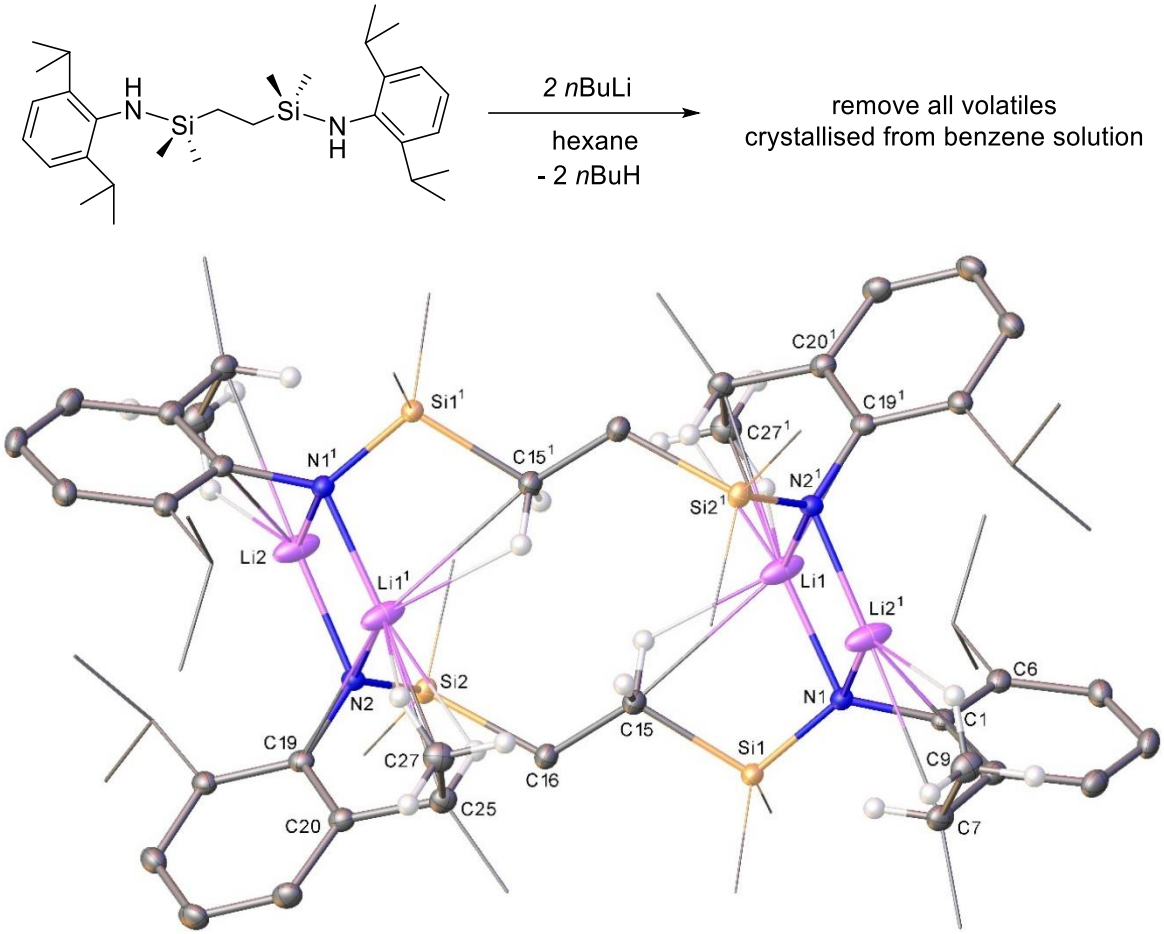

Figure 6. 1 : Displacement ellipsoid plot (30 % probability) of [{SiN^{Dipp}}Li$_2$]$_2$. Hydrogen atoms (except those which have potential interactions with Li) and solvent molecules have been removed, isopropyl groups (except those which have potential interactions with Li) are shown as wireframe for clarity. The asymmetric unit equates to half of a molecule, the remainder of which is generated *via* crystallographic inversion symmetry.

Crystal Data for $C_{30}H_{50}Li_2N_2Si_2$ (M =508.78 g/mol): triclinic, space group P-1 (no. 2), a = 9.4778(2) Å, b = 12.4773(3) Å, c = 15.1032(3) Å, α = 71.926(2)°, β = 72.329(2)°, γ = 67.921(2)°, V = 1537.59(7) Å^3, Z = 2, T = 150.00(10) K, μ(Cu Kα) = 1.174 mm^{-1}, D_{calc} = 1.099 g/cm^3, 16331 reflections measured (7.842° ≤ 2Θ ≤ 145.936°), 6117 unique (R_{int} = 0.0335, R_{sigma} = 0.0447) which were used in all calculations. The final R_1 was 0.0374 (I > 2σ(I)) and wR_2 was 0.0979 (all data).

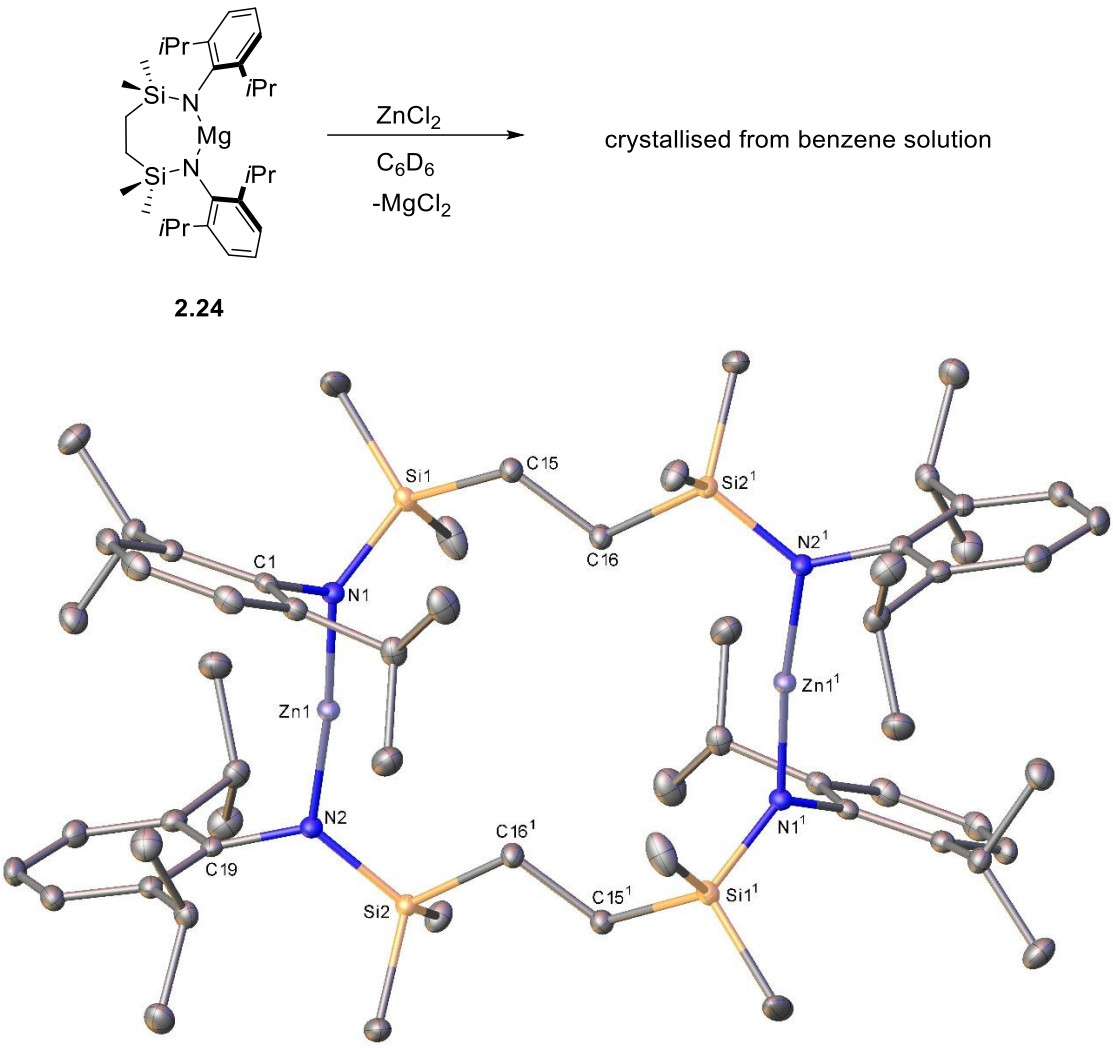

Figure 6. 2 : Displacement ellipsoid plot (30 % probability) of [{SiN^{Dipp}}Zn]$_2$. Hydrogen atoms have been removed for clarity. The asymmetric unit equates to half of a molecule, the remainder of which is generated *via* crystallographic inversion symmetry.

Crystal Data for $C_{30}H_{50}N_2Si_2Zn$ (M =560.27 g/mol): triclinic, space group P-1 (no. 2), a = 9.4322(2) Å, b = 12.5598(4) Å, c = 15.3306(5) Å, α = 70.229(3)°, β = 74.127(3)°, γ = 68.951(3)°, V = 1570.99(9) Å^3, Z = 2, T = 150.00(10) K, μ(Cu Kα) = 1.949 mm^{-1}, D_{calc} = 1.184 g/cm^3, 16886 reflections measured (7.828° ≤ 2Θ ≤ 146.02°), 6246 unique (R_{int} = 0.0308, R_{sigma} = 0.0393) which were used in all calculations. The final R_1 was 0.0302 (I > 2σ(I)) and wR_2 was 0.0769 (all data).

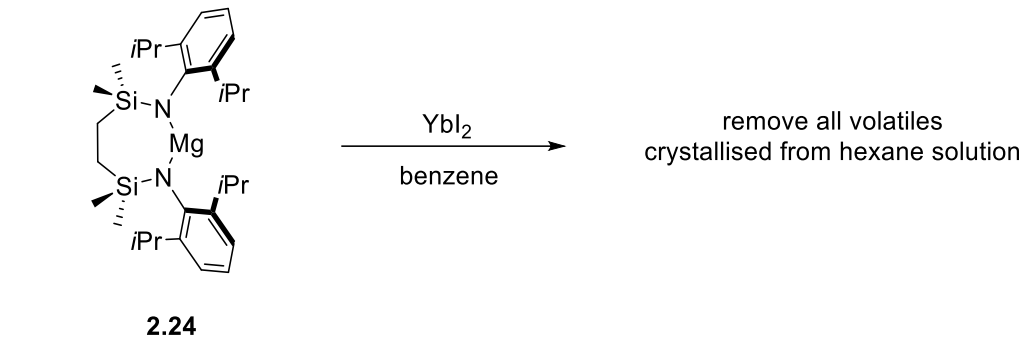

2.24

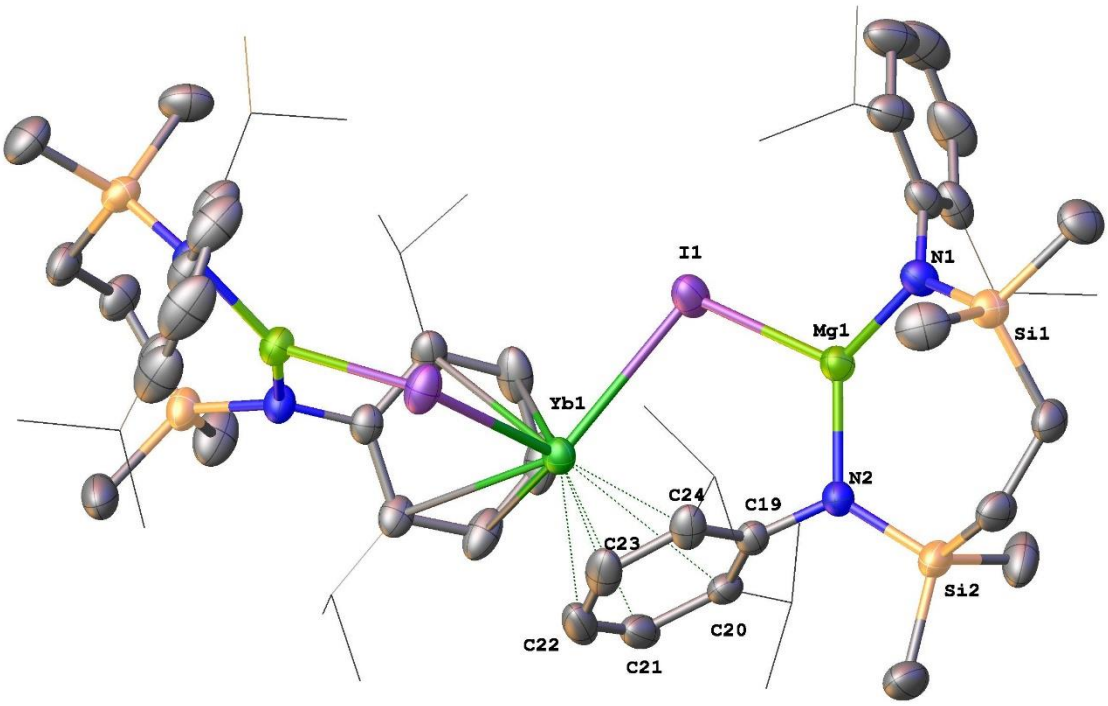

Figure 6. 3 : Displacement ellipsoid plot (30 % probability) of [{SiN^{Dipp}}Mg-IYbI-Mg{SiN^{Dipp}}]. Hydrogen atoms have been removed for clarity. The asymmetric unit equates to half of a molecule, the remainder of which is generated via crystallographic inversion symmetry.

Crystal Data for $C_{29.8}H_{49.3}IMgN_2Si_2Yb_{0.5}$ (M =379.37 g/mol): monoclinic, space group C2/c (no. 15), a = 15.14330(10) Å, b = 19.2981(2) Å, c = 23.6335(2) Å, β = 93.6540(10)°, V = 6892.54(10) Å^3, Z = 8, T = 150.00(10) K, μ(Cu Kα) = 98.930 mm^{-1}, D_{calc} = 5.849 g/cm^3, 37449 reflections measured (7.43° ≤ 2Θ ≤ 145.814°), 6833 unique (R_{int} = 0.0387, R_{sigma} = 0.0284) which were used in all calculations. The final R_1 was 0.0319 (I > 2σ(I)) and wR_2 was 0.0878 (all data).

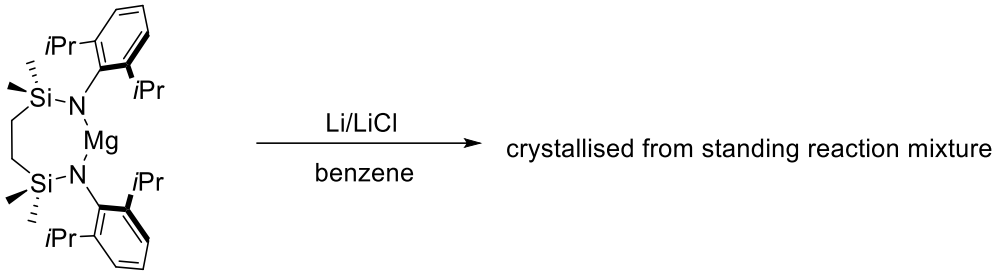

2.24

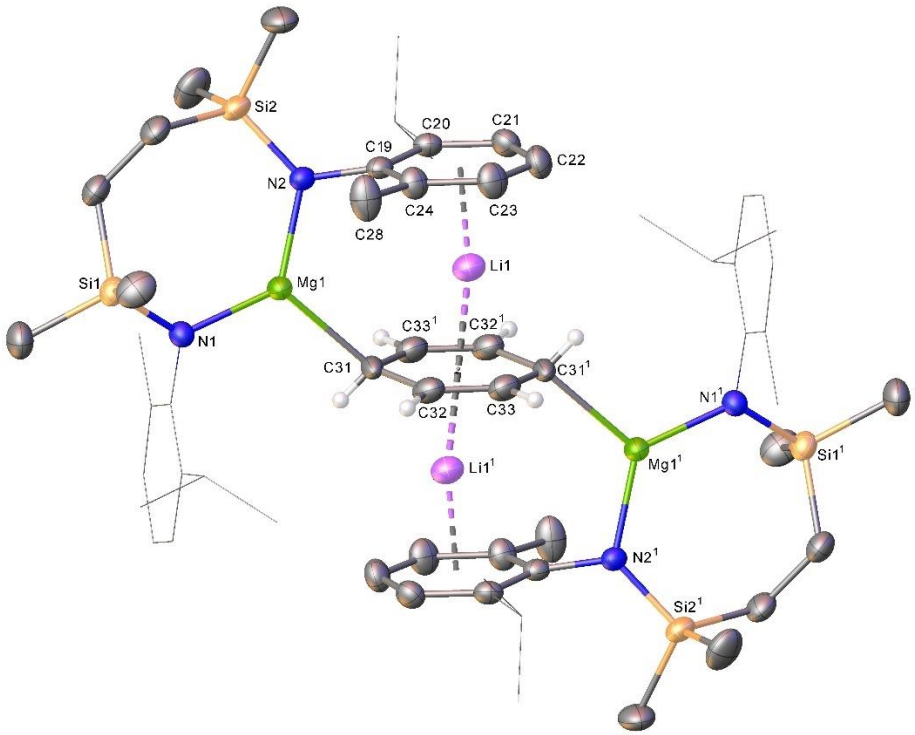

Figure 6. 4 : Displacement ellipsoid plots (30 % probability) of [{SiN^{Dipp}}MgLi-C_6H_6-LiMg{SiN^{Dipp}}]. Hydrogen atoms and solvent molecules have been removed; selected groups are shown as wireframe for clarity.

Crystal Data for $C_{33}H_{53}LiMgN_2Si_2$ (*M* =565.20 g/mol): monoclinic, space group $P2_1/n$ (no. 14), *a* = 17.0664(2) Å, *b* = 10.53860(10) Å, *c* = 20.5499(2) Å, *β* = 107.8730(10)°, *V* = 3517.65(7) Å^3, *Z* = 4, *T* = 150.00(10) K, μ(Cu Kα) = 1.240 mm^{-1}, *Dcalc* = 1.067 g/cm^3, 45587 reflections measured (8.072° ≤ 2Θ ≤ 146.294°), 7016 unique (R_{int} = 0.0322, R_{sigma} = 0.0215) which were used in all calculations. The final R_1 was 0.0443 (I > 2σ(I)) and wR_2 was 0.1191 (all data).

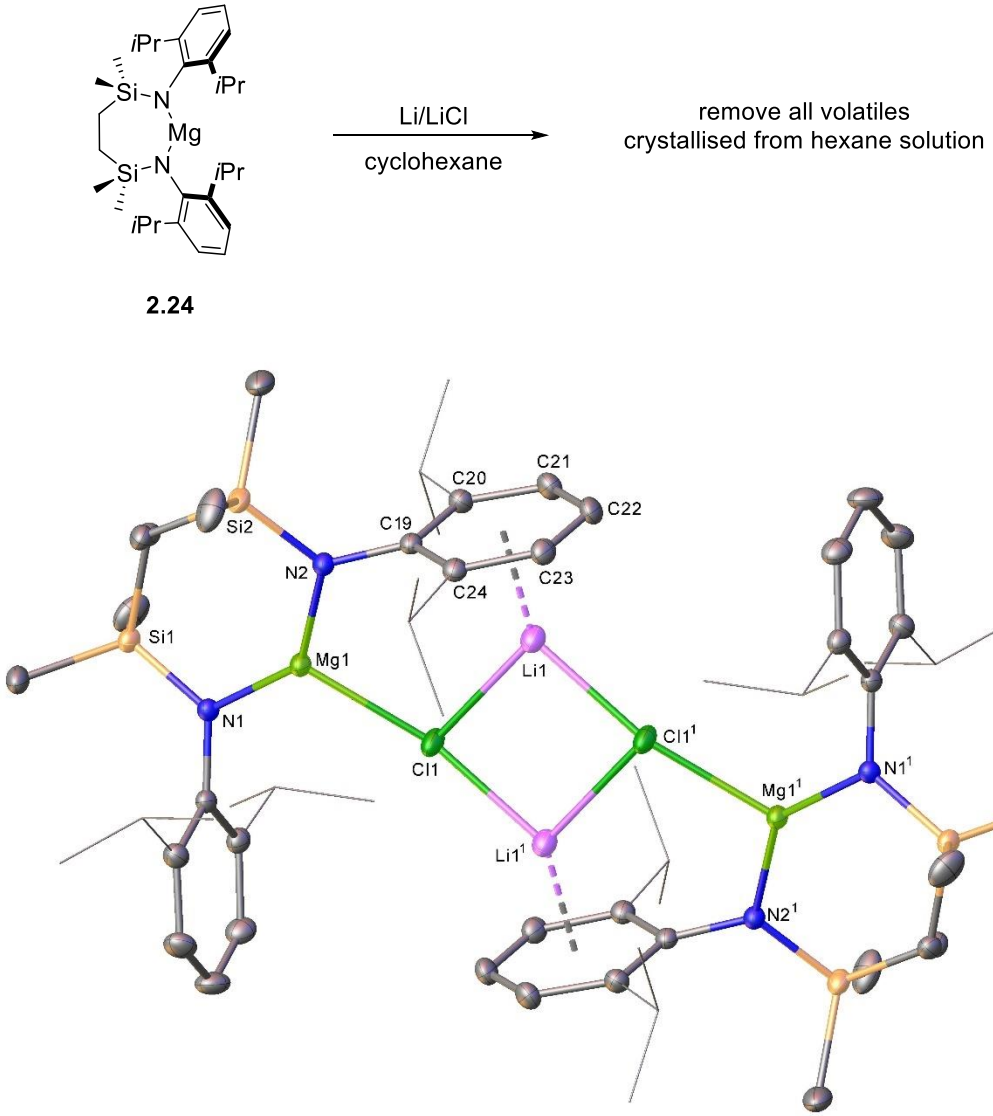

Figure 6. 5 : Displacement ellipsoid plots (30 % probability) of [{SiN^{Dipp}}MgClLi]$_2$. Hydrogen atoms and solvent molecules have been removed; some groups are shown as wireframe for clarity.

Crystal Data for $C_{37}H_{64}ClLiMgN_2Si_2$ (M =659.78 g/mol): monoclinic, space group $P2_1/c$ (no. 14), a = 17.34130(10) Å, b = 11.12930(10) Å, c = 21.41010(10) Å, β = 99.7460(10)°, V = 4072.44(5) Å^3, Z = 4, T = 150.00(10) K, μ(Cu Kα) = 1.720 mm^{-1}, *Dcalc* = 1.076 g/cm^3, 56040 reflections measured (8.38° ≤ 2Θ ≤ 145.844°), 8107 unique (R_{int} = 0.0341, R_{sigma} = 0.0216) which were used in all calculations. The final R_1 was 0.0321 (I > 2σ(I)) and wR_2 was 0.0883 (all data).

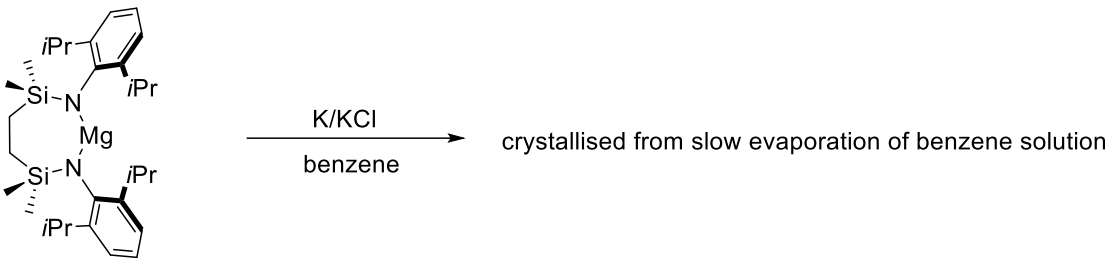

2.24

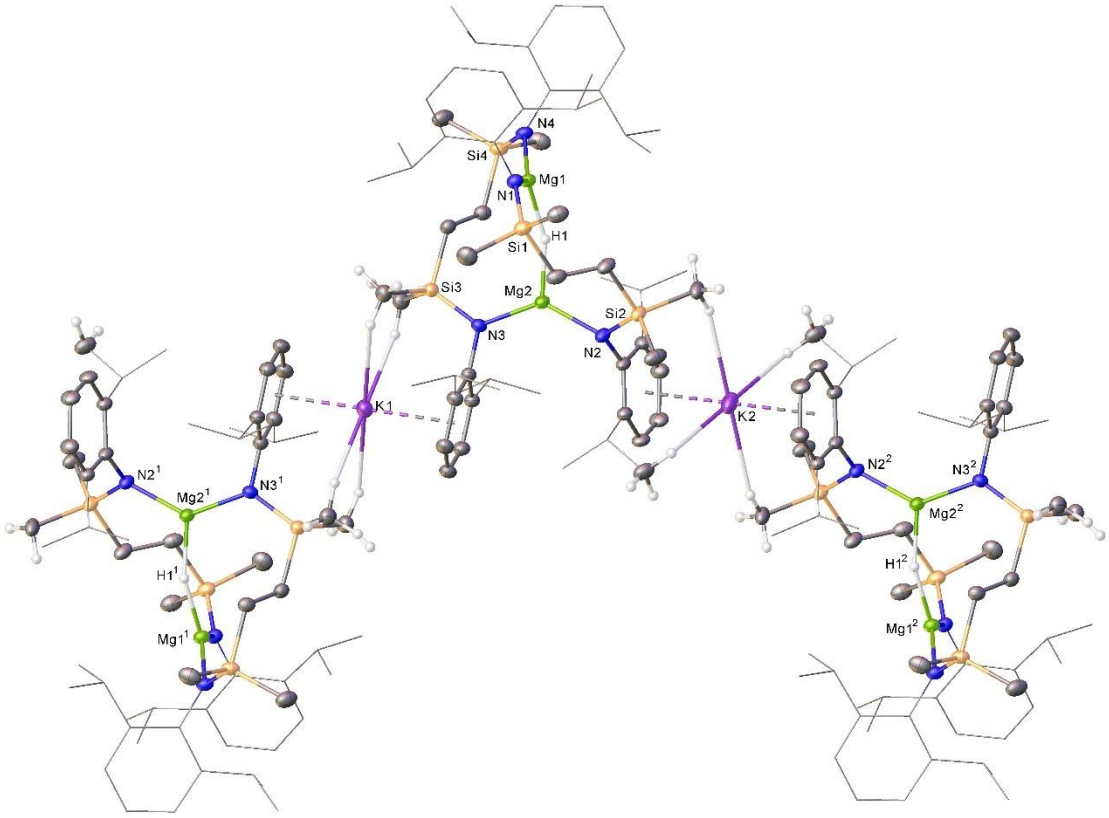

Figure 6. 6 : Displacement ellipsoid plots (30 % probability) of [{SiN^{Dipp}}Mg-H-Mg{SiN^{Dipp}}]K. Hydrogen atoms and solvent molecules have been removed; some groups are shown as wireframe for clarity.

Crystal Data for $C_{60}H_{101}KMg_2N_4Si_4$ (M =1078.52 g/mol): triclinic, space group P-1 (no. 2), a = 12.7527(4) Å, b = 13.6314(5) Å, c = 20.3895(7) Å, α = 92.993(3)°, β = 105.878(3)°, γ = 107.087(3)°, V = 3224.7(2) Å^3, Z = 2, T = 150.15 K, μ(CuKα) = 1.901 mm^{-1}, $Dcalc$ = 1.111 g/cm^3, 32457 reflections measured (7.594° ≤ 2Θ ≤ 145.696°), 12740 unique (R_{int} = 0.0409, R_{sigma} = 0.0598) which were used in all calculations. The final R_1 was 0.0670 (I > 2σ(I)) and wR_2 was 0.1950 (all data).

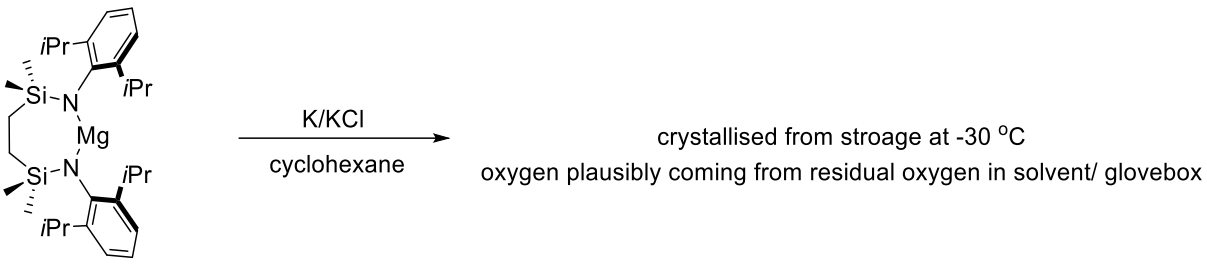

2.24

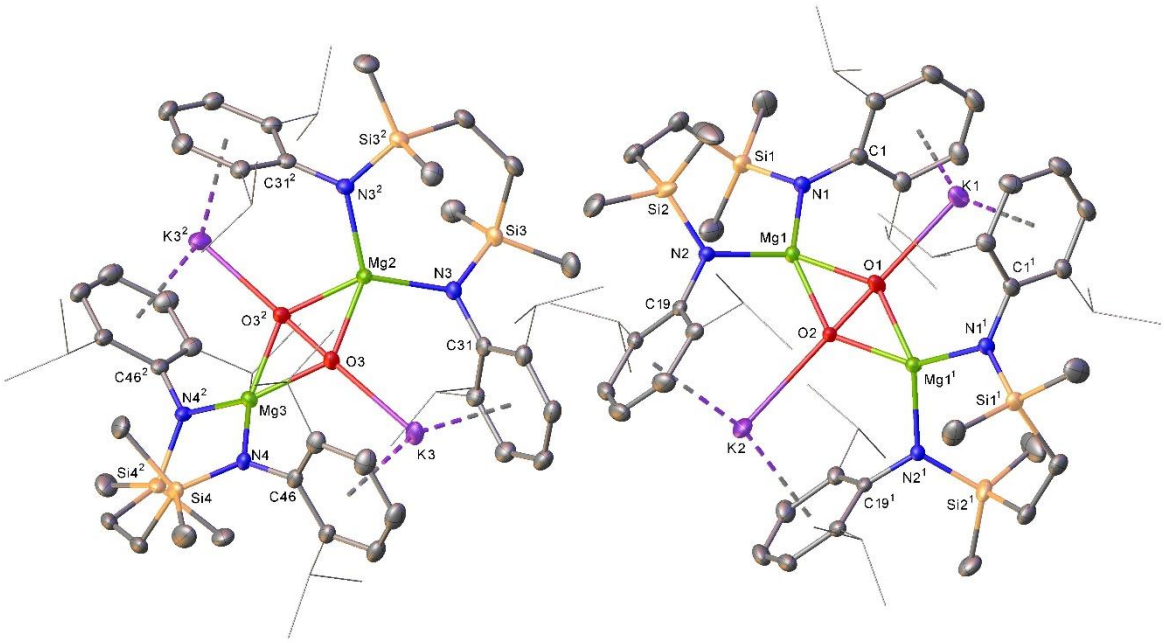

Figure 6. 7 : Displacement ellipsoid plots (30 % probability) of [{SiN^{Dipp}}Mg-(O_2)-Mg{SiN^{Dipp}}]K_2. Hydrogen atoms and solvent molecules have been removed; some groups are shown as wireframe for clarity.

Crystal Data for $C_{74}H_{116}K_2Mg_2N_4O_2Si_4$ (M =1332.88 g/mol): monoclinic, space group I2/a (no. 15), a = 22.2273(3) Å, b = 27.7481(3) Å, c = 26.8624(4) Å, β = 111.026(2)°, V = 15464.7(4) Å^3, Z = 8, T = 150.00(10) K, μ(Cu Kα) = 2.169 mm^{-1}, *Dcalc* = 1.145 g/cm^3, 89255 reflections measured (7.514° ≤ 2Θ ≤ 146.368°), 15403 unique (R_{int} = 0.0433, R_{sigma} = 0.0266) which were used in all calculations. The final R_1 was 0.0481 (I > 2σ(I)) and wR_2 was 0.1299 (all data).

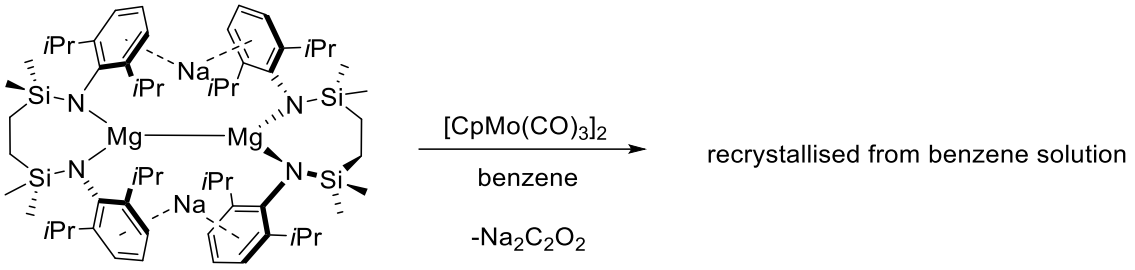

2.25

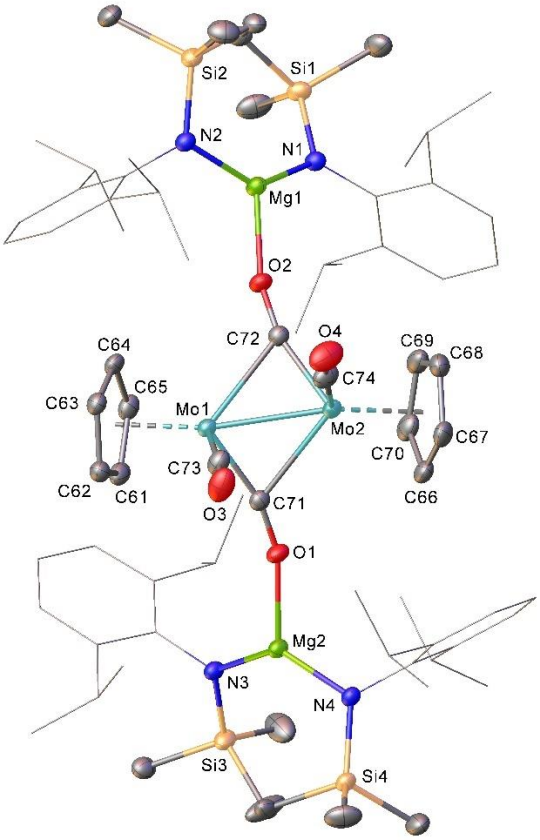

Figure 6. 8 : Displacement ellipsoid plots (30 % probability) of [{SiN^{Dipp}}Mg-OC-{$Cp_2Mo_2(CO)_2$}-CO-Mg{SiN^{Dipp}}]. Hydrogen atoms and solvent molecules have been removed; Dipp groups are shown as wireframe for clarity.

Crystal Data for $C_{86}H_{122}Mg_2Mo_2N_4O_4Si_4$ (M =1628.73 g/mol): triclinic, space group P-1 (no. 2), a = 13.0209(2) Å, b = 18.6587(3) Å, c = 19.2841(2) Å, α = 90.5160(10)°, β = 95.9290(10)°, γ = 109.4880(10)°, V = 4388.38(11) Å^3, Z = 2, T = 150.00(10) K, μ(Cu Kα) = 3.373 mm^{-1}, D_{calc} = 1.233 g/cm^3, 94541 reflections measured (6.982° ≤ 2Θ ≤ 145.936°), 17420 unique (R_{int} = 0.0362, R_{sigma} = 0.0250) which were used in all calculations. The final R_1 was 0.0276 (I > 2σ(I)) and wR_2 was 0.0755 (all data).

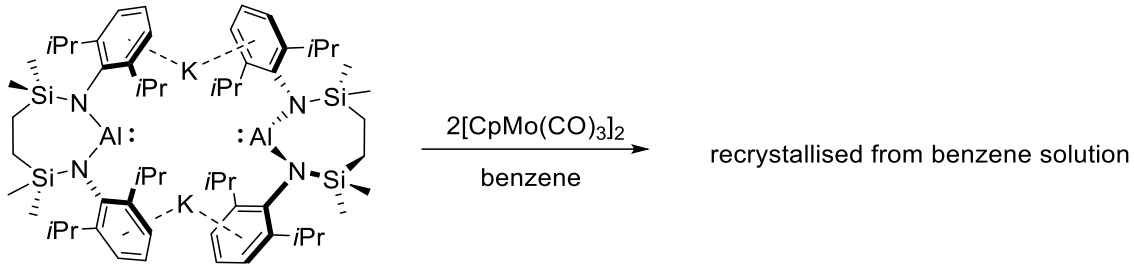

3.12

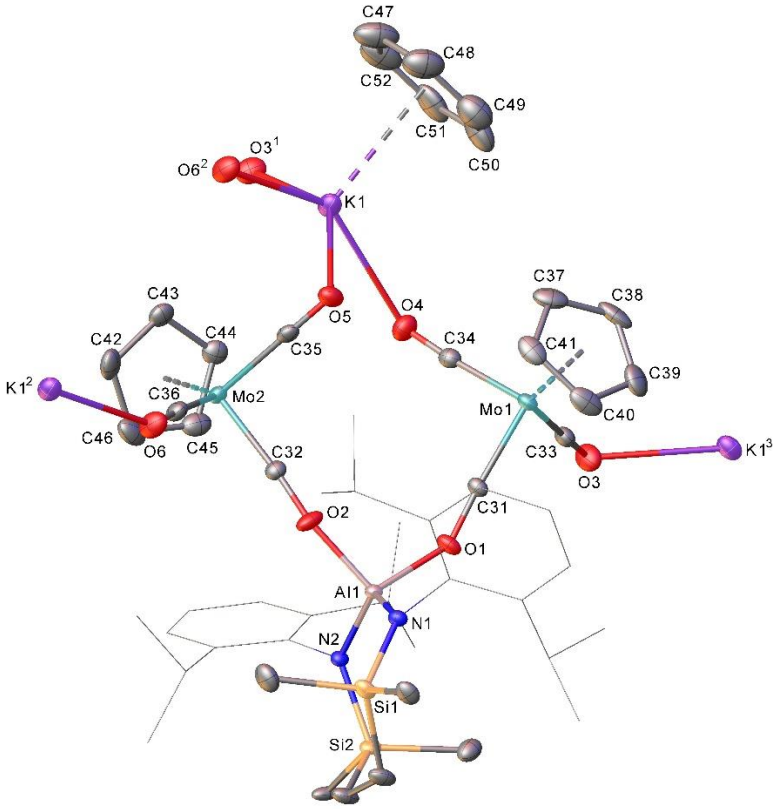

Figure 6. 9 : Displacement ellipsoid plots (30 % probability) of a polymeric section of [{SiN^{Dipp}}Al{$Cp_2Mo_2(CO)_3$}K]. Hydrogen atoms have been removed; Dipp groups are shown as wireframe for clarity.

Crystal Data for $C_{52}H_{66}AlKMo_2N_2O_6Si_2$ (M =1129.20 g/mol): monoclinic, space group $P2_1/c$ (no. 14), a = 17.7122(2) Å, b = 12.89460(10) Å, c = 24.3395(2) Å, β = 96.2460(10)°, V = 5525.94(9) Å^3, Z = 4, T = 150.01(10) K, μ(Cu Kα) = 5.331 mm^{-1}, D_{calc} = 1.357 g/cm^3, 76659 reflections measured (7.308° ≤ 2Θ ≤ 145.91°), 10980 unique (R_{int} = 0.0567, R_{sigma} = 0.0370) which were used in all calculations. The final R_1 was 0.0297 (I > 2σ(I)) and wR_2 was 0.0731 (all data).

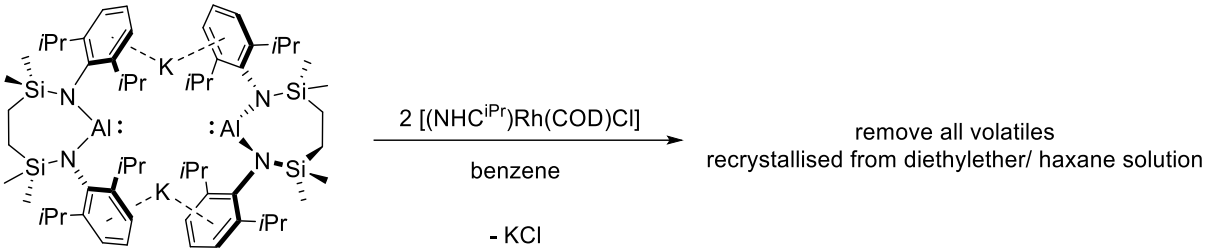

3.12

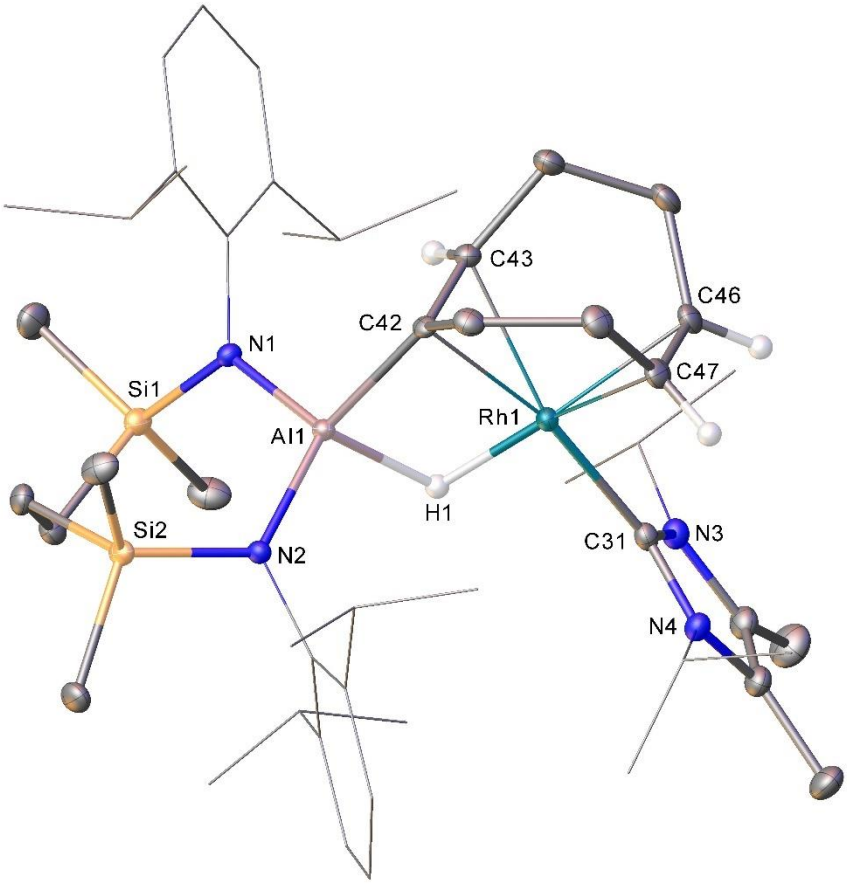

Figure 6. 10 : Displacement ellipsoid plot (30 % probability) of [(NHC^{iPr})Rh(H)(COD)Al{SiN^{Dipp}}]. Hydrogen atoms (except the Rh-H, and those on C43, C46, and C47) have been removed; Dipp and *iso*-propyl groups are shown as wireframe for clarity.

Crystal Data for $C_{49}H_{82}AlN_4RhSi_2$ (M =913.25 g/mol): monoclinic, space group $P2_1/c$ (no. 14), a = 16.15710(10) Å, b = 12.70830(10) Å, c = 24.3013(2) Å, β = 99.7010(10)°, V = 4918.42(7) Å^3, Z = 4, T = 150.00(10) K, μ(Cu Kα) = 3.709 mm^{-1}, D_{calc} = 1.233 g/cm^3, 64767 reflections measured (7.876° ≤ 2Θ ≤ 146.016°), 9780 unique (R_{int} = 0.0392, R_{sigma} = 0.0259) which were used in all calculations. The final R_1 was 0.0242 (I > 2σ(I)) and wR_2 was 0.0585 (all data).

"Everything will be alright in the end, if it is not alright it is not the end."

– Deborah Moggach, *The Best Exotic Marigold Hotel*, 2011.